

POLITECNICO DI TORINO

Collegio di Ingegneria Chimica e dei Materiali

**Master of Science Course
in Materials Engineering**

Master of Science Thesis

Characterization of Powders to Be Used in a Laser Powder Bed Machine. Analysis of the Critical Parameters and Relationship with Powder Flowability



Tutors

.....

Prof. Sara Biamino

.....

Ing. Enrico Maria Orsi

Candidate

.....

Alessandro Carrozza

October 2017

Table of Contents

1. Introduction	1
1.1. Additive Manufacturing (AM)	1
1.2. AM Limitations	8
1.3. Powder Bed Fusion (PBF)	9
1.4. Powders	12
1.4.1. Atomization Process	13
1.4.2. Powder Flowability and Processability	16
2. Materials and Methods	21
2.1. SEM/EDS	22
2.2. Helium Pycnometer	25
2.3. Particle Size Distribution	28
2.4. Powder Flow Test	30
2.5. Moisture Content	35
2.6. Powder Rheometer	36
2.6.1. Stability and Variable Flow Rate Test	43
2.6.2. Aeration Test	53
2.6.3. Permeability Test	56
2.6.4. Compressibility Test	57
2.6.5. Shear Cell	58
3. Results and Discussion for AlSi10Mg powders	62
3.1. SEM/EDS	62
3.1.1. Shape and Morphology	62
3.1.2. Chemical Composition Analysis	66
3.2. Density Measurement	75
3.3. Particle Size Distribution	76
3.4. Powder Flow Test	84
3.4.1. Comparison Between Powder Flow Test and SEM results	87
3.4.2. Comparison Between Powder Flow Test and Particle Size Distribution	90
3.5. Moisture Content	92
3.6. Powder Rheometer	94
3.6.1. Stability Test and Variable Flow Rate Test Results	94
3.6.2. Aeration Test Results	97
3.6.3. Permeability Test Results	103
3.6.4. Compressibility Test Results	107

3.6.5. Shear Cell Results.....	115
4. Results and Discussion for the A205 Powder.....	122
4.1. SEM/EDS	122
4.1.1. Shape and Morphology.....	122
4.1.2. Chemical Composition Analysis	124
4.2. Density measurement	125
4.3. Particle Size Distribution.....	125
4.4. Powder Flow Test	127
4.5. Moisture Content.....	127
4.6. Powder Rheometer	129
4.6.1. Stability Test and Variable Flow Rate Test Results	129
4.6.2. Aeration Test Results.....	130
4.6.3. Permeability Test Results.....	131
4.6.4. Compressibility Test Results.....	133
4.6.5. Shear Cell Results.....	134
5. Conclusions	136
6. List of Symbols.....	140
7. References	142

Sommario

L'Additive Manufacturing (AM) è una tecnica di produzione additiva, che consiste nella creazione di un manufatto, a partire direttamente dal progetto CAD del componente, tramite consolidamento di strati successivi, con l'ausilio del calore o di un legante. Nel caso dei materiali metallici, il materiale di partenza si trova sotto forma di polvere e non è necessario l'uso di alcun legante. Per gli scopi di questo elaborato si considererà solamente una sottocategoria di processi AM, ossia quelli a letto di polvere. Quest'ultimi si dividono a loro volta in base al mezzo tramite il quale viene fornito il calore necessario ai vari strati per fondere localmente e risolidificare. Le due tecniche possibili prevedono l'utilizzo di un laser (LBM) oppure di un fascio elettronico (EBM) (Fig. 1). Il mio lavoro di tesi qui riassunto è stato svolto presso Renishaw PLC (Stone, Staffordshire, UK), un'azienda che si occupa di produzione di macchine di Selective Laser Melting. Per questo motivo in questo lavoro si fa particolare riferimento a questa tecnica.

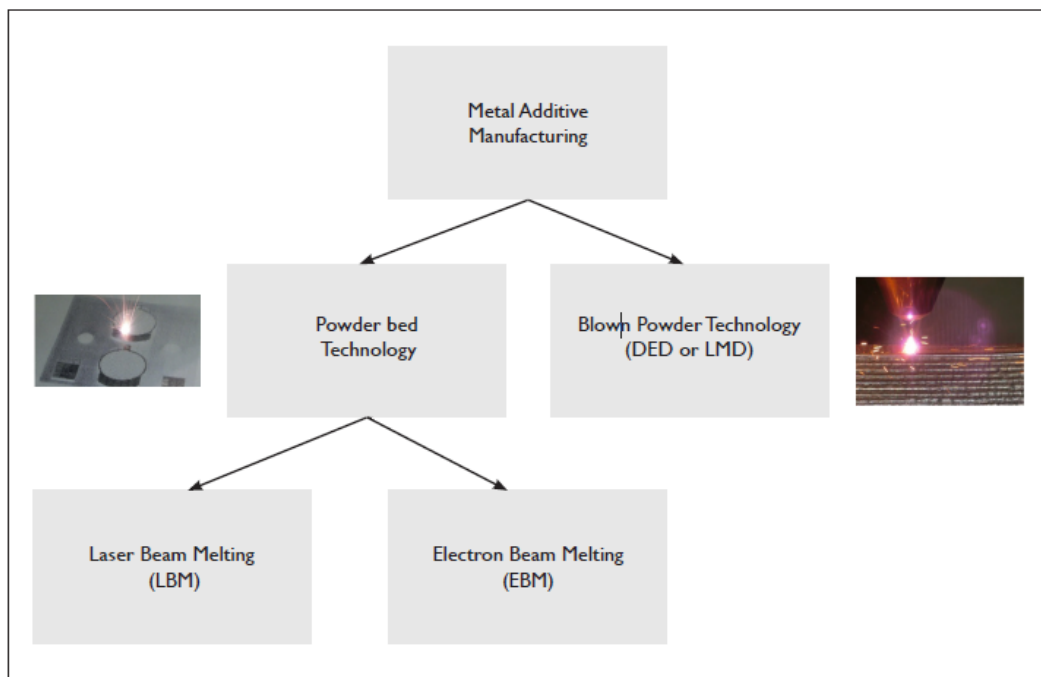


Figura 1: Schematizzazione delle principali tecniche AM per i materiali metallici.

Questa tecnica produttiva relativamente nuova possiede alcuni vantaggi peculiari, tra cui:

- Possibilità di produrre pezzi molto complessi geometricamente;
- Capacità di produrre il componente direttamente dal progetto, evitando di conseguenza costi relativi al cambiamento dell'impianto;
- È possibile produrre componenti dalle forme più complesse in materiali non convenzionalmente utilizzabili;
- L'assemblaggio, con i relativi problemi strutturali, può essere evitato, costruendo il componente come un unico blocco;

- Possono essere create microstrutture molto fini;
- Si tratta di una tecnologia valida anche nel caso di produzione di lotti molto piccoli;
- Non essendoci costi relativi al cambiamento dell'impianto fisico, nel caso di modifiche al progetto iniziale del componente, si può raggiungere un grado di versatilità estraneo alle altre classiche tecniche di produzione.

Tramite SLM possono essere lavorate svariate tipologie di leghe metalliche, tra cui acciai, leghe di Ti, Al, Ni, ecc. I componenti prodotti posseggono generalmente un elevato valore aggiunto e vengono utilizzati in svariati campi, come ad esempio biomedica, aerospazio, gioielleria, componentistica, ecc.

Un parametro fondamentale, da considerare per questa tecnica produttiva, sta nella qualità delle polveri utilizzate. Quest'ultime non devono presentare solamente le corrette caratteristiche composizionali, ma anche tutta una serie di caratteristiche (taglia granulometrica, contenuto di umidità, distribuzione della dimensione delle particelle), estranee alle tecniche fusorie, necessarie per il corretto svolgimento del processo, in maniera che non vengano compromesse le proprietà finali del manufatto. La qualità delle polveri inserite in macchina è strettamente legata non soltanto alle proprietà finali del componente prodotto, ma anche a quanto facilmente il processo potrà essere condotto. Infatti una polvere iniziale dalle scarse caratteristiche porta solitamente a fenomeni di intasamento del sistema di distribuzione, stesura non ottimale della polvere sulla piattaforma di lavoro e una bassa densità del letto. Questi fenomeni possono comportare un non corretto funzionamento del macchinario e/o una non ottimale densificazione del componente, con relativo abbassamento delle proprietà finali del manufatto. È conseguentemente necessario stabilire tramite un'ampia serie di test quali siano le caratteristiche e i parametri fondamentali da considerare per poter ottimizzare il cosiddetto "*Flowing Behaviour*".

L'obiettivo del lavoro svolto presso Renishaw PLC (Stone, Staffordshire, UK) consisteva nel fare una caratterizzazione più ampia possibile di polveri utilizzate nelle loro macchine. Questa azienda si occupa della produzione di macchinari per la produzione additiva, del tipo SLM. Di conseguenza, sono state caratterizzate 8 differenti polveri di lega di alluminio (AlSi10Mg, A205) provenienti da differenti produttori (L, S, T, V) e lotti differenti provenienti dal medesimo produttore. I campioni sono stati analizzati con tecniche classiche e consolidate (SEM, analizzatore di distribuzione della dimensione delle particelle, picnometro, valutazione del tenore di umidità, Flowability Test), ai cui risultati sono stati affiancati i dati ottenuti tramite reometro per polveri (FT4, Freeman Technology, UK). Questo strumento è principalmente utilizzato all'interno del settore farmaceutico, tuttavia si sta cominciando ad applicarlo anche al settore della produzione additiva, vista la necessità di trovare metodi sempre più efficienti per potere analizzare le polveri. I test che questo strumento è in grado di effettuare sono molteplici e sono qui di seguito elencati: stability and variable flow rate test, aeration test, permeability test, compressibility test, shear cell.

In accordo con l'approccio Renishaw al problema della *flowability* delle polveri, il punto di partenza dell'analisi sono i risultati del flowability test. Quest'ultimo consiste nel posizionare una quantità nota di polvere (50 g) all'interno di uno specifico contenitore normato con dimensione di foro sul fondo nota. Esistono due contenitori differenti, chiamati Hall funnel (con foro da 2,5 mm) e Carney funnel (con foro da 5 mm) (Fig. 2).



Figura 2: Hall funnel (sinistra) e Carney funnel (destra).

La polvere viene fatta fluire sotto la sola azione della gravità e viene cronometrato il tempo necessario affinché l'intero contenitore si svuoti. Il test viene condotto nell'Hall funnel, a meno che la polvere non sia in grado di passarvi attraverso, in questo caso si ricorre al Carney funnel. Naturalmente una polvere che passa attraverso il primo, ha una migliore flowability di una che scorre solo attraverso il secondo.

In accordo con il metodo Renishaw PLC, le polveri che scorrono nell'Hall funnel sono considerate avere una buona flowability e di conseguenza riescono ad essere utilizzate all'interno dei macchinari. I campioni che invece sono passati solamente attraverso il Carney funnel hanno un comportamento incerto e potrebbero non causare danni all'interno del macchinario, tuttavia non è automatico e può succedere che invece insorgano delle problematiche. Infine, le polveri che non fluiscono nemmeno attraverso il secondo funnel sono considerate di scarsa qualità e di conseguenza non verranno utilizzate.

I risultati del flowability test sono mostrati in tabella 1:

Tabella 1: Risultati del flowability test.

Powder	Vessel	Tap	Average Flow (s/50g)	Average angle of repose (°)
L 0001	Carney	No	12.5	30.10
L 0002	Hall	Yes	63.4	30.19
L 0003	Did not flow			
L UK3359	Hall	Yes	70.6	31.88
S 16D0534	Carney	Yes	13.5	29.87
T 0425.2.5	Carney	No	11.3	28.26
V 14-5034S	Did not flow			

Un altro test "classico" utile a determinare importanti caratteristiche chiave è la valutazione della distribuzione della taglia granulometrica delle particelle che formano la polvere o PSD (Particle Size Distribution). Questi dati sono stati ricavati tramite un analizzatore a diffrazione laser (Mastersizer 3000, Malvern, UK) (Fig. 3).



Figura 3: Analizzatore a diffrazione laser Mastersizer 3000.

Questo strumento è in grado di creare dei grafici di distribuzione della taglia delle particelle, in base a come un fascio laser viene diffratto, venendo in contatto con quest'ultime, in sospensione grazie ad un flusso d'aria. I risultati del test sono mostrati in Tabella 2 e Fig. 4.

Tabella 2: Risultati del test di analisi della PSD.

Powder	D(10) (μm)	D(50) (μm)	D(90) (μm)
L 0001	30.2	49.3	80.2
L 0002	29.1	47.9	78.3
L 0003	28.1	47.6	79
L UK3359	29.6	46.3	71.6
S 16D0534	20.6	34.7	56.2
T 0425.2.5	23.4	49.9	84.7
V 14-5034S	18.7	31.8	53.4

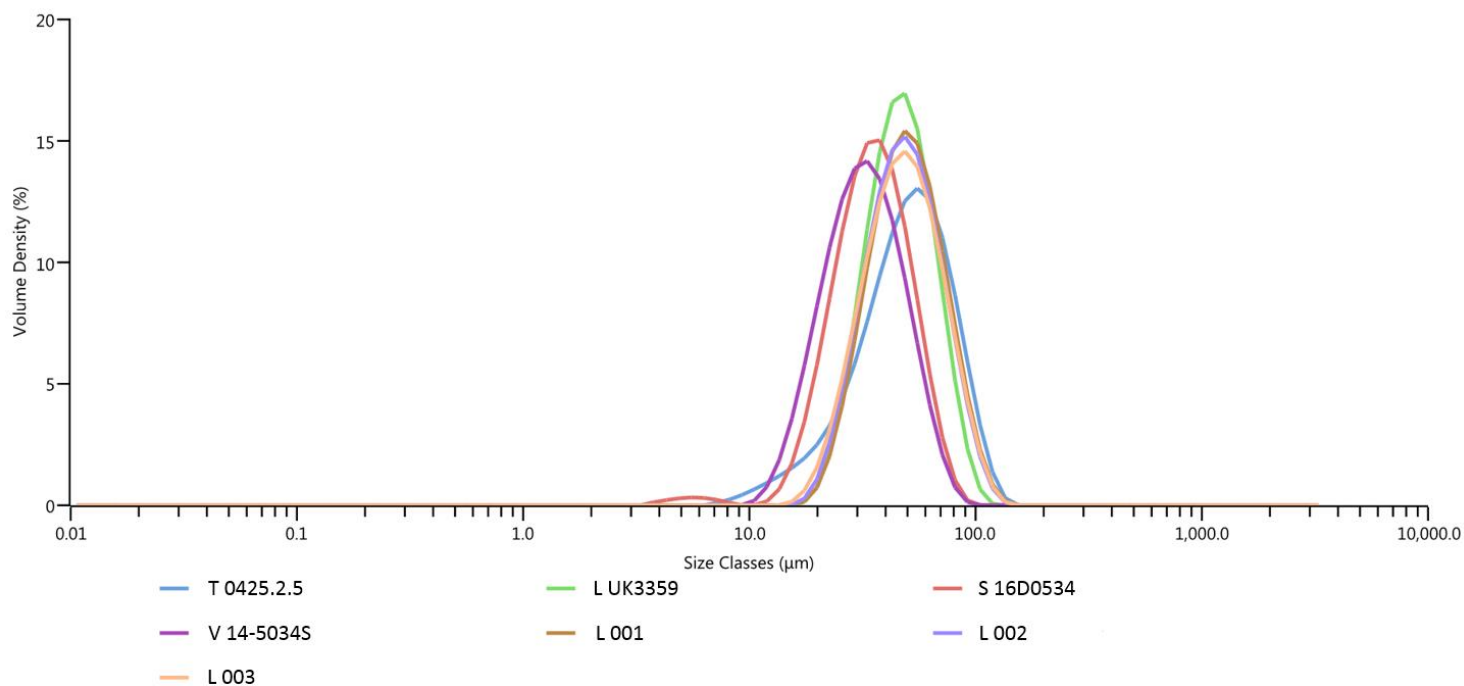


Figura 4: Grafico dei risultati dell'analisi della PSD.

I valori D(10), D(50) e D(90) rappresentano, a partire dal punto più a sinistra del grafico, il valore di diametro (in µm) che viene raggiunto considerando rispettivamente il 10%, il 50% e il 90% dell'area sottesa alla curva.

Come è possibile notare, confrontando i risultati di questi due test, le polveri che hanno presentato una buona flowability (L 0002, L UK3359) presentano curve strette e simmetriche. Le curve a flowability incerta sono più complicate:

- T 0425.2.5 è altamente asimmetrica, perciò una parte del suo comportamento, peggiore rispetto alle polveri che sono passate attraverso l'Hall funnel, è sicuramente dovuta alla taglia delle sue particelle;
- S 16D0534 presenta il picco spostato più a sinistra delle altre polveri, che porta ad un peggioramento delle caratteristiche, poiché le particelle più fini tendono maggiormente ad agglomerare. Inoltre, questa polvere è anche bimodale, ossia presenta due picchi. Anche quest'ultimo fenomeno peggiora le caratteristiche di flowability, poiché è facile che le particelle più piccole riempiano efficientemente gli spazi presenti fra quelle più grandi, portando alla formazione di una polvere più coesa, che di conseguenza scorre in maniera peggiore;
- L 0001 presenta invece una buona curva, la causa dell'esito del flowability test va quindi cercata altrove ed è poco probabilmente legata alla sua PSD.

Per quanto riguarda invece le polveri che non hanno superato il flowability test, V 14-5034S presenta una PSD molto spostata verso sinistra, mentre L 0003 presenta una buona curva, perciò, anche in questo caso, sarà necessario trovare le cause della sua scarsa flowability tramite qualche altro test.

La successiva prova, necessaria per analizzare le polveri, consiste nell'analisi delle immagini ottenute a vari ingrandimenti delle polveri tramite SEM (Scanning Electron Microscope). Tramite questo passaggio, è stato possibile correlare i risultati della PSD con un riscontro visivo. Inoltre si è riusciti a determinare le cause della diminuzione della flowability

delle polveri L 0001 e L 0003, rispetto alla controparte L 0002 e L UK3359. È infatti insolito che delle polveri così simili, dal punto di vista della PSD, presentino comportamenti così spiccatamente differenti.

La causa di queste differenze è stata trovata nella presenza di agenti contaminanti all'interno delle polveri stesse, sotto forma di fibre di tipo organico, che non è stato possibile caratterizzare completamente a causa dei limiti dell'analisi EDS, e particelle estranee, che sono state analizzate tramite EDS, in modo da poter capire, anche se approssimativamente, la loro composizione (Fig. 5, Fig. 6, Tabella 3, Fig. 7)

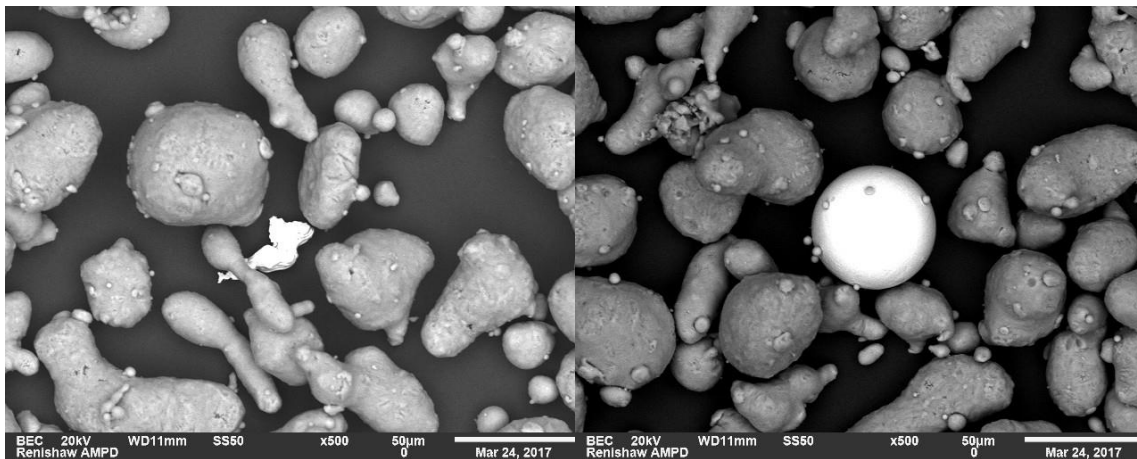


Figura 5: Immagini SEM della polvere L 0001 con relative particelle estranee trovate nel campione (backscattered electrons, 500x).

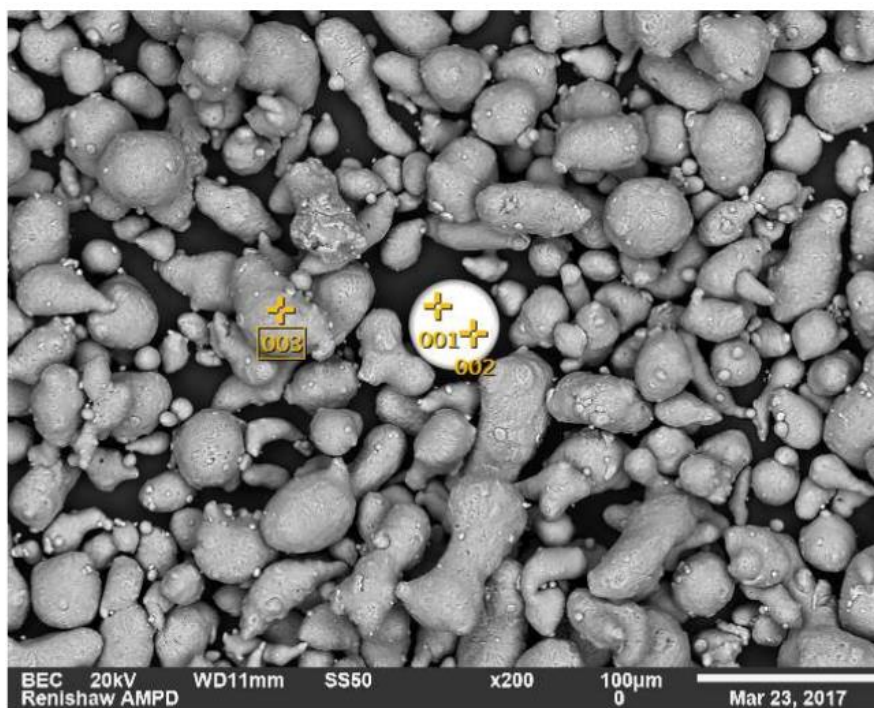


Figura 6: Punti selezionati per l'analisi EDS di una particella estranea trovata nel campione L 0001 (200x)

Tabella 3: Composizione chimica, rilevata tramite EDS, dei tre punti in Fig. 6.

Spot	Al (%)	Si (%)	Mg (%)	Fe (%)	Ti (%)	Cr (%)	Ni (%)	Nb (%)	Mo (%)
Spot 1	4.31	-	-	20.72	0.91	19.58	54.48	-	-
Spot 2	10.39	0.75	-	17.29	0.77	16.77	47.35	4.07	2.62
Spot 3	87.22	12.52	0.26	-	-	-	-	-	-

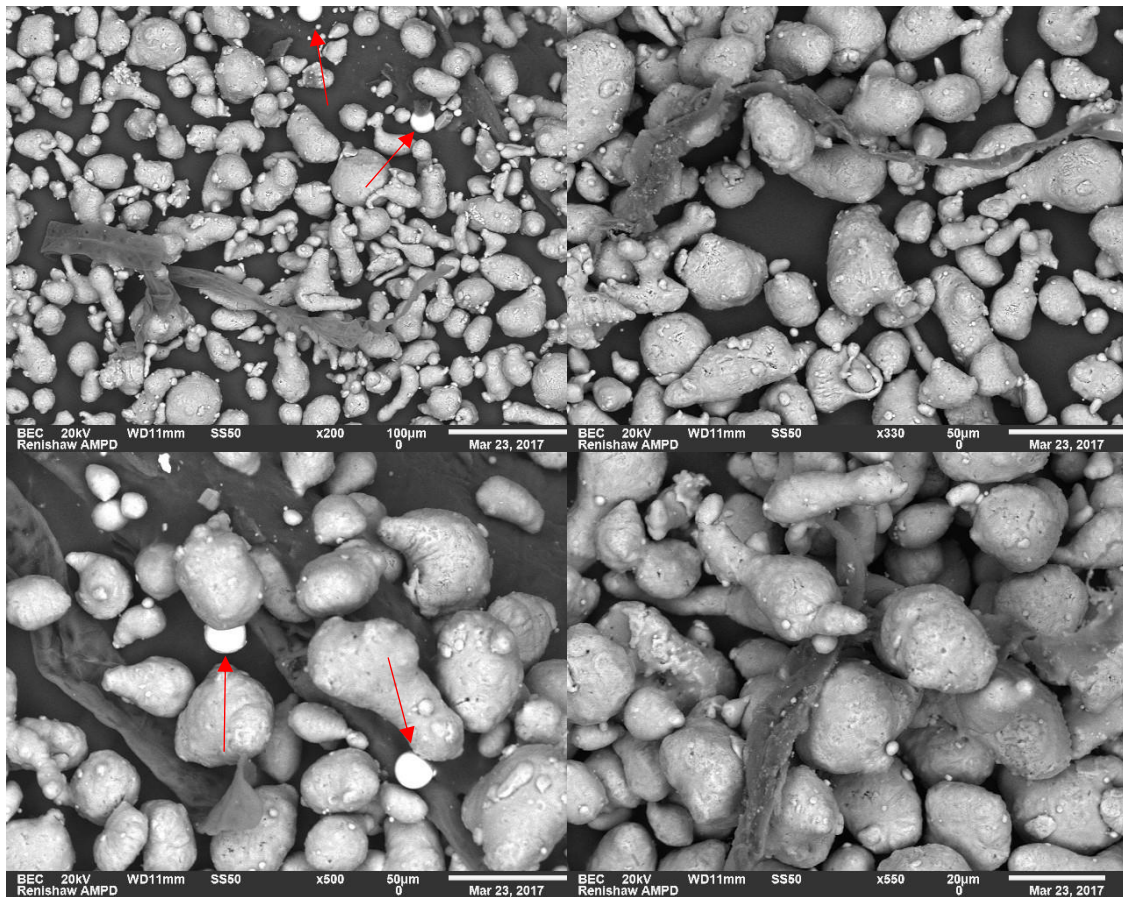


Figura 7: Immagini SEM della polvere L 0003 con relative fibre e particelle estranee trovate nel campione (backscattered electrons, 200x, 330x, 500x e 550x).

La presenza di questi agenti contaminanti sicuramente impatta negativamente sulla flowability delle polveri, la presenza di fibre in particolare è critica, poiché possono attorcigliarsi e creare con le particelle strutture molto ingombranti (Fig. 8).

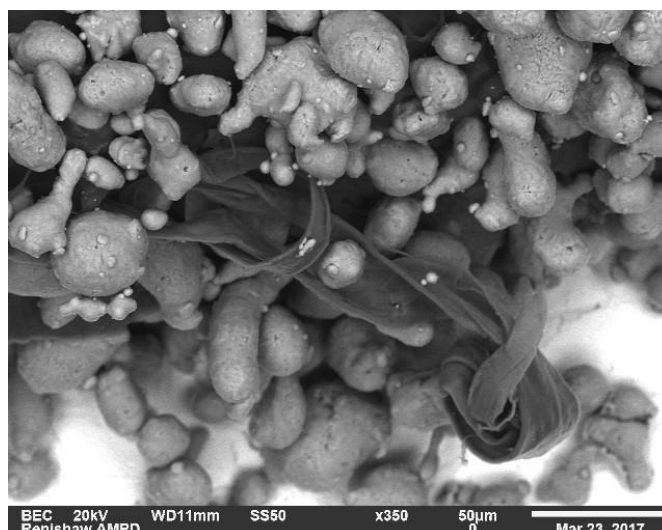


Figura 8: Esempio di fibra attorcigliata con particelle, trovato nel campione L 0003 (backscattered electrons, 350x).

All'interno delle polveri L 0001 e L 0003 sono state inoltre trovate particelle di leghe di Ni, leghe di Ti, acciai.

I risultati dei test di valutazione del tenore di umidità e della densità delle polveri non hanno dato risultati che permettessero di differenziare le polveri fra di loro. L'unico avvenimento degno di nota, consiste nell'agglomerazione superficiale (Fig. 9) che la polvere V 14-5034S ha mostrato dopo essere stata rimossa dal forno in vuoto, all'interno del quale è stata processata durante il test volto a valutare il tenore di umidità.



Figura 9: Agglomerazione superficiale del campione V 14-5034S dopo essere uscito dal forno in vuoto.

Questo fenomeno conferma ciò che era stato intuito dal flowability test e successivamente confermato dalla valutazione della PSD: questo campione presenta problemi di agglomerazione, che ne compromettono la flowability, probabilmente a causa del basso valore medio della taglia delle sue particelle.

Terminati i test classici che vengono generalmente effettuati in Renishaw per determinare le caratteristiche delle polveri, il proseguimento del lavoro è consistito nell'utilizzare un reometro per polveri (Fig. 10) per effettuare una serie di test.

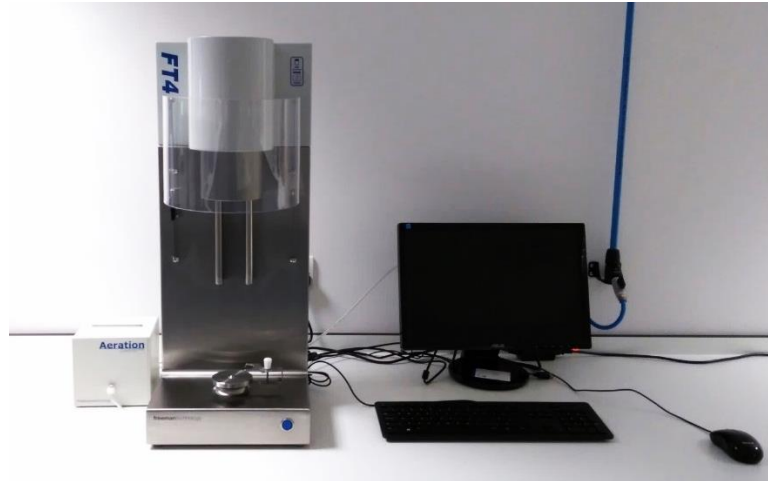


Figura 10: Reometro per polveri FT4.

Tramite questo strumento, è stato possibile effettuare numerosi test, che prevedono l'utilizzo di svariate componenti, teste (Fig. 11) ed accessori (Fig. 12), ognuno con una specifica funzione.



Figura 11: Differenti teste utilizzate nel reometro per polveri (23.5 mm blade a sinistra, compression piston al centro, shear head a destra).



Figura 12: Principali accessori utilizzati nel reometro per polveri.

I risultati più importanti ottenuti con il reometro sono quelli relativi al permeability test. Tramite questo esperimento è possibile determinare quanto una polvere sia permeabile, ossia quanto facilmente trasmetta un fluido. Questo dato è molto importante, poiché dà informazioni sia riguardanti le proprietà fisiche del campione (PSD, livello di coesione, densità, ecc.) che eventuali fattori esterni che ne influenzano il comportamento (stress di consolidamento). Dopo una iniziale fase di consolidamento del campione, effettuate tramite la 23.5 blade (Fig. 11, sinistra), viene utilizzato il pistone (Fig. 11, centro) per comprimere dall'alto la polvere a livelli di stress crescenti (1, 2, 4, 6, 8, 10, 12, 15 kPa), mentre allo stesso tempo un flusso di aria costante (2 mm/s) attraversa la polvere dal basso. Per ogni livello di stress, viene valutata la caduta di pressione nel letto di polvere, che consiste praticamente nella resistenza che il materiale oppone al flusso d'aria attraverso di esso.

I risultati del test sono mostrati in Fig. 13.

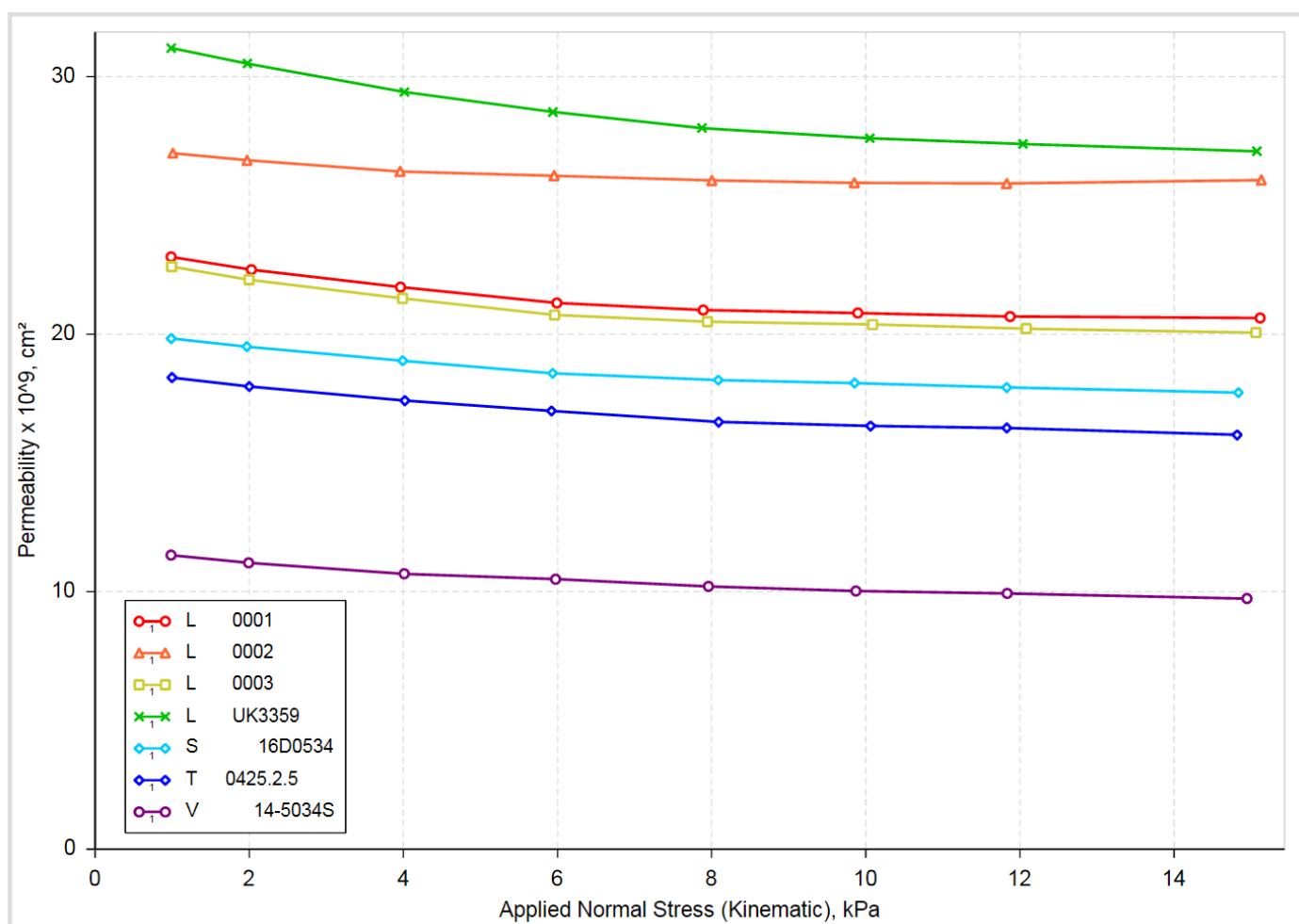


Figura 13: Risultati del permeability test.

Confrontando i risultati di questa prova con il flowability test, si può notare come le due polveri che sono passate attraverso l'Hall funnel (L 0002 e L UK3359) si trovino nella parte alta del grafico; tutte le polveri dal comportamento incerto, ossia in grado di passare attraverso il Carney funnel, ma non l'Hall funnel, si trovano invece nella parte centrale, mentre V 14-5034S, il campione che non è stato in grado di passare attraverso nessun funnel, si trova al fondo del grafico. L'unica eccezione a questo andamento è rappresentata dalla polvere L 0003, che verrebbe classificata come polvere dal comportamento incerto, quando invece non ha passato il flowability test. Tuttavia questa deviazione del modello è probabilmente dovuta al fatto che il peggioramento del comportamento di questa polvere sia dovuto alla massiccia presenza di fibre e particelle estranee al suo interno. Questa caratteristica è probabilmente difficilmente rilevata dal test, poiché una volta che dell'aria viene fatta fluire attraverso il letto di polvere, la presenza di agenti contaminanti diventa meno critica.

In conclusione, questo metodo pare comunque essere un'alternativa valida al flowability test, purché si rimanga all'interno della categoria dei campioni non contaminati, che comunque rappresenta la maggior parte dei casi nell'industria AM. Va inoltre considerato che le polveri che presentano particelle estranee spesso devono essere scartate in ogni caso, per motivi composizionali.

1. Introduction

1.1. Additive Manufacturing (AM)

Developed for the first time during the 1980s, additive manufacturing (AM) is a manufacturing technology, which is also known as rapid manufacturing, 3D printing, additive fabrication, freeform fabrication or rapid prototyping [1]. It is defined by the American Society of Testing and Materials (ASTM) as “*The process of joining materials to make objects from 3D model data, usually layer upon layer, as opposed to subtractive manufacturing methodologies*” (e.g. Machining) [2]. In particular, the term *3D Printing* is intended as a technique that implies the fabrication of an object, performed depositing a material using a print head or nozzle [3].

It basically consists in bonding successive layers, typically by deploying heat or a binder. This technique consists then in the progressive building of the component, directly from the Computer-Aided Design (CAD) file. This approach is the opposite of the classical subtractive methods, in which the material is progressively removed from a larger piece. [4]

A wide variety of materials can be used for AM, ranging from polymers to ceramics, metals and composites. In this work, the attention is focused on metallic materials.

The manufacturing of a component using AM begins with 3D modelling (Fig. 1.1). Before producing it, it is necessary to position the support structures, necessary to avoid the object from falling during the layer-by-layer deposition phase, and then to slice the model (Fig 1.2).

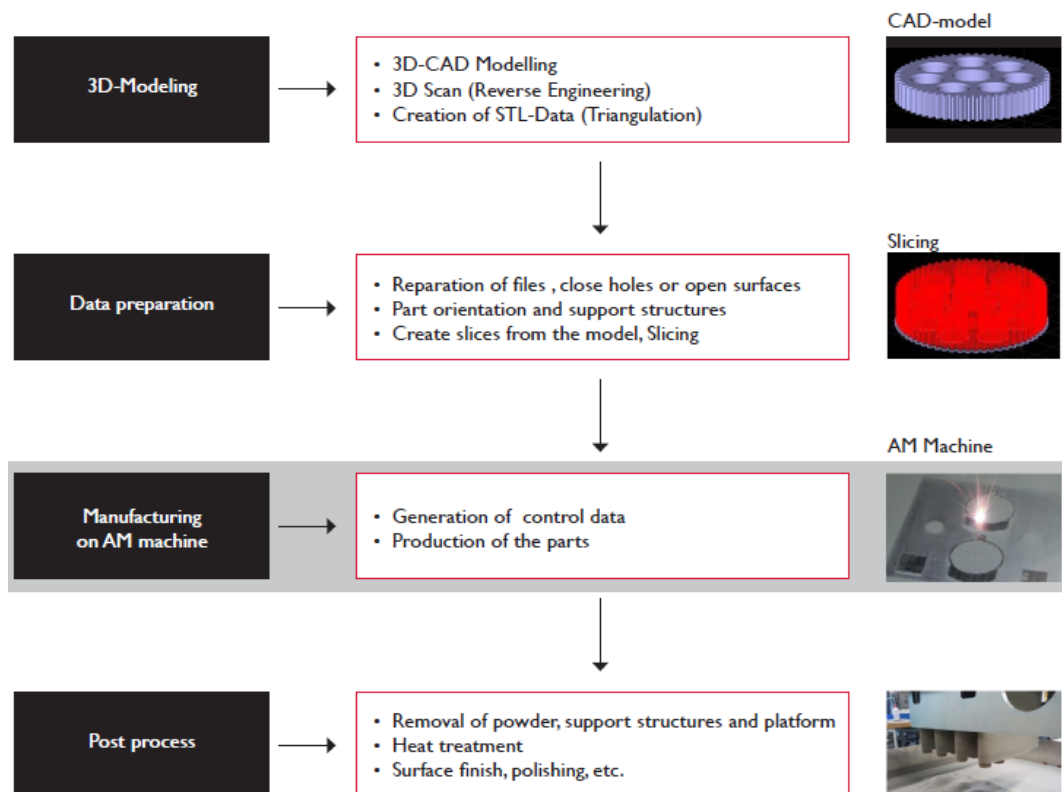


Figure 1.1: Summary of process steps. [5]

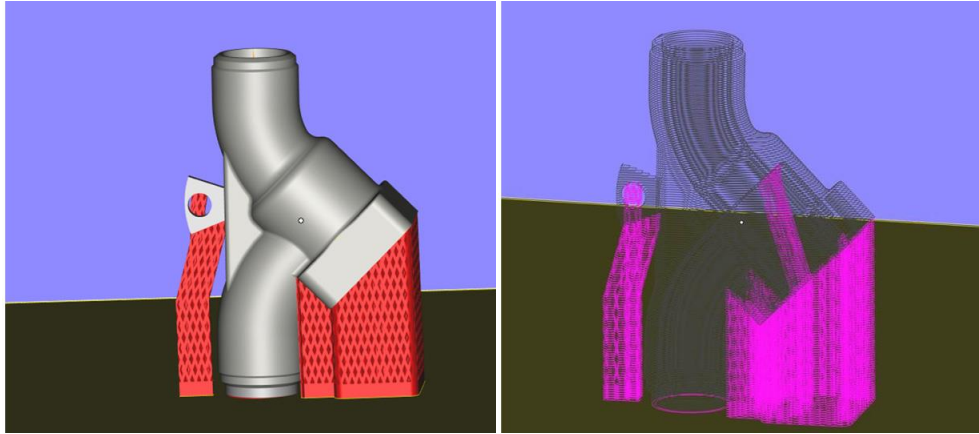


Figure 1.2: Model supports and file slicing. [5]

After the manufacturing phase itself, post-processing operations are usually needed. Some of these processes can include:

- Machining,
- Grinding,
- EDM (Electrical Discharge Machining),
- Polishing, surface treatments,
- HIP (Hot Isostatic Pressing),
- Heat treatments,
- Etc. [5]

Additive manufacturing shows several advantages that discriminate it from the other traditional processes, in which material is removed:

- Extremely intricate parts can be produced. In fact, complex geometries, internal features, specifically engineered porosities and gradients are realizable. AM can be the only available process usable to produce a certain type of components, in some cases. In Fig. 1.3 is shown a prototype of a vacuum permeator (AISI 316L), manufactured by IK4-Lortek, that is intended to be used in ITER (International Thermonuclear Experimental Reactor). This apparatus is impossible to manufacture by using any other conventional process. [5, 6]

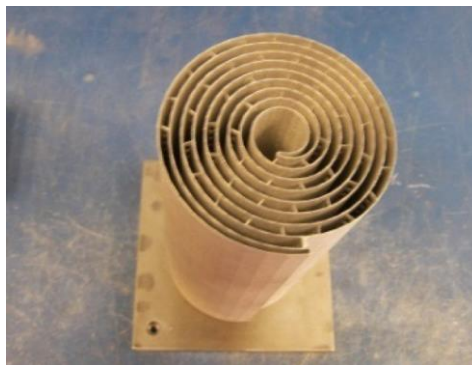


Figure 1.3: Vacuum permeator manufactured using an AM technique. [5]

- Components can be produced directly from design information, granting an extremely elevated level of customizability and avoiding all the phases that are necessary to set up a productive line (e.g. creating a mould), typical of other manufacturing techniques. As a consequence of that, the process is very versatile and grants more freedom, making it inexpensive and quick to eventually change the project.

- Possibility to produce components made of hard metals. This is the typical limit for the other classical manufacturing techniques, because of the intrinsic difficulty to machine with a removal process these materials. [6]

- Potential to reduce waste. Not using a technique that implies material removal, the material usage percentage is extremely high (typically greater than 97%) [7]. Hence, less material is used. For example, up to 25 less material is consumed, if compared to a traditional machining process. [5]

- Possibility to build objects that otherwise must be split into several components and assembled, if manufactured using different methods. Thus, dramatically facilitating production planning and making the component itself less critical.

- Efficient solution for producing just a few components (even just one), especially if volume is low. This is possible because there is not any additional cost linked to setting up the production line.

- It is possible to use materials with comparable characteristics, sometimes even better, to those achievable using traditional manufacturing methods. [3]

- Light-weight structures can be achieved. These are obtained by wisely using lattice design or planning to put the material only where it needs to be.

- Short production cycle time, for certain components. Very complex parts can be produced layer-by-layer in just a few hours. Adding post-processing, the usual total time needed to create a component equals roughly a few days or a week. This amount of time is lower than the several months needed if a conventional metallurgical process was chosen.

- Due to the quick solidification process, a very fine microstructure can be obtained. [5]

- It is a brand-new technology; hence research, development and optimization are still ongoing. As a consequence of that, it can be expected for the near future to have a better understanding of the physical phenomena involved, leading to an optimization of the process, an expansion of the usable material pool and maybe the fabrication of complex integrated systems. [3] This is proved by the fact that recently AM received constantly increasing attention both in scientific journals and conventional press. For example, from 2011 to 2012, the quantity of publications on that subject raised by an order of magnitude. Approximately 1600 papers were written in 2011, whilst over 16000 in 2012. [6]

AM is very appreciated in some specific fields. One of the main important is the aerospace industry, in which the necessity of extremely complex parts makes the components, produced using these technology, are ideal (e.g. metal fuel nozzle used in aircraft engines [6]).

The medical sector is also very suitable, in particular the possibility to create highly personalized parts is valuable in orthodontics, orthotics, implants and prosthetics (e.g. metal jaw replacement [6]). The latter has been the first biomedical field in which 3D printing has proved to be very successful, particularly for skull anatomy reproduction (Fig. 1.4) and hip prosthesis. [8]



Figure 1.4: Cranial implant produced using an AM technique. [5]

Recently, AM technologies have been successfully used in the radio-frequency (RF) field. They are studied to develop new microwave and millimetre-wave devices, intended to operate from few to hundreds GHz. Some possible applications in this field include communication systems, wireless networks, wearable sensors, automotive collision avoidance sensors, HR imaging systems, satellite communication sensors and MEMS (MicroElectroMechanical Systems) devices. AM is also appreciated in the industrial sector, in which high-precision and customizable parts are commonly used. Layer-by-layer technologies can be also used for consumer goods, such as jewellery. [3]

Energy engineering is another field in which AM technologies are valuable; for example, in Fig. 1.5 is shown a gas turbine demonstrator manufactured using Selective Laser Melting (SLM), an AM technique. Using this method, it is possible to reduce the number of parts produced, so no assembly is needed, hence it is a weight saving process, that can lead to an increase in performance. [5]



Figure 1.5: Gas turbine demonstrator (Al, Ti and Ni powders). [5]

Some of the main applications of this technology are shown in Fig. 1.6 and Fig. 1.7.

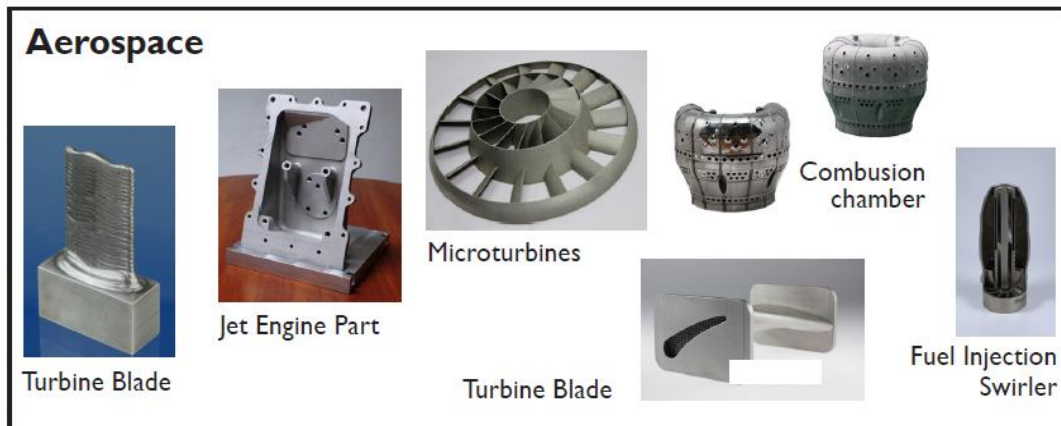


Figure 1.6: Some of the aerospace and Medical applications of additive manufacturing. [3]

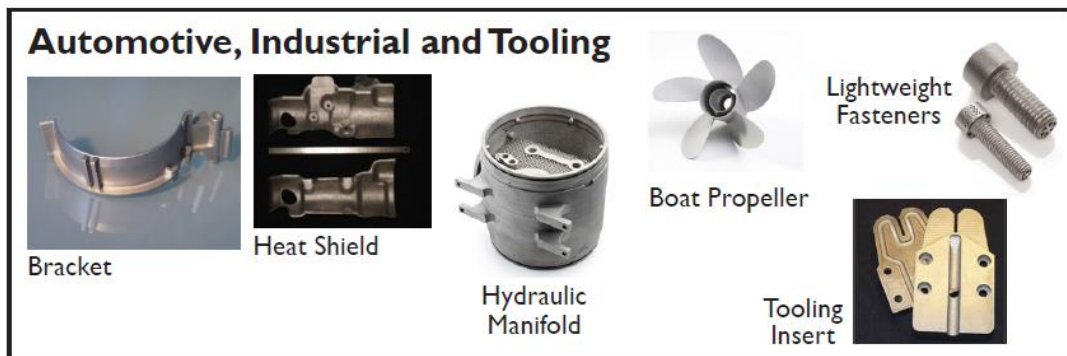


Figure 1.7: Some of the industrial and consumer goods applications of additive manufacturing. [3]

The application of additive manufacturing to the production of metallic components is a brand new and flourishing industrial sector, with a lot of leading companies based in Europe. It was initially intended to build only prototypes, but nowadays it is becoming a solid and suitable process choice to manufacture complex net shape components.

AM is complementing the other powder metallurgy (PM) technologies. While other PM technologies (e.g. HIP) are better for massive productions (till to hundreds of kilograms) of near net shape parts, AM is more suitable for smaller production (few kilograms) of little components. In this niche production, it shines thanks a much greater design freedom. Other PM technologies are MIM (Metal Injection Moulding) and Press & Sinter. These are both reliable techniques to produce net shape parts, but are recommended just for larger productions, where the high cost of the equipment can be split among a high number of piece produced. In Fig. 1.8 *Figure*, the position of AM, in a part weight & size vs. No. of parts graph, is shown. From this image, it is possible to confirm, as it was stated before, that 3D printing truly complements the other PM technologies.

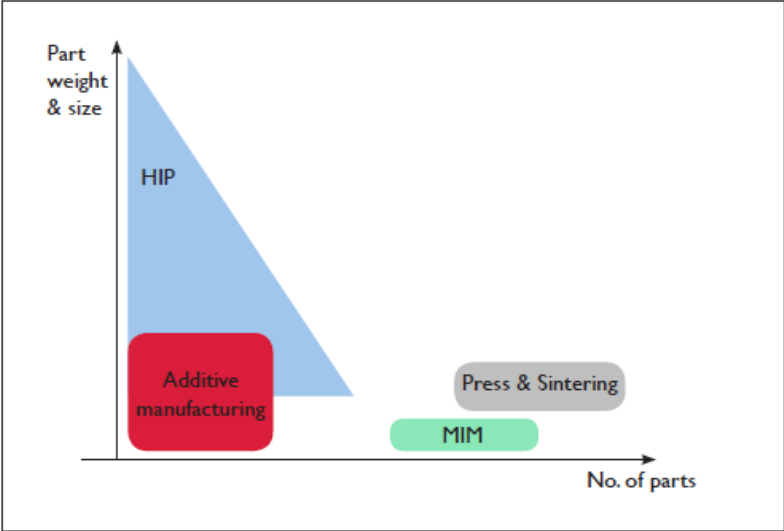


Figure 1.8: PM technologies according to part weight or size and number of pieces produced. [5]

As it is possible to understand from the previous graph, AM is the best option when the lot size is very small. From the previous paragraphs, it has also been understood how 3D printing is the best alternative when the component that must be built shows a high degree of complexity. These two concepts are shown in the graphs in Fig. *Figure*1.9, in which Laser Beam Melting, a typical AM technique, is compared to a conventional manufacturing process.

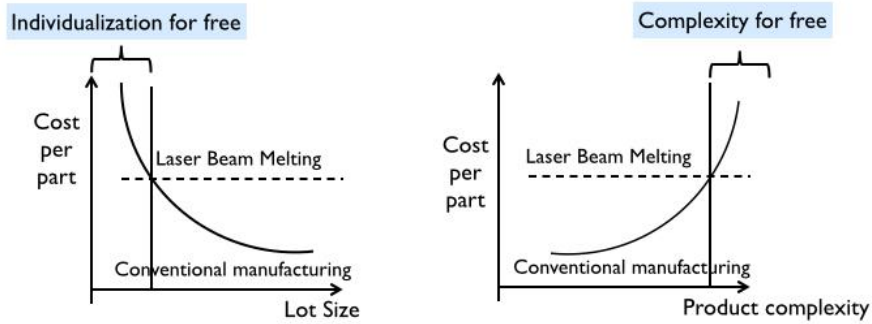


Figure 1.9: Cost per part function variation, according to changes in lot size and product complexity for an AM technique and a conventional manufacturing processes. [5]

From the graph on the left, it is possible to notice how the cost per part of a component manufactured using LBM is constant, not depending from the lot size at all. This happens because, as explained before, it is not necessary to set up a production line, hence it is not needed to produce as many components as possible to recover the initial investment. On the opposite, classical manufacturing techniques become more appealing in case of huge productive lots. The same thing happens when it comes to complexity, as shown on the graph on the right. While the complexity of a component does not affect the cost, if produced using an AM technique, it strongly influences the price of a part manufactured in a conventional way.

The great advantage of 3D printing lies in the possibility to produce very small lots and/or very complex parts without any increase in cost. That is why, as previously stated, it is so appealing in certain fields, where small, complex parts with a great added value are used (e.g. biomedical, energetic, etc.).

By looking at the graph in Fig. 1.10, that shows the number of units produced using AM methods in recent years, it is possible to notice the constant growth that this technology is showing, which is reflected on its impact on the market. AM technology is no longer used only for prototyping but now also for metal part production, hence the strong growth since 2012 of AM systems sales for metal parts production (see graph below).

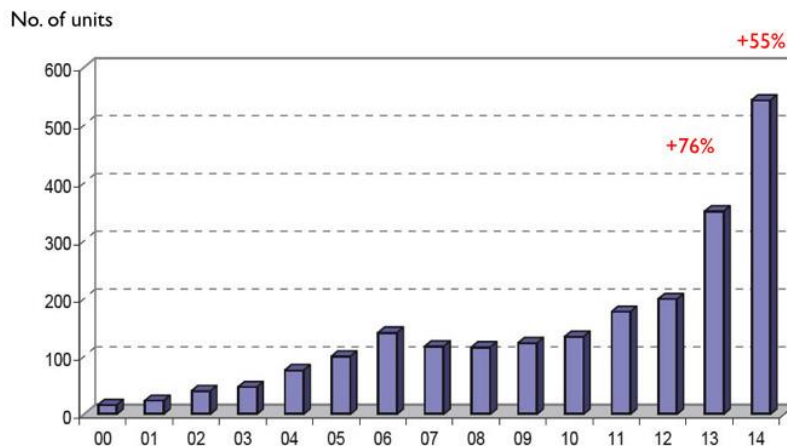


Figure 1.10: Sales of metal parts produced by AM systems. [5]

The sudden growth in production in 2012 (+76%) has been caused by the switch from using AM just for prototyping to apply it to metal part production.

Additive manufacturing complements also the other conventional production methods. It is possible to notice, from Fig. 1.11, that, as it happened when comparing this process to other PM techniques, it is the most suitable technology to produce very complex parts and when the production lot is small.

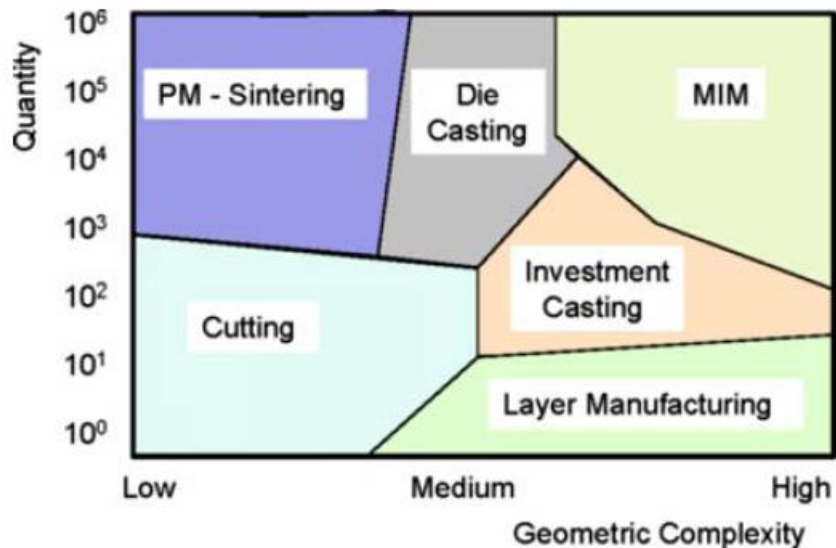


Figure 1.11: Comparison of AM technology with other production methods. [9]

1.2. AM Limitations

AM-produced components show a certain variability due to insufficient dimensional tolerances and surface roughness control. These characteristics still limit a wider acceptance for some critical applications. This variability can be somehow controlled with process control, but the lack of effective process measurement methods (“metrology issues”) is still a critical factor. This is mostly caused by the fact that today’s development is based on experimental data and attempts, while a complete understating of the whole process and its characteristics is still missing scientifically. Hence, real-time control is a huge limit of this techniques.

The widespread application of AM technologies is challenged by issues related to part quality (e.g. form errors), porosity, delamination of layers and achieved material properties in general.

It is very important to determine a correlation between the AM process parameters, the material and powder properties and the final component properties. [1]

Other limitations are:

- Slight anisotropy, mostly cause by the stacking layers during the process. [10]
- Part size. Especially for PBF technologies, the component final dimension is limited by the powder bed size (usually 250x250x250 mm).
- Productivity. In fact, as it was explained before, the process is very time-consuming.
- Material choices. Even if a lot of different materials are available, non-weldable alloys are not usable and the materials difficult to weld require specific and difficult approaches.

1.3. Powder Bed Fusion (PBF)

AM technologies can be divided into two main families (Fig. 1.12):

- Powder bed technologies. The most important are:
 - Selective Laser Melting (SLM), where powder melting is reached deploying a laser beam.
 - Electron Beam Melting (EBM), where the powder is melted using an electron beam.
 - Precision inkjet printing, where a mix of metal powder and a binder is printed and then sintered.
- Blown powder technologies (Laser Metal Deposition or Laser Cladding). In this technique, the powder is blown on a metallic base and then melted by a laser beam. [3]

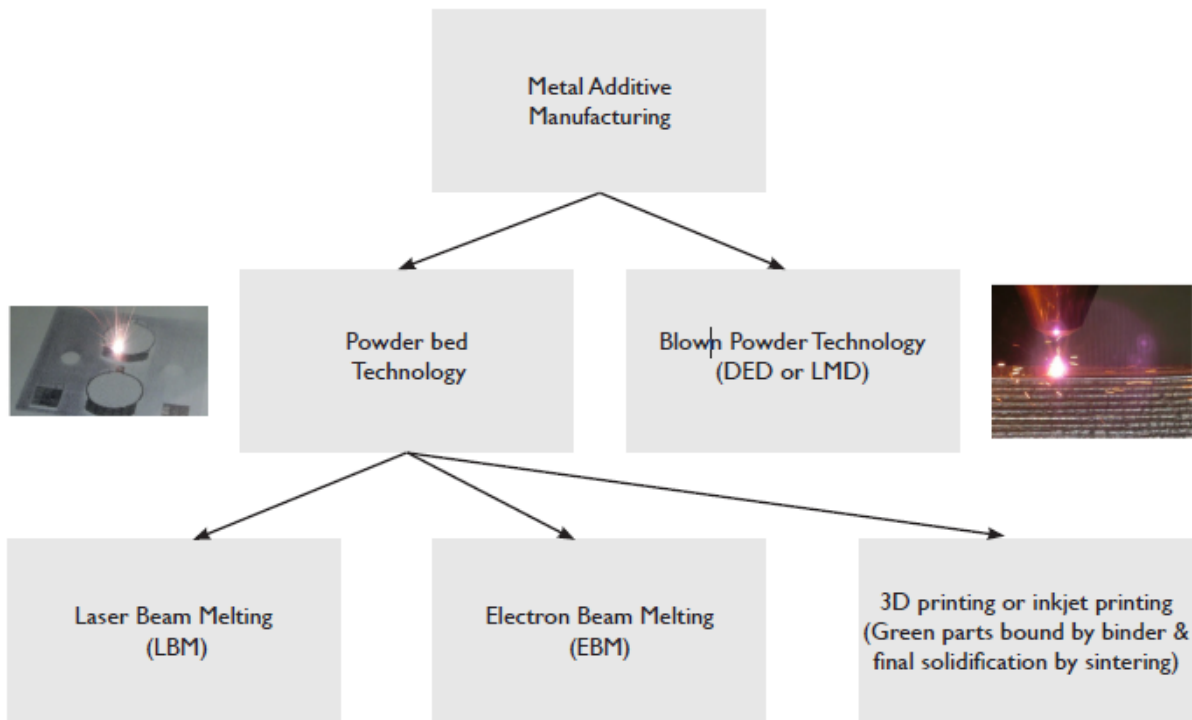


Figure 1.12: Main AM technologies tree. [5]

Nowadays, most of the commercially available AM systems are PBF based. SLM and EBM are the most commonly used; they both deploy a high-energy beam to completely melt the powder particles, that then fuse to the other layers when cooling occurs. Repeating this layer-by-layer process results in fully dense parts. [1] Powder bed technologies, also known as Powder Bed Fusion (PBF) are specifically defined in ASTM F2792 [2].

From the following pages, the attention will be focused on the PBF processes, in particular on SLM.

This process has been developed by Dr. M. Fockele and Dr. D. Schwarze of F & S Stereolithographietechnik GmbH. [11] To melt layers of powder, it uses a high-energy laser, which diameter can reach up to 100 μm and power varies between 200 W and 1000 W. The process starts when a thin layer of metallic powder is laid on a plate by a recoater (blade or roller) (Fig. 1.13) and the laser melts a selected area (melt-pool), according to the data obtained from the CAD file. Melting occurs due to a phenomenon of energy absorption. The particles are then fused together when the molten material re-solidifies. Different scanning strategies lead to differences in surface roughness, porosity, microstructure. Hence this process must be optimized.

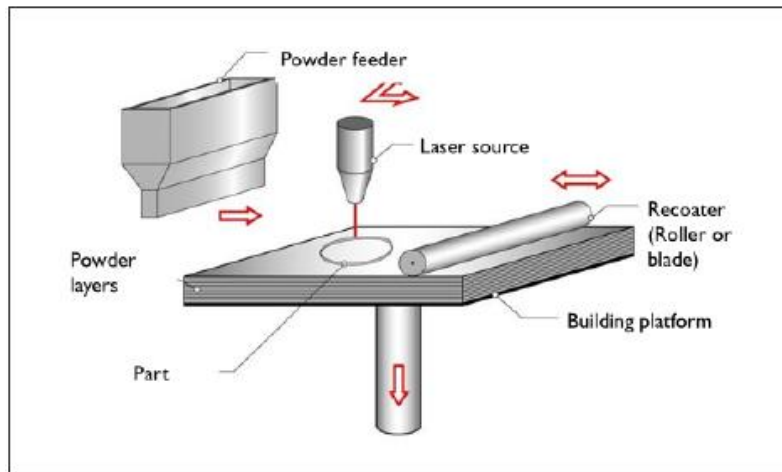


Figure 1.13: Schematics of a SLM machine. [5]

When the laser scanning is completed, it is possible to lower the building platform, by the prevented layer thickness (75-150 μm [8]), and deposit the next powder layer from the dispenser platform on top of the previous one (over the building platform). This process is then repeated until the component is complete (Fig. 1.14), that usually takes hundreds of cycles, hence the process itself is very time-consuming. It must be noted that the complete component is buried within the powder at the end of the process.

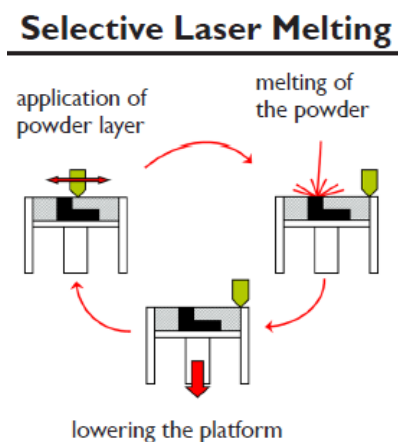


Figure 1.14: SLM process steps summarization. [3]

Due to the high temperature and energetic level involved, it is necessary to operate under a controlled oxygen content atmosphere, for preventing oxidation and the subsequent lowering

of the mechanical properties. To do so, usually inert gases, such as argon or nitrogen, are used. The typical process-controlling parameters are: laser power, scanning speed, layer thickness and hatching distance. [1, 5, 10]

The main parts of a SLM machine (recoating blade, build platform and dispenser platform) are shown in Fig. 1.1 *Figure 5*.

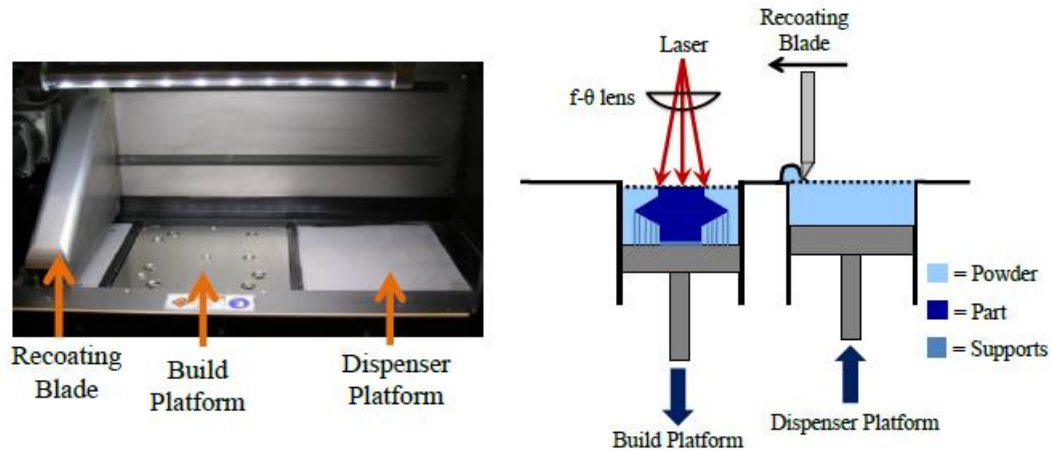


Figure 1.15: Main parts of a SLM machine. [1]

The alloys most commonly used for this process include:

- **Steels.** In particular, maraging steels (aged martensitic steels) are appreciated because of their good mechanical properties, such as high strength and good toughness, dimensional stability during heat treatments and weldability. These materials are widely appreciated in the aerospace sector, where superior mechanical properties and weldability are very important. Also, stainless steels (e.g. 17-4 PH), especially AISI 316L, are investigated a lot, due to their high number of applications in several fields, such as marine, biomedical equipment and fuel cells.

- **Co-Cr-Mo based superalloys.** Characterized by excellent mechanical performances, but most of all corrosion and temperature resistance. These materials have been used in biomedical applications, such as dental restorations and orthopedic implants (e.g. joints). They proved to be useful materials because of their characteristic of being the hardest known biocompatible alloy.

- **Ni-based superalloys** (e.g. Inconel). These materials show a very good damage tolerance combined with creep, oxidation and corrosion resistance. They also have superior mechanical properties and generally find their use in fields such as turbines (Fig. 1.16), airframe parts, high-temperature fasteners and bolts and nuclear engineering components.



Figure 1.16: Hollow Inconel 718 turbine, build using SLM. [5]

- **Aluminium alloys.** These are mostly interesting for lightweight applications in automotive and aerospace. AlSi10Mg is a particularly appreciated cast alloy, age-hardenable and with good mechanical properties. It also shows good castability and weldability, as a result of its composition being close to eutectic.

- **Titanium alloys.** These materials, in particular Ti-6Al-4V (duplex), can show higher strength if manufactured using SLM, instead of a conventional technique. This is caused by the different solidification process that happens during 3D printing, that directly impacts the $\alpha + \beta$ microstructure. Ti-6Al-4V found room for application in the aerospace industry and in maxillofacial applications, due to its exceptional corrosion resistance when in a physiological environment. [10]

It must also be noted that other alloys are being evaluated and studied. Some of them are copper and magnesium alloys, precious metals (gold, silver, platinum) and refractory metals, such as tungsten and WC. The application of AM for metal composites seems also promising. [5]

1.4. Powders

It is very important to establish a relation between process parameters and the final component quality. *Process parameters* basically determine the energetic rate delivered to the powder and its interaction. These parameters can be categorized into *controllable parameters*, that can be continuously modified during the process (laser power, scan speed), and *predefined parameters*, which must be defined at the beginning of each build (material properties). Instead, product quality can be divided into geometrical, physical and mechanical qualities.

In this work, a lot of attention is going to be dedicated on predefined parameters, in particular some material properties linked to powder quality, such as powder size and distribution. These features influence, for example, the activation energy needed to coalesce, the ability of the powder bed to pack efficiently, leading to density values closer to the theoretical one. Higher density then leads to a reduction of internal stress in the final component, and less distortion and porosity in the final part. [1]

Ideally, for PBF machines, metal powders should have the following characteristics:

- A shape as close as possible to a sphere, to ensure good flowing properties to the powder itself and the ability to efficiently coat the other layers. Typical defects such as elongated particles, satellites and hollow particles must be preferably avoided.

- A general particle size distribution ranging between 15 μm and 150 μm . Of course, the range varies a lot, usually getting smaller, depending on the technique adopted, the machine used and the finishing needed. It must be noted though that finer particles (10-20 μm) are usually avoided, because they are detrimental to the powder flowability. [5]

- Chemical composition as controlled and constant as possible.
- Controlled gas content. [3]

As previously stated, metal powder quality has a major influence on the final component mechanical properties, but it also affects the reproducibility of the part, in fact more controlled and constant powders lead to more homogeneous and similar components. Moreover, it influences the presence of defects.

1.4.1. Atomization Process

The most common way to produce powders for PBF technologies is usually the *gas atomization* process. It is an expensive method, but able to create high-quality powders, necessary for AM. During gas atomization, a molten metal stream, that already has the composition of the wanted powders, is atomized by a high-pressure inert gas jet. The collision cause the molten material to form a lot of small droplets that quickly solidify and form powder particles. It is possible to use water instead of gas, but the latter is less beneficial, because it produces particles characterized by irregular shape, hence bad flowing properties and an inferior capability to pack efficiently, thus leading to a less dense powder bed. Instead, gas atomization is more beneficial, because the powders produced are more spherical and the particle size distribution is narrower, which is a good feature for AM.

The process starts when the molten metal is poured through a nozzle into a chamber, called atomization tower, where a neutral gas jet (usually nitrogen or argon) hits it. The collision causes the formation of small droplets that quickly solidify, due to the beneficial surface over volume ratio, while falling inside the atomization tower. These particles can then be collected from the bottom of the chamber into a can. The entire process is summarized in Fig. 1.17.

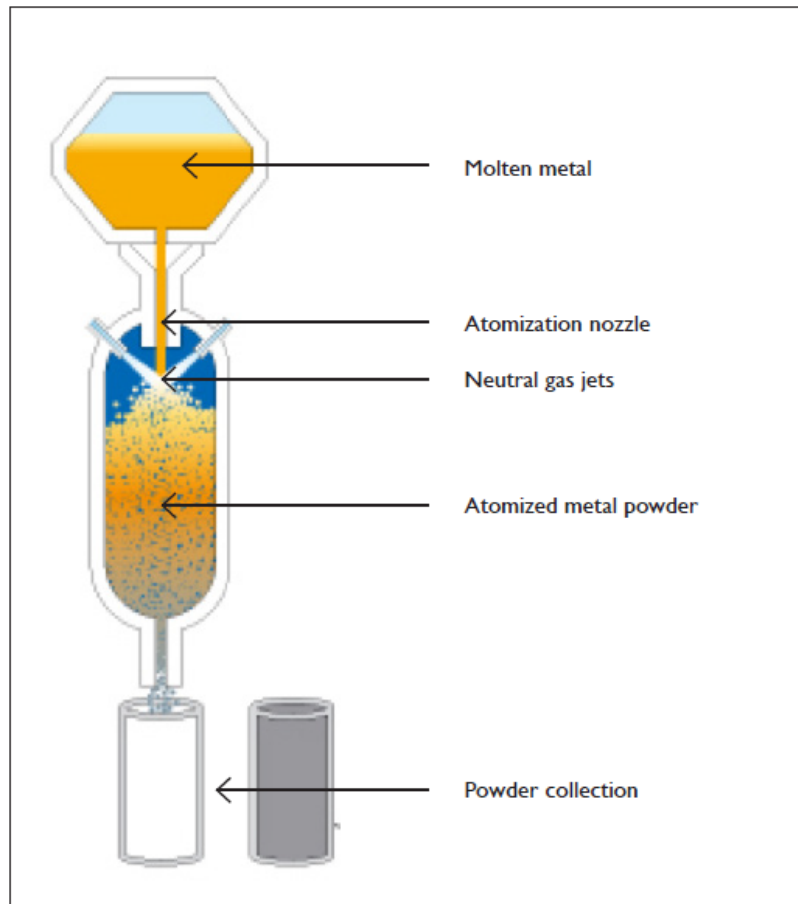


Figure 1.17: Gas atomization process steps. [5]

Inert gas atomization can be combined with several melting techniques, thus defining different systems that are available on the market.

The leading power-making process consists in the combination of inert gas atomization and melting performed in vacuum. This process is called VIGA (Vacuum Induction melting Gas Atomization), it comprises a VIM (Vacuum Induction Melting) furnace, in which the metal is melted in a ceramic crucible and degassed. The following step is the atomization process, during which, as previously mentioned, the metal is inserted via a tundish system into a gas nozzle. After that, the molten material is disintegrated because due to the high-pressure inert gas. The metal droplets then solidify during the fall and can be gathered in the bottom of the atomizing tower. After the atomization process, the particles obtained are moved through a convey tube, that leads them to a cyclone, used to separate the powder from the gas. During this phase, particles separation based on size is possible and it is usually implemented. A diagram showing a gas atomization tower and the relative VIM furnace is available in Fig. 1.18.



Figure 1.18: Schematics of a VIGA system. [12]

Several other systems are available and differ on the technique adopted to melt the metal before the atomization process (Fig. 1.19).

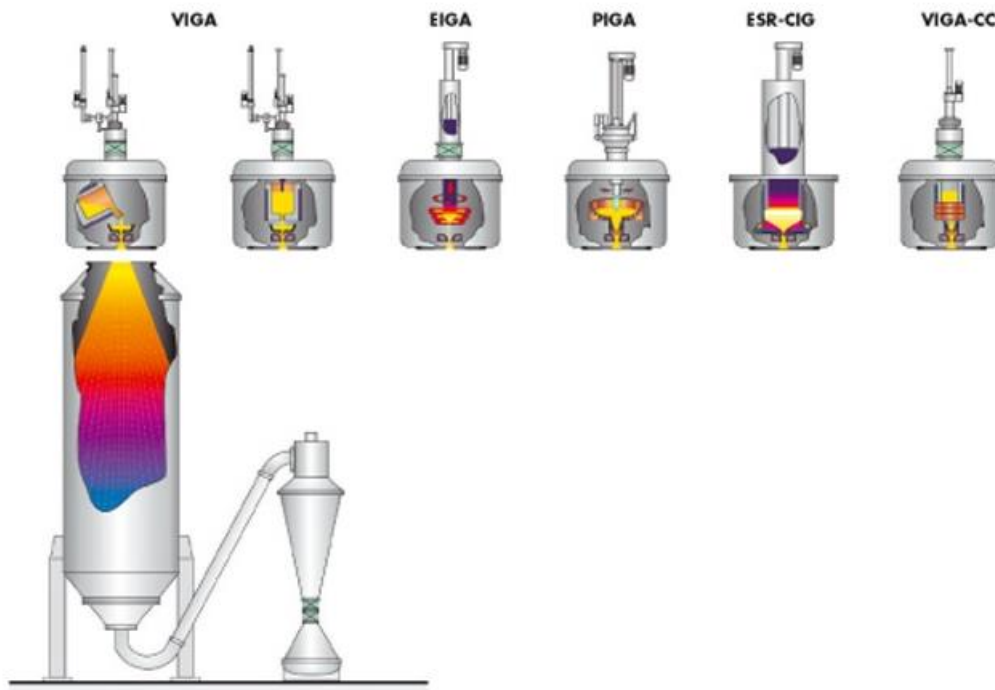


Figure 1.19: Main melting processes adopted for gas atomization. [12]

The other systems available are:

- EIGA (Electrode Induction melting Gas Atomization). In this system, the feedstock consists in prealloyed rods, that form an electrode, which is inductively melted. By proceeding that way, a crucible is not needed.
- PIGA (Plasma-melting Induction-guiding Gas Atomization). This technique is usually preferred for very reactive and/or high-melting alloys. It basically consists in a plasma jet induced melting, performed in a water-cooled copper crucible.
- VIGA-CC (Vacuum Induction melting Gas Atomization – Cold-wall Crucible). It is mainly adopted for reactive metals, such as titanium alloys, or some intermetallic, for example TiAl. It is similar to the VIGA system, but the crucible is in copper and equipped with a bottom pouring system. This final part is attached to a CGI (Cold-wall induction Guiding) system (ALD patent).
- ESR-CIG (ElectrSlag Remelting – Cold-wall Induction Guiding). This technique has been expressively developed for high-performance superalloys used in the aircraft industry. For these materials, the so called “triple melting” process is performed. An ESR process is performed in a ceramic-free environment (CIG) to grant a high level of cleanliness and purity, fundamental for the above-mentioned applications. The material feedstock is in form of an electrode, which is slowly lowered into the slag. Once it is wetted, droplets of the refined material pass through the slag layer and create a melt pool beneath the slag. This molten metal is then guided through the cold-wall system into the atomizing tower. [12]

1.4.2. Powder Flowability and Processability

Powder flowability is a very important parameter to consider and it should be high enough to let the powder create a good-quality powder layer. Although it is more important to evaluate the powder “*processability*”. This term refers to several parameters (Fig. 1 *Figure .20*), which combination influences the manufacturing process itself and the final part properties too. It includes physical and chemical properties of the material, the layer creation device (e.g. a roller or a ruler) and it also depends on the powder properties, such as particle size distribution and related powder density, flowability. It must be noted that these characteristics also affect the thermal and optical properties of the powder. [13]

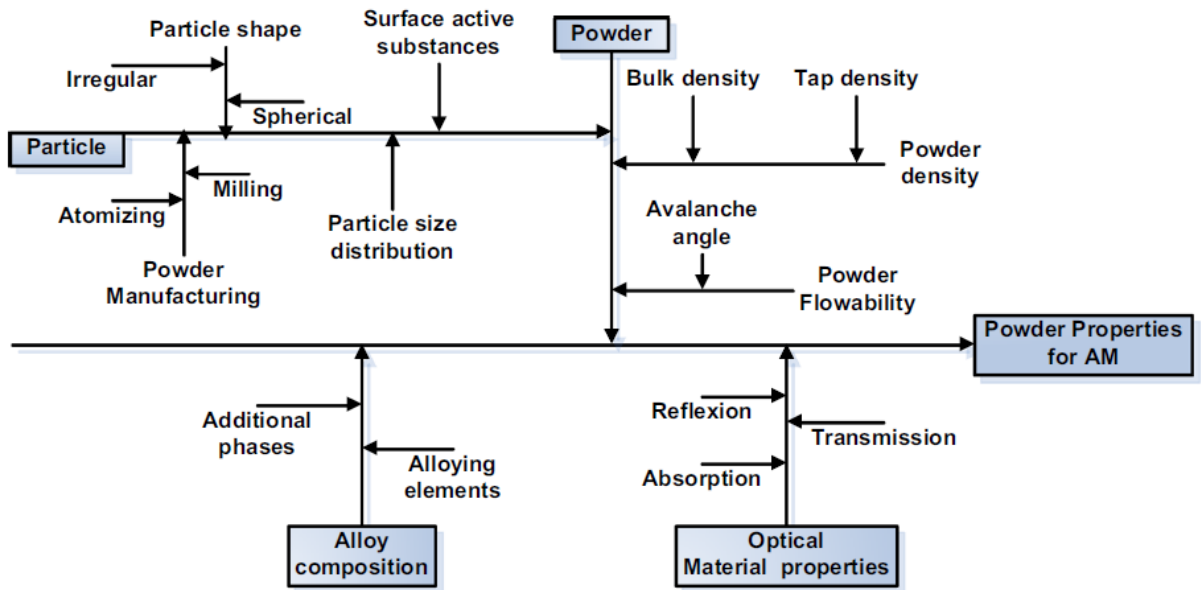


Figure 1.20: Most important properties that influence a powder processability. [13]

A good flowability is essential, it is although insufficient to grant a good processability. Krantz [14] concluded that an accurate measurement technique must be as close as possible to the manufacturing environment, especially when evaluating the stress state of the particles.

AM powders optimization is still a serious challenge for researchers. This is partially caused by the triple dependence of powder behaviour on its interaction with the AM system, the bulk solid material properties and particle consolidation phenomena.

It has been shown in several studies the importance of particle shape, size and surface roughness, especially for PBF processes. [15, 16, 17] These morphological properties have a major impact on powder density after deposition. Hence, they must be meticulously studied and controlled to ensure a good degree of reliability and repeatability for the whole process. To do so, all the major powder properties must be investigated from both a morphological, chemical and microstructural point of view, as summarized in Fig. 1.21.

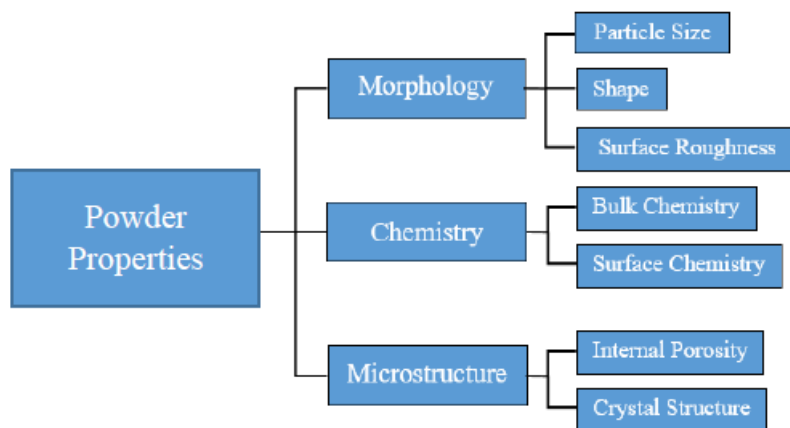


Figure 1.21: Classification of powder properties. [4]

This work consists in a characterization as complete as possible of the powders I studied during the period I spent in Stone (Staffordshire, UK), when I was working for Renishaw plc. To do so, the first step consisted in analysing what was available in literature, focusing on what has already been done for characterizing AM powders. The results of this review are shown below.

Today, the solution to the lack of sensitivity seems to be a long analysis, which incorporates a combination of shear, dynamic and bulk properties. This process is more accurate, but widely inadequate from an industrial point of view, because of its expensiveness and the relative required time. [6] Even if this kind of analysis is more suited for a laboratory analysis, than is it applicable to an industrial reality, the goal of this work consists in trying to provide a complete powder characterization, not just relative to bulk properties but also from a dynamically and shear point of view.

Slotwinski et al. [6] stated the several challenges that the wide-spread diffusion of AM has to face nowadays, in particular they focused their attention on the limits linked to the powder properties measurement and their connection with the processability during manufacturing. According to the authors, there must be a greater effort in standardization. Some of the main issues described in this article include:

- Poor comprehension of the relationship between the properties of powder and bulk material.
- Lack of knowledge on the causes of machine-to-machine and day-to-day variability.
- General need to better understand how to properly understand and characterize AM materials, both in input (powders) and output (component).
- Need to create a certified and standardized method to qualify and certificate AM-produced parts; according to the author, the classical techniques are impractical due to their lack of cost-effectiveness and the great amount of time and effort they require.
- Inexistence of standardized AM-specific methods, that could allow easier interlaboratory studies.

The main issue is the lack of comprehension on how the local physics of particles interactions is linked to the powder macroscopic mechanical behaviour. Because of that, a general empirical approach is usually preferred. [18]

Leturia et al. [19] compared the results obtained through traditional methodologies (powder flow tester, moisture content evaluation, particle size distribution, etc.) and compared them with the data from an FT4 Powder Rheometer. They determined that analysis on the bulk material are completely unreliable to determine the powder properties. Moreover, to completely characterize the flow properties of a powder it is necessary to test it in several ways and in different conditions. Shear tests are particularly useful, because they are able to give intrinsic parameters; although it must be stated that this kind of tests are very time-consuming. They also determined that the parameters that are usually applied when analysing powders, are accurate just in very restrictive and specific, usually almost theoretical, conditions (e.g. free surface condition). Several other authors [20, 21, 22] proved that intrinsic material properties are poorly useful for AM applications, if compared to dynamic properties, due to the presence of Van der Waals, electrostatic and/or capillary forces that become preponderant in powders. These phenomena are the direct consequence of the extremely high surface area-to-volume ratio, typical of fine powders used in AM.

Clayton et al. [23] also stated the necessity to use more accurate methodologies to analyse powder properties. Their study agrees with the previous one in the necessity to adopt powder rheometers, due to their ability to detect even subtle changes in the bed properties, which are very impactful on the AM machines. The importance of a multivariate approach is also stated.

Valverde [24] stated the importance of a good flowing behaviour, which is critical because of the several operations that a powder must withstand during processing (e.g. fluidization, aeration, etc.). Processability has a direct impact on the final product quality, but also on the efficiency of the manufacturing process itself. Thus, a poorly flowing powder can lead to wastage, machinery issues and consequent maintenance downtime, with associated cost. According to the previously mentioned author, Freeman [25] explained how every test that can be performed is individually unable to represent all the conditions that a powder can face while processed. Hence, a wide range of characterization techniques must be adopted if the goal is to predict the flowing behaviour of a powder in an environment as complex as the inside of an AM machine is. This prediction is more accurate if the analysis is carried by taking into account the results of several different tests.

According to Taylor et al. [26] and Leturia et al. [19], even if the most common characterization techniques in use today (e.g. angle of repose evaluation, bulk density tests, etc.) are well understood and documented, these methods were developed decades ago and often prove not to be sensitive enough to detect subtle variation in a powder behaviour. For example, two powders with the same test results can show act in two different ways once processed, even if they should show the same behaviour. These phenomena cannot be completely explained by a lack of accuracy in the instruments, instead it is more plausible that the key parameters controlling the powder behaviour during AM processing are still not completely understood. Hence, even if the investigation methods are sensitive enough, the real issue is the determination of which parameter is more impacting than the others. The development of new characterization techniques will probably solve this issue, granting the possibility to find new parameters more influencing on the powder processability.

The necessity of new characterization techniques is then vital, although “classical” testing is still fundamental. As it was previously mentioned, determining “static” parameters, such as particle size distribution, average particle shape, etc., keeps being mandatory, due to the huge impact that these factors have on the powder flowability and general behaviour. For example, Cervera et al. [27] and Gusarov et al. [28] showed that a higher relative powder density, linked mainly to particle size distribution and particles morphology, leads to a greater thermal conductivity, concerning the powder bed. Thus, lowering the energy barrier required to create a melt pool and giving the possibility to use a lower laser intensity, making the whole process relatively more cost effective. This effect was also proved by Liu et al. [29], that tested two powders with the same particle size mean value, but characterized respectively by a narrow and a wide particle size distribution. The latter, which was also the powder showing a greater powder bed density, due to the better particles packing efficiency, always required a lower laser intensity, even if tested at very different values of scanning speed and laser power. The reduction of internal stresses, distortion and porosity in the final part are other advantages of a relatively denser powder. [30] It must be noted that a high particle packing efficiency leads to process-related issued, such as clogging and a decrease in flowability. Hence, it is necessary to find the right balance for the powder relative density value.

2. Materials and Methods

Eight different aluminium alloy powders, from five different suppliers, have been characterized during the experiments that will be described later. A complete list is provided in Table 2.1:

Table 2.1: List of Powders and relative Supplier

Material	Supplier	Lot / Batch No.
A205	V	15-6053S
AlSi10Mg	L	0001
AlSi10Mg	L	0002
AlSi10Mg	L	0003
AlSi10Mg	L	UK3359
AlSi10Mg	S	16D0534
AlSi10Mg	T	0425.2.5
AlSi10Mg	V	14-5034S

All the listed powders have been characterised by a series of tests, as described in Table 2.2, that will be described in the following sections.

Table 2.2: List of Tests performed and relative Apparatus

Test	Apparatus
Shape and morphology evaluation	SEM
Chemical composition analysis	SEM-EDS
Density measurement	Helium pycnometer
Particle size distribution	Laser diffraction particle size analyser
Powder flow test	Hall flow / Carney flow
Moisture content	Vacuum oven
Stability and variable flow rate test	Powder Rheometer
Aeration test	Powder Rheometer
Permeability test	Powder Rheometer
Compressibility test	Powder Rheometer
Shear cell	Powder Rheometer

2.1. SEM/EDS

One of the most important properties to analyse is the powder chemical composition. Knowing the percentage of each element forming the material used is generally important for every industrial process, including additive manufacturing techniques. In fact, the use of a laser is involved, which parameters have been optimized for a certain chemical composition, which means that it is important to check if the powder composition is within the acceptable range set on the laser.

The other very important property that must be considered is the particle shape, that affects not just the flowing properties of the powder, but also the capability of the powder to give a dense initial powder bed, fundamental in order to avoid residual porosities in the produced component.

Both these key characteristics have been evaluated using an electron microscope (JSM-6010PLUS/LA, Jeol, JP) (Fig. 2.1), even if usually an EDS analysis is not a precise method for chemical analysis; other techniques are then generally preferred (e.g. ICP, LECO). The parameters used were: 20 kV voltage and 50 SS (spot size) when doing the chemical analysis (EDS), 60 SS when just acquiring images.



Figure 2.1: JSM-6010PLUS/LA electron microscope.

The SEM has an electron gun, which is able to produce an electron beam that targets the powder sample. By using lenses and electromagnetic fields, it is possible to direct that beam and change its size and shape. When the electrons generated get in contact with the sample, particles (other electrons) and X-rays can be emitted, as shown in Fig. 2.2.

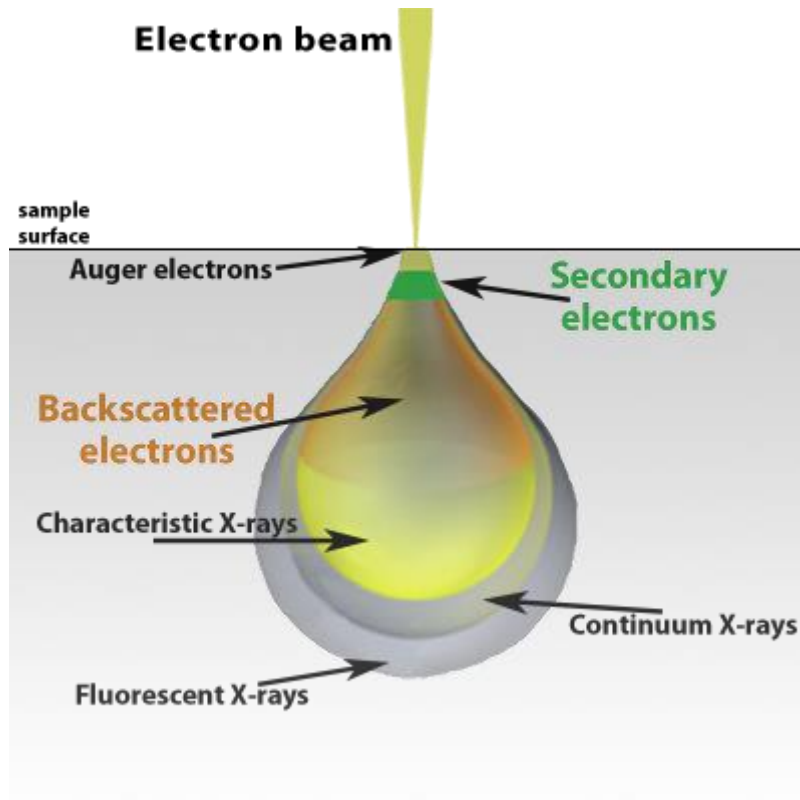


Figure 2.2: Electron-matter interaction. [31]

The different possible emissions are collected by detectors, that send that kind of information to a signal processing system that can convert it into images or data.

In the experiment, a small amount of powder was attached to a brass cylinder by using a carbon sticker. The cylinder is then being inserted into the sample holder, shown in Fig. 2.3



Figure 2.3: Sample holder with 3 brass cylinders and relative powder slotted in.

The sample holder is then put into the SEM (Fig. 2.4), which is consequently closed and vacuumed.

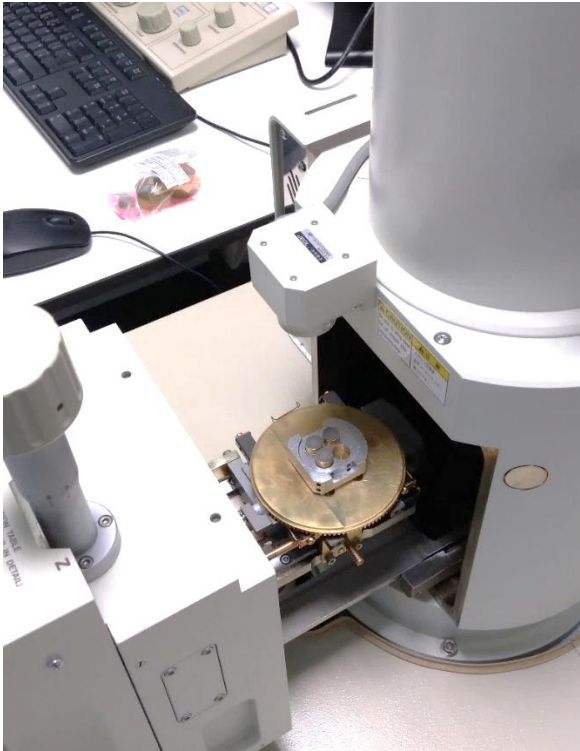


Figure 2.4: Sample holder slotted in the SEM.

The analysis performed and the relative parameters are shown in Table 2.3:

Table 2.3: Relationship between flow properties for AM powders and angle of repose.

Analysis	Magnification	Electrons analysed	SS
SEM (imaging)	50x	Backscattered	60
	50x	Secondary	60
	100x	Backscattered	60
	100x	Secondary	60
	200x	Backscattered	60
	200x	Secondary	60
	400x	Backscattered	60
	800x	Backscattered	60
EDS	350x	Backscattered	50
	500x	Backscattered	50

In this work, the EDS analysis has been performed by using a single point analysis, instead of an entire surface one, hence the relative results refer to just single spots. During the experiment, for every image ten relevant points, usually the centre of the bigger particles, have been considered and analysed. The result will then be provided as the average composition and standard deviation obtained from all those spots. Note that the EDS analysis just provides information about the elements that form the powder, but not the way they are bonded together. The interpretation of the results, in fact, is usually difficult for this reason.

In case of anomalies in the sample (e.g. impurities or foreign particles), further EDS analysis are carried.

2.2. Helium Pycnometer

To determine the true density of the particles forming a powder, without the result to be influenced by the presence of voids or entrained air, a measurement can be done via gas displacement. In that case, a gas displacement helium pycnometer (AccuPyc II 1340 Pycnometer, Micromeritics, USA) (Fig. 2.5) and an analytical balance, with at least four digits' precision, (XS205 DualRange, Mettler Toledo, UK) (Fig. 2.6) were used.



Figure 2.5: AccuPyc II 1340 Pycnometer.



Figure 2.6: XS205 analytical balance.

Using this pycnometer, it is possible to perform a non-destructive test which measures the absolute volume and density of a certain sample by evaluating the pressure variation of helium in a chamber that has a calibrated volume. A 3.5 cm^3 cup has been used (Fig. 2.7, centre). It has been filled for approximately two thirds of its volume, weighted and then slotted into the sealed chamber (Fig. 2.7, right).



Figure 2.7: Lid (left), 3.5 cm^3 cup (centre) and sealed chamber(right).

The chamber is then slotted into the pycnometer, as explained in Fig. 2.8



Figure 2.8: Pycnometer before (left) and after (right) the chamber has been slotted.

The inert gas is consequently admitted into the room, then expanded into another one, with a precise and calibrated internal volume. The variation of pressure noted when the gas goes from the first chamber, filled with powder, to the second one (empty), makes it possible to compute the volume of the solid phase in the filled chamber. The density can then be evaluated as it follows:

$$Density = \frac{powder\ mass}{Volume} \quad (2.1)$$

Note that the precision is extremely high, because helium molecules can quickly fill even pores as small as 1 Å.

The process is summed up in Fig. 2.9.



Figure 2.9: Schematics of the process. [32]

The pycnometer makes 10 measurements for every test. The final result is the average, also standard deviation is provided.

2.3. Particle Size Distribution

For evaluating the particle size distribution, a laser diffraction analyser (Mastersizer 3000, Malvern, UK) has been used (Fig. 2.10) in conjunction with the Aero S unit.



Figure 2.10: Mastersizer 3000 and Aero S unit.

This test has the main purpose to define the particle size distribution of a sample, an important property to evaluate, because it greatly influences the packing properties and the flowability of the analysed powder.

During the test, the sample is hit by a laser beam that is diffracted when passing through the powder. It then scatters at fixed angles, depending on the particle size distribution. In fact, a certain particle size corresponds to a certain diffraction angle. The light emitted from the particles creates a pattern, evaluated by detectors. It is then analysed to determine the particle size distribution itself.

A schematic diagram of the process is shown in Fig. 2.11.

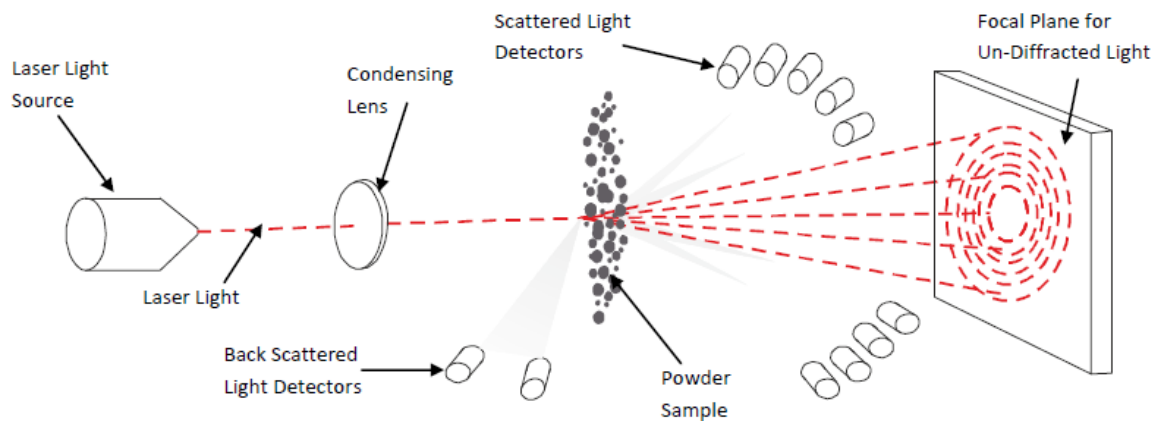


Figure 2.11: Representation of the Laser diffraction analysis process (Courtesy of Renishaw).

The Mastersizer 3000 uses both red and blue light, the latter has the purpose to grant higher resolution measurement when the particle size is below $1\ \mu\text{m}$. The combination of both gives better results on a wider particle size range ($0.01\ \mu\text{m}$ - $3500\ \mu\text{m}$) [33] (Fig. 2.12).

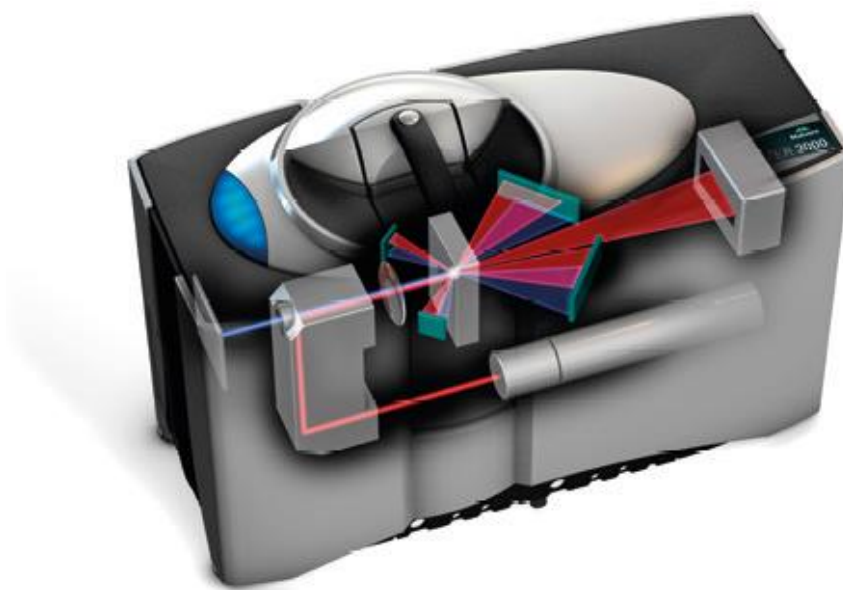


Figure 2.12: Representation of the testing chamber with laser light. [33]

The Aero S unit is a so called “dry unit”: its purpose is to disperse the powder and feed it to the analysing chamber. To achieve that, a stream of air is used.

Three tests have been conducted for each powder, evaluating the average as the final test result.

2.4. Powder Flow Test

The powder flow test is a simple experiment used to determine a powder flowability and flow rate. The necessary equipment that has been used consists of: Hall Funnel (ACuPowder, USA) (Fig. 2.13 left), Carney Funnel (ACuPowder, USA) (Fig. 2.13, right), pressure/humidity/temperature datalogger (SD700, EXTECH, USA) (Fig. 2.14), infrared thermometer (AutoPro ST25, Raytek, USA) (Fig. 2.15), precision balance (Pioneer PA413C, OHAUS, USA) (Fig. 2.16), Manual tapper (Fig. 2.17) and the clamp support (Fig. 2.18). A camera and a chronometer are also required.



Figure 2.13: Hall funnel and Carney funnel.



Figure 2.14: Datalogger.



Figure 2.15: Infrared thermometer.

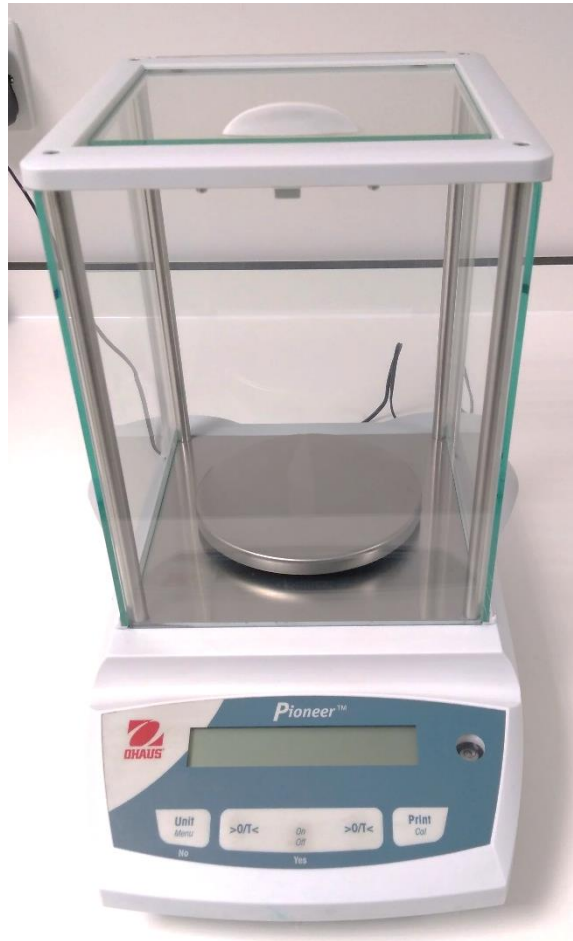


Figure 2.16: Precision balance.



Figure 2.17: Manual taper.



Figure 2.18: Clamp stand.

The testing procedures follow the ASTM B213: to determine the flow rate, it is necessary to evaluate the time that 50g of powder require to flow through the Hall funnel, that is strictly standardized (Fig. 2.19) and has a known orifice of 2.5mm.

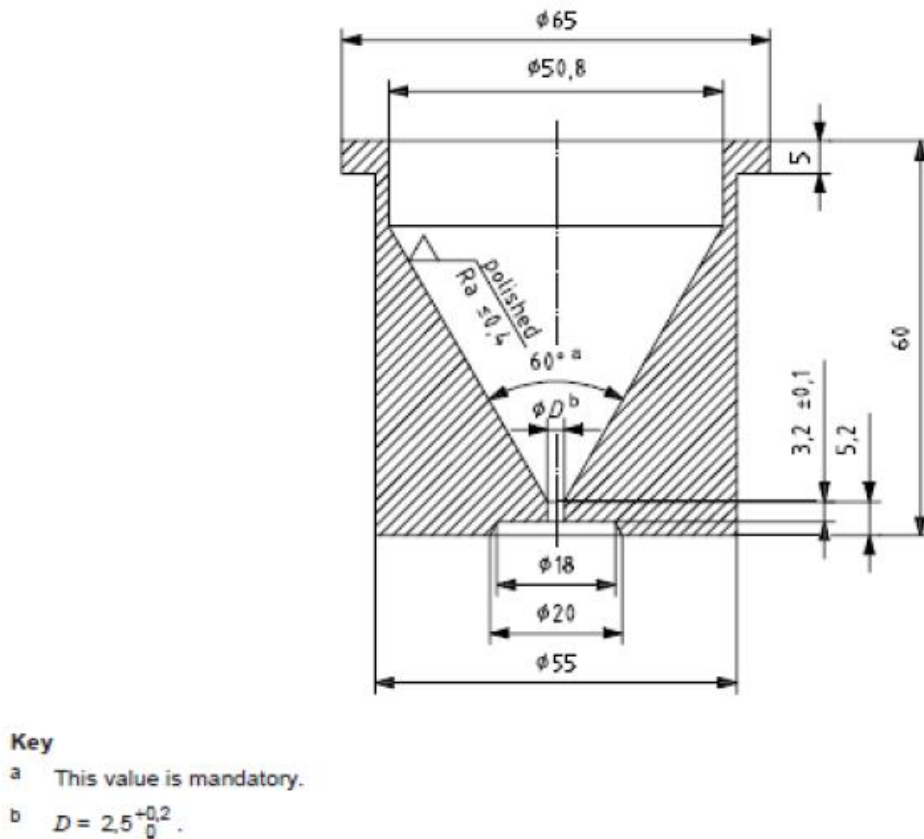
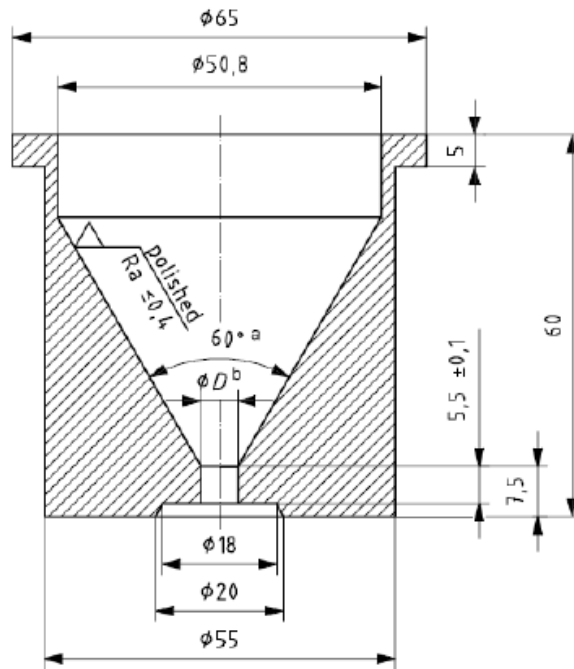


Figure 2.19: Hall funnel schematics (Courtesy of Renishaw).

During the test, the powder must be poured into the vessel, while the orifice is blocked by the operator finger, so that the powder cannot flow through it. When everything is ready the powder must be let free to flow under the action of gravity, while at the same time a chronometer is recording the time necessary for the whole powder to flow through the orifice.

The test works in that way just for powders that flow freely in this kind of system, sometimes it can happen that, because of several causes (e.g. moisture content, agglomeration, etc.), the powder is not able to move. In that case, it is possible to tap the funnel once and, if the powder starts to flow, the test can be carried on as usually, with the only difference being that it must be noted that a tap was required. Because of the tap being operator dependant, it has been decided to use a manual tapper (Fig. 2.17) to try to make the test as objective as possible.

If the tap is not enough, that means that the powder is too cohesive to be tested that way and the funnel must be switched to the Carney funnel (Fig. 2.20) (ASTM B964), which is similar with the previous one. The main difference between the two is that the second has a bigger orifice (5mm). The way the test it's carried is the same for both funnels.



Key

a This value is mandatory.

b $D = 5^{+0.2}_0$

Figure 2.20: Carney funnel schematics (Courtesy of Renishaw).

At the beginning of the test, it is also necessary to note the environmental humidity percentage and temperature, because these two parameters can affect the result of the test.

After flowing, the powder accumulates on the metallic plate shown in Fig. 2.18. By analysing the way the powder piled up, it is possible to determine useful parameters, like the angle of repose, that can be directly correlated with the flowability of the sample. That angle can be easily evaluated by taking a picture and analysing it, an example of angle of repose is shown in Fig. 2.21.

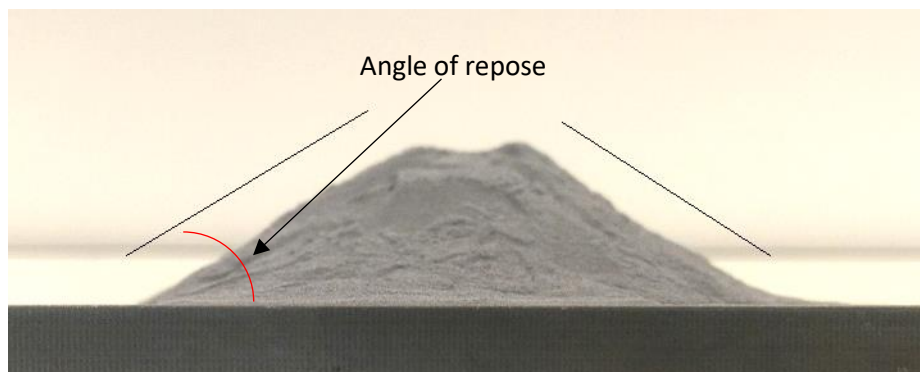


Figure 2.21: An example of angle of repose evaluation.

In general, the results are analysed according to the values showed in Table 2.4:

Table 2.4: Relationship between flow properties for AM powders and angle of repose. [34]

Flow property	Angle of repose (°)
Excellent	25-30
Good	31-35
Fair – aid not needed	36-40
Passable – may hang up	41-45
Poor – must agitate/vibrate	46-55
Very poor	56-65
Very, very poor	≥66

2.5. Moisture Content

When analysing the moisture content of a certain sample, the goal is to determine the percentage of water contained in it. For this test a precision balance (Pioneer PA413C, OHAUS, USA) (Fig. 2.16) and a vacuum oven (Vacutherm, Thermo Scientific, USA) (Fig. 2.22) have been used.



Figure 2.22: Vacutherm vacuum oven.

At the beginning, approximately 50g of powder are used to fill an aluminium boat. It is then weighted with the precision balance and the results are noted. The sample is then left in the vacuum oven at 180°C for 2 hours. At the end of the cycle, the sample is cooled in a desiccator, which is essentially an isolated cabinet with the bottom filled with silica, that absorbs water instead of the sample inserted, in that way the powder does not accumulate moisture again before being weighted.

Once the sample is cooled, it can be weighted again. The weight loss can be then related to the initial mass as a percentage, which is the moisture content:

$$\text{Moisture content (\%)} = \frac{\text{weight loss}}{\text{initial mass}} \cdot 100\% \quad (2.2)$$

A vacuum oven is used instead of a normal one, because the synergic effect of heating and vacuum is very effective to remove bulk and absorbed water. Moreover, the use of a vacuum environment makes it possible to work at lower temperatures. In that way, the powder is also protected from oxidation.

2.6. Powder Rheometer

The Powder Rheometer (FT4, Freeman Technology, UK) (Fig. 2.23) main purpose is to characterise the rheology, hence the flow properties, of powders. But as time went by, a lot of functionalities have been implemented so that now it can be considered a universal powder tester.

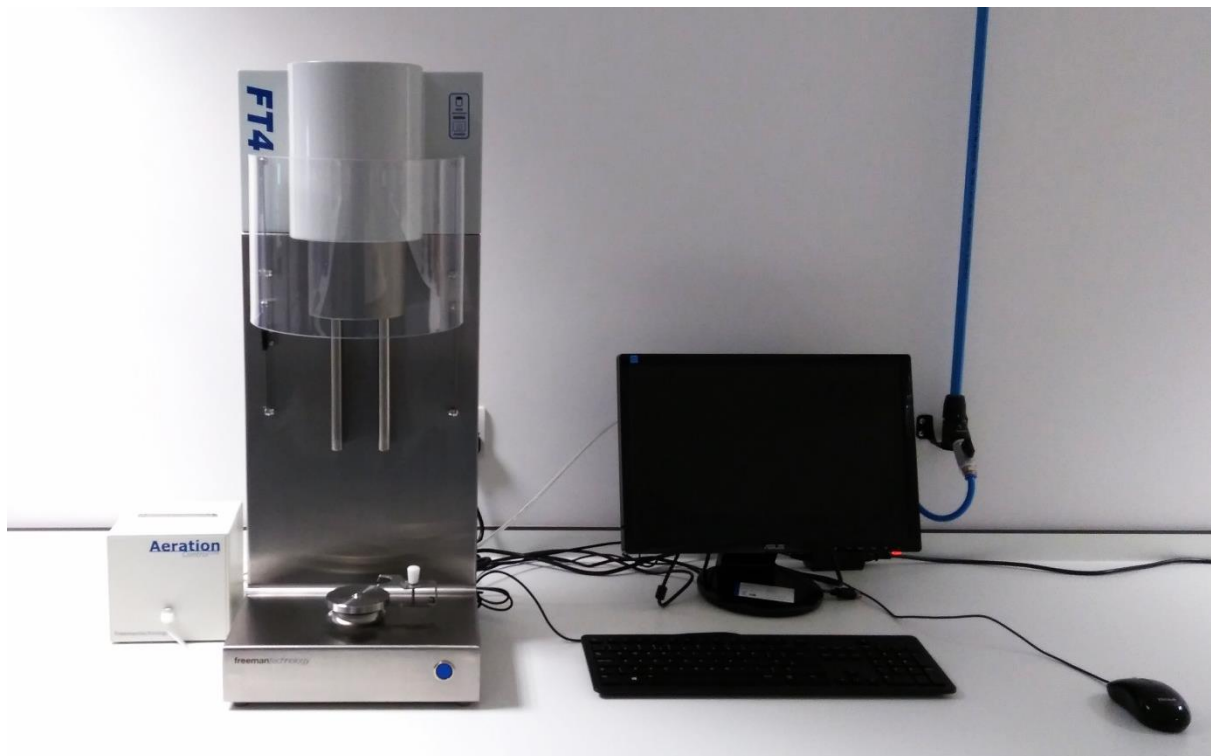


Figure 2.23: FT4 Powder Rheometer used, comprehensive of the Aeration Unit.

It has been used for a relevant number of tests, because it makes possible to determine a big variety of properties due to being able to perform up to seven different tests, as summarized in Table 2.5:

Table 2.5: Test available using the FT4 (performed highlighted) and relative analysed properties.

Type of properties analysed	Dynamic Flow Properties	Bulk Properties	Shear Properties
Test name	Stability and Variable Flow Rate	Compressibility	Shear Cell
	Aeration	Permeability	Wall Friction
	Consolidation		

Five out of seven available tests have been performed, as highlighted in the previous table, and they will be explained later in this chapter.

All the tests, in particular the ones that determine dynamic properties, use a patented blade methodology, which main goal is to evaluate the flow energy. In addition to that, a variety of shear cells, wall friction modules and other accessories (Fig. 2.24) can be used for measuring also bulk and shear properties.



Figure 2.24: FT4 Powder Rheometer accessories.

The key factor to be understood is that, by analysing at the same time data coming from different methodologies, it is possible to evaluate and relate several properties to many variables and packing states, from aerated to consolidated. So not just flow energy is obtainable, but also density (in different conditions), compressibility, permeability, etc. These are also relatable to process variables, like moisture content, attrition and segregation.

One of the most important components is a 23.5 mm Blade (Fig. 2.25), that is used in all the FT4 tests for conditioning the sample, when determining bulk and shear properties, and both for conditioning and testing, when used to determine the dynamic flow properties.



Figure 2.25: 23.5 mm Blade.

The blade must be inserted in the upper part of the machine, as shown in Fig. 2.26. By doing so, it is possible to both use the blade to apply several types of stresses to the powder (shear, normal) and to gather numerical information, given by sensors, about the applied forces and the reaction that the bulk shows to the blade movement.



Figure 2.26: 23.5 mm Blade inserted in the machine.

As previously mentioned, the blade is used during all the tests that involve the FT4 Powder Rheometer, even if it gathers information only during the stability and the aeration test. Other tests require the use of different components, that are inserted in the machine in the same place where the blade was, substituting it. Even so, the blade is initially used in every single test to condition the powder. It practically gently displaces the powders particles to achieve a state where the sample shows both low stress and low content of entrained air. [35]

One of the components that substitutes the blade during the other three tests is the vented piston (Fig. 2.27).



Figure 2.27: Vented piston.

Being a piston, its main feature is to compress the powder homogeneously. Its key part consists in its compression face (Fig. 2.28), the one that goes in contact with the powder, constructed from a woven stainless-steel mesh, allowing the air in the powder to escape uniformly across the surface of the powder bed. [36]



Figure 2.28: Vented piston compression face.

The compression face itself is composed of two different components: the metallic mesh (Fig. 2.29) and the cylinder (Fig. 2.30).



Figure 2.29: Metallic mesh, part of the vented piston.



Figure 2.30: Cylinder, part of the vented piston.

In Fig. 2.30 it can also be noticed the presence of an O-ring that, once the piston is assembled, prevents direct contact between cylinder and mesh. That is useful to avoid wear and decrease this component lifetime, but its main goal is to prevent air from flowing through the gap between cylinder and mesh. By doing so, the gas is forced to flow through the mesh. That avoids possible obstructions due to powder accumulating inside the piston.

The last component that substitutes the blade is the rotational shear cell head, shown in Fig. 2.31.

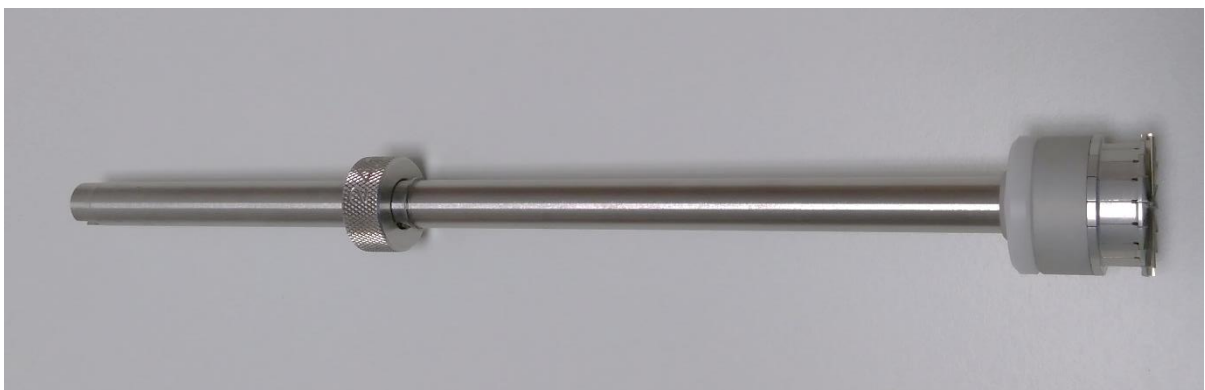


Figure 2.31: Rotational shear cell head.

It is mainly used during the shear cell test to induce both a normal stress, acting as a piston, and a shear stress, thanks to its unique face structure (Fig. 2.32) that allows to effectively shear the powder, even while compressing at the same time.



Figure 2.32: Shear cell head compression face.

Another important component to be considered is the vessel (Fig. 2.33), that is often different in every single test. Not all the vessels that were used are going to be shown. It will be discussed instead when it is necessary to use a different base and the splitting functionality.



Figure 2.33: One of the several vessels that are used during an FT4 test.

Some tests require air to flow through the powder sample. To achieve that, the commonly used plastic-made base (Fig. 2.34) must be substituted with its metallic, porous counterpart, called aeration base (Fig. 2.35).



Figure 2.34: Commonly used base.



Figure 2.35: Aeration base.

That component is made of AISI 316L stainless steel and is made up of five layers of mesh, with the finest being the central layer. Its function is to make the air flow through its pores and to prevent the powder to go the other way around. It is connected, with the use of a plastic tube, to the aeration unit, visible in Fig. 2.23 to the left of the machine, that provides the controlled air flow (Fig. 2.36).



Figure 2.36: Example of vessel with aeration base connected to the aeration unit.

The other important functionality of some vessels is the possibility to split them, as shown in Fig. 2.37.

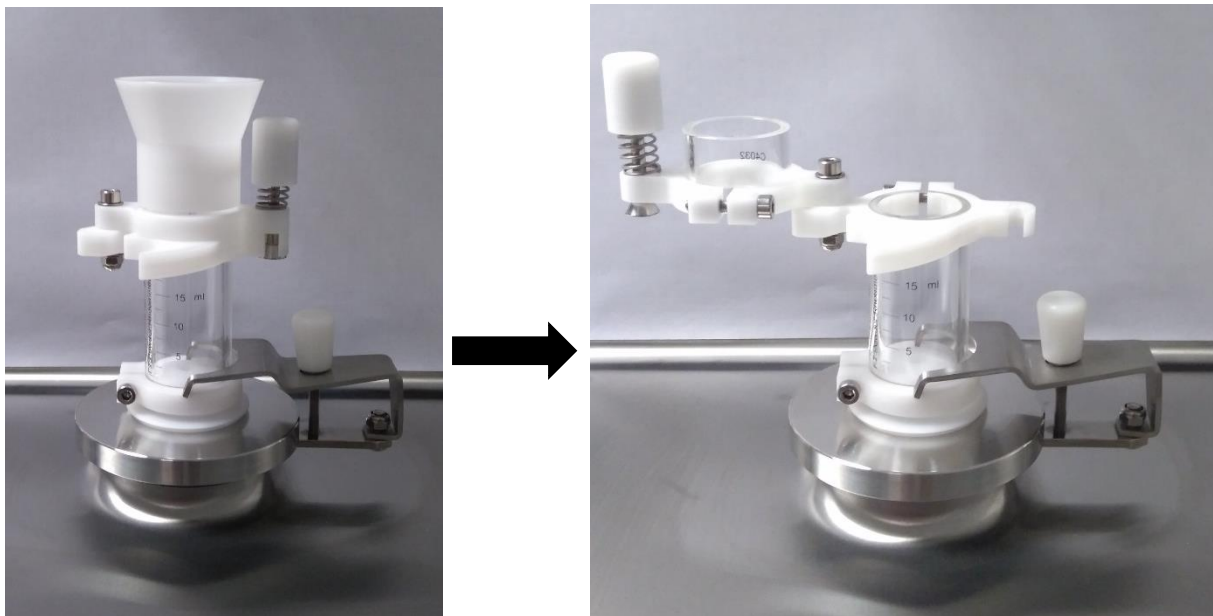


Figure 2.37: An example of a splitting vessel before (left) and after (right) splitting.

Splitting is a necessity when in need to evaluate a density. By doing so, the volume evaluation is not influenced by the powder in excess, which is over the lower cylinder and then cut out. This is why usually the vessel is not split at the beginning of the test: the separation of the upper part usually happens after the powder conditioning, with the 23.5 mm blade, that leads the bulk to a low-stress and low-air status, in which the density evaluated is known as conditioned bulk density (CBD).

2.6.1. Stability and Variable Flow Rate Test

The test was carried out using a powder rheometer (FT4, Freeman Technology, UK) using a 25mm x 25ml split vessel and a 23.5 mm blade.

A lot of phenomena can happen during a powder characterization, like changes in particle size or shape, and that can result in a variation in the flow properties. The goal of the stability test is to determine whether the powder is going to change in consequence of being tested. That is done by evaluating the variation of flow energy (positive or negative).

The test sequence consists of a series of identical conditioning and test cycles (Fig. 2.37), during which the required energy to make the powder flow is evaluated. The results of every test are different just if the powder changed during the test itself.

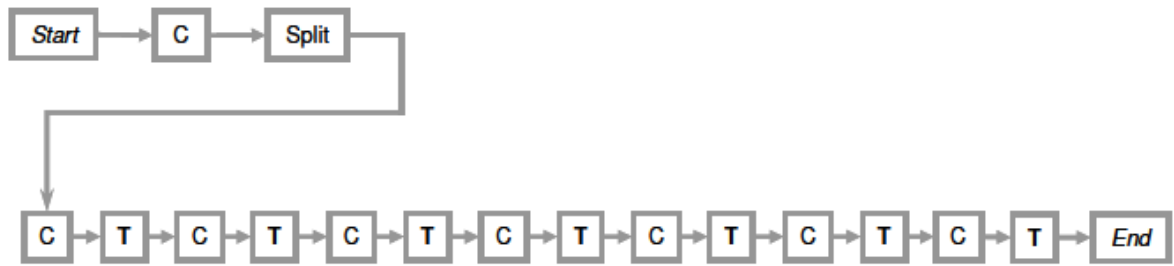


Figure 2.38: Stability test sequence (C = conditioning cycle, T = test cycle) (Courtesy of Freeman Technology). [37]

The vessel is split at the beginning of the sequence to provide a precise volume of powder for measurement. The conditioning process consists in the powder loosening and aeration, due to the 23.5 mm blade motion. The aim is to disturb and drop each particle to construct a homogeneously packed powder bed. This process removes any pre-compaction or excess air. The flow pattern, while evaluating the required energy to make the powder flow, consists in a downward anti-clockwise motion of the 23.5 mm blade (Fig. 2.39) that generates a high stress compressive flow mode in the powder. [35, 37, 38]

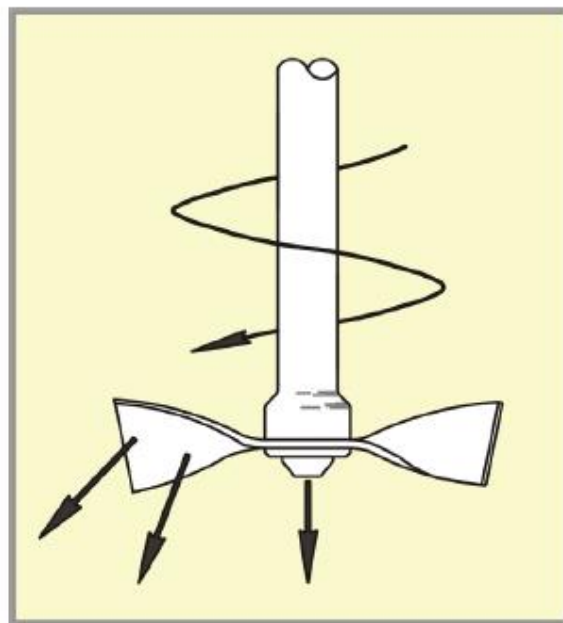


Figure 2.39: Graphical representation of the blade motion (Courtesy of Freeman Technology). [39]

The flow energy is calculated in every test as the work required to move the blade through the powder from the top to the bottom of the vessel.

One of the indexes obtainable from this test is the stability index (SI):

$$SI = \frac{E_{Test 7}}{E_{Test 1}} \quad (2.3)$$

Where:

$$E_{TEST\ n} = \text{Flowing energy evaluated at the end of test number } n \text{ [mJ]}$$

If the Stability index is not close to 1 ($0.9 < SI < 1.1$), the possible causes for instability can be investigated, as shown in Table 2.6:

Table 2.6: Possible causes of powder instability. [37]

SI > 1	SI < 1
De-aeration	Attrition
Agglomeration	De-agglomeration
Segregation	Over blending of an additive
Moisture uptake	Coating of vessel and blade by additive
Electrostatic charge	

Another index that can be obtained during this test is the basic flowability energy (BFE):

$$BFE = E_{Test\ 7} \text{ (mJ)} \quad (2.4)$$

It can be defined as the energy required to promote flow in a precise volume of powder that has been conditioned and that is the reason why it is considered the seventh test instead of a previous one. For stable powders, the energy obtained from the first test can be used instead, because the variation is small. It is preferable to study the powder after several conditioning processes, because in that way it acts more similarly to a real processed powder. [37, 38]

In general, it can be considered that a low BFE is typical of powders with “good” flow properties, while a high BFE generally results in a powder that flows poorly.

Even if it is arguably one of the easiest parameter to measure, its interpretation can be complex. In fact, it is dependent on many properties, both physical (e.g. particle size and distribution, cohesivity, density, porosity, etc.) and environmental (moisture content, surface additives, etc.), and their interaction.

Of course, the influence of each property varies from powder to powder, nonetheless it can be said that usually the most influential property is particle size: in fact, powders that consist of smaller particles are often more cohesive and vice versa. At the same time, the opposite can also be true, for example a poorly cohesive powder characterised by local agglomeration in a single spot can result in a very high BFE. Hence, this information must be analysed with care, because it can provide counter-intuitive results. Cohesivity of powder particles is mainly dependent on the packing efficiency of the powder bulk, affected by gravitational and interparticulate/cohesive interaction forces (Fig. 2.40).

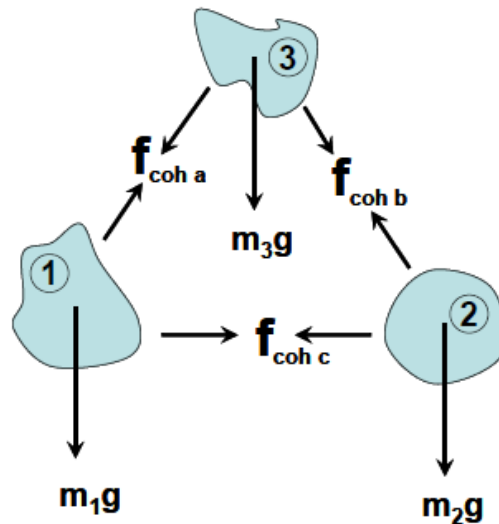


Figure 2.40: Force diagram (the other mechanical forces are ignored) (Courtesy of Freeman Technology). [39]

A “good” flow behaviour is generally associated with the ability of the powder to flow under gravity. It is linked to the ability of each particle to flow away from its neighbour. Considering that, powders with a small particle size usually behave as cohesive. In fact, the high degree of specific surface makes the cohesion forces relatively high compared to gravity. This kind of powders are able to trap a large amount of air within the powder bulk. For obvious reasons, powders with a larger particle size behave in a non-cohesive way instead. They are able to grant a more efficient packing structure and less entrained air. As a consequence of that, the powder bed is stiffer and relatively incompressible.

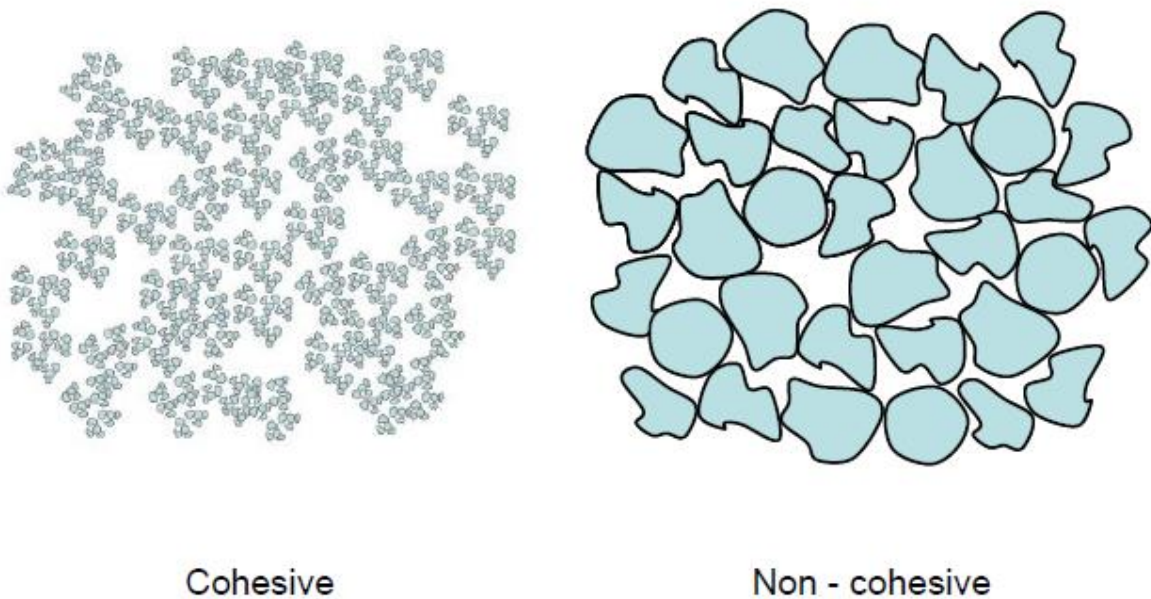


Figure 2.41: Example of cohesive and non-cohesive packing structures (Courtesy of Freeman Technology). [39]

As previously stated, the blade motion, during both the conditioning and analysing cycle, generates a highly compressive stress. Due to the powder being also constrained by the vessel, its compressibility plays a major role in the BFE values. So it must also be considered that the behaviour during the test dramatically changes in function of how cohesive and compressible the powder is.

Cohesive powder flow can be accommodated by the air pockets present between agglomerates. As a consequence of that, the stress transmission zone is localised (Fig. 2.42).

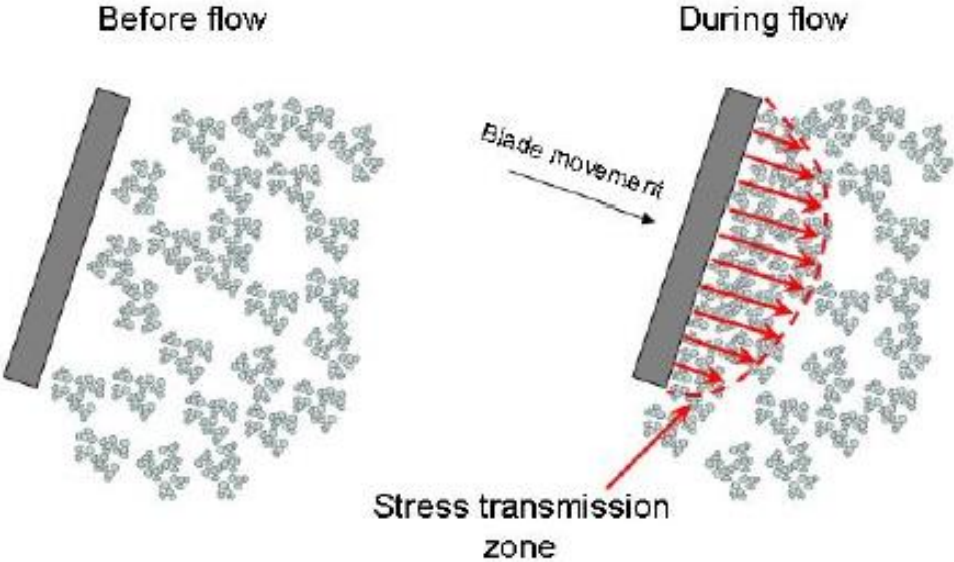


Figure 2.42: Cohesive powder flow during test (Courtesy of Freeman Technology). [39]

On the other hand, for a non-cohesive powder (packed efficiently), the blade movement cannot be accommodated by excess air, so the flow zone is able to be transmitted far ahead of the blade (Fig. 2.43), deep into the bulk. That means that friction gets relevant and contact stresses contribute significantly to the BFE.

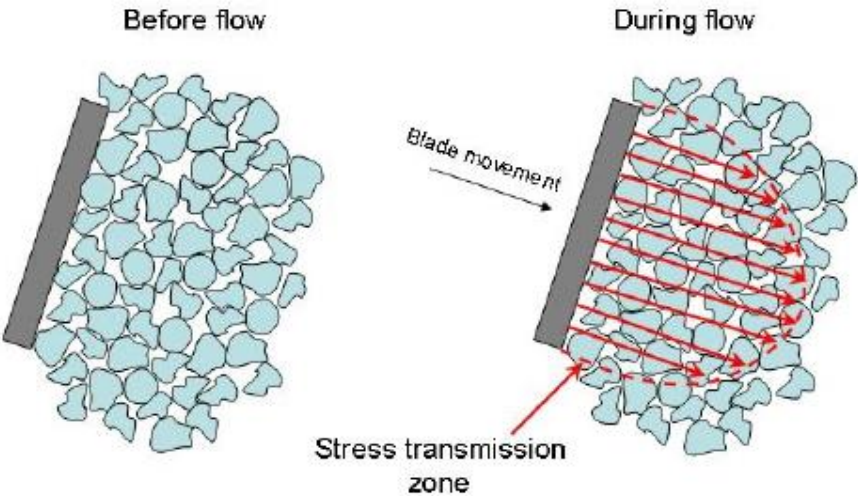


Figure 2.43: Non-cohesive powder flow during test (Courtesy of Freeman Technology). [39]

That is the kind of counter-intuitive result previously mentioned. In fact, in that case, a non-cohesive powder shows a high BFE, linked to a “bad” flow behaviour. As previously stated, the BFE interpretation is complex, not just because of possible contradictory interpretation of the result, but also because the main properties (cohesivity, packing efficiency, particle size) linked to this possible source of misunderstanding are also the most influencing on the index itself.

In addition to this, every powder, even if hydrophobic, is affected to some extent by water presence. In fact, the level of moisture influences the mechanical bonds and electrostatic charges existing between particles (Fig. 2.44).

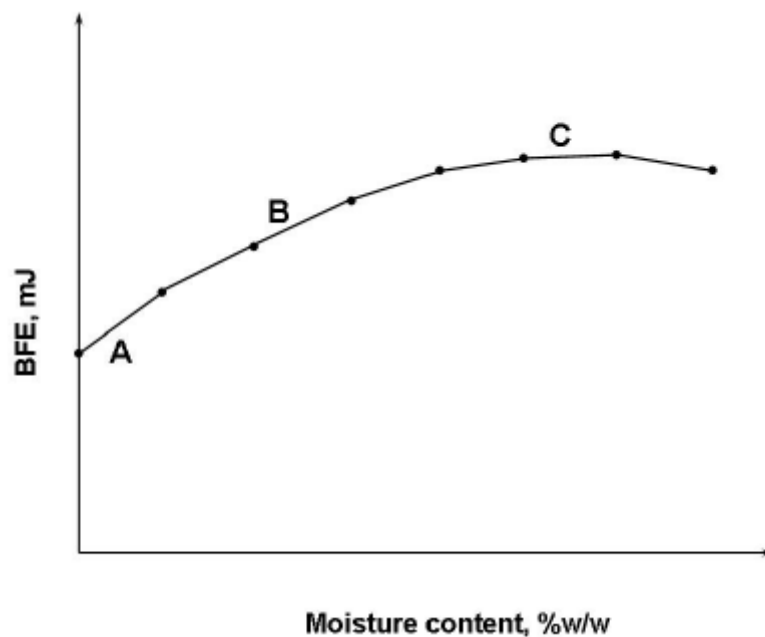


Figure 2.44: Effect of moisture content on BFE (Courtesy of Freeman Technology). [39]

As previously stated, particle size distribution and morphology are key properties when it comes to flowability, hence any change in these parameters is probably going to affect the powder behaviour. That can happen when some particle face a high enough stress (attrition) to break them apart. This situation can result in two different and opposite results:

a) Initially uniformly shaped particles break into irregular ones, which usually causes flow properties to worsen (Fig. 2.45, left).

b) Initially irregularly shaped particles break into particles with a more homogeneous and spherical shape, which may cause an improvement in flowability (Fig. 2.45, right).

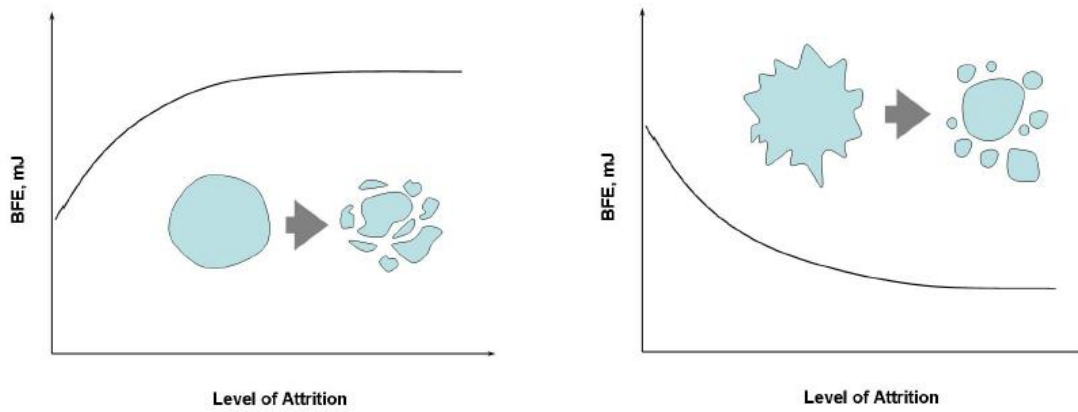


Figure 2.45: Effect of attrition on BFE (Courtesy of Freeman Technology). [39]

About the previous graph, attrition can be induced in several ways, depending from the analyst. The most common one is to establish an aggressive flow pattern using the blade, that makes particle contact more severe according to how fast is the blade motion. In general, it can be considered that “level of attrition”, used in the graph in Fig. 2.45, can be considered a synonym of stress applied to the sample, that is transmitted through particles and mediated by attrition.

Another phenomenon that can occur is segregation, particularly relevant in powders characterised by a wide particle size distribution. It consists in a reorganization of the sample particles from a homogenised distribution to a size-based hierarchy (Fig. 2.46).

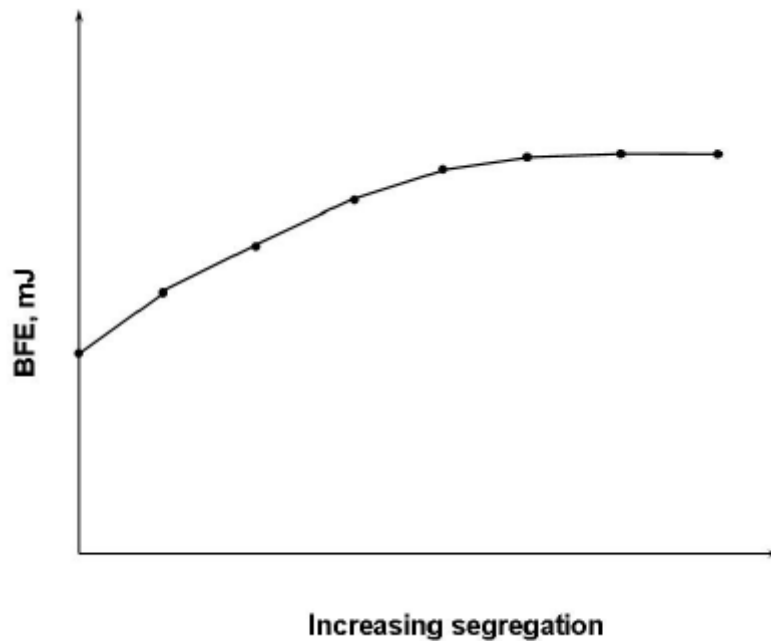


Figure 2.46: Effect of segregation on BFE (Courtesy of Freeman Technology). [39]

To obtain the previous graph instead, it was not considered the same powder processed in different ways, instead every single point is a different powder. As an approximation, it can be considered that the more the corresponding point on the graph lies on the right, the more segregation is relevant of course, so the wider the powder particle size distribution is. [39]

Another index obtainable is the specific energy (SE), which is obtained through a dynamic measurement, similarly to the basic flow energy. However, the major difference is that this index is evaluated when the blade is moving upwards (Fig. 2.47).

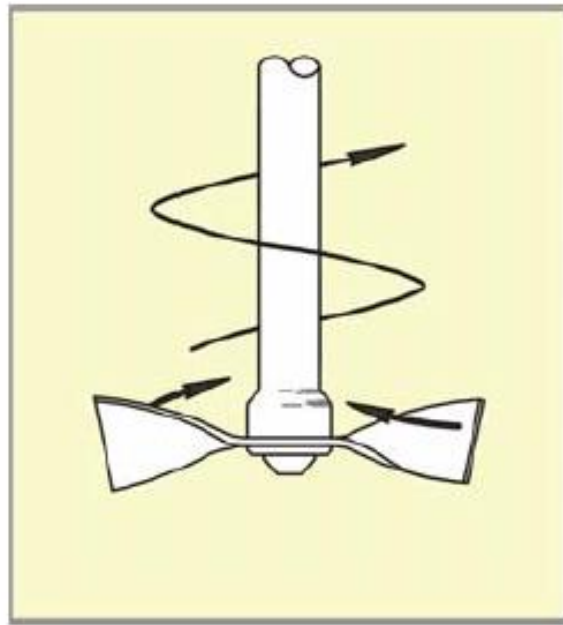


Figure 2.47: Graphical representation of the blade motion when evaluating the SE (Courtesy of Freeman Technology). [40]

It is defined as:

$$SE = \frac{\left(\frac{E_{up,Cycle\ 6} + E_{up,Cycle\ 7}}{2} \right)}{m_{split}} \quad (mJ/g) \quad (2.5)$$

Where:

$E_{up,Cycle\ n}$
= *Flowing energy when the blade is moving upward during test number n [mJ]*

m_{split} = *Sample mass once the vessel has been split [g]*

It is evaluated as the work necessary to move the blade from the bottom of the vessel to the top. It is normalised against mass, because, not being the powder constrained, mass conservation is not guaranteed and some particles can be pushed outside of the vessel.

By moving upwards instead of downwards, this test results in a lower stress applied to the particles, due to the powder not being constrained (there is no lid), unlike the case of BFE. Cohesion (Fig. 2.48) is usually the property that influences this kind of powder flowability the

most, due to the low stress environment. It has been reported that the specific energy is well correlated with the flow performance in low stress situations, in particular when the powder is fed gravimetrically (e. g. Die filling). [40]

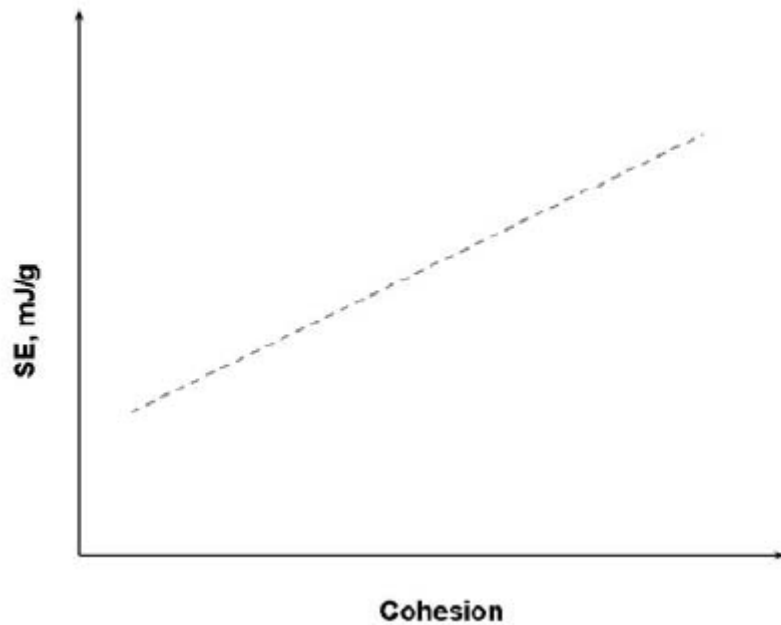


Figure 2.48: Correlation between the specific energy and the cohesion of the powder (Courtesy of Freeman Technology). [40]

To analyse the results of the test, the specific energy value obtained must be compared with the ranges provided in Table 2.7:

Table 2.7: Relation between specific energy and cohesion. [40]

Specific energy range	Cohesion
SE < 5	Low
5 < SE < 10	Moderate
SE > 10	High

At the end of that test, the rheometer automatically performs the variable flow rate test too. The goal of this test, similar to the previous one, is to verify the powder properties at different flow rate values. That is very important because even the most basic processes require the powders to flow at low rates in some places and high rates in elsewhere. Hence determining a powder sensitivity to flow rate is an important parameter. Commonly, a change in flow rate has a greater impact on the properties of a more cohesive powder, mainly because of its air content. [41]

The test sequence is shown in Fig. 2.49:

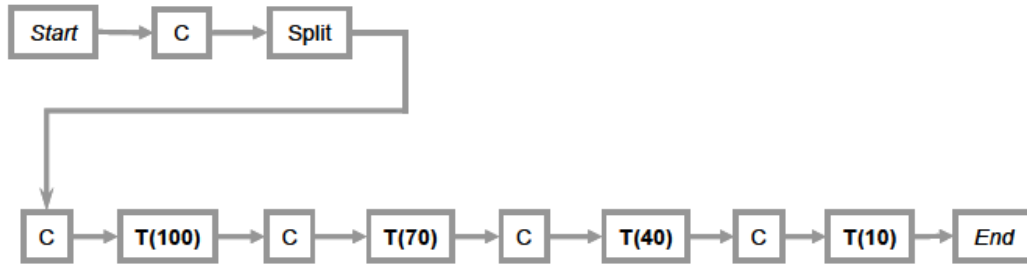


Figure 2.49: Variable flow rate test sequence (C = conditioning cycle, T = test cycle, () = Blade tip speed in mm/s) (Courtesy of Freeman Technology). [41]

The flow energy is measured at four different flow rates. It is fundamental that the results are considered reliable only if the powder proved to be stable during the previous test.

The index obtained from that test is the flow rate index (FRI):

$$FRI = \frac{E_{Test\ 4}}{E_{Test\ 1}} \quad (2.6)$$

Where:

$E_{Test\ n}$ = Energy at the end of test number n [mJ]

Note that the numeration used in the previous equation just refers to the test run when evaluating the variable flow rate. Referring to the previous figure, T(100) is Test 1 and T(10) is Test 4.

Its interpretation is explained in Table 2.8:

Table 2.8: Relation between flow rate index, type of powder and relative powder characteristics. [41]

Flow rate index	Type of powder	Powder characteristics
FRI > 3.0	High flow rate sensitive	Cohesive
3.0 > FRI > 1.5	Average flow rate sensitive	Average
FRI ≈ 1.0	Flow rate insensitive	Large particle size
FRI < 1.0	Pseudoplastic/Newtonian flow rate	Contains flow enhancers (e.g. magnesium stearate)

Flow rate sensitivity is influenced by various factors that must be considered, the major ones are:

- High flow rate means more entrained air. Air acts as a lubricant, because it reduces the contact between particles and it also makes the material more compressible. Both these characteristics reduce the energy needed to flow.
- Lower flow rates lead to less entrained air, hence to a locally more consolidated material, because of the blade action. The slower the it moves, the further the consolidated zone spreads, so the higher is the total energy consumed.

This phenomenon is possible only if the powder is relatively non-cohesive. Of course, it is influenced by other properties, such as shape, size distribution and density, but cohesion is by far the most important.

However, if the cohesive forces between particles are higher, complete separation is forbidden and there is formation of air channels (fig. 2.52) through the bulk. In that case, being frictional forces and mechanical interlocking still relevant, flow energy keeps being relatively high.

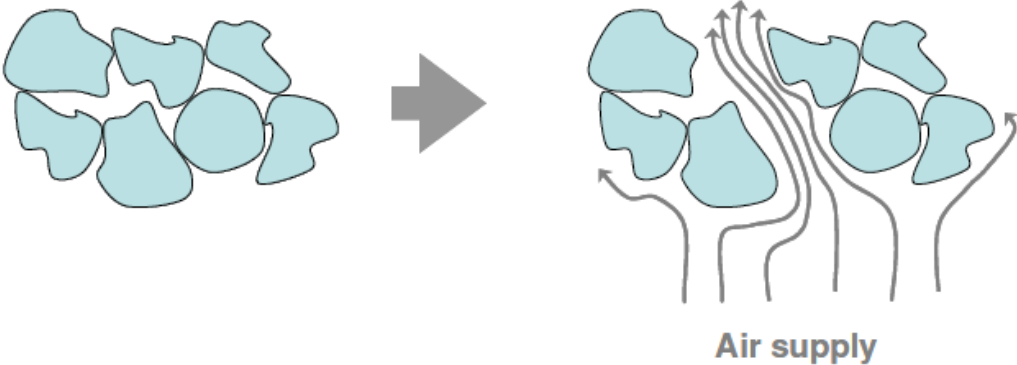


Figure 2.52: Fluidisation of a cohesive powder (Courtesy of Freeman Technology). [27]

As shown in Fig. 2.53, for flow to occur, the gravitational force must exceed all the other interactions so that the considered particle can flow away from its neighbours.

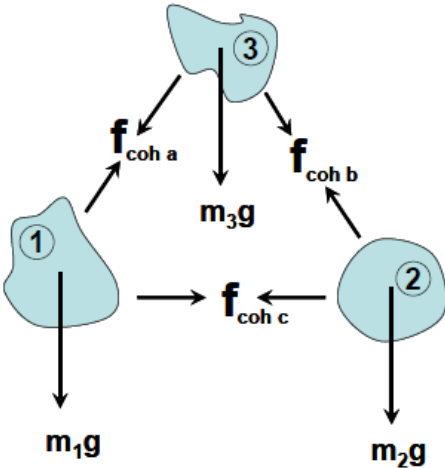


Figure 2.53: Force diagram (the other mechanical forces are ignored) (Courtesy of Freeman Technology). [27]

In particular, for the simple case shown:

$$m_1g > f_{y,coh a} + f_{y,coh c} \tag{2.7}$$

Where:

$$m_1 = \text{Mass of particle 1 [kg]}$$

$g = \text{Gravitational acceleration } [m/s^2]$

$f_{y,coh a} = \text{Vertical component of the cohesive force between 1 and 3 } [N]$

$f_{y,coh c} = \text{Vertical component of the cohesive force between 1 and 2 } [N]$

In any case, the ability of a powder to become aerated or fluidised strictly depends on the existing cohesive forces between every particle and its neighbour. Hence quantifying the sensitivity to aeration of a certain powder gives useful information about its behaviour during processes that implies the intentional introduction of air. However, it can be important also for laser powder bed fusion processes since this test can be used to better understand the powder cohesion and its behaviour when flowing under gravity.

The test sequence consists of a series of conditioning and test cycles (Fig. 2.54). Its goal is to determine whether the powder properties changed, and to which extent, as a consequence of aeration or not.

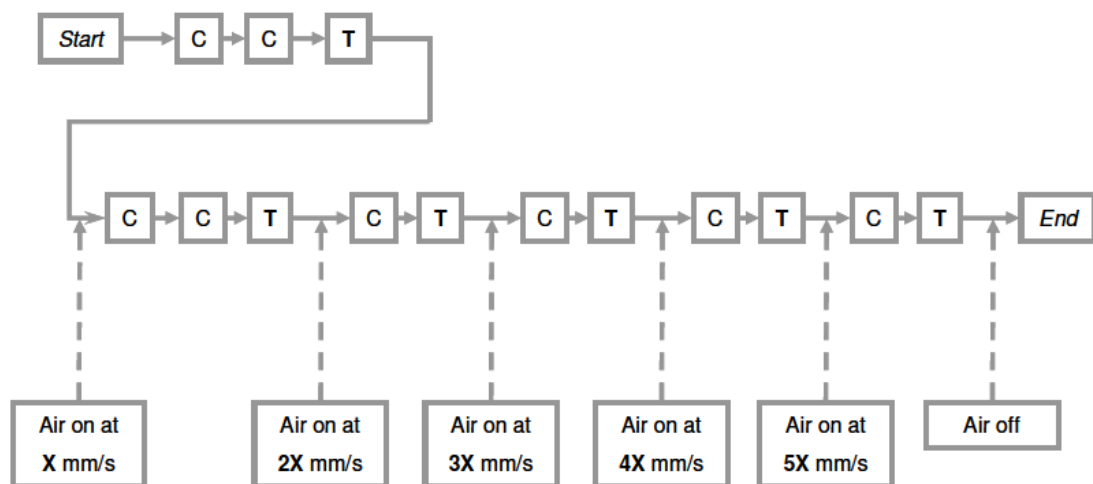


Figure 2.54: Stability test sequence (C = conditioning cycle, T = test cycle, X = air velocity) (Courtesy of Freeman Technology). [42]

Note that the first conditioning cycle is necessary to have a stable sample. The second one ensures that air is homogeneously distributed.

The aeration ratio (AR) index is obtainable, which defines the powder sensitivity to aeration and is directly correlated with its cohesion. It is defined as:

$$AR = \frac{E_{(air\ velocity=0)}}{E_{(air\ velocity=10)}} \quad (2.8)$$

Where:

$$E_{(air\ velocity=n)} = \text{Flowing energy when the air velocity equals } n \text{ } mm/s \text{ } [mJ]$$

It is interpreted as shown in Table 2.9:

Table 2.9: Relation between specific energy and cohesion. [42]

Aeration ratio range	Sensitivity to aeration	Cohesion
≈ 1	Absent	Very high
$2 < AR < 20$	Average	Average
$AR \gg 20$	High (probably fluidised)	Very low

Other information that can be obtained from that test are:

- **Basic flowability energy**, evaluated exactly as in the stability test, but during the first test (air velocity = 2 mm/s).
- **Aerated energy**, that is the energy value during the last test (air velocity = 10 mm/s). [42]

2.6.3. Permeability Test

It is defined as permeability the measure of how easily a certain material is able to transmit a fluid, which is air for this experiment, through its bulk. Being able to understand how permeable a powder is can be considered important, because it provides information about both physical properties (particle size and distribution, cohesivity, bulk density, etc.) and possible influencing external factors, such as consolidation stress, that can lead to a variation of certain powder properties, like porosity and particle contact surface areas. In general, the least permeable powders are the more cohesive, they usually consist of sub 30-micron particle size. Granular powders instead, are typically more permeable. If there are simultaneously large and fine particles, a tight packed structure takes place, where the fine particles fill the empty spaces between the larger ones, thus leading to a less permeable bulk.

The test was carried out using a powder rheometer (FT4, Freeman Technology, UK) using a 25mm x 10ml split vessel and a 23.5 mm blade. The air velocity value for the first test was 2 mm/s and the stress sequence was: 1, 2, 4, 6, 8, 10, 12, 15 kPa.

During the test, the powder is preliminary conditioned using the blade, then that must be changed for the vented piston, which will be used to compress the powder under increasing normal stress, while at the same time air flows from the bottom through the bulk at a constant rate (2 mm/s). The complete sequence is shown in Fig. 2.55:

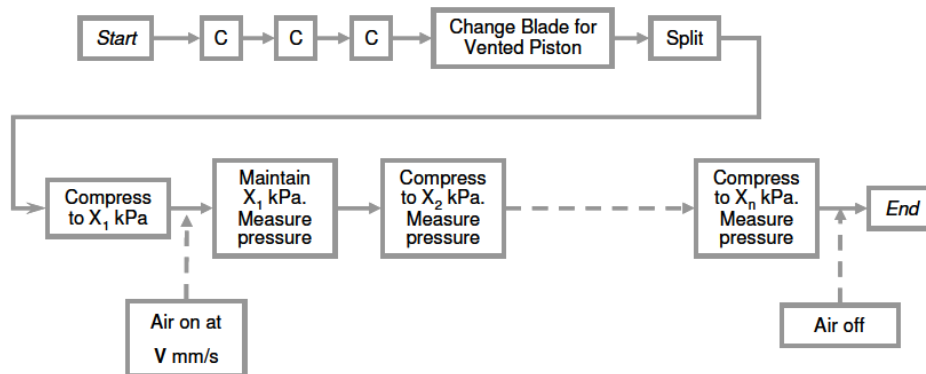


Figure 2.55: Permeability test sequence (C = conditioning cycle, V = air velocity, X = normal stress) (Courtesy of Freeman Technology). [43]

The piston holds the stress value fixed for a certain amount of time to allow the powder to reach equilibrium. It is then evaluated, for each level of stress, the pressure drop across the powder bed, that practically consists in the resistance that the material provides to the air flowing through it. [43]

2.6.4. Compressibility Test

During this test, it is measured how density deviates from the initial value when the applied normal stress increases. The importance of this measure is due to compressibility being directly influenced by many factors dependent on the powder quality, such as particle size distribution, shape, texture, cohesivity, etc. Note that it is not a direct measurement of flowability.

The results can be analysed similarly to the previous test ones, generally the most compressible powders are the more cohesive, they usually consist of sub 30-micron particle size. Granular powders instead, are typically less compressible.

The test was carried out using a powder rheometer (FT4, Freeman Technology, UK) using a 25mm x 10ml split vessel and a 23.5 mm blade. The stress sequence was: 1, 2, 4, 6, 8, 10, 12, 15 kPa.

The test sequence is shown in Fig. 2.56:

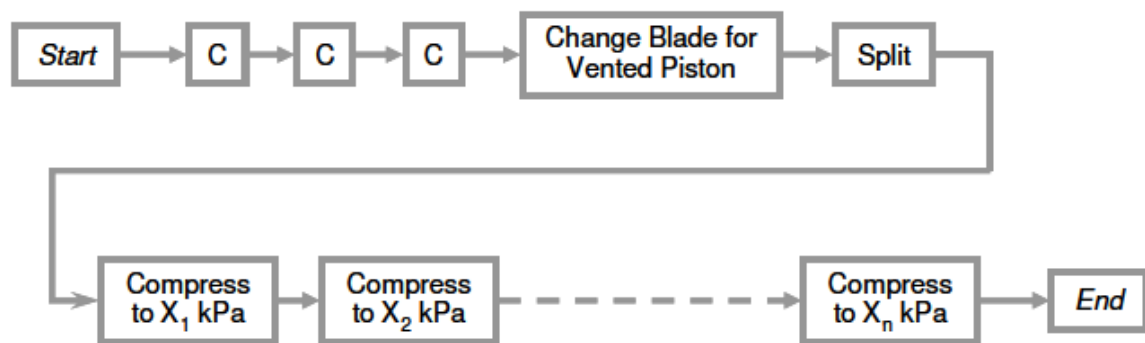


Figure 2.56: Compressibility test sequence (C = conditioning cycle, X = normal stress) (Courtesy of Freeman Technology). [36]

At the beginning, the powder is prepared by being conditioned with the 23.5 mm blade, after that the vessel is split, to provide a fixed volume for the test. The core of the process consists in the vented piston compressing, without rotating, the sample under increasing normal stress. The piston holds the stress value fixed for a certain amount of time, usually 60 seconds, to allow the powder to reach equilibrium. It is then the distance travelled by the piston for each level of normal stress. Compressibility is immediately calculated as a percentage change in volume, in fact, being the vessel cylindrical, the height variation and the volume are directly correlated. [36]

2.6.5. Shear Cell

When working with powders, shear properties are relevant. They are useful to understand how and when a consolidated powder (e.g. previously at rest) will begin to flow. Not just industrial processes, but also storage will cause the powder to be subjected to consolidation stresses that will lead to variations in density and interparticle forces. One important value that must be determined is the yield point, which represents the minimal stress required for flow to occur. It is influenced by several properties, such as particle size, shape and surface characteristics, or other variables like moisture content. This test provides also useful information that can be used to predict how the powder will behave during processing, for example if it will flow or whether blockages or stoppages can happen.

The most important component used during this test is the shear head (Fig. 2.31). At the beginning, it induces a normal stress σ on the powder, by keeping moving downwards, and then it slowly starts to rotate, inducing a shear stress τ (Fig. 2.57). Of course, the powder bed will resist the head rotation, so the shear stress will be increased until the bed will shear or fail, when the maximum shear stress (Yield Point) will be observed. During the whole process, the normal stress is kept constant.



Figure 2.57: Shear head and applied stresses (Courtesy of Freeman Technology). [44]

For each measurement of the previously mentioned value after the first one, the shear head rotates backwards to nullify the shear stress applied during the previous test.

The test was carried out using a powder rheometer (FT4, Freeman Technology, UK) using a 25mm x 10ml split vessel and a 23.5 mm blade. The applied pre-consolidation stress is 9 kPa and the normal stress sequence during the test is: 7.00, 6.00, 5.00, 4.00, 3.00 kPa

During the test sequence (Fig. 2.58) the powder is initially conditioned using the 23.5 mm blade, with the usual goal to achieve a homogeneous, low stressed sample. Then the blade is switched with the vented piston, used to induce a precise consolidation stress. In the end, the

vessel is split and the powder is reconsolidated, before the shear sequence, by the shear cell head.

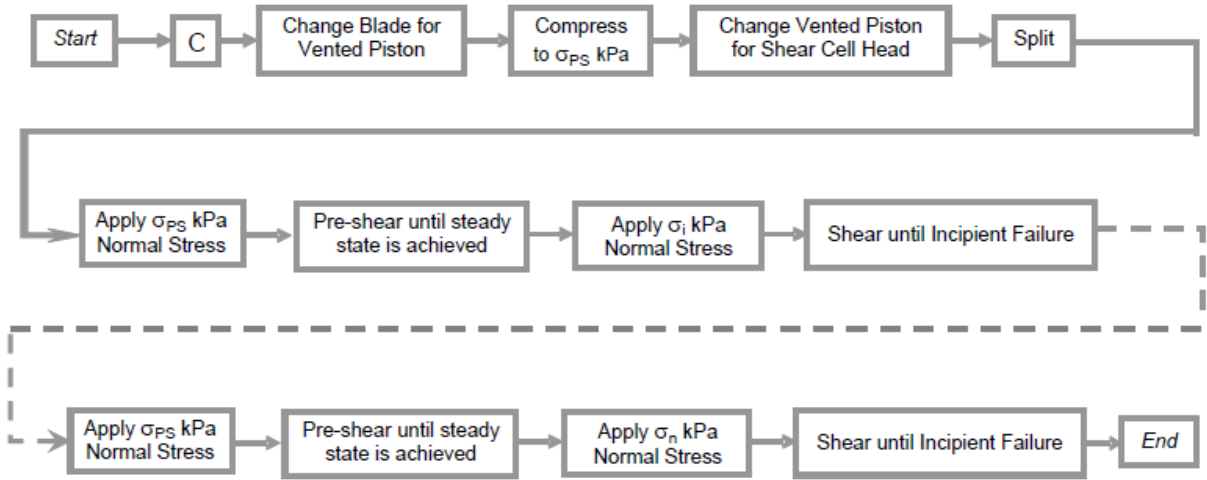


Figure 2.58: Shear cell sequence (σ_{PS} = pre-consolidation stress, σ_i = normal stress in test number i) (Courtesy of Freeman Technology). [44]

The vented piston is used for the pre-consolidation phase, because it allows an easy escape for entrained air. Note that the sample is pre-consolidated before performing the splitting procedure, so that the shear cell will not be surrounded by excess powder, that can negatively impact the result of the test.

To sum up, the real test involves the use of the shear cell head and provides different shear stress values (yield points) for several pre-determined normal stress levels, after a pre-consolidation at 9 kPa. To clarify that, in Fig. 2.59 and Fig. 2.60 it is provided an example of how the normal and shear stress change in function of time. [44]

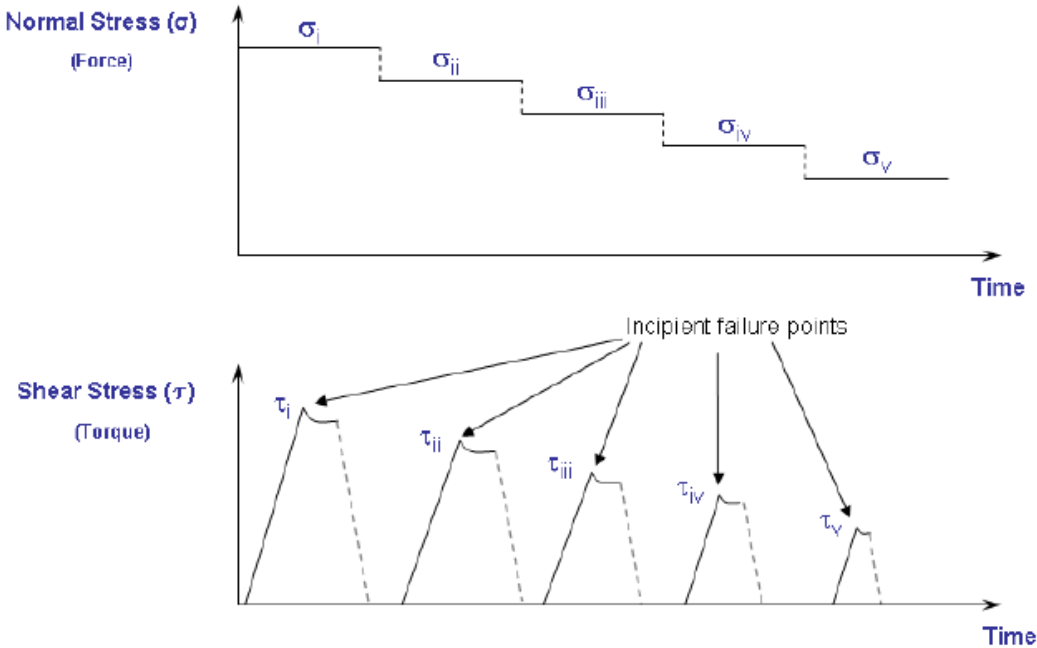


Figure 2.59: Normal and shear stress tendency as the test goes on (not considering pre-consolidation) (Courtesy of Freeman Technology). [44]

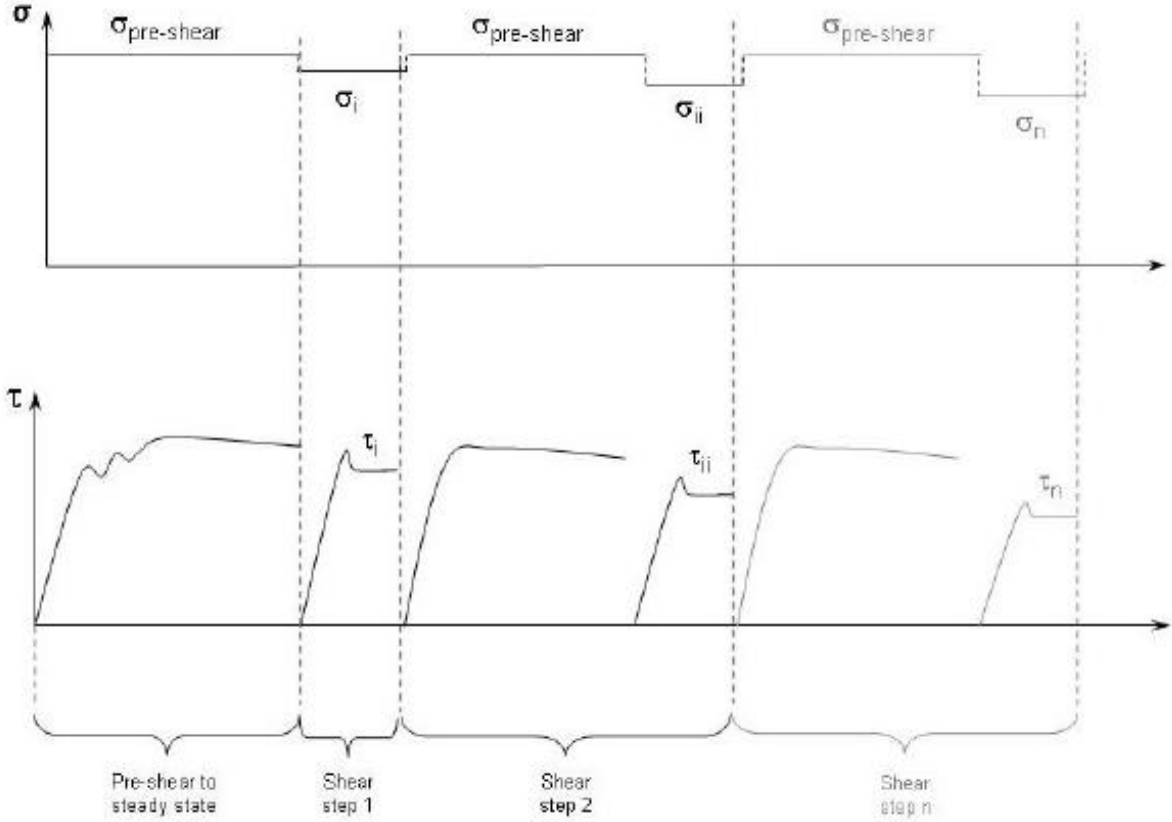


Figure 2.60: Normal and shear stress tendency as the test goes on (including pre-consolidation) (Courtesy of Freeman Technology). [44]

3. Results and Discussion for AlSi10Mg powders

3.1. SEM/EDS

3.1.1. Shape and Morphology

Being the available images too many, it has been decided, for the purpose of this report, to analyse group of powders instead of every single one. The analysed samples will be grouped as explained in Table 3.1:

Table 3.1: Powder groups.

Group	Powder (Supplier and Batch)			
Group A	L 0001	L 0002	L 0003	L UK3359
Group B	S 16D0534	T 0425.2.5	V 14-5034S	

The reasons that justify this way of grouping the powders consist mainly in the fact that the ones from group A are supplied from the same company and that powders in the same group share some characteristics (general shape, presence of satellites, etc.).

It can be noticed from the results of the secondary electrons analysis at a 200x magnification (Fig. 3.1) that the group A powder shown (L 0001 top, L UK3359 bottom) exhibit a general irregular particle shape, usually elongated. This is a common trend for that group

On the other hand, if the previous images are compared with two powders from group B (Fig. 3.2) (S 16D0534 top, V 14-5034S bottom), it is easy to notice that in this case the particle shape is in general more regular (rather spherical), but the presence of satellites is massive.

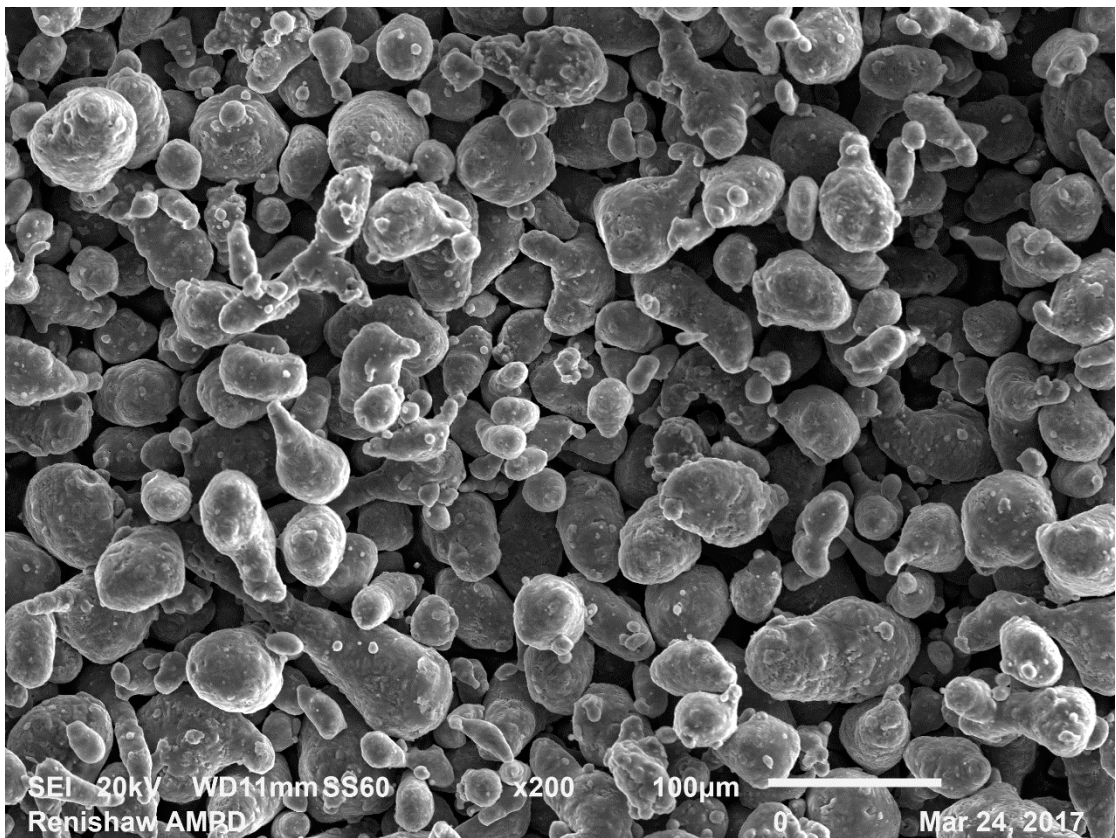
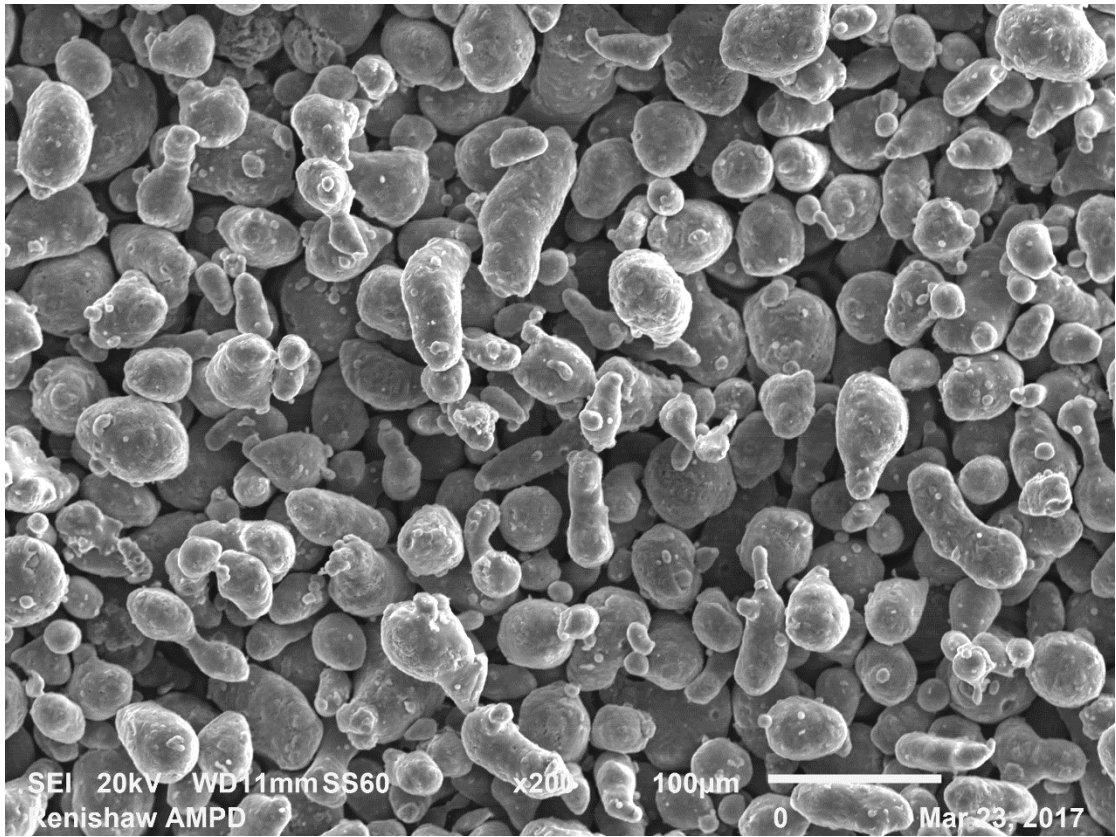


Figure 3.1: SEM image (secondary electrons, 200x) of L 0001 (top) and L UK3359 (bottom).

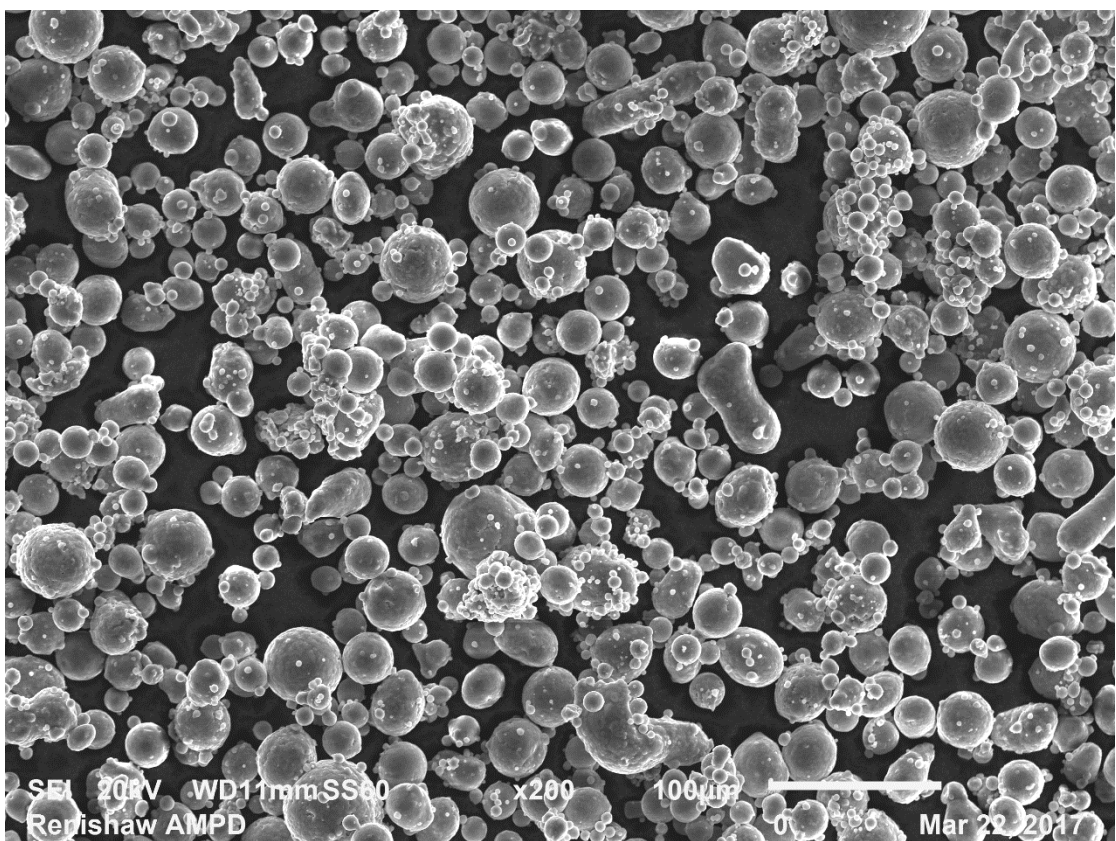
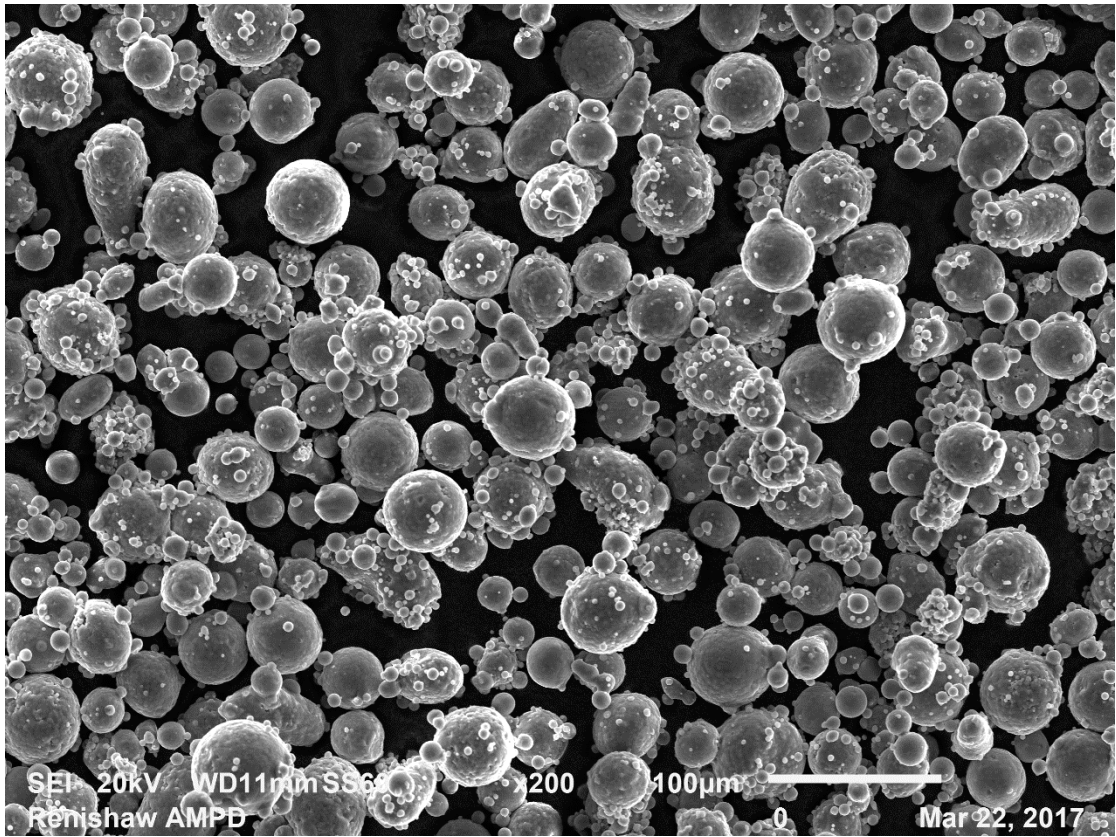


Figure 3.2: SEM image (secondary electrons, 200x) of S 16D0534 (top) and V 14-5034S (bottom).

Using a greater magnification makes evaluating the presence of satellites in the particles of group B easier. An example of that can be provided by Fig. 3.3 and Fig. 3.4:

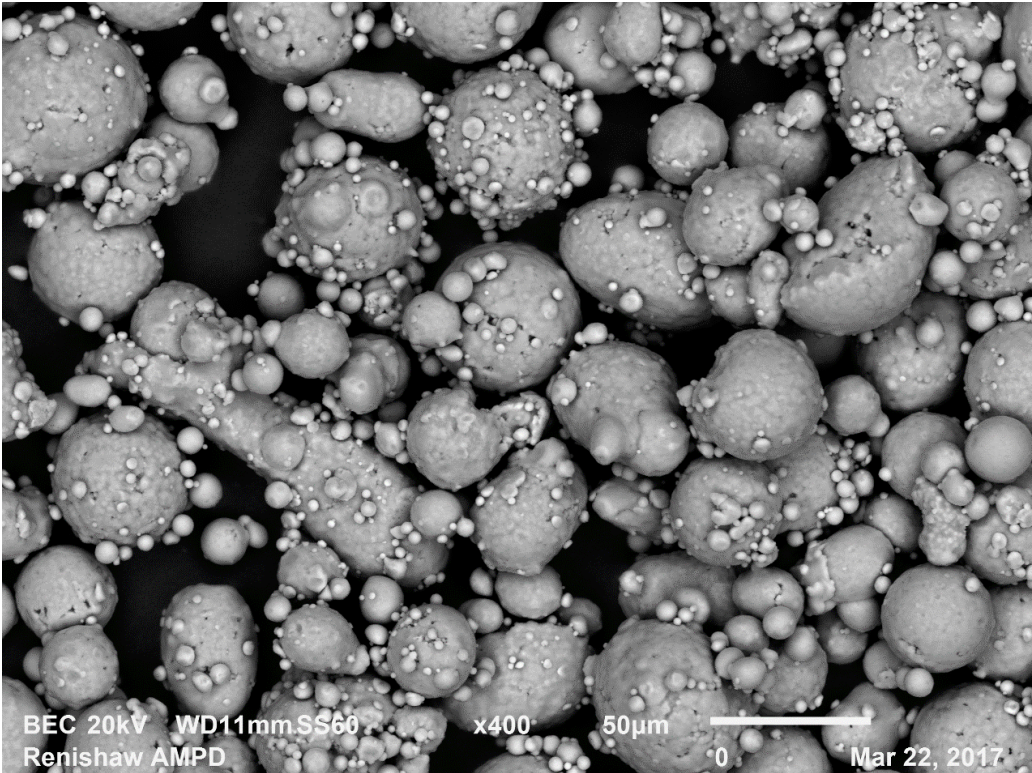


Figure 3.3: SEM image (backscattered electrons, 400x) of S 16D0534.

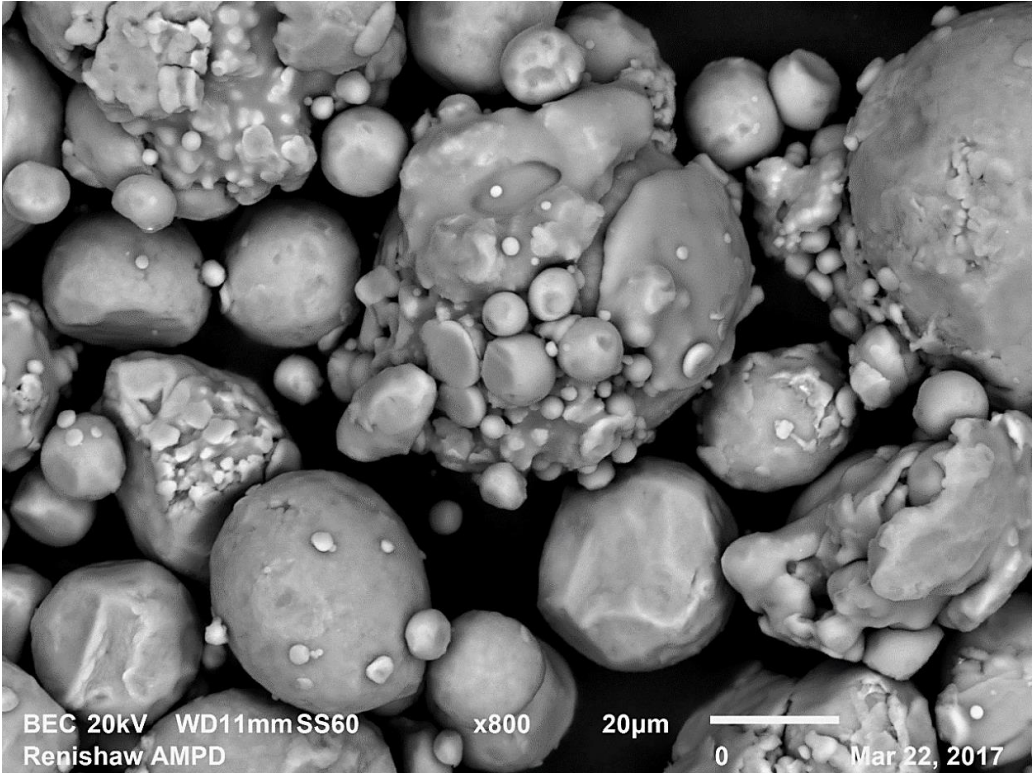


Figure 3.4: image (backscattered electrons, 800x) of T 0425.2.5.

3.1.2. Chemical Composition Analysis

As explained in the previous chapter, the results of the EDS analysis will be provided as an average composition of the evaluated spots, an example of that is shown in Fig. 3.5:

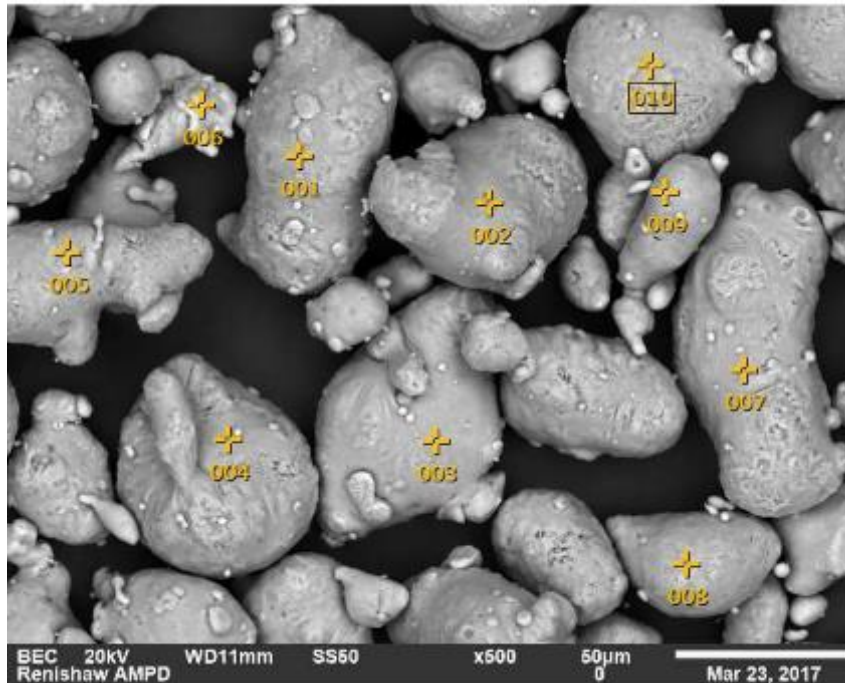


Figure 3.5: Selected spots for the EDS analysis (500x) of L UK3359.

The results of the test have been slightly manipulated to prevent the analysis from providing wrong results. It is possible to exclude some elements in the analysis or force the software to add others. In fact, it usually excludes elements which percentage is below a certain low limit. The elements that have been eliminated are:

- C, because it is the main component of the sticker, which is in direct contact with the powder.
- O, which is for sure present at least in a small amount (e.g. oxidized aluminium), although the machine is not that reliable in detecting non-metallic elements. If there is an issue with oxygen content, it is usually recommended to carry other types of analysis.

Mg instead has been manually added to every test result. This action was necessary because, even considering the powder composition to be the theoretical one in every single spot, its ideal content is quite low. Considering also that the EDS analyses single spots, it is not unusual for one of them to have a composition different from the bulk one, hence Mg element content can be locally even lower.

The results of the analysis are shown in Table 3.2:

Table 3.2: EDS analysis results.

Magnification	Composition	L 0001	L 0002	L 0003	L UK3359	S 16D0534	T 0425.2.5	V 14- 5034S
350x	Al (%)	88.07	89.91	87.51	89.56	86.40	84.58	88.17
	St Dev (%)	1.21	0.37	0.58	1.29	1.26	0.48	0.43
	Si (%)	11.63	9.79	10.00	10.29	13.26	15.09	11.61
	St Dev (%)	1.20	0.35	0.84	1.30	1.26	0.55	0.43
	Mg (%)	0.30	0.29	0.29	0.15	0.34	0.34	0.23
	St Dev (%)	0.01	0.02	0.02	0.01	0.00	0.07	0.01
500x	Al (%)	87.41	87.18	88.00	85.61	88.08	85.67	88.95
	St Dev (%)	0.43	0.13	2.04	1.50	0.30	1.73	0.94
	Si (%)	12.25	12.57	11.39	14.18	11.62	13.87	10.71
	St Dev (%)	0.45	0.10	1.92	1.47	0.30	1.72	0.92
	Mg (%)	0.34	0.25	0.39	0.23	0.29	0.46	0.34
	St Dev (%)	0.02	0.03	0.05	0.03	0.00	0.01	0.01

The ones presented in the previous table are the general results that can be analysed all together and be compared. It is although necessary to consider some singular cases that deviated from the average behaviour.

The first case analysed is the EDS analysis (350x magnification) of the L 0003 powder (Fig. 3.6).

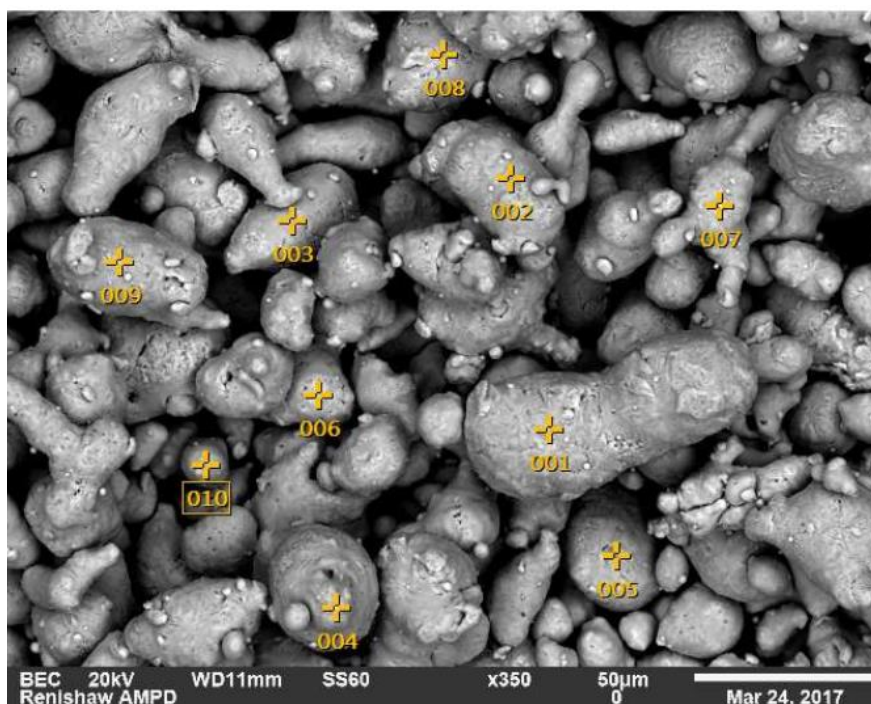


Figure 3.6: Spots selected for the EDS analysis (350x) of L 0003.

As opposed to what happens to the other analysed powders, the results did not show just the presence of Al, Si and Mg, but also Cu and Zn. In particular, spot number 8 and spot number 10 (in Fig. 3.6) exhibited the compositions visible in Table 3.3:

Table 3.3: Anomalous compositions in the EDS analysis of L 0003 (350x).

Spot	Al (%)	Si (%)	Mg (%)	Cu (%)	Zn (%)
Spot 8	72.96	7.58	0.57	6.82	12.08
Spot 10	89.33	7.34	0.22	-	3.11

Two possible causes have been given to try to explain this phenomenon. The first one considers the possibility that in some way the sample holder (brass) was analysed, maybe there was a cut in the carbon sticker and the electron beam, that has a certain radius, hit both the particle and the sample holder. The other possible explanation is that the actual local composition is shown and the analysed powder particle contains those elements. The latter seems more likely, because looking at the picture, especially point 8, the analysed spot was chosen as closer as possible to the centre of the particle and it seems very unlikely that the electron beam hit something else.

L 0003 showed a spot with an anomalous composition even when analysed at a 500x magnification in another area of the sample (Fig. 3.7).

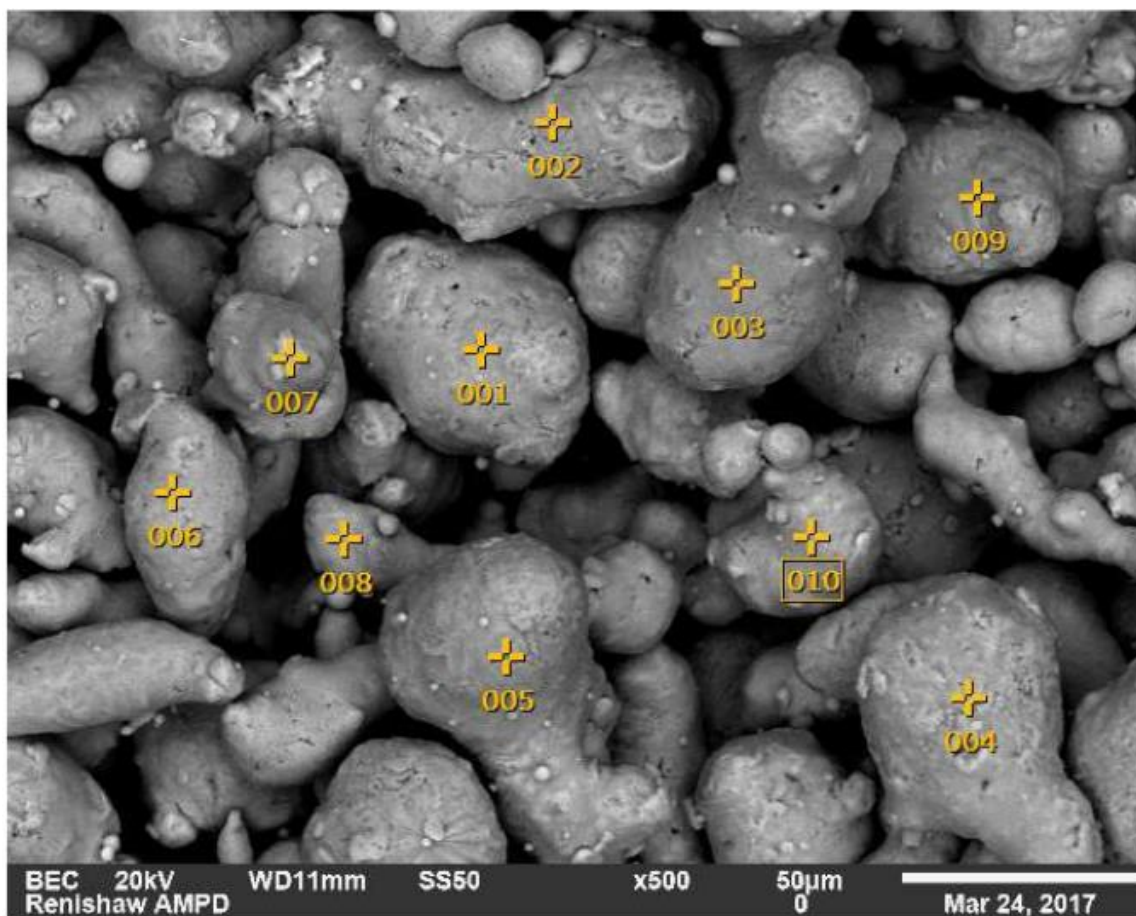


Figure 3.7: Spots selected for the EDS analysis (500x) of L 0003.

Spots 5 and 8 showed a relevant Fe content, as summarized in Table 3.4:

Table 3.4: Anomalous compositions in the EDS analysis of L 0003 (500x).

Spot	Al (%)	Si (%)	Mg (%)	Fe (%)
Spot 5	95.18	2.68	0.65	1.50
Spot 8	88.09	10.83	0.40	0.67

To explain that, the sample holder cannot be considered a cause this time. The possible explanations can then be an actual variation in composition or the presence of foreign particles in the powder (contamination).

It will be now briefly discussed the presence in the analysed powders of contaminants, that do not differ from the surrounding for slight chemical composition fluctuations, instead they are actual particles or objects made with completely different materials and shapes.

Traces of foreign objects have been found in L 0001, L 0002, L 0003.

Concerning L 0001, Fig. 3.8 shows the presence of a contaminant particle.

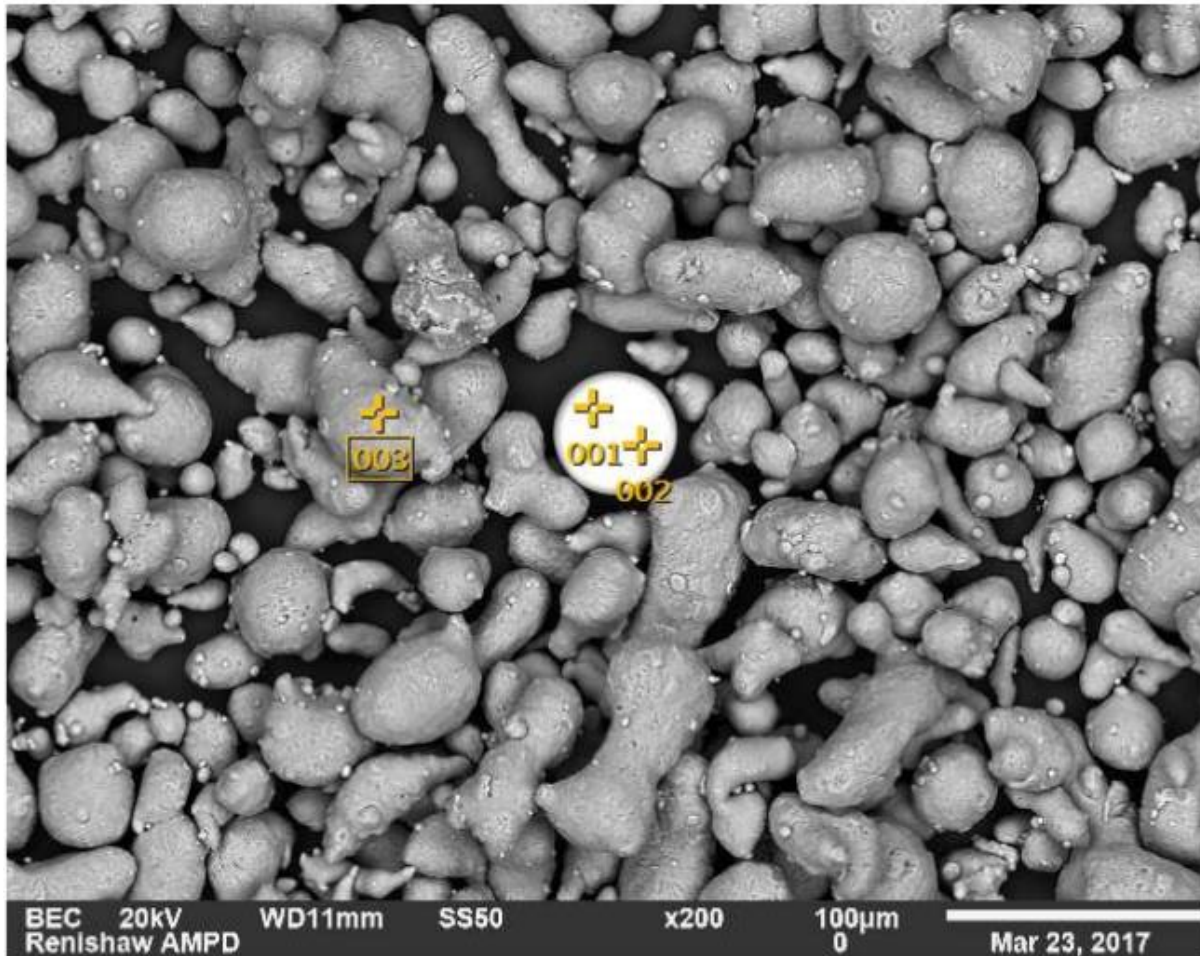


Figure 3.8: EDS analysis of L 0001 and a foreign particle (200x).

By comparing the results of the EDS analysis (Fig. 3.9, Fig. 3.10 and Table 3.5), it is possible to conclude what is evident even just having a look at the image, without the composition analysis: that particle is not AlSi10Mg, in fact it does not have the same colour and its shape is too regular.

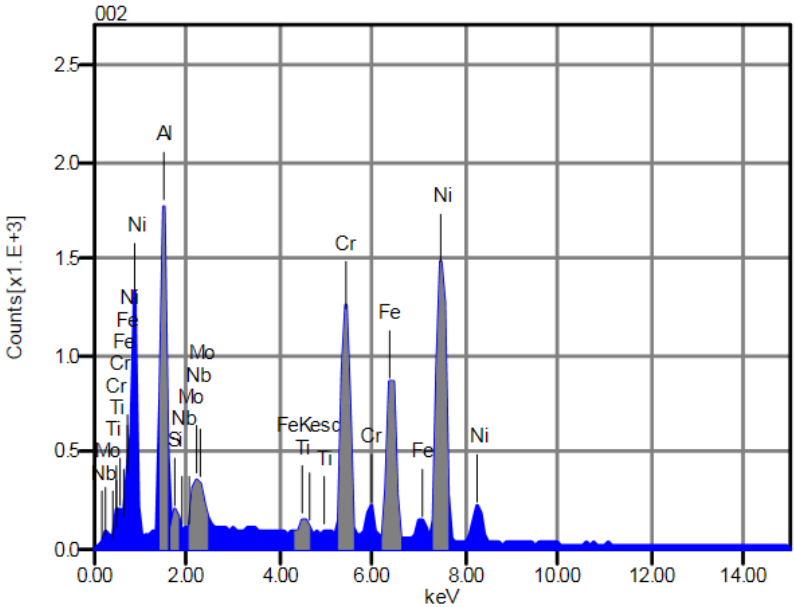


Figure 3.9: EDS analysis of spot 2.

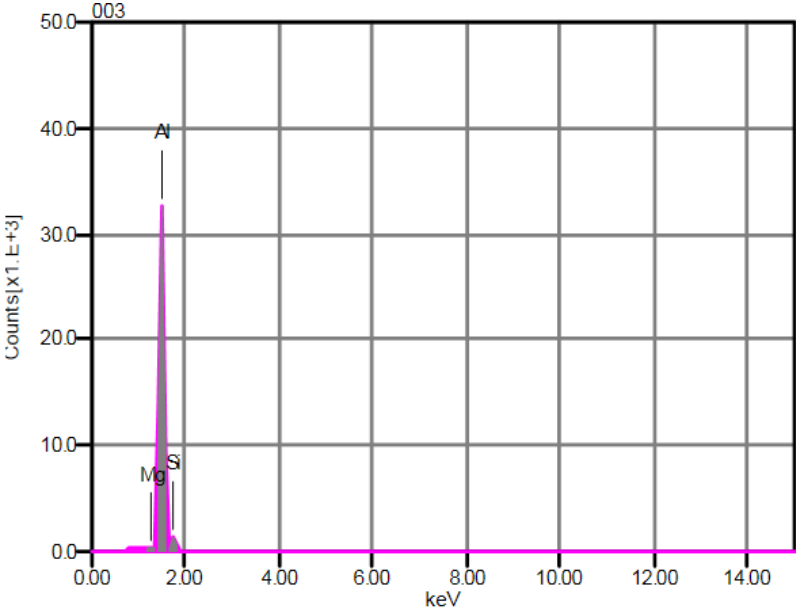


Figure 3.10: EDS analysis of spot 3.

Table 3.5: Chemical composition of L 0001 (spot 3) and foreign particle (spot 1 and 2).

Spot	Al (%)	Si (%)	Mg (%)	Fe (%)	Ti (%)	Cr (%)	Ni (%)	Nb (%)	Mo (%)
Spot 1	4.31	-	-	20.72	0.91	19.58	54.48	-	-
Spot 2	10.39	0.75	-	17.29	0.77	16.77	47.35	4.07	2.62
Spot 3	87.22	12.52	0.26	-	-	-	-	-	-

More tests like the one previously described were conducted on that powder, but on different samples, and there was always some form of contaminant.

It is interesting to notice that in L 0001 sample were found also other types of foreign objects. Some sort of fibres was detected (Fig. 3.11), in addition to some other particles (Fig. 3.12) which chemical composition is very similar to the one showed in Table 3.5.

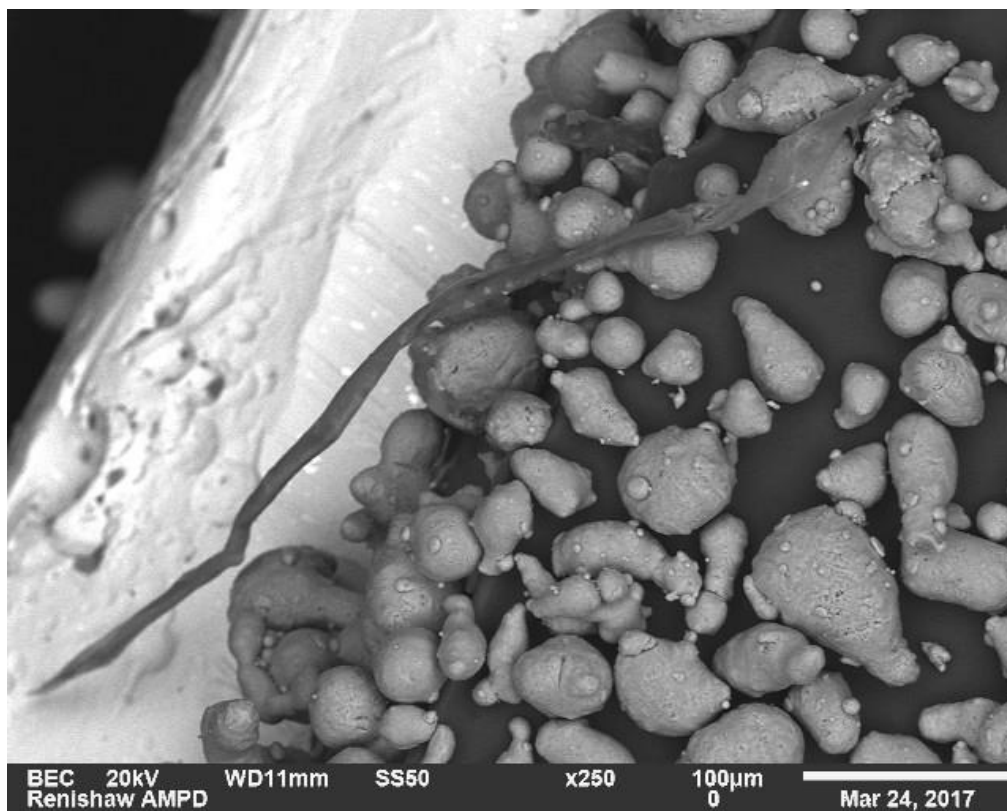


Figure 3.11: Image of L 0001 and a fibre (backscattered electrons, 250x).

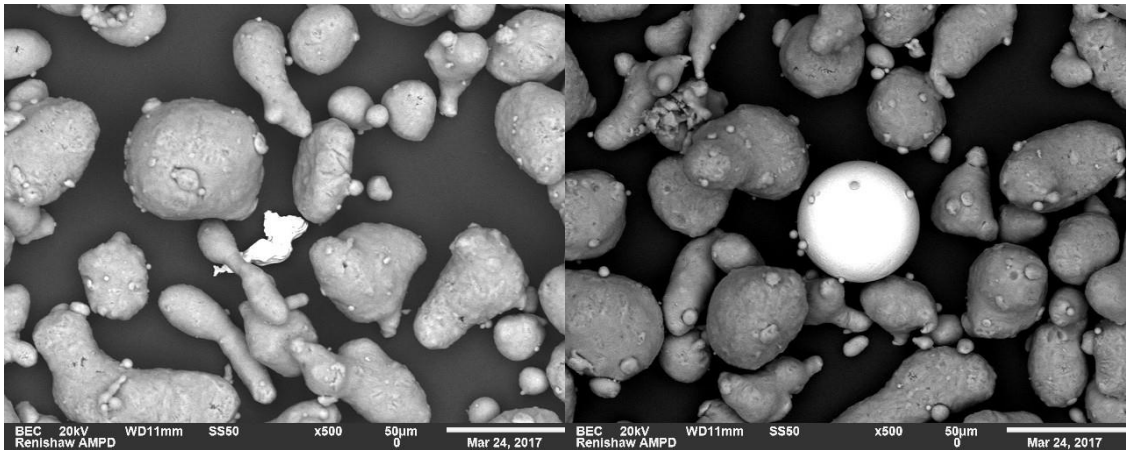


Figure 3.12: Image of L 0001 and some Ni alloy particles found (backscattered electrons, 500x).

Regarding the nature of the fibre shown, its EDS analysis is not going to be provided because it is too affected by the surrounding. In fact, the fibre is quite thin and probably organic, hence its analysis is greatly influenced by the aluminium in the surrounding and it is not possible to distinguish if the detected carbon comes from the fibre itself or from the sticker.

These fibres were not an L 0001 prerogative, in fact they showed up also during the analysis of the L 0002 (Fig. 3.13) and especially L 0003 powder, in a much greater quantity (Fig. 3.14, Fig. 3.15).

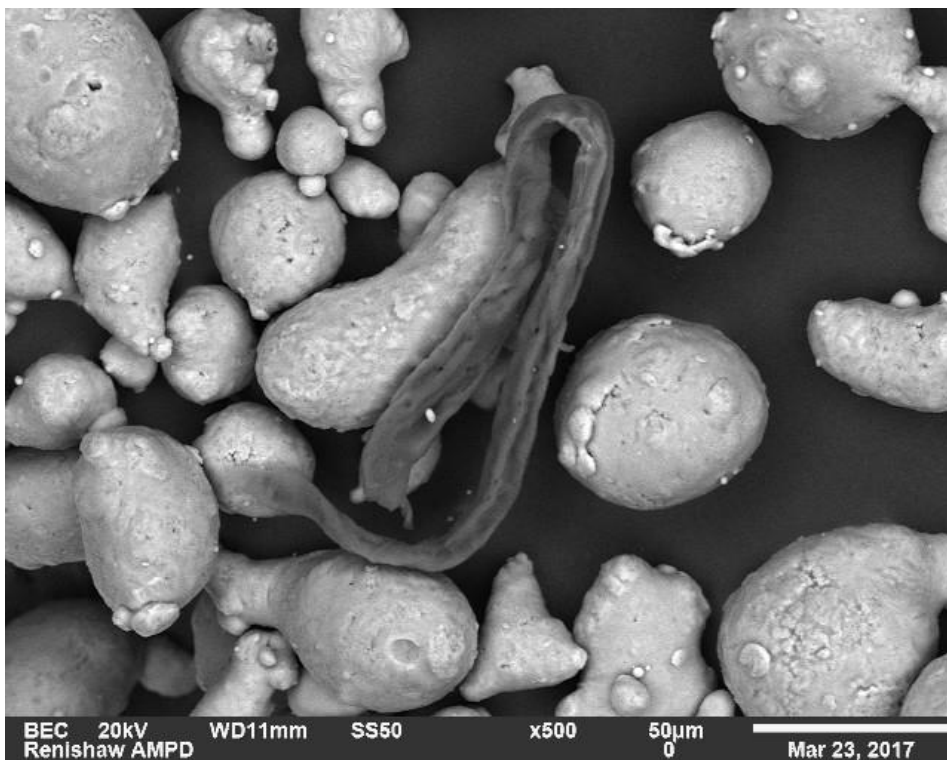


Figure 3.13: Image of L 0002 and a fibre (backscattered electrons, 500x).

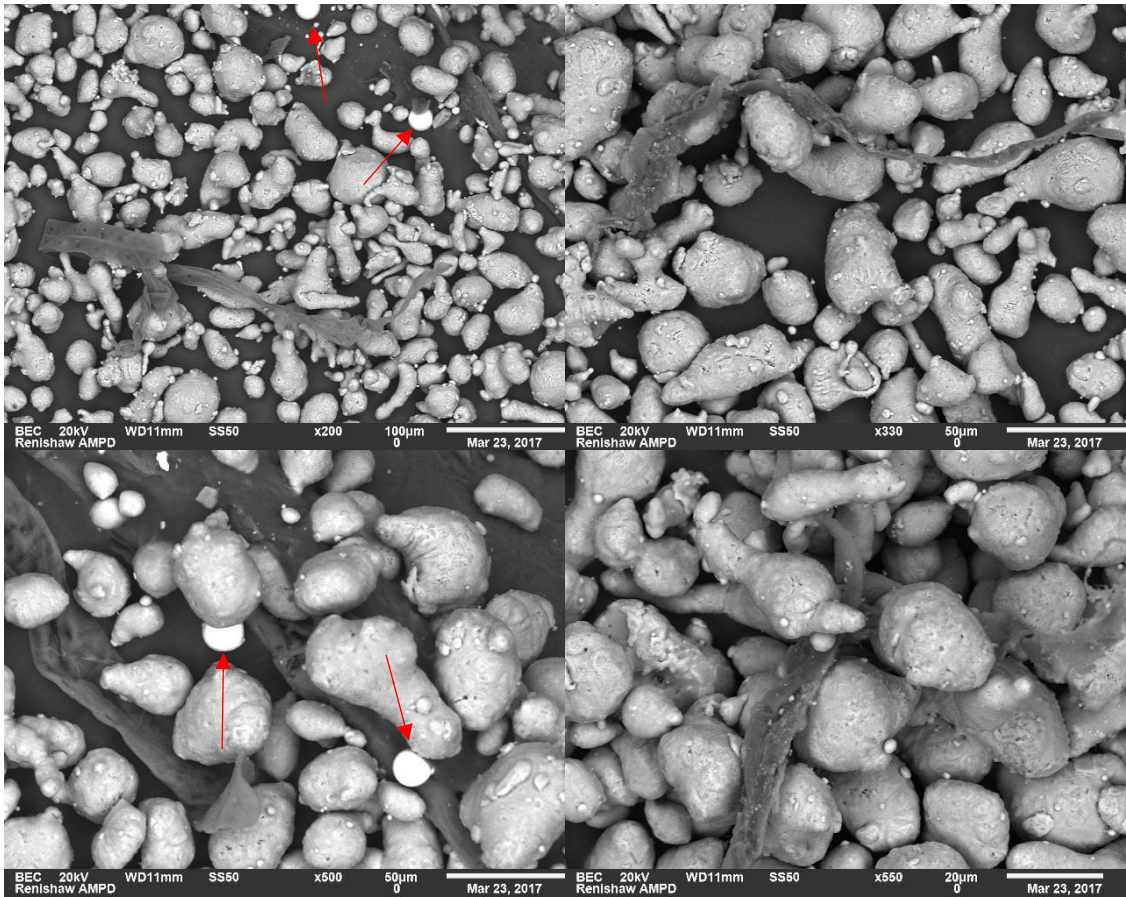


Figure 3.14: Image of L 0003 with fibres and particles found in the sample (backscattered electrons, 200x, 330x, 500x and 550x).

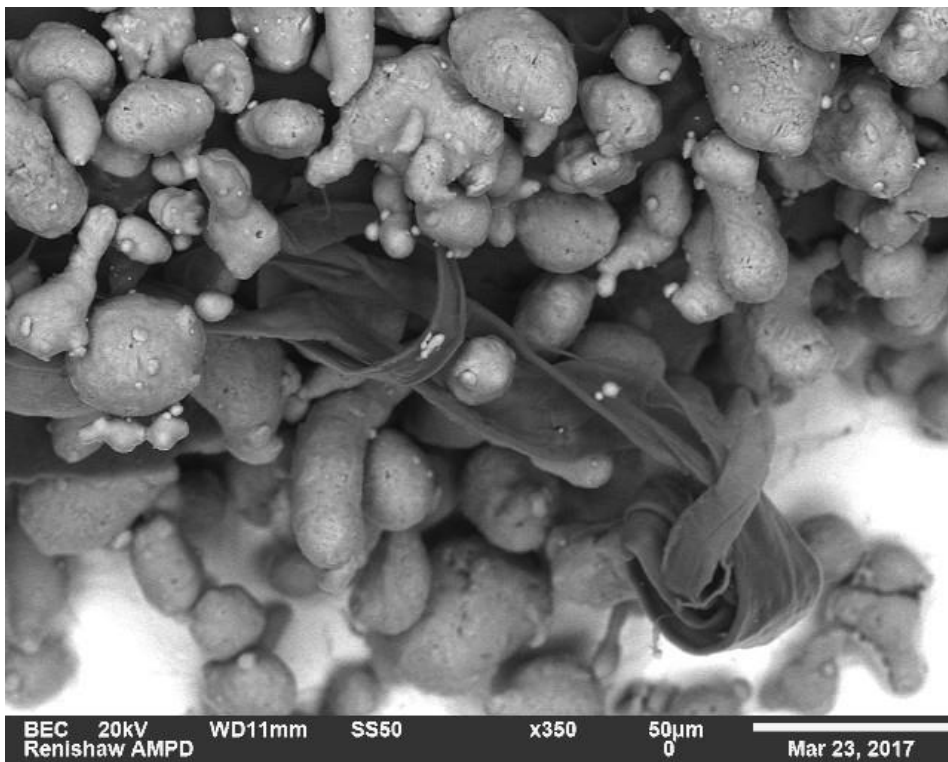


Figure 3.15: Image of L 0003 and a tangled fibre (backscattered electrons, 350x).

Even in the L 0003 powder a lot of foreign particles with different chemical compositions, ranging from Ti alloys (Fig. 3.16, Fig. 3.17, Table 3.6) to Ni alloys, were found.

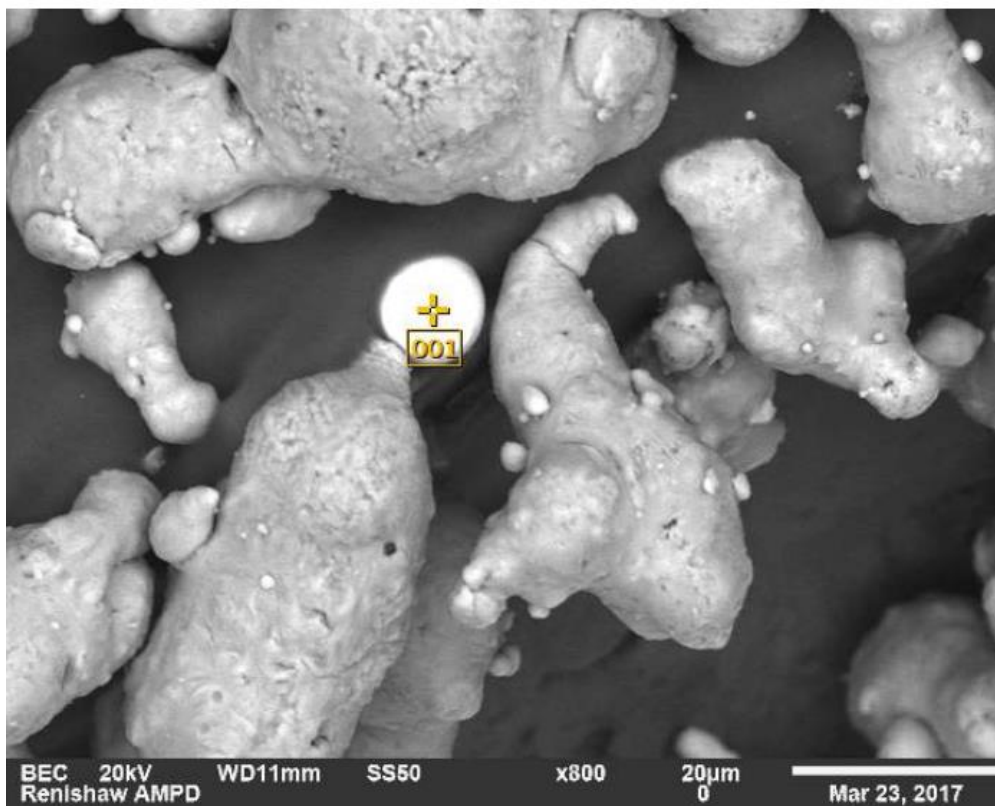


Figure 3.16: Spot selected for the EDS analysis of the contaminant found in L 0003 (backscattered electrons, 800x).

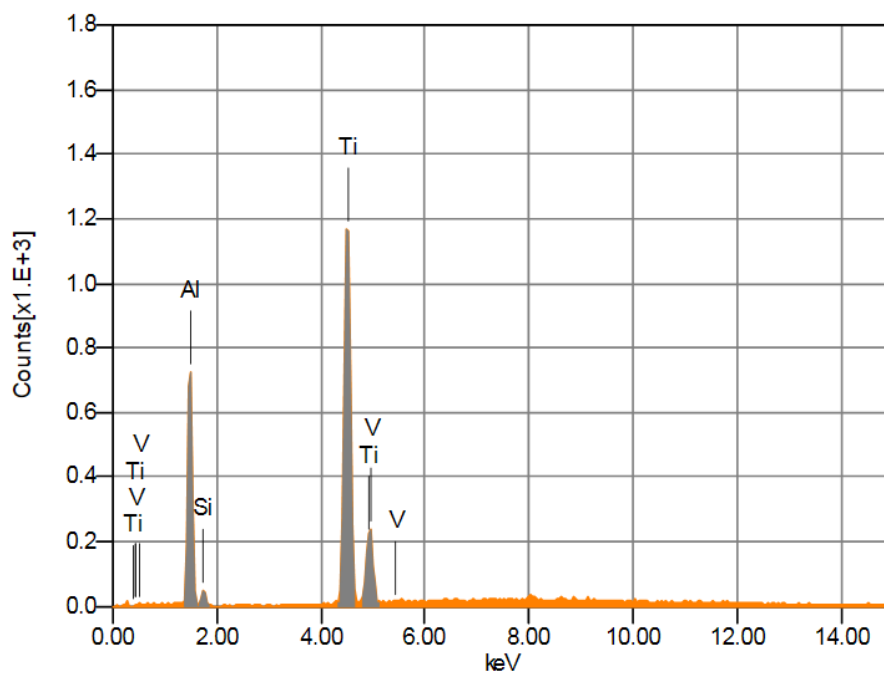


Figure 3.17: EDS analysis of the contaminant found in L 0003.

Table 3.6: Chemical composition of the contaminant found in L 0003.

Al (%)	Si (%)	Ti (%)	V (%)
18.36	1.65	73.91	6.08

It is difficult to determine how the contaminants reached the powder. There are several possibilities, for example it can be a production issue, a container cleanliness problem or it may have been contaminated after being sold. It is not even possible to understand if the contamination was caused by the person who conducted the tests or not.

Although the possibility that somehow the samples were contaminated before leaving the producer's facility seems to be more likely. Considering, as an example, Fig. 3.15, it seems very unlikely that a fibre like that went in contact with the powder just before the test, when the container was opened. Its shape and the way it is tangled, make it look more like a pre-existing contamination.

Another consideration that makes it seem more likely for these powder to have been contaminated during the producing or storing steps, is the fact that all the powders were tested the same day using the same equipment. Considering that, it would be odd if the contamination were caused by the operator and just three powders were affected. Moreover, the contaminants are very different (Ti particles, Ni particles, fibres) and it would be hard for an operator to contaminate a sample in such different ways.

3.2. Density Measurement

The absolute density for each sample has been evaluated, the results are provided in Table 3.7:

Table 3.7: Absolute density analysis results.

Powder	Density (g/cm ³)	Standard Deviation
L 0001	2.6640	0.0004
L 0002	2.6523	0.0012
L 0003	2.6511	0.0009
L UK3359	2.6471	0.0008
S 16D0534	2.6831	0.0006
T 0425.2.5	2.6393	0.0003
V 14-5034S	2.6515	0.0003

The variation of temperature and density throughout the entire test are also available. In Fig. 3.18 is shown, as an example, the case of L 0002, because it is the powder with the highest standard deviation. It can be noticed that the variations of both the properties are very little, hence the test can be considered reliable, not just for this powder, but also for all the others.

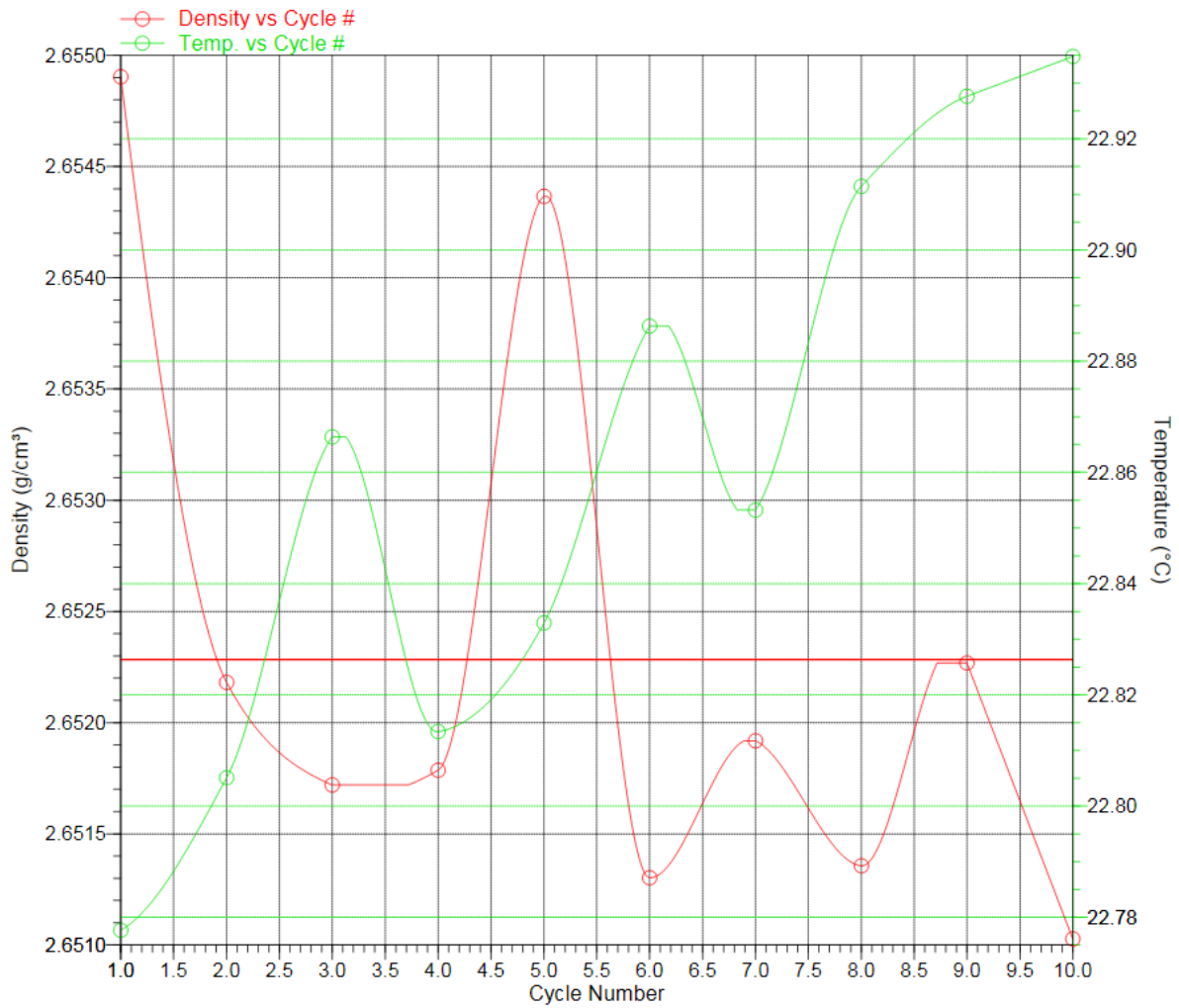


Figure 3.18: Temperature and density trend during the L 0002 test.

3.3. Particle Size Distribution

The average results of the test conducted with the particle size analyser are shown in Fig. 3.19 and Table 3.8:

Table 3.8: Particle size distribution analysis results.

Powder	D(10) (µm)	D(50) (µm)	D(90) (µm)
L 0001	30.2	49.3	80.2
L 0002	29.1	47.9	78.3
L 0003	28.1	47.6	79
L UK3359	29.6	46.3	71.6
S 16D0534	20.6	34.7	56.2
T 0425.2.5	23.4	49.9	84.7
V 14-5034S	18.7	31.8	53.4

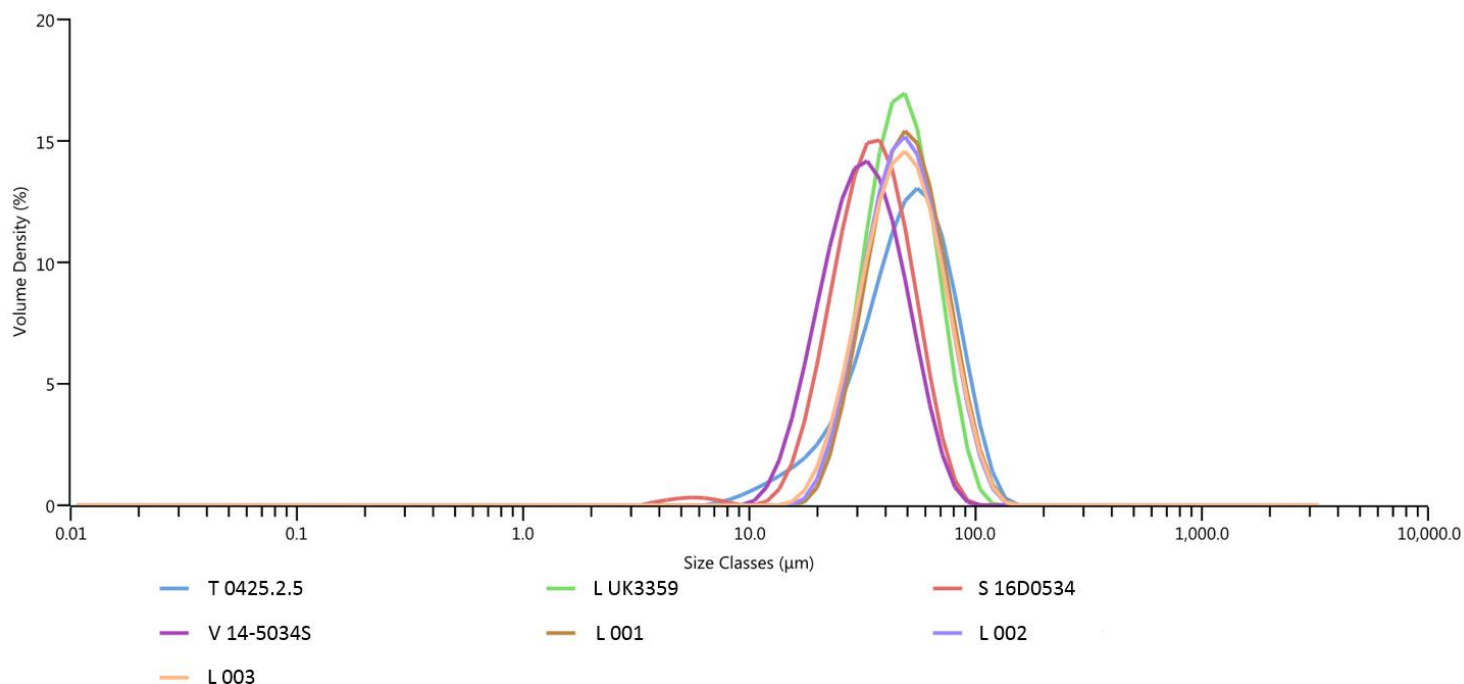


Figure 3.19: Particle size distribution graph.

In the above graph, a certain percentage of the total volume is shown for different values of particle size, evaluated as the average diameter of the particle. It must be considered that AlSi10Mg particles are in general not very regular and their shape is quite different from a sphere. Because of that the size evaluation cannot be considered as reliable as it can be with more regular particles. It is still a good instrument to compare powders of the same material.

The indexes shown in table 3.8 are the corresponding diameters values in μm reached when considering, from the left to the right, respectively 10%, 50% and 90% of the area under the curve. They can be used to evaluate and compare the different curves, the most important one is usually $D(50)$, also known as mass median diameter.

It is fundamental to consider that all the results are volume-based. In fact, if for example 15% of the distribution lies in the range 16.4 - 18.7 μm , it means that 15% of the total volume of all the particles is in that range. That can lead to some counterintuitive results: for example, if a sample consists of just two sizes of particles and 50% of them have a 1 μm diameter, while the other half has a 10 μm diameter, and assuming that all particles are spheres; the latter group volume fraction is 1000 times of the volume of the other one. Hence 50% of the particles consist in 99.9% of the volume particle size distribution.

Assuming the particle shape as a perfect sphere is an approximation, especially for aluminium particles that are usually very irregular. The Mastersizer 3000 uses the volume of a particle to determine its shape, hence its diameter. This process will now be explained through an example (Fig. 3.20). [45]

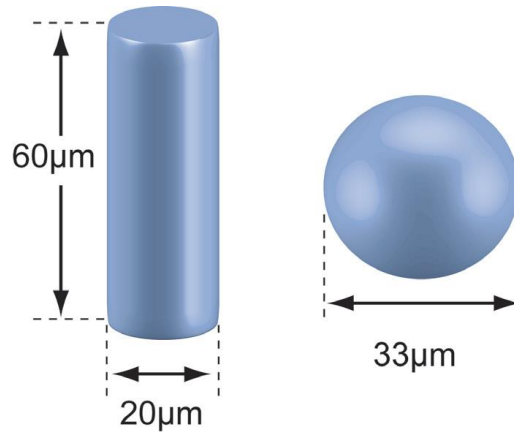


Figure 3.20: example of irregular particle and relative sphere with the same volume value. [45]

The particle shown on the left in the previous figure is a cylinder and its volume can be evaluated as:

$$V = \pi \cdot (10 \mu m)^2 \cdot 60 \mu m \approx 18850 \mu m^3 \quad (3.1)$$

The corresponding sphere of equivalent volume has a diameter of:

$$\sqrt[3]{\frac{6V}{\pi}} = 33 \mu m \quad (3.2)$$

From the analysis of the previously shown results, some information can be gathered to try to explain any possible difference between the several studied powders, concerning the flowing behaviour.

First of all, it can be noticed that S 16D0534 and V 14-5034S have a lower D(50) with respect to the other samples, in fact it can be noticed, by looking at Fig. 3.19, that these two powders peaks present lower diameter values. As a consequence of that, in that case, particles from a powder with a bigger D(50) (e.g. L 0001) can be considered bigger on average. This conclusion can be confirmed by comparing two images of these powders acquired with the SEM at the same low magnification (Fig. 3.21).

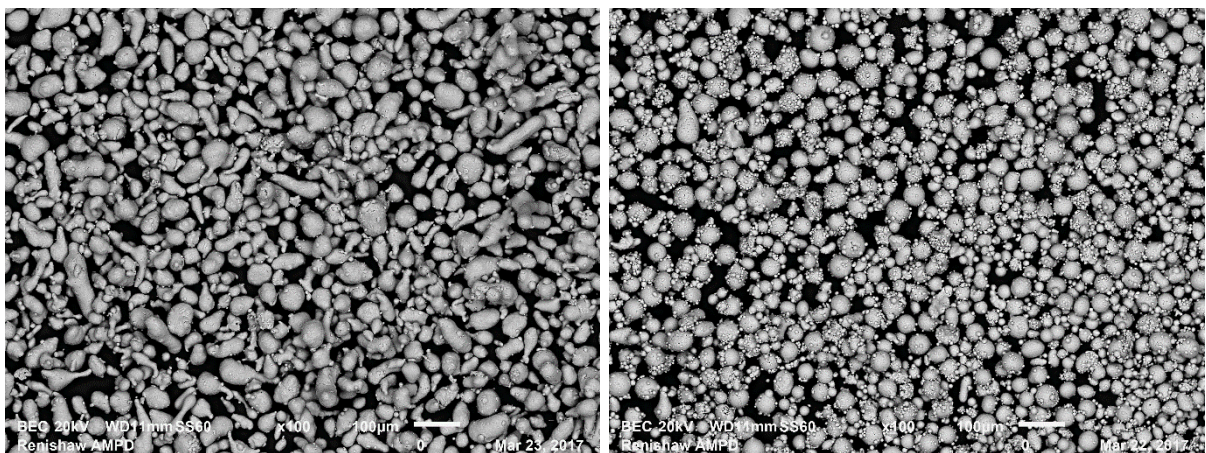


Figure 3.21: SEM image (backscattered electrons, 100x) of L 0001 (left) and S 16D0534 (right).

It can also be noticed that T 0425.2.5, unlike the other powders, has a very asymmetric curve (Fig. 3.22). This can also be confirmed by the fact that its D(10) is concretely lower than the D(10) for other powders with a similar D(50) value (e.g. L 0001)

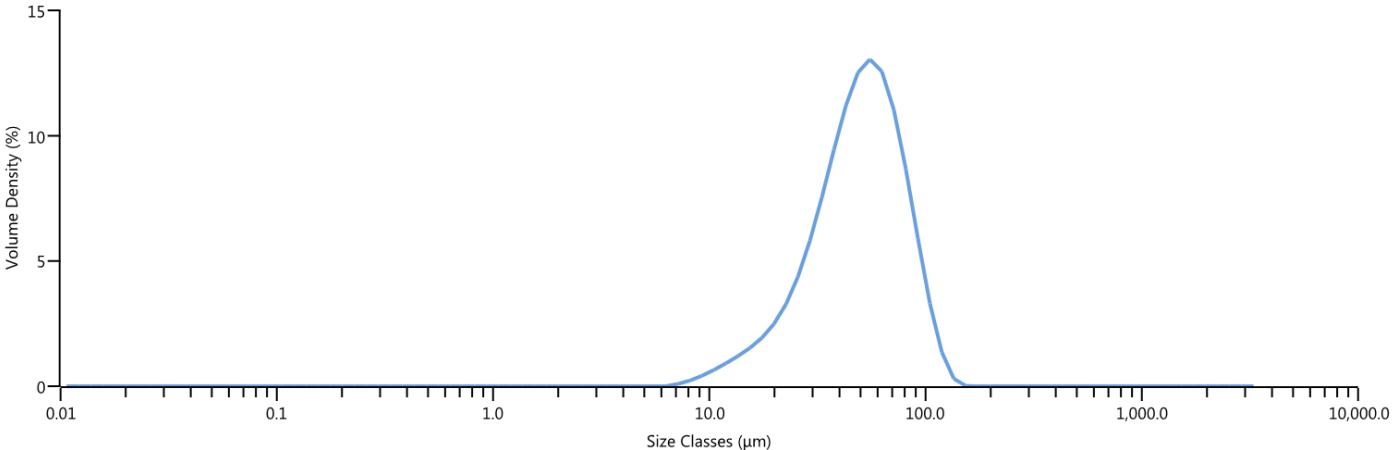


Figure 3.22: Particle size distribution graph of T 0425.2.5.

According to the previous analysis, it is expected for this powder to show a greater number of small particles, if visually analysed. A comparison between this one and a powder with a more symmetric curve shape (L 0002) is shown in Fig. 3.23.

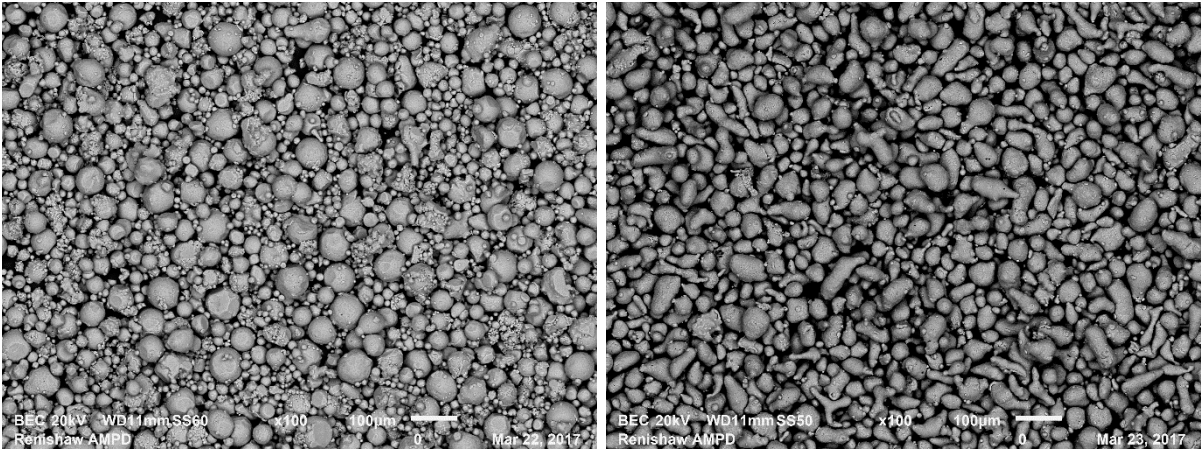


Figure 3.23: SEM images (backscattered electrons, 100x) of T 0425.2.5 (left) and L 0002 (right).

By comparing these images, it is evident that T 0425.2.5 has a wider particle size range, in fact L 0002 appears a lot more homogeneous.

Another important result obtained during the test is relative to the powder S 16D0534 (Fig. 3.24).

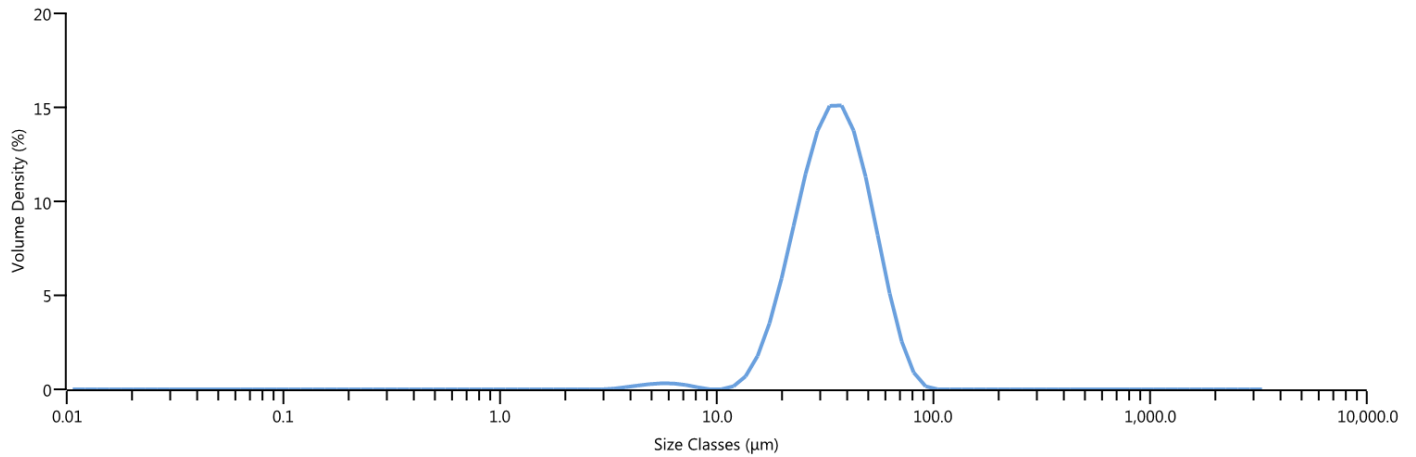


Figure 3.24: Particle size distribution graph of S 16D0534.

That kind of powders are called bimodal, because they have a secondary peak independent from the first one. By analysing the particle size distribution table obtained from the experiment (Fig. 3.25), it can be stated that the secondary Gaussian curve lies approximately in the 3µm - 8µm range, with the peak in the middle.

Size (µm)	% Volume In
2.13	0.00
2.42	0.00
2.75	0.00
3.12	0.03
3.55	0.10
4.03	0.17
4.58	0.24
5.21	0.28
5.92	0.27
6.72	0.21
7.64	0.10
8.68	0.00
9.86	0.00
11.2	0.12

Figure 3.25: Particle size distribution results table, relative to the secondary Gaussian part of the graph.

To try to understand the causes of this behaviour during the test, the SEM images of the powder must be analysed (Fig. 3.26, Fig. 3.27).

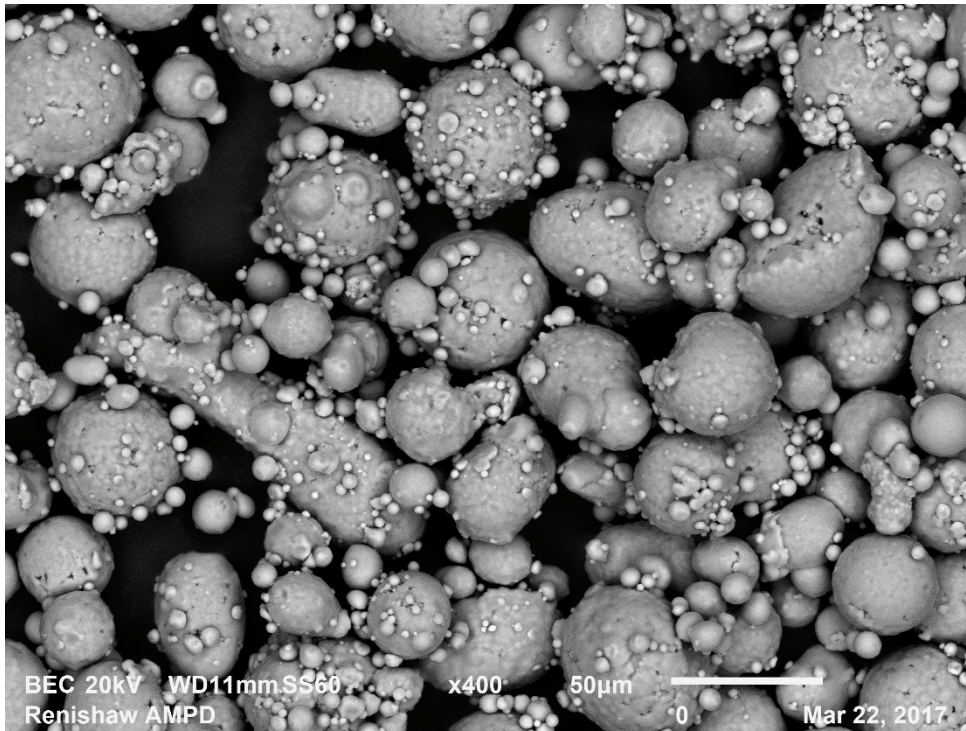


Figure 3.26: SEM image (backscattered electrons, 400x) of S 16D0534.

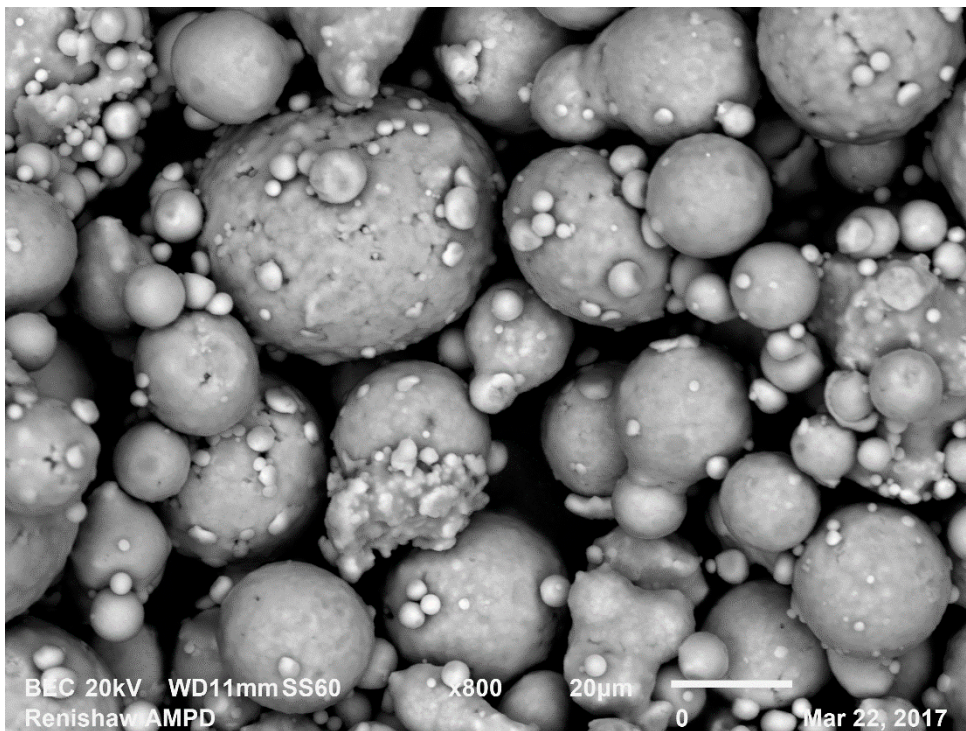


Figure 3.27: SEM image (backscattered electrons, 800x) of S 16D0534.

It does not seem to be present a fraction of the powder with the size described by the particle size distribution test. Especially analysing Fig. 3.27, it can be noted that the only particles that can meet the size requirements are the satellites, but they are not counted as

particle on their own by the test. Moreover, other powders have a similar quantity of satellites (e.g. V 14-5034S, Fig. 3.28) but are not bimodal (Fig. 3.29).

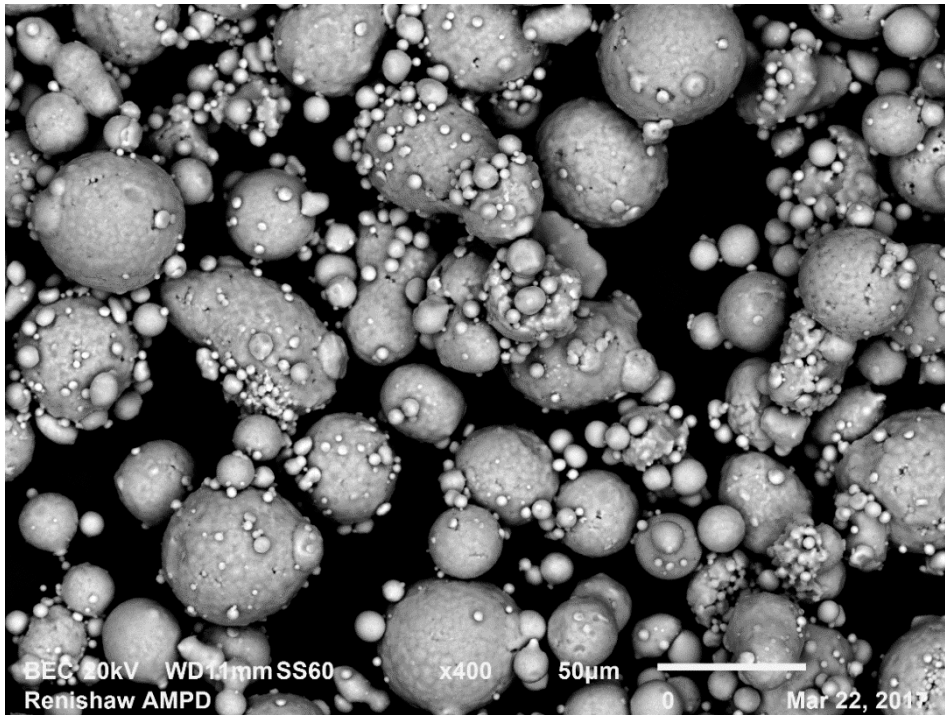


Figure 3.28: SEM image (backscattered electrons, 400x) of V 14-5034S.

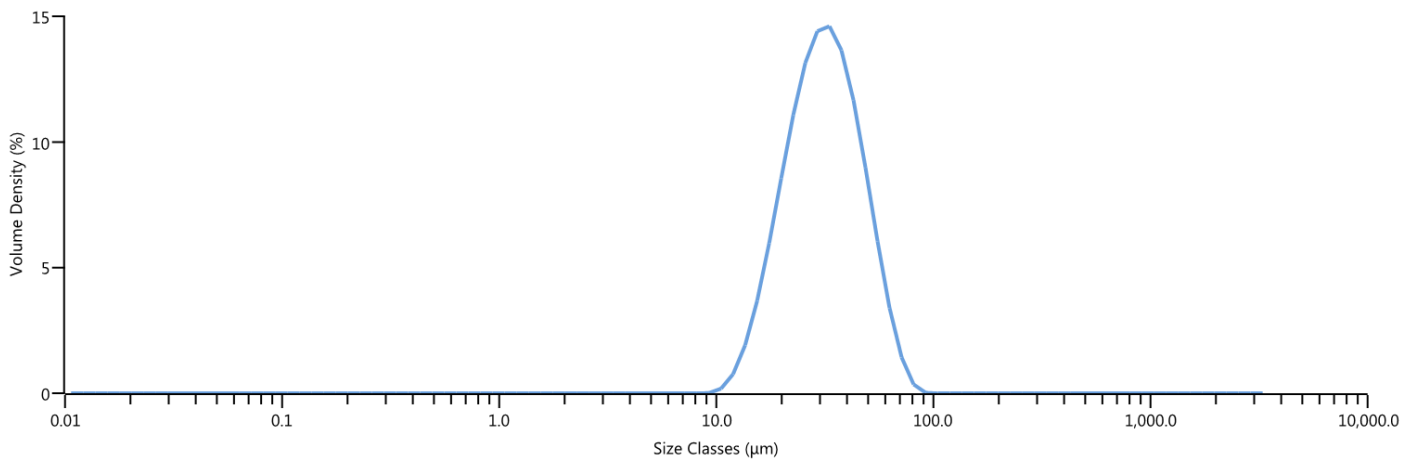


Figure 3.29: Particle size distribution graph of V 14-5034S.

By comparing Fig. 3.26 and Fig. 3.28, the two analysed powders result being morphologically very similar. There must be then a characteristic or a phenomenon that makes this relevant difference between these two particles possible. Considering that the only particles of acceptable size to be counted as part of the bimodal curve, are the satellites, the cause must be linked to their properties.

It has been investigated the possibility that the satellites were not strong enough to remain attached to the biggest particles during the test, that involves vibrations and air flowing. That would make them become particles on their own and then form a secondary peak during the

particle size distribution analysis. To prove that it has been tried to analyse the powders again after a vigorous shaking.

The experiment results of the shaken powder proved that, even if the satellite content was decreased for S 16D0534 (Fig. 3.30) or pretty much nullified for V 14-5034S (Fig. 3.31), the particle size distribution practically did not change. (Fig. 3.32, Fig. 3.33).

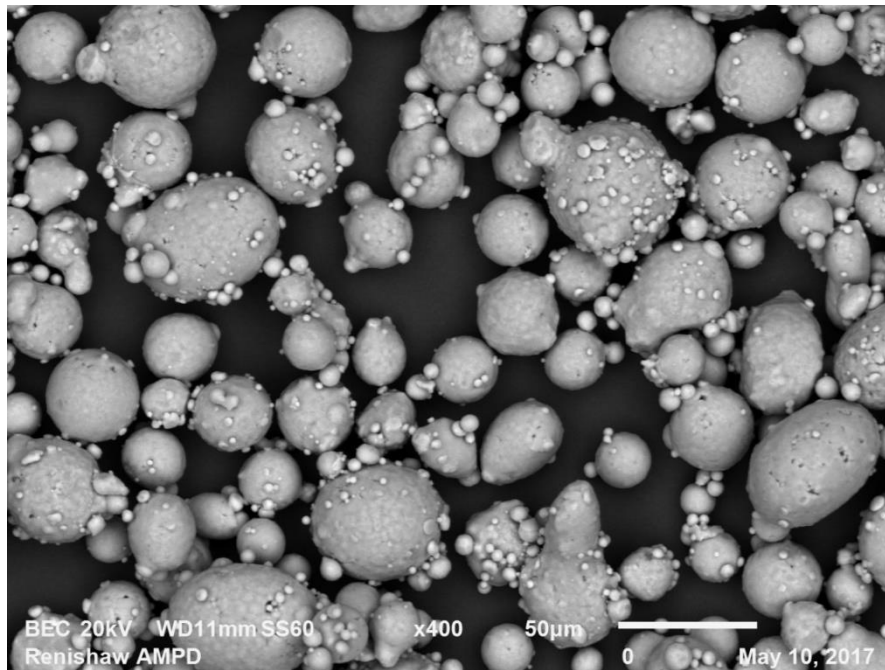


Figure 3.30: SEM image (backscattered electrons, 400x) of S 16D0534 after shaking.

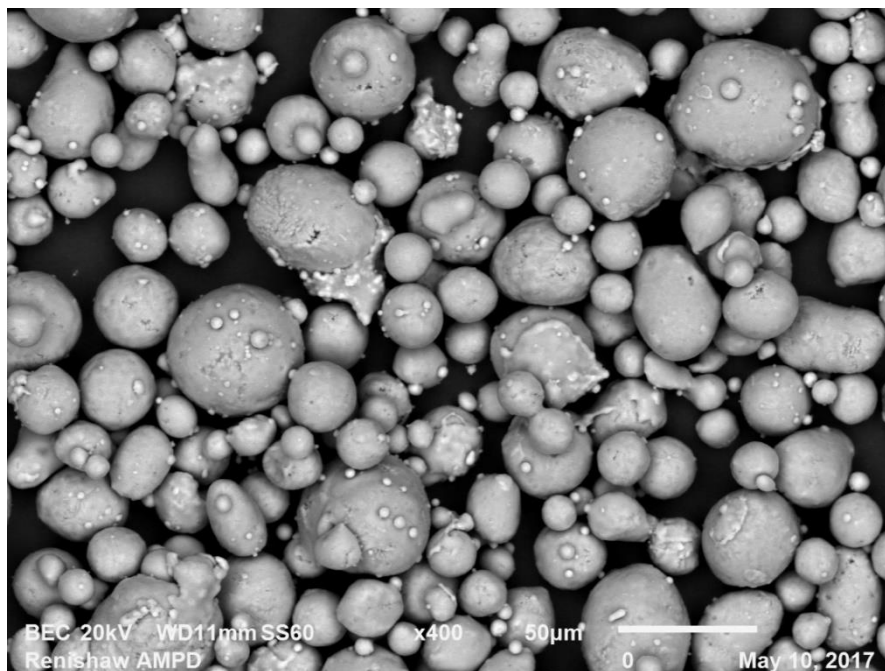


Figure 3.31: SEM image (backscattered electrons, 400x) of V 14-5034S after shaking.

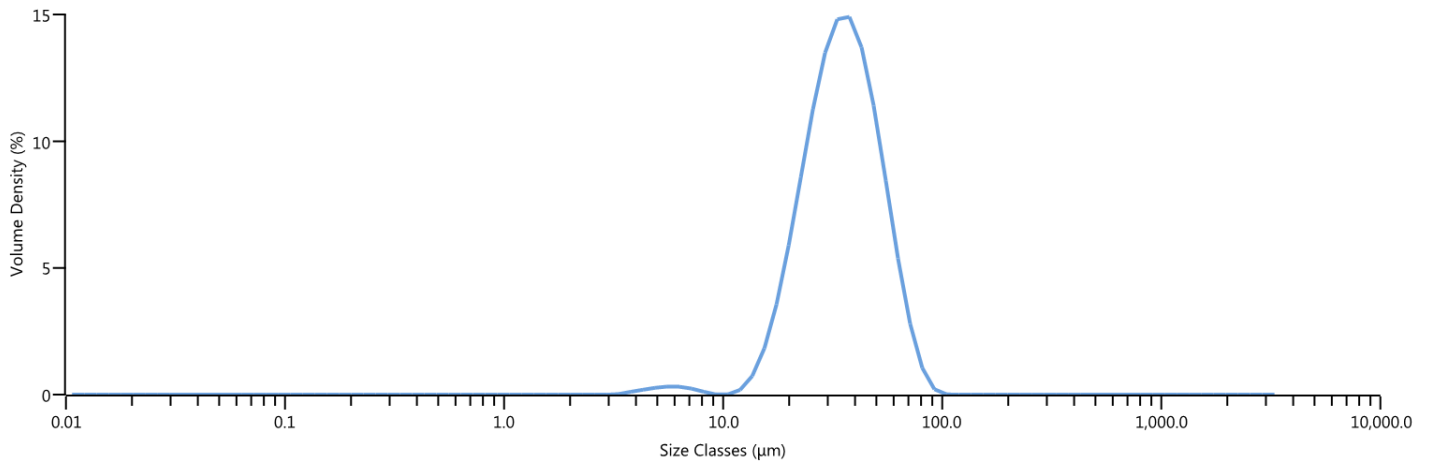


Figure 3.32: Particle size distribution graph of S 16D0534 after shaking.

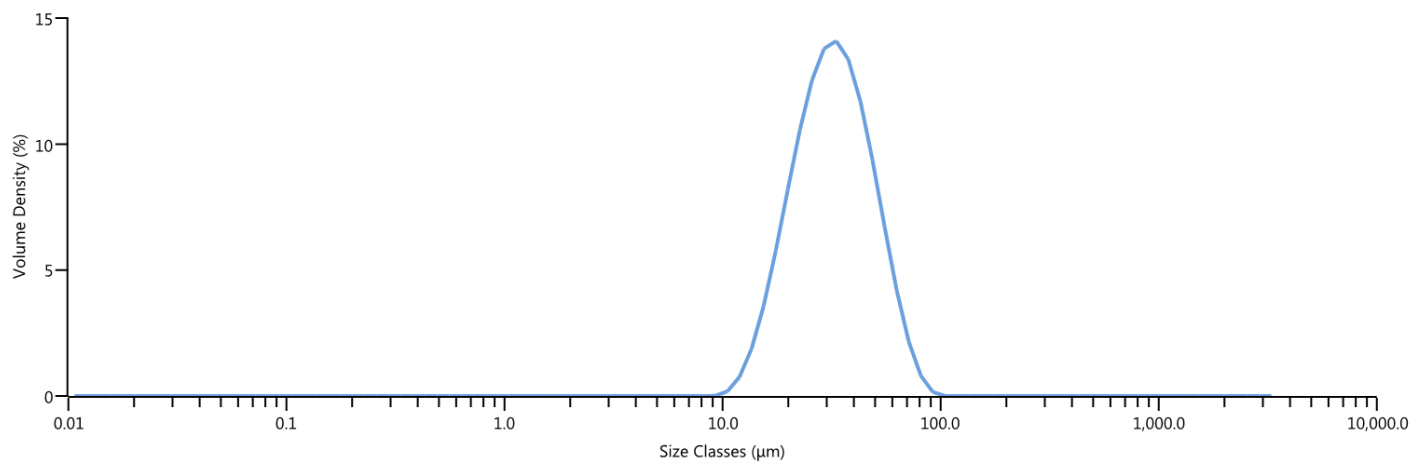


Figure 3.33: Particle size distribution graph of V 14-5034S after shaking.

These results look contradictory. In fact, the whole explanation, for which the secondary peak is formed by satellites particles that breaks apart during the particle size distribution evaluation, seems likely. Although, if this is true, then the V 14-5034S behaviour is odd: its particles should be strong enough to resist without breaking the stress exerted by the air flow during the particle size distribution test, which is strong enough to break apart S 16D0534's satellites, but, at the same time, they should be weak enough to be completely broke apart by the forces exerted during the shaking process, which are not strong enough to break apart most of the other powder's satellites. Hence V 14-5034S particles should be at the same time stronger and weaker than the other powder's ones.

It must be also considered that the previously described situation may be true, in fact shaking and aerating are two different mechanical solicitations, hence materials resist to them in different ways and the fact that a powder may be stronger than another one under certain circumstances, but weaker in other scenarios is possible.

3.4. Powder Flow Test

The results obtained from the powder flow test are shown in table 3.9:

Table 3.9: Powder flow test results.

Powder	Vessel	Tap	Average Flow (s/50g)	Average angle of repose (°)
L 0001	Carney	No	12.5	30.10
L 0002	Hall	Yes	63.4	30.19
L 0003	Did not flow			
L UK3359	Hall	Yes	70.6	31.88
S 16D0534	Carney	Yes	13.5	29.87
T 0425.2.5	Carney	No	11.3	28.26
V 14-5034S	Did not flow			

It can be noticed that all the powders tested showed similar average angle of repose values, hence, according to the table showed in the previous chapter (Table 2.4), they have a good/excellent flowability. However, it must be noticed that this value doesn't mean that these powders will have a "good" flowing behaviour once processed, instead it means that they meet the minimum requirement to be considered processable. The most important thing to evaluate is whether the powder flowed and which vessel was required. Generally, a powder that flows through the Hall funnel shows an appropriate behaviour once processed in the additive manufacturing machine. On the opposite, a powder that does not flow, even through the Carney funnel, is considered to have "bad" flow properties, because it will probably cause problems in the machine (e.g. clogging).

The powders that did flow through the Carney funnel are considered critical, because it is not possible, just by analysing the results of that test, to define if they will behave properly or not.

All the samples tested can then be divided into three groups, as shown in table 3.10:

Table 3.10: Powders groups, as stated by their predicted machining behaviour.

"Good" behaviour	Uncertain behaviour	"Bad" behaviour
L 0002	L 0001	L 0003
L UK3359	S 16D0534	V 14-5034S
	T 0425.2.5	

For each powder, has been taken a picture of the internal part of the funnel once the powder flowed through it, to visually analyse its residue. It is interesting to compare the differences between the powder residue for a sample that easily flowed through the Hall funnel (good behaviour), like L UK3359 (Fig. 3.34) and a sample that required a tap to flow through the Carney funnel (uncertain, probably bad, behaviour), like S 16D0534 (Fig. 3.35).



Figure 3.34: Powder residue of L UK3359 in the Hall funnel.



Figure 3.35: Powder residue of S 16D0534 in the Carney funnel.

By comparing the previous images, it can be noticed that in the first case the powder residue is more homogeneous, while in the Carney funnel it is visibly irregular, with some spots when the powder did not flow. That can be linked a phenomenon like local agglomeration.

Another important parameter from Table 3.9 is the average flow. To obtain it, the operator must use a chronometer to evaluate the time that the powder requires to fully flow through the funnel, that leads of course to a great level of uncertainty on the results, dependent on how ready the operator was. If the powder mass was not 50g, the results must be related to that quantity. Obviously, the time is dependent on the funnel used, in fact it can be noticed that the powders that were tested with the Carney funnel required less time, this is linked to the orifice dimension.

It can generally be considered that a lower value of average hall flow leads to a more performing powder that flows more easily.

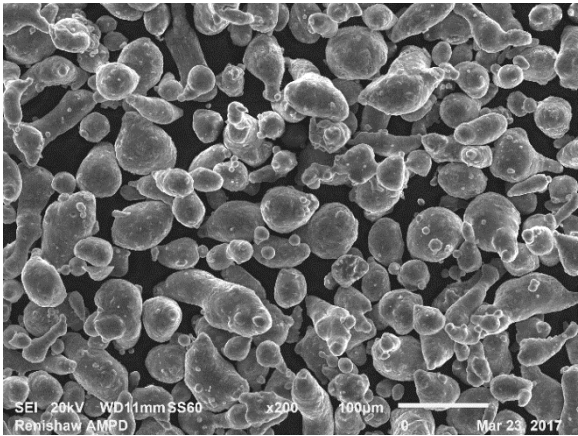
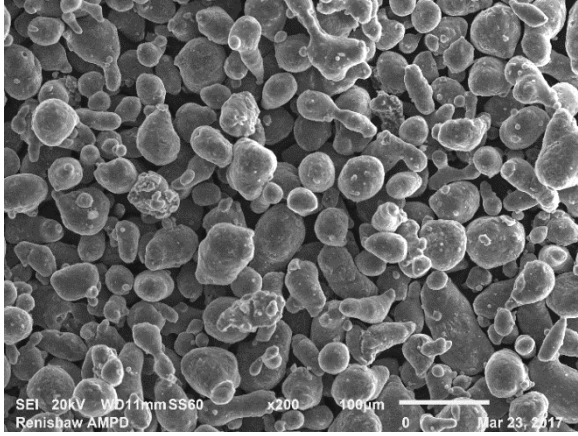
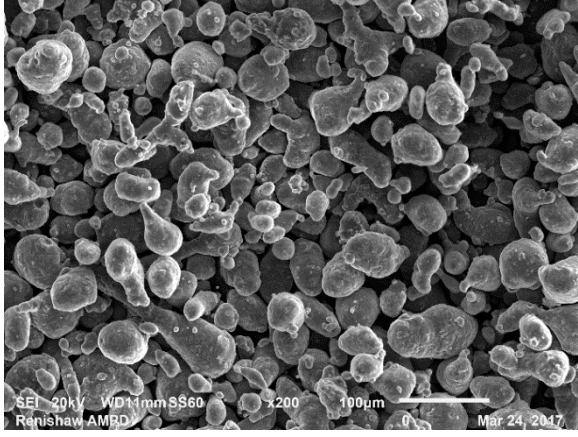
The necessity of a tap is also very important: the fact that a powder needs an external stimulus to begin to flow, hence it cannot freely move just under the influence of gravity, means that it has a worse behaviour than its counterpart that does not require a tap. In fact, it can be noticed that S 16D0534 (Carney funnel, tap required) has a greater value of average flow than L 0001 and T 0425.2.5 (Carney funnel, tap not required), hence it is confirmed that, for these results, its flowing behaviour will be worse.

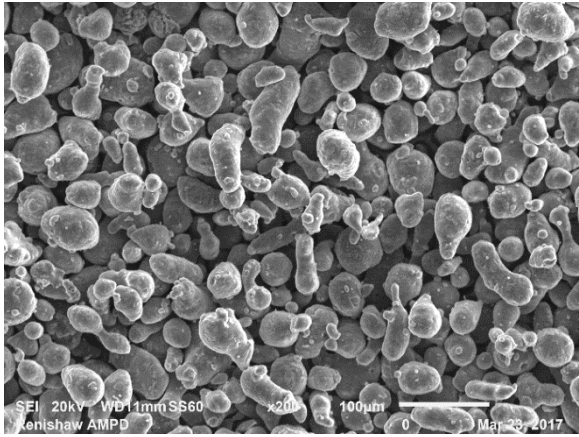
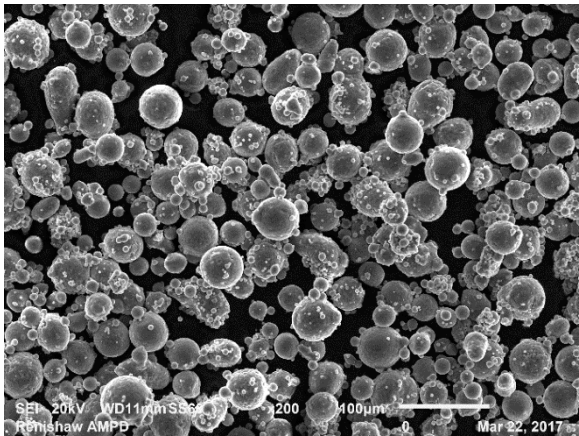
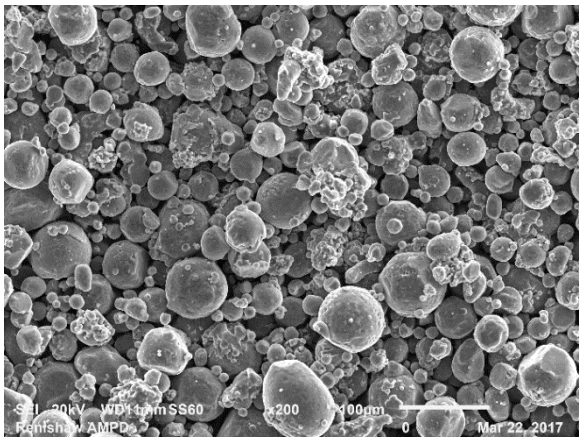
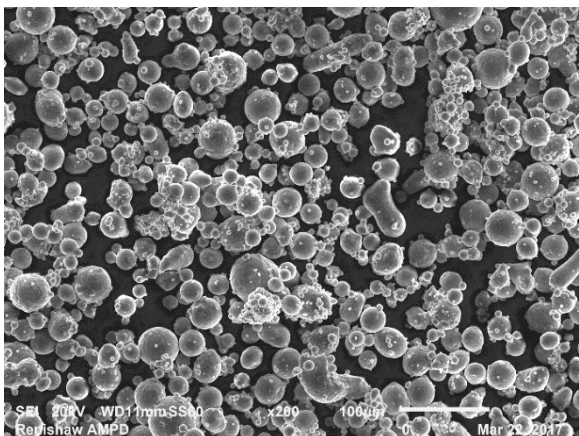
It is interesting to compare the results of that test with the ones obtained from the previous ones, especially because this simple procedure is the one used more often and considered quite reliable when it comes to evaluate the flowing properties, hence the quality, of a powder used for additive manufacturing.

3.4.1. Comparison Between Powder Flow Test and SEM results

Considering the SEM images, some key characteristics that can be studied are the general shape of the particles and the presence of satellites. The results of the images comparison are summarized in Table 3.11:

Table 3.11: Sum up of the morphological features of the powder studied.

Powder	Satellites amount	Shape	SEM image (secondary electrons, 200x)
L 0001	Small	Quite irregular, elongated	
L 0002	Small	Quite irregular, elongated	
L 0003	Small	Irregular, elongated	

<p>L UK3359</p>	<p>Small</p>	<p>Quite irregular, elongated</p>	 <p>SEM 20kV WD11mm SS60 x200 100µm 0 Mar 23, 2017 Kentshaw AMPD</p>
<p>S 16D0534</p>	<p>High</p>	<p>Regular</p>	 <p>SEM 20kV WD11mm SS60 x200 100µm 0 Mar 22, 2017 Kentshaw AMPD</p>
<p>T 0425.2.5</p>	<p>Small</p>	<p>Regular</p>	 <p>SEM 20kV WD11mm SS60 x200 100µm 0 Mar 22, 2017 Kentshaw AMPD</p>
<p>V 14- 5034S</p>	<p>High</p>	<p>Generally regular, some elongated particles</p>	 <p>SEM 20kV WD11mm SS60 x200 100µm 0 Mar 22, 2017 Kentshaw AMPD</p>

S 16D0534 and V 14-5034S show very similar morphological properties. Their particles have a regular shape, but the satellites content is very high, especially if compared with the other powders. This last factor seems to be critical if we compare that with the powder flow test results, in fact S 16D0534 was just able to flow through the Carney funnel with a tap, V 14-5034S did not even flow. It seems that the presence of satellites is a crucial factor that can make a powder with generally morphological good properties flow poorly. This is probably due to the particle size being very irregular (non-sphere like), that leads to the presence of a lot of contact point between particles and mechanical interlocking, increasing friction and making the powder flow poorly.

The T 0425.2.5 situation is similar to the previous one: the powder morphology is decent, but there is an element that makes it impossible for the powder to flow through the Hall funnel. To better understand it, it will be highlighted in Fig. 3.36:

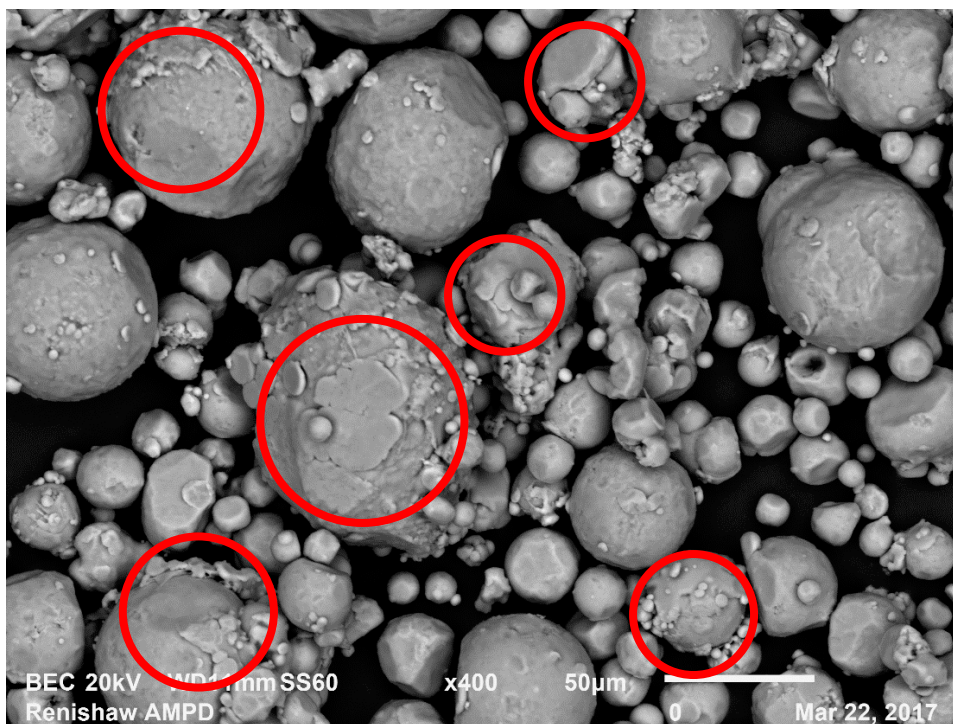


Figure 3.36: SEM image (backscattered electrons, 400x) of T 0425.2.5 with highlighted critical areas.

The highlighted unusual “splashed” surface structures are a consequence of the production process: they appear when two solidifying particles, so not fully solid, crash. These “splashes” can explain why that powder, which otherwise has a pretty good morphology, did not flow very well. Their effect can be considered similar to the one caused by the presence of satellites. It probably causes mechanical interlocking within particles and the irregular surfaces increase friction, leading to a sample that flows poorly. Although it must be noted that these phenomena cannot be directly compared because they happen in two different powders and in different quantities. Because of that, it is unknown if the T 0425.2.5 flowing properties are better than the two previous powder ones because of the different quantities involved, in fact there are less splashes than satellites, or this morphological feature is less critical, because it forms a particle with a shape closer to a sphere than a particle with satellites.

The flowing behaviour of the L powders seems to be contradictory: they both share a similar morphological quality, so it would be expected for them to have a similar flowing behaviour too, but that does not happen. These powders range from flowing through the Hall funnel (e.g. L UK3359) to not flowing at all (L 003). A possible explanation for these significant differences can be found in the presence of impurities in the different samples. It must be considered in fact that the contaminant content found in these powders was not the same, but varied for each one of them. Considering that, a general trend appears: L 0002 had the lowest contaminant content and it is the powder that flows better with L UK3359, in which no contaminants were found. On the other hand, L 0003 had the highest content of impurities and it did not even flow. It seems to be a direct correlation between how many impurities are contained in the powder and how badly it flows. Of course, for this consideration not all the contaminants are equal and for sure fibres impact on the flowing properties is more significant, because of their elongated shape that can block multiple particles at the same time. To sum up, it seems to be an inverse relation between the impurities content and the flow quality, as summarized in Fig. 3.37.

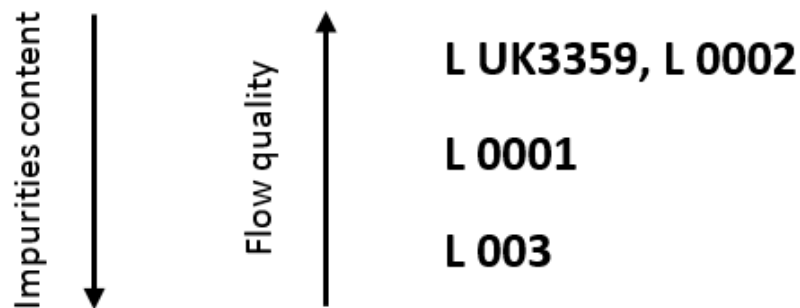


Figure 3. 37: Summarization of the relation between impurities and flowability.

3.4.2. Comparison Between Powder Flow Test and Particle Size Distribution

All the L powders have similar particle distribution curves (Fig. 3.38). Their curves are symmetrical and there is a low D(50) variation, in fact it ranges from 46.3 μm (L UK3359) to 49.3 μm (L 0001). These facts are coherent with the theory that all the L powders would flow similarly if they had a similar impurities content.

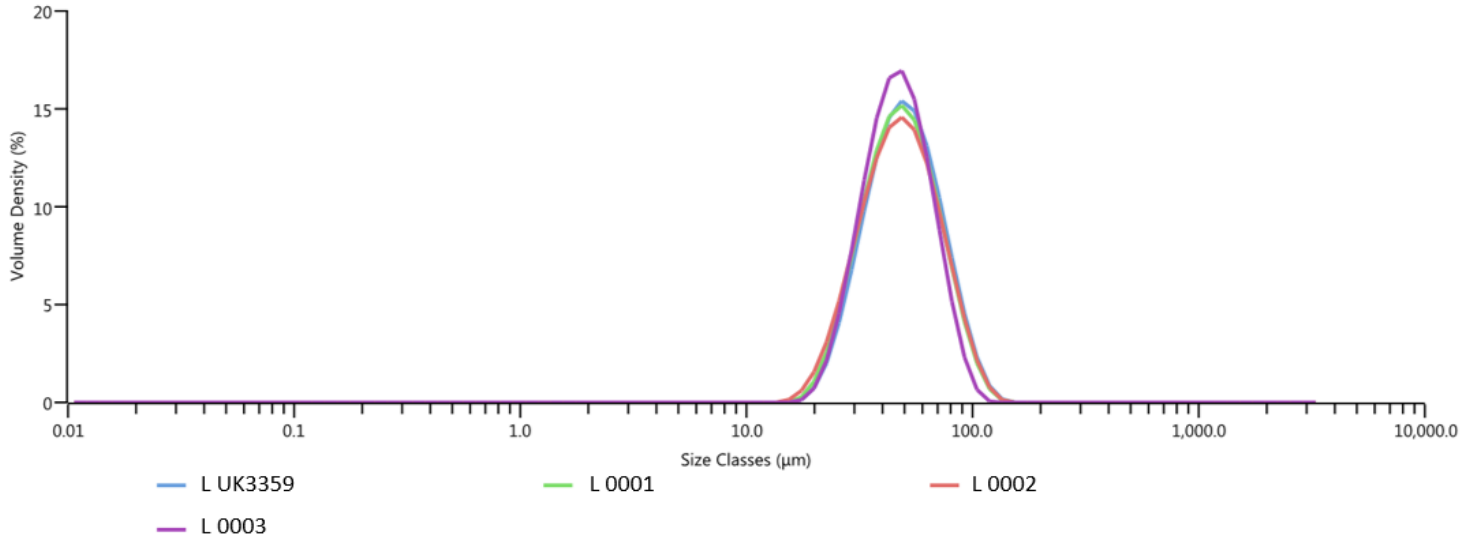


Figure 3.38: Particle size distribution graph for the L powders.

The other powders lack of ability to flow through the Hall funnel can be linked to some of their particle size distribution curves:

- Presence of a secondary peak (S 16D0534). As explained in sec. 2.3, the causes are unknown, but the consequences are clear: it leads to a more efficiently packed structure, where the smaller particles can fill the voids between the bigger ones. Agglomeration is more likely to happen and in general it is more difficult (i.e. more energy is required) to make the powder flow due to the lack of voids that can accommodate the movement of the particles.

- Asymmetric curve (T 0425.2.5). The presence of a large quantity of small particles affects the flowing behaviour of a powder, acting in a similar way to the previous case. Again, the small particles efficiently fill the voids, make agglomeration more likely and it is more difficult for the powder to flow freely. Considering that, as explained in sec. 1.6.1, smaller particles are more subjected to cohesion than bigger ones, it is not surprising that an increasing percentage of smaller particles leads to a more cohesive, hardly flowing powder.

- Low D(50) (S 16D0534, V 14-5034S). These characteristics can be considered as the particle size distribution curve was shifted to the left. Because of that, it can be considered as all the particles are on average smaller. That leads again to more consistent cohesion forces, that make it easier for the powder to resist to other external stimuli that can trigger the flow (e.g. gravity).

When comparing S 16D0534 and V 14-5034S, an apparently counterintuitive phenomenon is noted: the latter does not flow, even through the Carney funnel, whilst the other one flows. By analysing the powder from a morphological point of view, it is hard to explain that, because the powders are very similar (SEM analysis) and, according to the particle size distribution evaluation, S 16D0534 should be worse. In fact, that powder has a low D(50) and it is bimodal. The other one has just a low D(50). A comparison between these two powders is shown in Fig. 3.39.

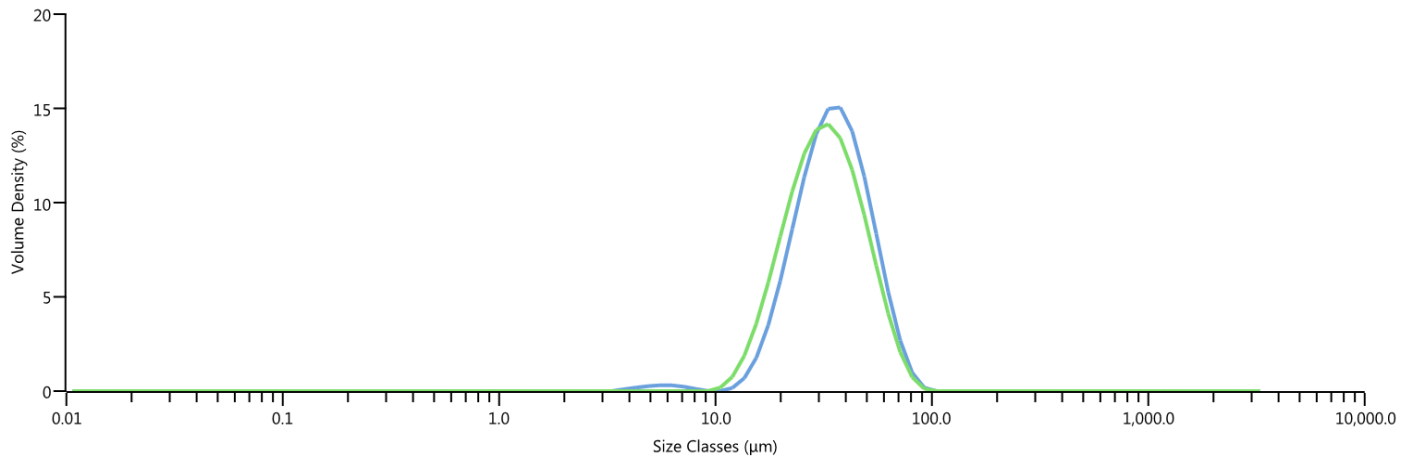


Figure 3.39: Particle size distribution graph for S 16D0534 and V 14-5034S.

As it is visible in the graph although, even if they both have a low $D(50)$, V powder has it lower, as shown in Table 3.7. Another thing that can be evaluated is the percentage of powders with size lower than $21.2 \mu\text{m}$, which is the area under the curve from that size value to the left, graphically represented for V 14-5034S in Fig. 3.40.

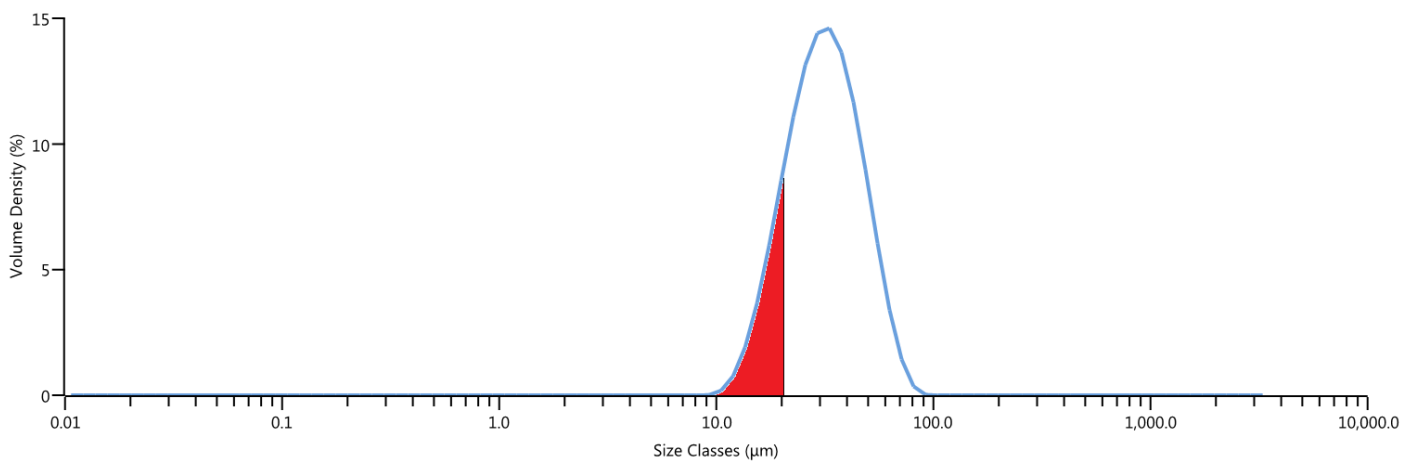


Figure 3.40: Percentage of particles with size lower than $21.2 \mu\text{m}$ for V 14-5034S.

For the S 16D0534 powder, that value is 18.33%, while it is 26.7% for V 14-5034S. That is probably why, in the end, the latter has a worse flowing behaviour during the flowability test: even if the other powder has smaller particles, V 14-5034S is formed by a much greater number of small particles, that makes it an overall more cohesive powder.

3.5. Moisture Content

The results of this test, shown in Table 3.12, proved that in general the moisture content is quite limited in all the analysed powders.

Table 3.12: Moisture content test results.

Powder	Moisture content (%)
L 0001	0.006
L 0002	0.008
L 0003	0.014
L UK3359	0.070
S 16D0534	0.041
T 0425.2.5	0.010
V 15-5034S	0.039

At the end of the test, an interesting phenomenon was noted on the V 15-5034S surface: quite a relevant amount of powder agglomerated (Fig. 3.41).



Figure 3 41: Agglomeration on the V 14-5034S sample.

This is coherent with the results from the previous experiments, in fact that sample did not flow during the powder flow test. Moreover, the massive presence of satellites and its low $D(50)$, that means smaller particles on average, which leads to stronger adhesion forces (the surface/volume ratio is higher), make this phenomenon almost expected for this powder.

3.6. Powder Rheometer

3.6.1. Stability Test and Variable Flow Rate Test Results

The results of the stability and variable flow rate test are shown in Fig. 3.42, graph in which the total energy required to make the blade move is evaluated as the number of tests go on, and Table 3.13:

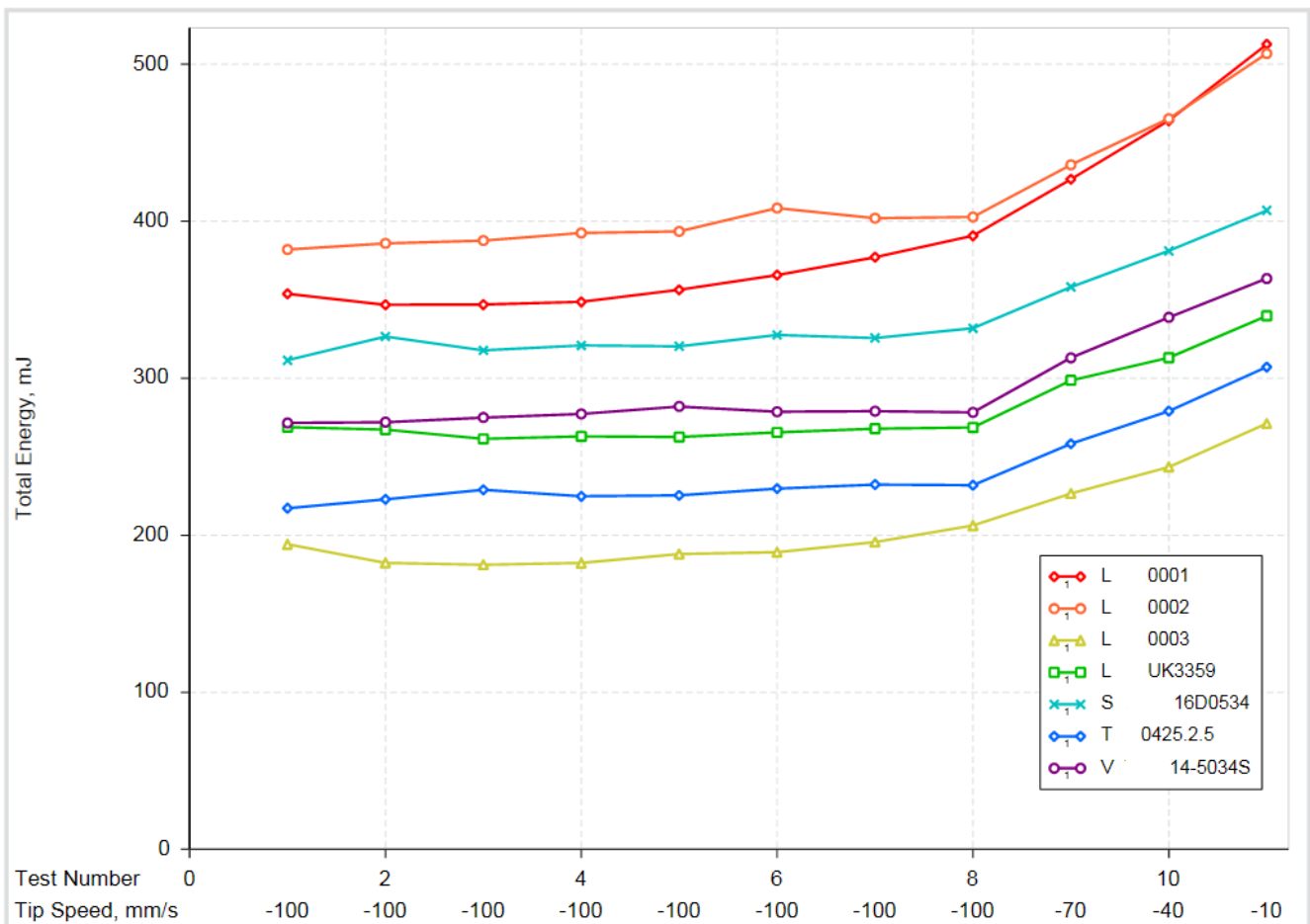


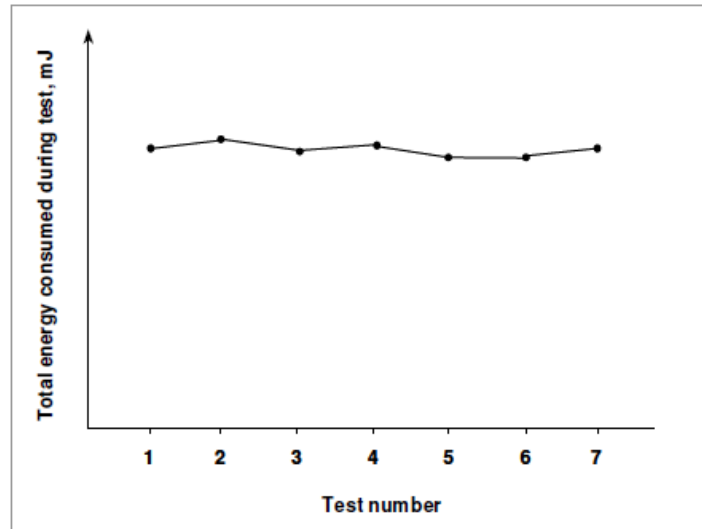
Figure 3.42: Stability and variable flow rate test results.

Table 3.13: Stability and variable flow rate test results.

Powder	SI	BFE (mJ)	SE (mJ/g)	FRI	CBD (g/cm ³)
L 0001	1.07	377	4.02	1.21	1.36
L 0002	1.05	402	4.31	1.26	1.36
L 0003	1.01	196	3.01	1.32	1.31
L UK 3359	0.997	268	3.55	1.26	1.37
S 16D0534	1.05	326	4.66	1.23	1.25
T 0425.2.5	1.07	232	3.02	1.32	1.39
V 14-5034S	1.03	279	4.49	1.31	1.40

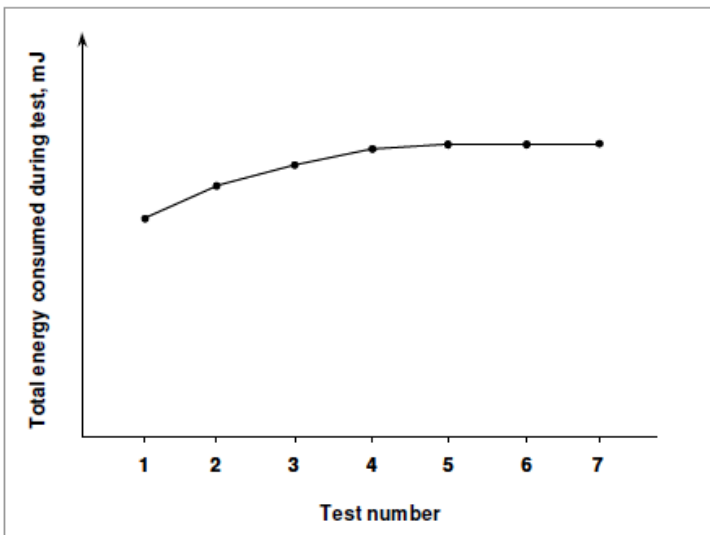
It must be noted that the first seven spots of every curve are referred to the stability test, while the last four are part of the variable flow rate test results.

By looking at Fig. 3.42, a first preliminary interpretation of the available data can be done just by looking at the curves shapes. In general, the stability of a powder can be roughly determined as shown in Fig. 3.43 and Fig. 3.44:

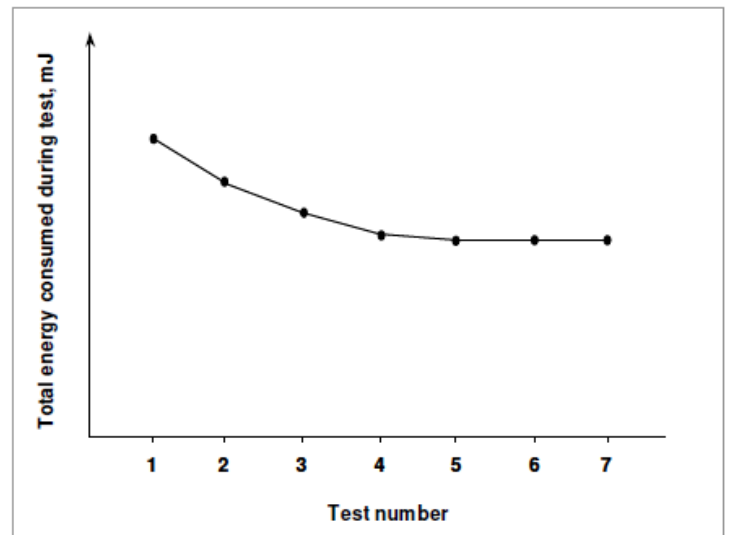


Stable

Figure 3.43: general stability test graph for stable powders (Courtesy of Freeman Technology). [37]



Unstable



Unstable

Figure 3.44: general stability test graph for unstable powders (Courtesy of Freeman Technology). [37]

Per this initial analysis, all the powders seem to be stable enough. As explained in the previous chapter, a mean that can be used to evaluate the powder stability is the stability index (SI). The results obtained by its evaluation substantially agree with what was just stated looking at the graph: all the powders seem to be stable. In fact, considering $SI = 1$ as the perfect stability value, it has been decided that all the acceptable powder were the ones for which $0.9 < SI < 1.1$, which means all the previously analysed ones.

To compare the powders in an easier way it is possible to change the graph in Fig. 3.42, so that it shows the normalised total energy on the Y-axis (Fig. 3.45). To evaluate that, for all the powders the energy value for test 7, that corresponds to the BFE, the end of the stability test and the beginning of the variable flow rate test, has been considered to be 1. The rest of the graph is a direct consequence of that change.

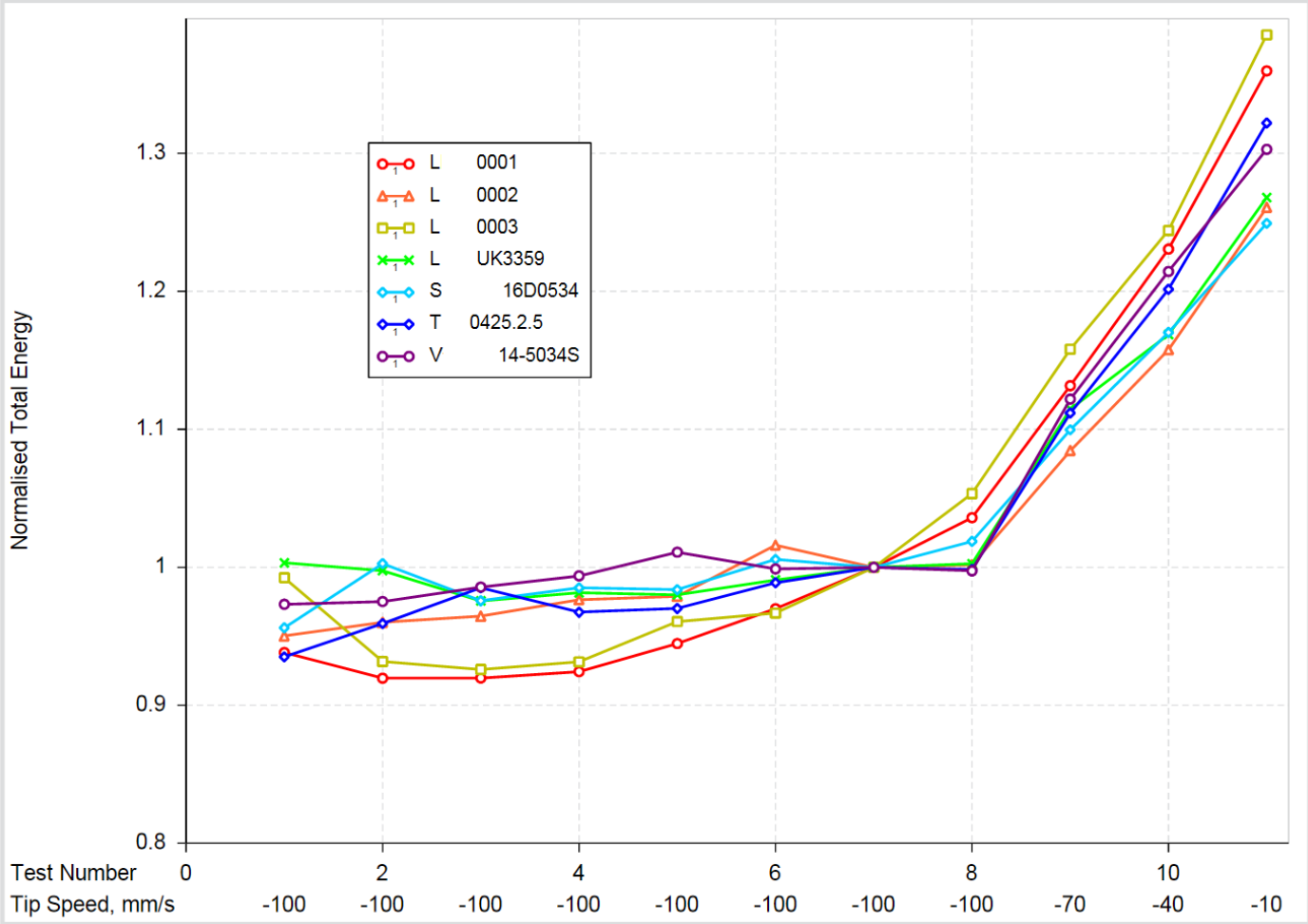


Figure 3.45: Stability and variable flow rate normalised test results.

It is easier to evaluate the powder stability from the previous graph, where it can be easily noticed that the maximum variation is lower than 10% of the BFE, in fact every graph is above the 0.9 normalised total energy values.

The analysis of the basic flowability energy is more complex, mostly because, as previously stated, that index is dependent on a high number of properties and parameters. It also does not necessarily relate to how a powder flows, in fact an experiment like the flowability test

evaluates the flowing properties under gravity, in that case a shear stress is applied. To evaluate the flowing behaviour, it is more useful to study this parameter variation during other tests.

It is not possible yet to make considerations about the impact on the BFE of segregation or attrition, but, from the results of the moisture content test (Table 3.12), it is possible to affirm that probably the BFE has not being influenced considerably by the presence of water. That can be considered as a reliable information because the moisture content was quite low in all the powders. Moreover, water is probably not the cause of the high BFE values variation, because its content was pretty much the same in all the samples analysed.

The specific energy (SE) values analysis proves that all the powders can be labelled as having low cohesion. It is although interesting to notice that the two highest values (4.66 mJ/g for S 16D0534 and 4.49 mJ/g for V 14-5034S) define as more cohesive the two powders that were already described before as very similar from a morphological point of view. They also share a low value of their D(50) in the particle size distribution test, which suggests their particles to be more efficiently packed and smaller on average, hence cohesive, coherently with the result of that test.

On the other hand, T 0425.2.5. has a very low SE value (3.02 mJ/g), that seems to be in contradiction with its poor flowing properties. Although It must be noted again that in the rheometer the characteristics linked to shearing are fundamental, and the flowability test is conducted in very different conditions. Because of that, some apparently contradictory results should be expected. It has been stated that the T 0425.2.5 morphology is good, but there are splashes. It is possible that this kind of defects are not as impactful on the test results as they were during the flowability test.

It must be stated that the overall best performing powder is L 0003 (SE = 3.01 mJ/g), which did not even flow during the flowability test. But in general, the SE interpretation for the L powders is difficult, because that value varies a lot from one powder to another, but all the tests performed so far are not able to provide results that make this kind of discrimination possible.

According to the FRI values analysis previously stated, all the powders fall in the range that describes them as flow insensitive and possibly characterised by a large particle size. These values variation makes it difficult to compare them, because they are all quite close. Moreover, it has been provided a general interpretation, this does not mean that they must be powders with a large particle size. In fact, the powder rheometer is designed to characterize all types of powders. The “small particle size” category is probably best suited for powders used in pharmaceutical or other applications.

The conditioned bulk density is very similar in all the powders. The only exceptions are L 0003 (1.31 g/ml) and S 16D0534 (1.25 g/ml).

3.6.2. Aeration Test Results

The results of the aeration test are shown in Fig. 3.46, graph in which the energy required for the blade to rotate is evaluated at different air velocities, and Table 3.14:

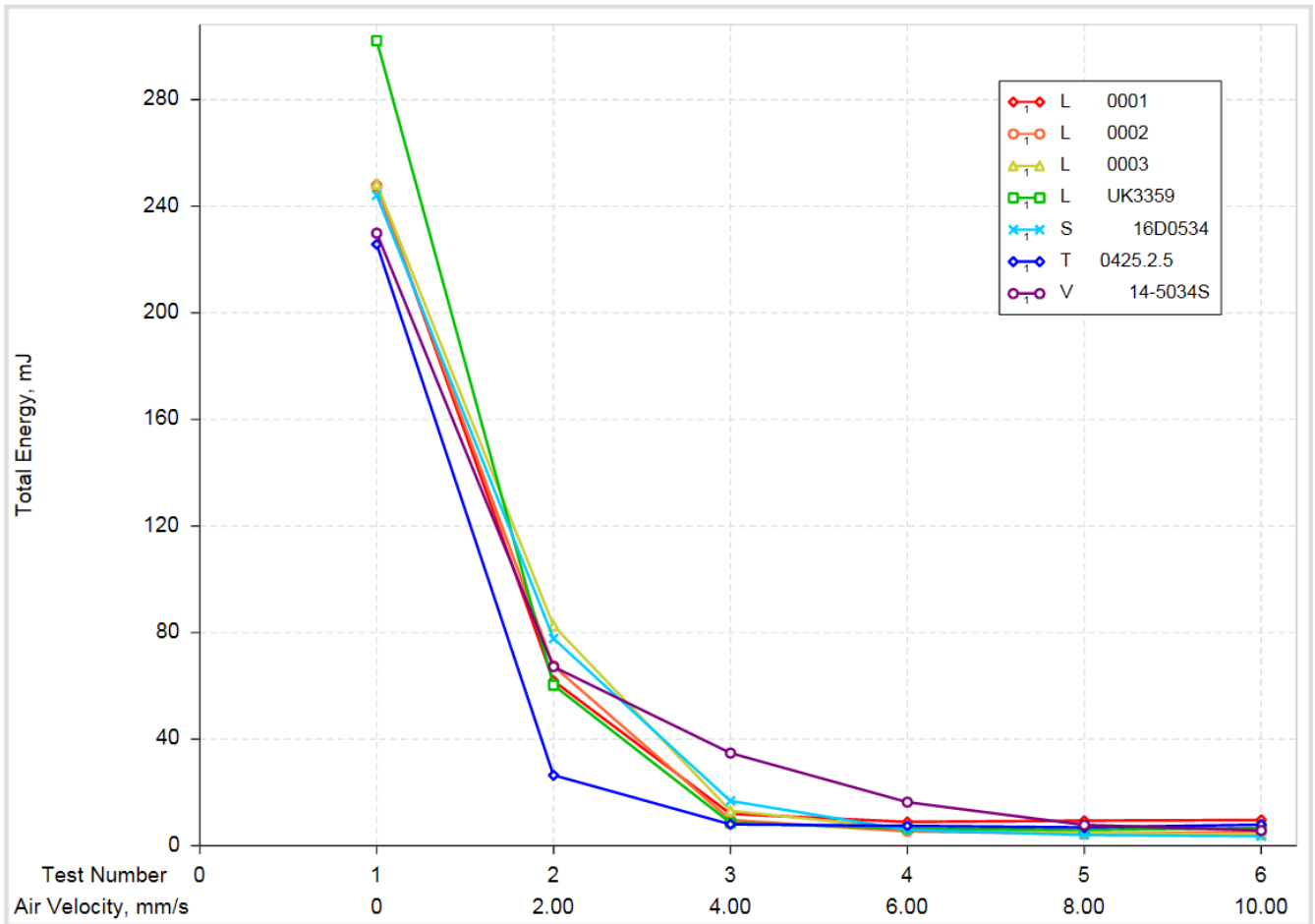
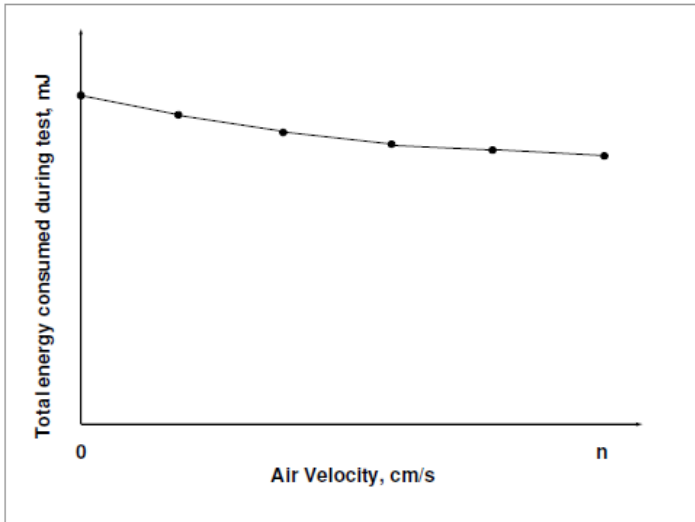


Figure 3.46: Aeration test results.

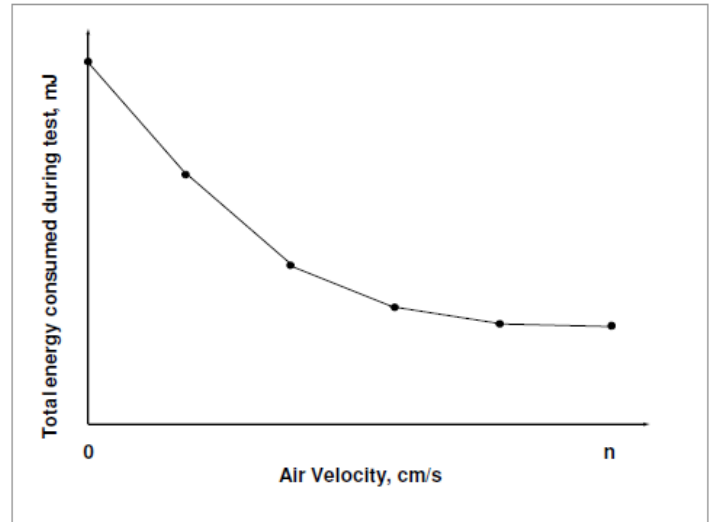
Table 3.14: Aeration test results.

Powder	AR_10	BFE (mJ)	AE_10 (mJ)
L 0001	25.6	248	9.68
L 0002	47.2	247	5.24
L 0003	58.2	248	4.27
L UK3359	45.6	302	6.62
S 16D0534	68.3	244	3.58
T 0425.2.5	28.4	226	7.94
V 14-5034S	40.4	230	5.69

Again, the first thing that must be done is looking at the graph and evaluate the curve shapes. The general interpretation is shown in Fig. 3.47 and Fig. 3.48:

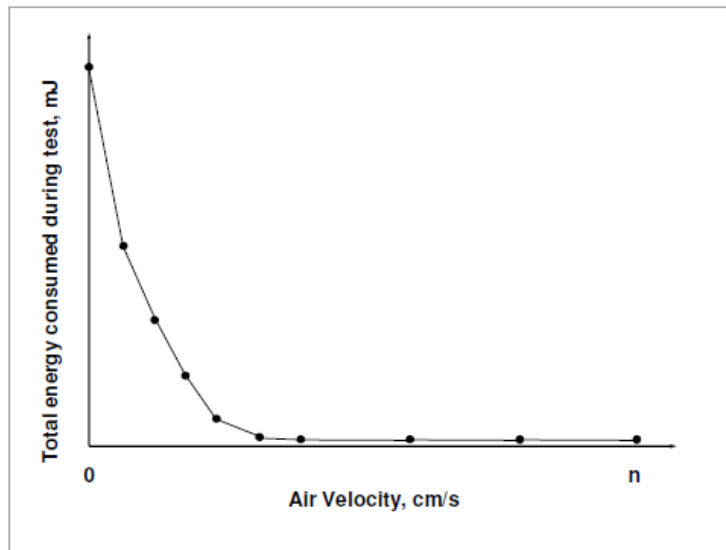


Cohesive



Typical

Figure 3.47: General aeration test graph for cohesive and typical powders (Courtesy of Freeman Technology). [42]



Non - cohesive

Figure 3.48: General aeration test graph for non-cohesive powders (Courtesy of Freeman Technology). [42]

All the analysed powders seem to have a non-cohesive behaviour, which is an appreciated characteristic. But it must be said again that this does not mean they will behave properly once processed, just that they have the potential for being used, as explained before.

As it was done for the stability test, using as parameter the normalised total energy, can make easier the comparison between the different samples (Fig. 3.49). In that way, it is possible to look at the data regarding relative differences. In that case, the energy value for

the first test, when the air velocity was null, has been considered as 1. Again, the rest of the graph has been derived as a consequence of that operation.

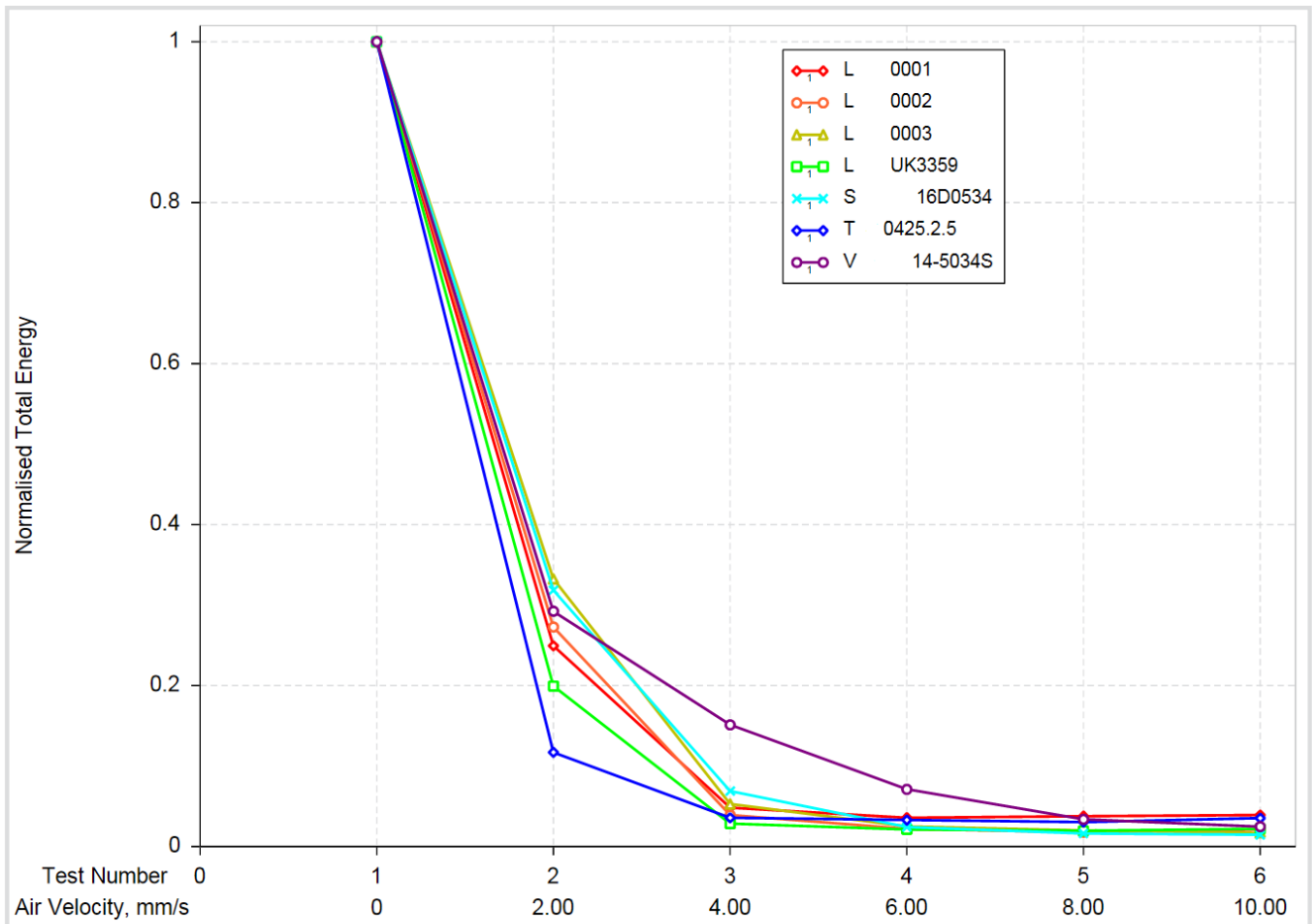


Figure 3.49: Aeration test normalised results.

A couple of considerations about the minimum fluidisation velocity can be done. It can be defined as the minimum air velocity required to establish fluidisation (aeration) in the powder bed. It occurs when the flow energy is reduced approximately to zero (usually 10 mJ or less). An example to explain that is Fig. 3.50, in which both powders reach a fluidised state, but at different air velocities (4 mm/s and 8 mm/s).

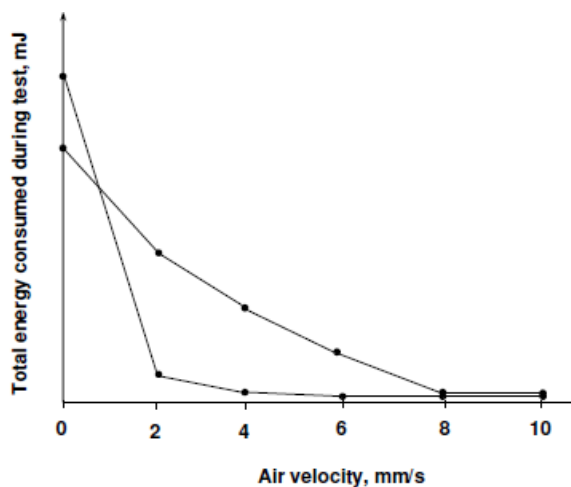


Figure 3.50: Example of two powders that become fluidised at different air velocities (Courtesy of Freeman Technology). [42]

By analysing the results, it can be said that approximately all the powders have a value of minimum fluidisation velocity that lies between 4.00 and 6.00 mm/s, exception done for V 14-5034S that needs a higher value of about 8.00 mm/s. All the powders become fluidised, in fact that is confirmed because all the AE₁₀ values are lower than 10 mJ. [42]

As it was explained in the previous chapter, one useful index obtained during this test is AR₁₀, which is evaluated as the ratio of the energy value when the air velocity is null to the energy value when the air velocity is 10 mm/s. All the powders show AR₁₀ > 20, hence they can be considered very sensitive to aeration, in fact they all become fluidised. Because of that, they are probably characterised by low cohesive strengths, confirming the results obtained by the SE values in the stability and variable flow test. Although it must be considered that T 0425.2.5, but especially L 0001 have AR₁₀ values not much greater, hence they can be considered slightly more cohesive than the other powders. In fact, for being considered as having low cohesivity, a powder should show a value for that index much greater than the 20 limit. Being their value so close, they will be considered as mid/low-cohesive powders.

The BFE values obtained during that test are the result of a procedure that is identical in the stability test. The BFE values for both tests are reported in Table 3.15:

Table 3.15: comparison between the BFE obtained from the stability test and from the aeration test.

Powder	Stability test BFE (mJ)	Aeration test BFE (mJ)
L 0001	377	248
L 0002	402	247
L 0003	196	248
L UK3359	268	302
S 16D0534	326	244
T 0425.2.5	232	226
V 14-5034S	279	230

It is quite easy to notice that BFE, for most of the powders analysed, varies a lot from a test to the other one. Two possible causes can lead to this behaviour:

- In the Aeration test the base is porous, while in the stability test it is dense. That is a big factor to consider, in fact the conditioning downward motion of the blade has the goal to displace particle and reduce the amount of entrained air. In case of a porous base, the air that fills the spaces between the particles can escape even from the bottom, making the process more efficient. On the other hand, during the stability test, the lack of pores makes it harder for the entrained air to break free.
- The aeration test base is made from stainless steel (AISI 316L), the stability test base instead is made of plastic. Because of that, there could be some interferences during the flowing energy measurement due to electrostatic effect/charging during the aeration test.

Base porosity seems to be the main factor to consider as it can explain why there is a general reduction of the BFE in the last test, drastic in some cases (e.g. L 0002). However, there are two scenarios (L 0003, L UK 3359) in which the trend is opposite: BFE increases in the aeration

test. Probably in that case the phenomenon is explained by electric effects. It all depends on which phenomenon is prevalent.

It must be also noticed that during the aeration test, the BFE values generally stabilised around the 240 mJ value. The variation between a powder and another one is much lower than in the previous test.

3.6.3. Permeability Test Results

The permeability test results are shown in Fig. 3.51, graph in which the pressure drop across the powder bed is evaluated as the normal applied stress increases:

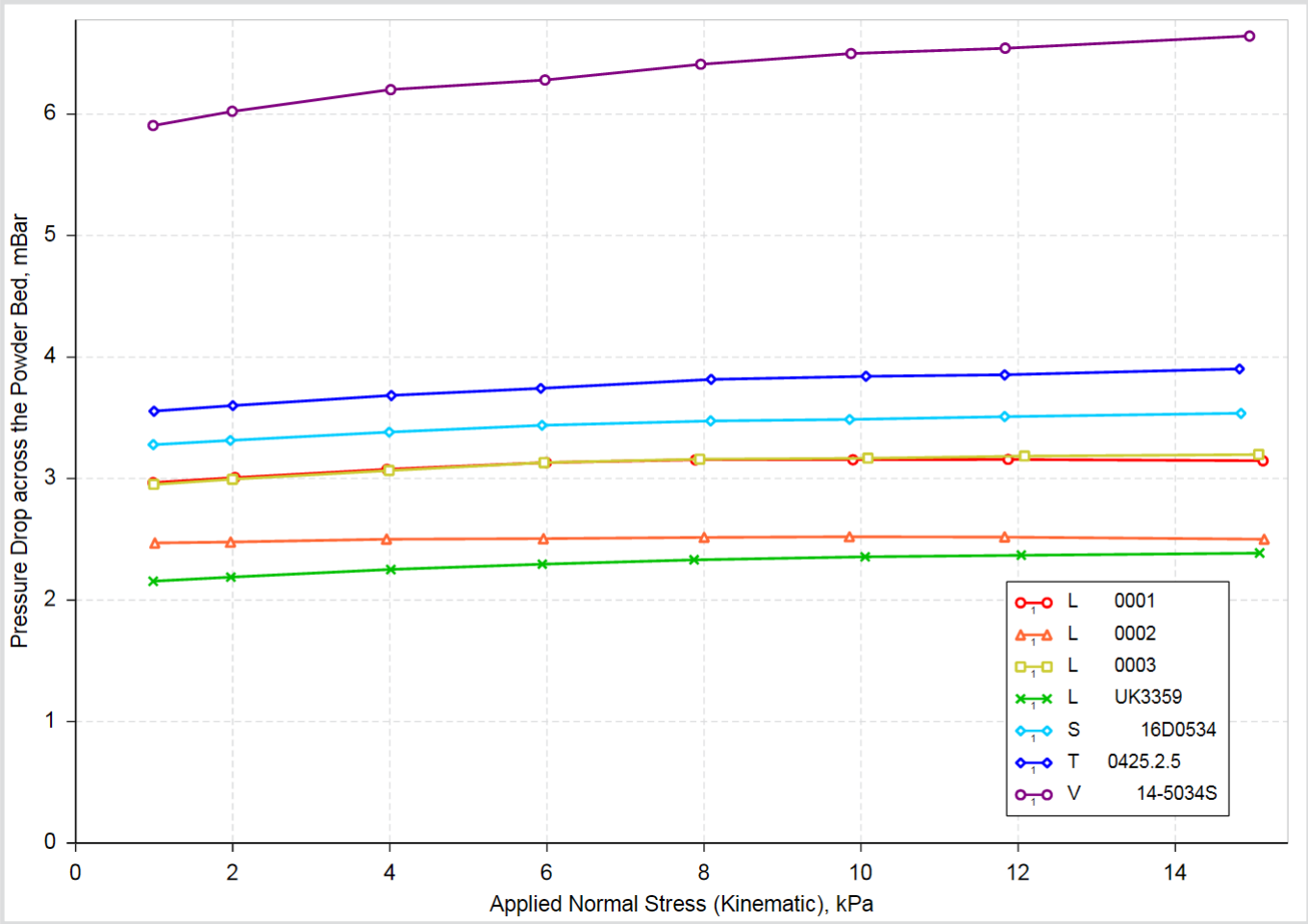


Figure 3.51: Permeability test results.

This test does not provide any specific index or numerical powder property. Any results evaluation must be performed looking at the previous graph. By doing that, it is possible to notice that all the L powders curves lay on the bottom part. Just considering them, the lowest ones are the one that flowed through the Hall funnel during the flowability test. Talking about the other powders instead, it can be immediately noted that the pressure value for V 14-5034S is far greater than it is for the other two. That can again be somehow linked with the flowability test results, in fact S 16D0534 and T 0425.2.5 could flow through the Carney Funnel, while V 14-5034S did not flow at all.

There seem to be some sort of correlation between that test results and the Flowability ones.

Supposing that L 0003 was not in the graph, it could be said that the powders would have been grouped exactly according to the flowability test results. In fact, on the bottom part of the graph there are the curves relative to L 0002 and L UK3359 (flowed through the hall funnel), going up there are L 0001, S 16D0534 and T 0425.2.5 (flowed through the Carney funnel) and on the top there is the V 14-5034S curve (did not flow). It must be questioned then why a trend so clear has been compromised by the presence of the L 0003 powder. A possible explanation may be that, unlike the other powders, the Ls different results during the flowability test are due to the presence of contaminants, so not morphological properties. That is why they are all close in the previous graph, because during this kind of test the presence of impurities is less important and these powders can be considered almost similar, because their other characteristics are close. That would be coherent both with the data interpretation that has been given before and prove again that the behaviour of the non-L powders is worse because of their morphology.

The resulting graph can be generally interpreted as suggested in Fig. 3.52:

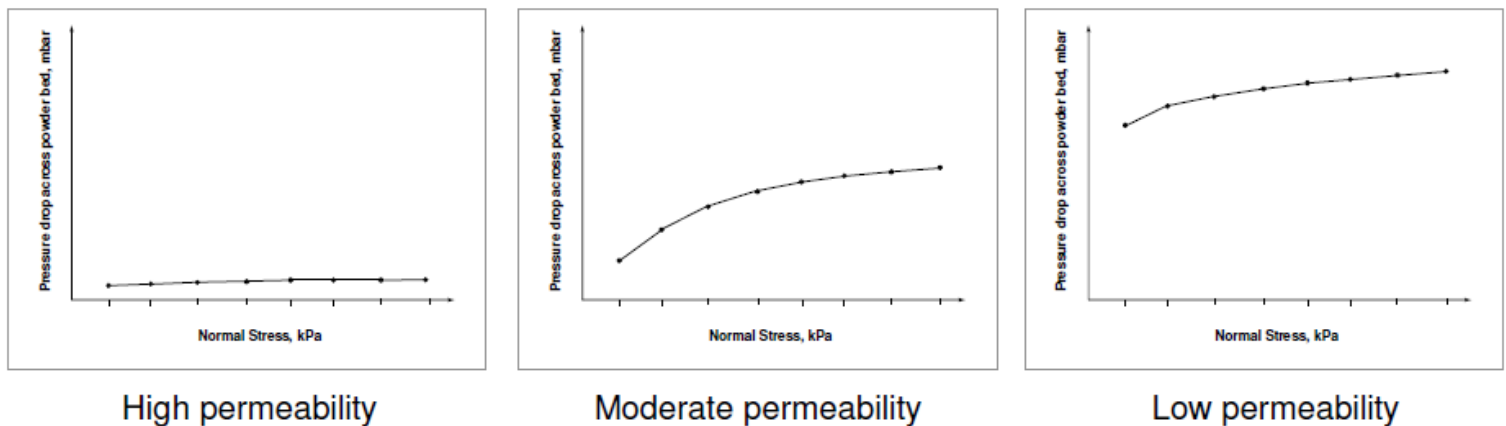


Figure 3.52: General permeability test graph for different types of powders (Courtesy of Freeman Technology). [43]

All the analysed sample can be considered as having low permeability, which means that, for making air flowing through the powder itself, it is necessary to apply a high pressure. Because of that, it can be considered that probably there are just a few channels between particles, probably small. As previously stated, an important contribution to that phenomenon is due to irregular particle shape. This kind of powders is likely to be cohesive and characterized by small particle size.

Most of the previous considerations were referred to permeability, even if it is not shown directly in the graph. It is true that in general a greater pressure drop corresponds to a less permeable powder, although It would be more useful to change the graph, to make it show directly this property.

Permeability strictly depends on powder porosity, which is a measure of the void space between the particles and it is significantly changed by compression, but also on particle properties like shape and texture. This is the reason why normal stress is considered as the main variable. [28] To put permeability in a graph, it must be still plotted against normal stress. To do so, Darcy's Law can be used:

$$Q = \frac{kA}{\mu} \cdot \frac{P_a - P_b}{L} \quad (3.3)$$

Where:

$Q =$ Air volume per unit time [cm^3/s]

$k =$ Permeability [cm^2]

$A =$ Area of the powder bed [cm^2]

$P_a - P_b =$ Pressure drop across the powder bed [Pa]

$\mu =$ Air viscosity [$Pa \cdot s$]

$L =$ Length of the powder bed [cm]

Rearranging the equation, it can be obtained:

$$k = \frac{q\mu L}{\Delta P} \quad (3.4)$$

Where:

$q =$ Flux, or air flow rate [cm/s]

$\Delta P =$ Pressure drop across powder bed [$mbar$]

Considering that P_b is assumed to be atmospheric pressure, then it can be stated:

$$\Delta P = P_a \quad (3.5)$$

Concerning the air viscosity, it can be approximated as:

$$\mu = 1.74 \cdot 10^{-5} Pa \cdot s = 1.74 \cdot 10^{-7} mbar \cdot s \quad (3.6)$$

Applying these changes, the graph showed in Fig. 3.53 is obtained:

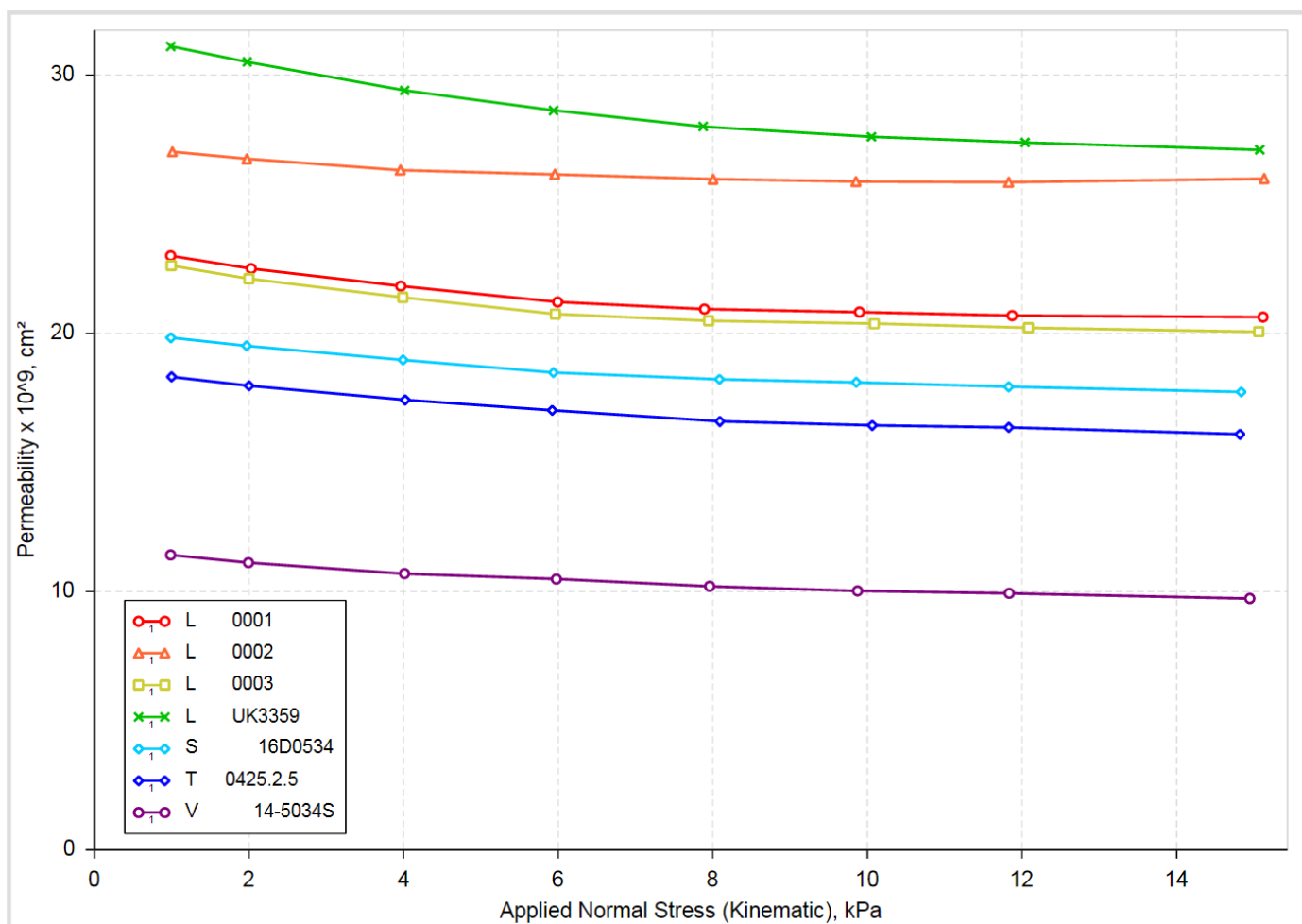


Figure 3.53: Permeability test results, where permeability is plotted instead of pressure drop.

It must be noted that the previous correlation between cohesivity and permeability must not be taken for granted. Sometimes the results are counter-intuitive and, for example, a less cohesive powder can show low permeability. In that case, this phenomenon can be caused by the very efficient packing state of the particles, that form a tightly packed mass that makes a homogeneous transmission of air through the sample almost impossible. On the other hand, very cohesive powders can exhibit a small pressure drop, suggesting high permeability, probably due to agglomeration, that makes groups of particles act as a singular big particle.

Because of that, these test results must always be compared with the data given by the other powder rheometer tests.

As suggested by the aeration test, the analysed powders should be non-cohesive, suggesting a very efficient packing of the powder, that leads to high permeability. To determine if this is the case, the results of these two tests will be compared with the ones from the compressibility test.

Although it must be stated that the low cohesivity option seems more likely, because, as noticed during the SEM analysis, the most permeable powder (Ls), even if more irregular shaped, lack the presence of satellites. This key characteristic makes powder packing more efficient, hence the powders more permeable, coherently with the previous explanation and in agreement with the aeration test results.

3.6.4. Compressibility Test Results

The compressibility test results are shown Table 3.16 and Fig. 3.54, graph in which the compressibility percentage is evaluated as the normal applied stress increases:

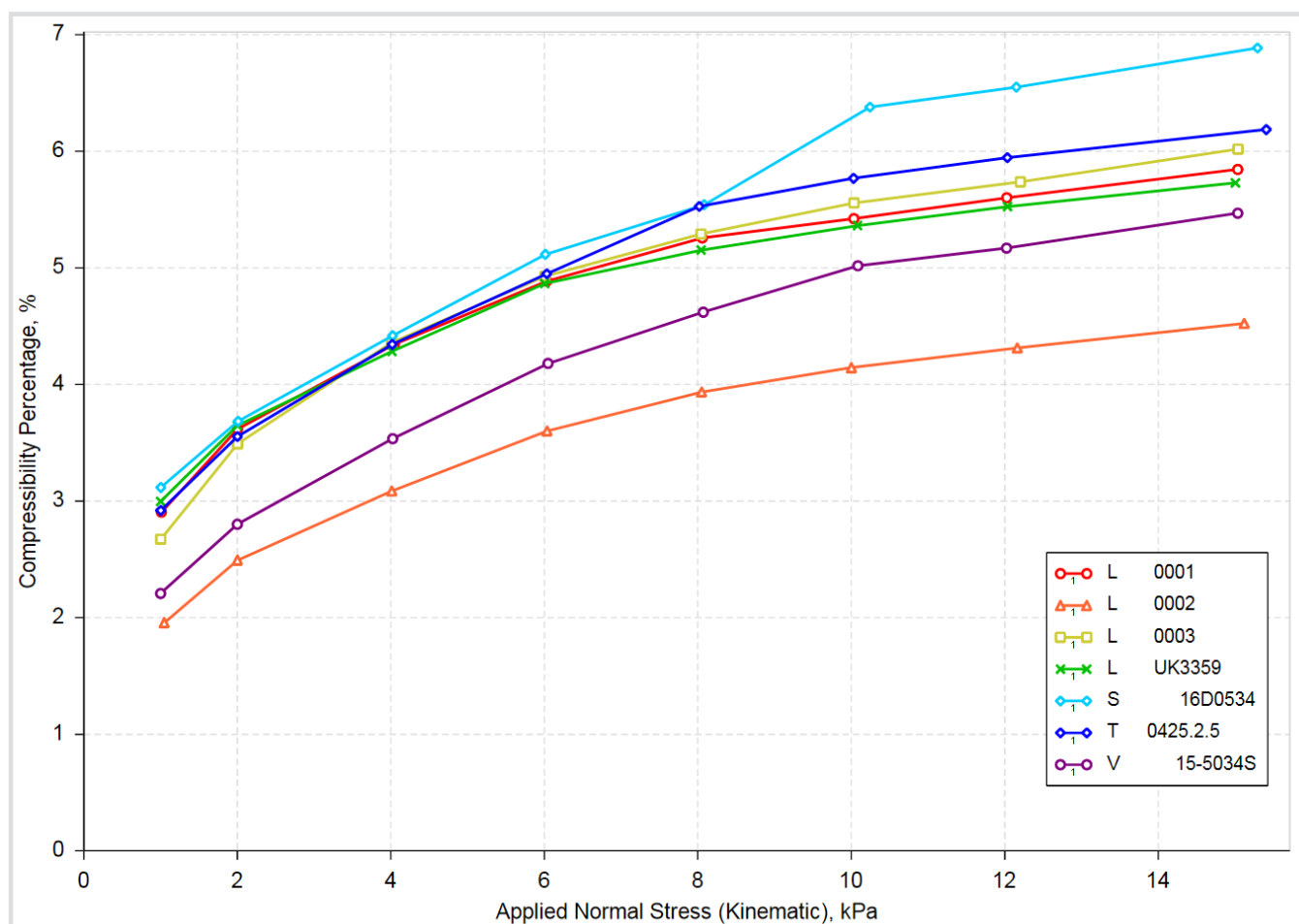


Figure 3.54: Compressibility test results.

Table 3.16: Compressibility test results.

Powder	CBD (g/cm ³)	Compressibility percentage at 15 kPa (%)
L 0001	1.34	5.84
L 0002	1.37	4.52
L 0003	1.32	6.02
L UK3359	1.37	5.73
S 16D0534	1.26	6.89
T 0425.2.5	1.39	6.19
V 14-5034S	1.45	5.47

Before analysing the test results, it is important to clarify that probably, because of the results obtained from the two previous tests, the rheometer was dealing with non-cohesive powders. These are usually characterised by a relatively high stiffness. Hence the force control must be checked, because an equilibrium, necessary for a good measurement, is unlikely to be reached. An example of that, is shown in Fig. 3.55:

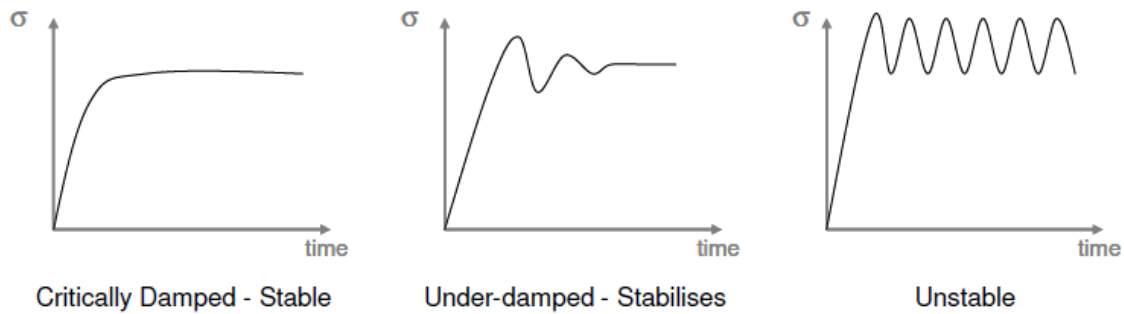


Figure 3.55: Examples of three different scenarios with different force control (Courtesy of Freeman Technology). [36]

A general view on the force trend during the tests is shown in Fig. 3.56:

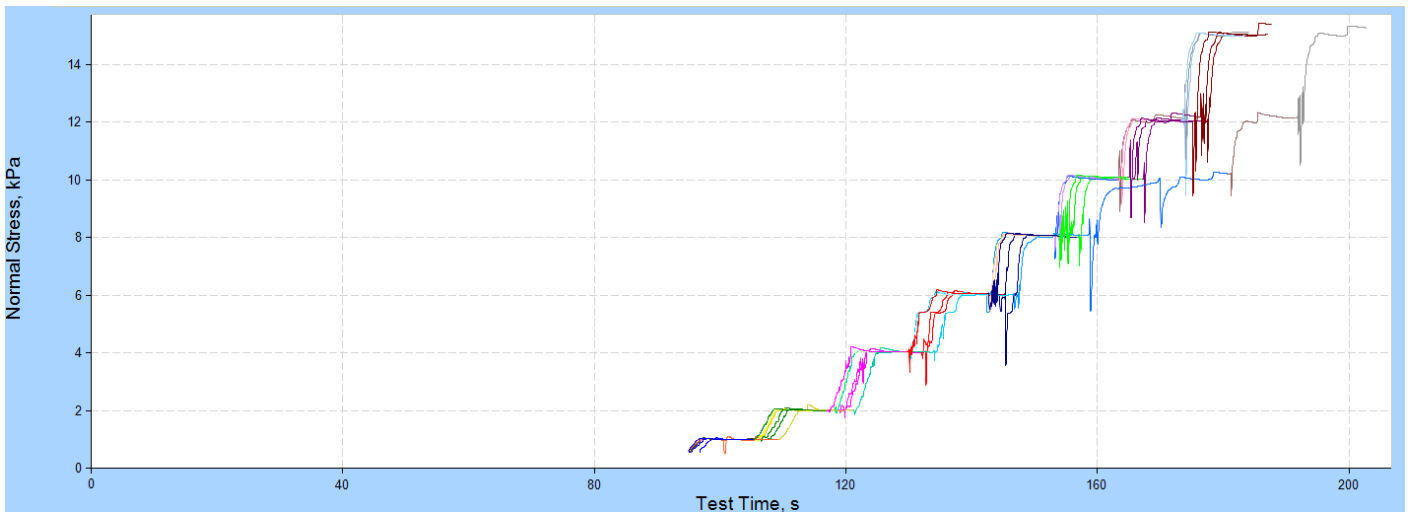


Figure 3.56: Force trend during the different tests.

As it can be seen, the general behaviour can be considered quite stable, so powders reach stress equilibrium quite quickly and keep being in that condition. Although there is a specific case (S 16D0534, Fig. 3.57) in which the behaviour would be better described by the central graph of Fig. 3.55. Hence the powder still reaches equilibrium stress, but slowly. This is probably due to the sample initially supporting the applied stress and collapsing in the end.

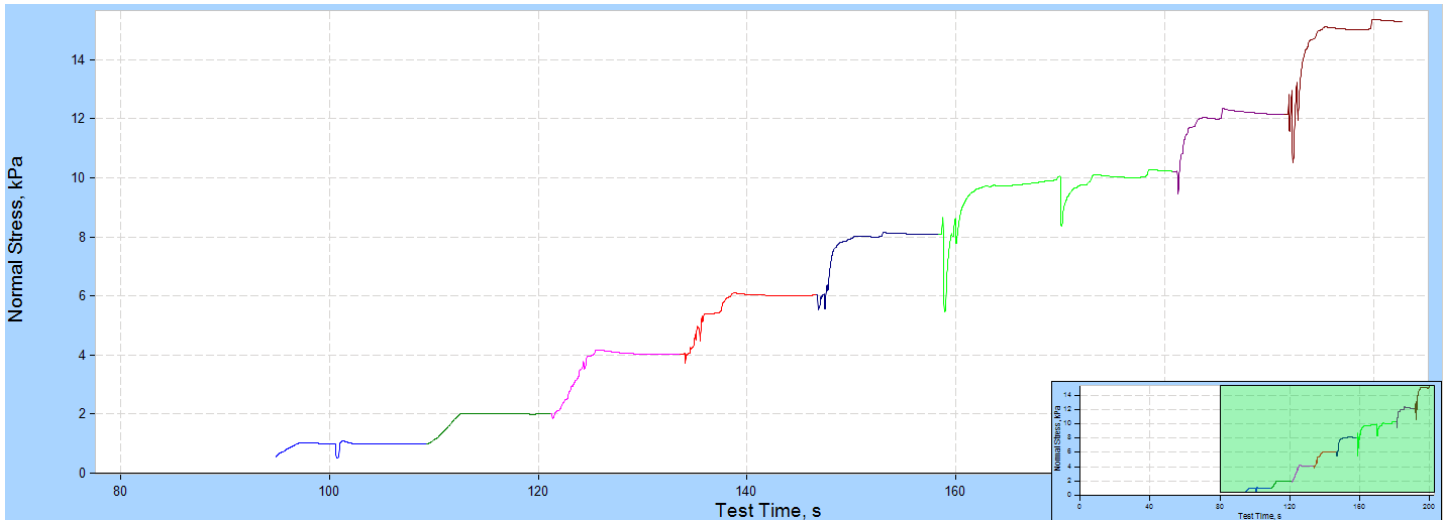


Figure 3.57: Force trend during the S 16D0534's compressibility test.

From the previous figure, in which every colour represents a test conducted at a different stress level, it can be noticed that the unstable behaviour is shown just after a certain minimum force is applied, in that case 8 kPa. Before that critical value, the curves are quite regular. It is interesting to compare that graph with one relative to a more stable powder, from that point of view, which is L UK3359 (Fig. 3.58).

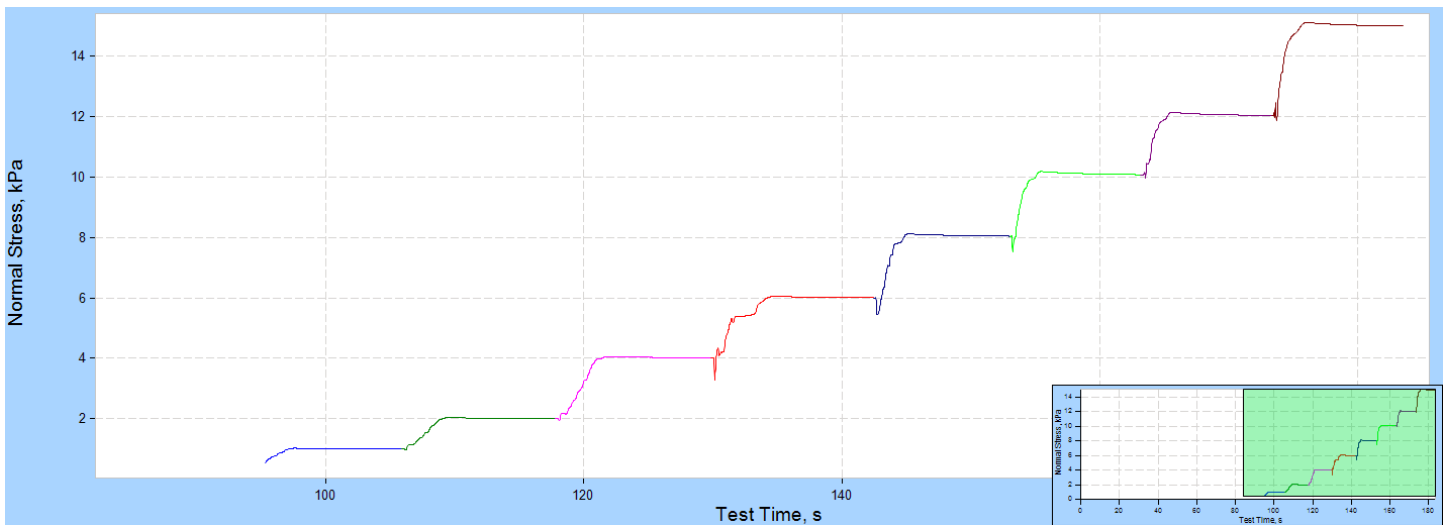


Figure 3.58: Force trend during the L UK3359's compressibility test.

By comparison, it is evident that the second one is more regular, at all the available stress level. It is important then to understand what could be the possible cause that make the S 16D0534 powder acts differently. Considering that the “unstable behaviour” of the S 16D0534 powder, shown in Fig. 3.57, begins at approximately 8 kPa, it is possible to notice that at this specific stress there is an above the average increase of the compressibility percentage in Fig. 3.54. In fact, if that powder is compared with other samples that had an initial (1.00 kPa) similar compressibility percentage value (e.g. L UK3359), it is possible to notice that the final compressibility (15.00 kPa) is much greater for the unstable powder. That is also confirmed by the numerical results shown in Table 3.16.

If the unusually low conditioned bulk density obtained is also considered, moreover noticing that in the end that powder is by far the most compressed, it is possible to link that result to the satellite issue that was discussed before in the particle size distribution test results section.

It has already been clarified that S 16D0534 had a high content of satellites, that directly impacts on particles packability, worsening it. In fact, that powder has the lowest conditioned bulk density, as shown in Table 3.16. It is now known that if an 8 kPa compression stress is applied, there will be a sudden compressibility increase. This phenomenon can be caused by the presence of entrained air that is released during compression, but it seems somehow unlikely that this quantity will increase suddenly without any other phenomenon explaining why. It has then been theorized that 8 kPa is approximately the critical stress value that on average breaks the satellites particles. That would explain the graph trend, because, by separating primary particles and satellites, the powder components would become more spherical, hence able to pack more efficiently and then be compressed more. That also explain the “instability” in Fig. 3.57, due to the satellites needing time to pack again after having been released.

With this new information, the S 16D0534 and V 15-5034S comparison can be further investigated.

First of all, it can be noticed from Fig. 3.54 that, unlike S 16D0534, the V 15-5034S powder does not show any sudden increase in its compressibility as the applied stress goes up. By analysing the force trend during the test (Fig. 3.59), it is also possible to notice that this powder can be classified as quite stable, as applied stress reaches equilibrium quickly.

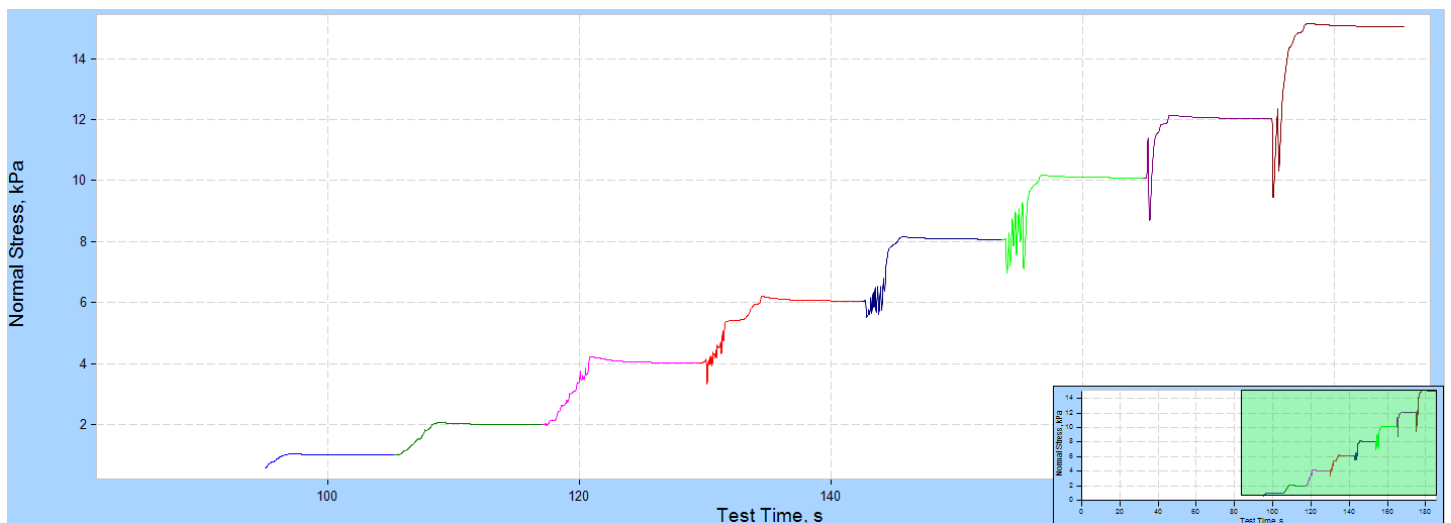


Figure 3.59: Force trend during the V 15-5034S' compressibility test.

But it must also be considered that morphologically these 2 powders are a lot alike, especially because they are both characterised by a high content of satellites. But again, as happened in the particle size distribution test, the fact that the two samples have a similar content of satellites in an unstressed state, does not mean they will maintain their similarities while testes. It has already been explained how S 16D0534, unlike V 15-5034S, kept a certain content of satellites after being shaken. Then it can be assumed that these two morphologically similar powders have satellites with different resistance, in particular S 16D0534's satellites are stronger than the others. It has been theorized that the satellites separation of V 15-5034S is not caused by the normal stress applied during the compressibility test, but from the shear stress

applied by the 23.5 mm blade during conditioning, which is a step common for all the tests conducted. To study that phenomenon, two samples of these powders have been imaged with the SEM after they took part in the stability test. It can be noted that the satellite content for S 16D0534 was still quite high after all the conditioning cycles of the test (Fig. 3.60). On the other hand, V 15-5034S did not almost show any satellite (Fig. 3.61).

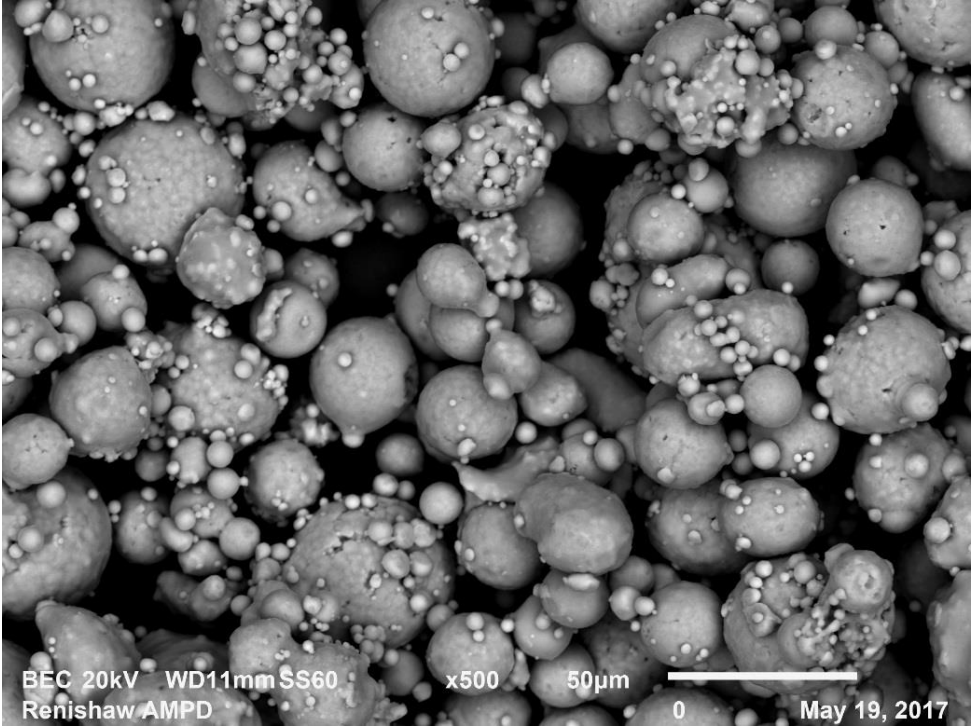


Figure 3.60: SEM image (backscattered electrons, 500x) of S 16D0534 after stability test.

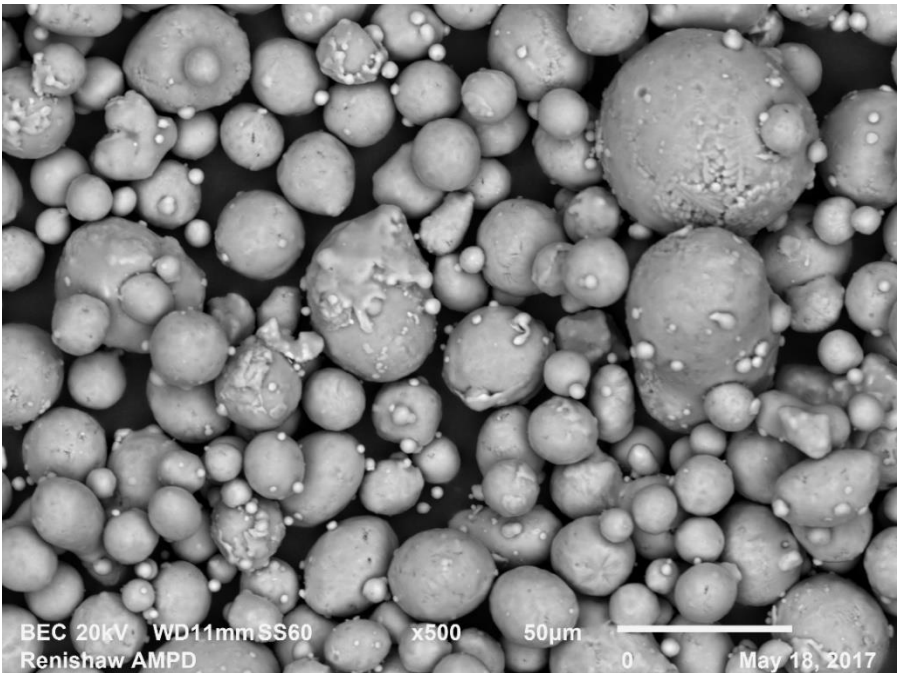


Figure 3.61: SEM image (backscattered electrons, 500x) of V 15-5034S after stability test.

It can be easily noted how different is the satellite content in these two powders, even if it was almost the same before testing them. It is reasonable again to ask where did the satellites from the V powder go. Probably it is hard to collect them on the carbon sticker used for the SEM analysis, because getting in contact with the sticker is prevented by the presence of bigger particles.

This proves again that, as explained before, these two powders show very different reactions to applied stress, depending on how the force is applied.

It has also been previously theorized that during the compressibility test S 16D0534's satellites break apart due to the increasing compression stress. To test if that is true, that powder has been imaged in the SEM after having been tested. In Fig. 3.62 it is possible to compare its morphology after it has just been conditioned by the 23.5 mm blade (left) and after the compression test (right).

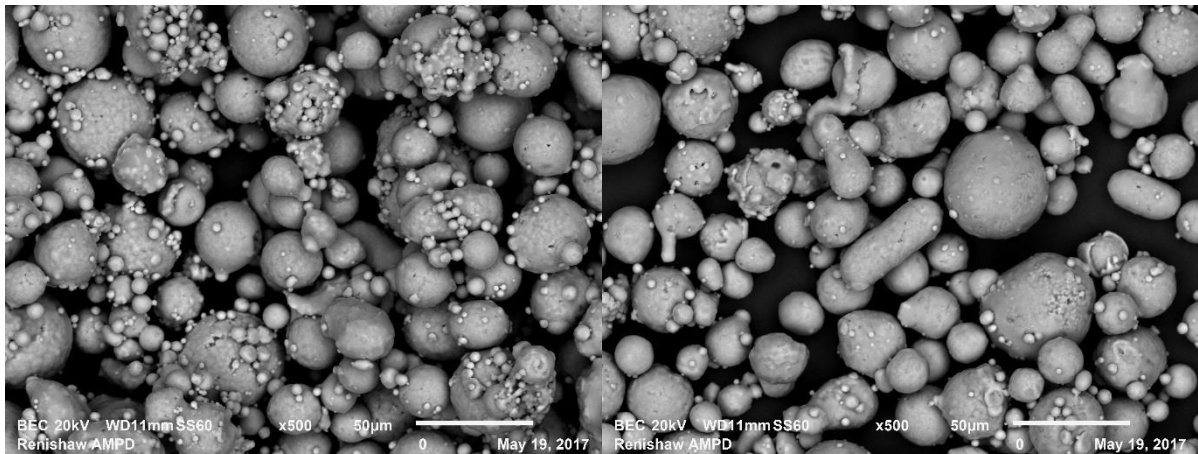


Figure 3.62: SEM image (backscattered electrons, 500x) of S 16D0534 after stability test (left) and after compressibility test (right).

It can be easily noted that in the second case the number of satellites is very low, suggesting that what was theorized can be true. To sum up, it can be said that this last powder's satellites are more resistant, in fact they can withstand the shear stress applied during the stability test without breaking apart, unlike the other powder's satellites. It has also been possible to determine the critical compressive stress value that leads to the particle-satellite separation in S 16D0534, which is around 8kPa. The fact that this separation happened is proved by the lack of satellites in the powder after the compressibility test.

That also explains these two powders' CBD values are so different from the others: that value is in fact evaluated after a conditioning cycle performed by the 23.5 mm blade. If the satellites separation already took place when CBD is evaluated, then S 16D0534's low value (1.26 g/cm^3) is due to the satellites interference with the particles packing process, that makes the amount of entrained air higher. Regarding V 14-5034S (1.45 g/cm^3), the satellites separation leads to a heterogeneous structure, from a particle size distribution point of view, which packs more efficiently, filling the voids between particles with the satellites, hence leading to a greater density.

As it has been previously stated, it is necessary to compare this test data with the results of the aeration and permeability test. The last two experiments seemed to describe the powders as

mainly non-cohesive. It has although been stated how sometimes the results can be counterintuitive, hence the necessity to make the comparison. To do that, it is now defined the Compressibility Index (CI) [36]:

$$CI = \frac{\text{Density (15 kPa)}}{CBD} \tag{3.7}$$

Where:

Density (15kPa) = Sample density after a 15 kPa compression $[g/cm^3]$

CBD = Conditioned Bulk Density $[g/cm^3]$

The density variation during the test is shown in Fig. 3.63:

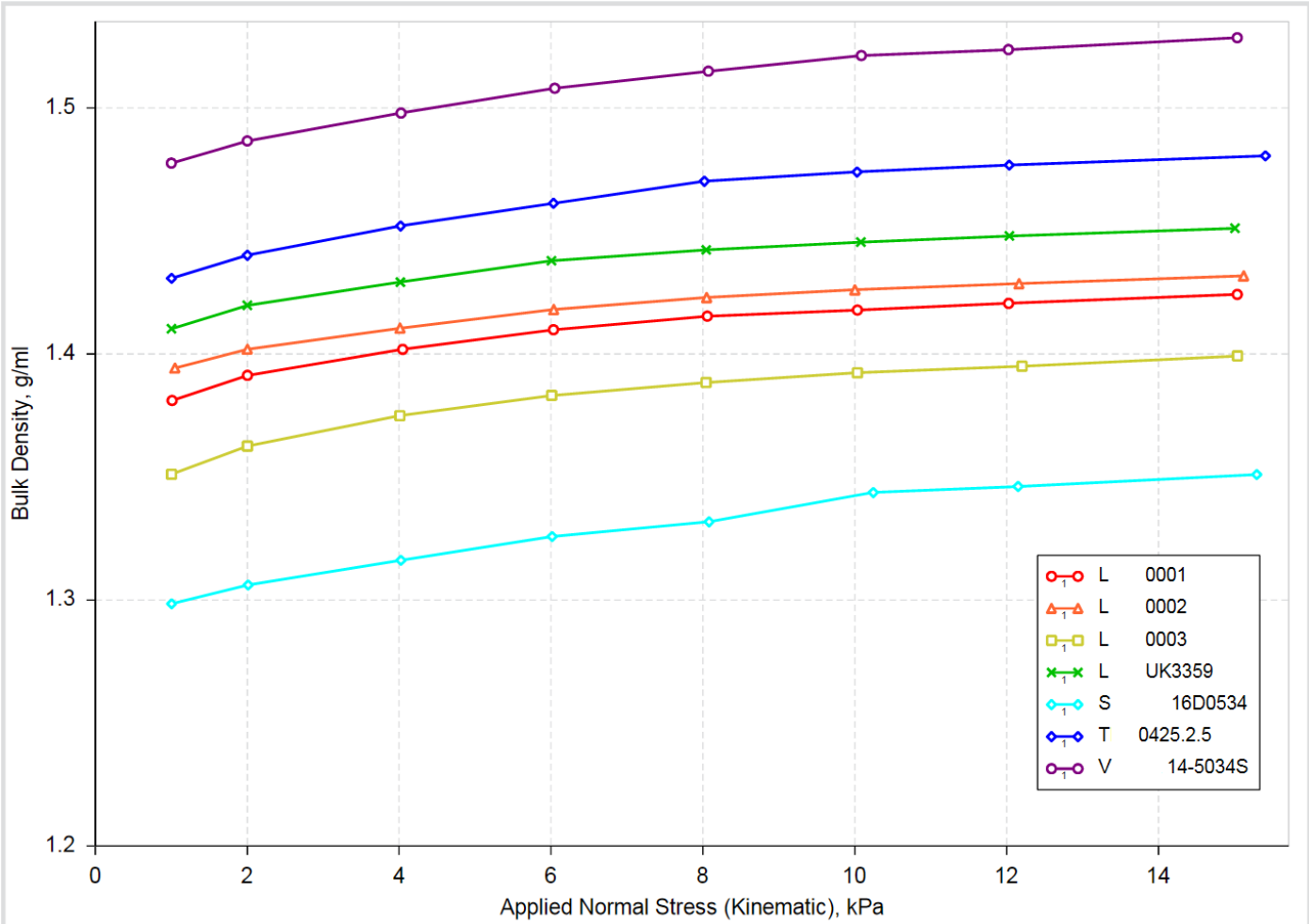


Figure 3.63: Bulk density variation in function of compression stress applied during the test.

It has been considered the compression value at 15 kPa, because it is the reached during the test. The relevant numerical data provided in Table 3.17 are graphically represented in Fig. 3.64:

Table 3.17: Numerical data relative to the compressibility index obtained during the test.

Powder	CBD (g/cm ³)	Density at 15kPa (g/cm ³)	Compressibility Index
L 0001	1.34	1.42	1.060
L 0002	1.37	1.43	1.036
L 0003	1.32	1.40	1.083
L UK3359	1.37	1.45	1.022
S 16D0534	1.26	1.35	1.151
T 0425.2.5	1.39	1.48	1.065
V 14-5034S	1.45	1.53	1.055

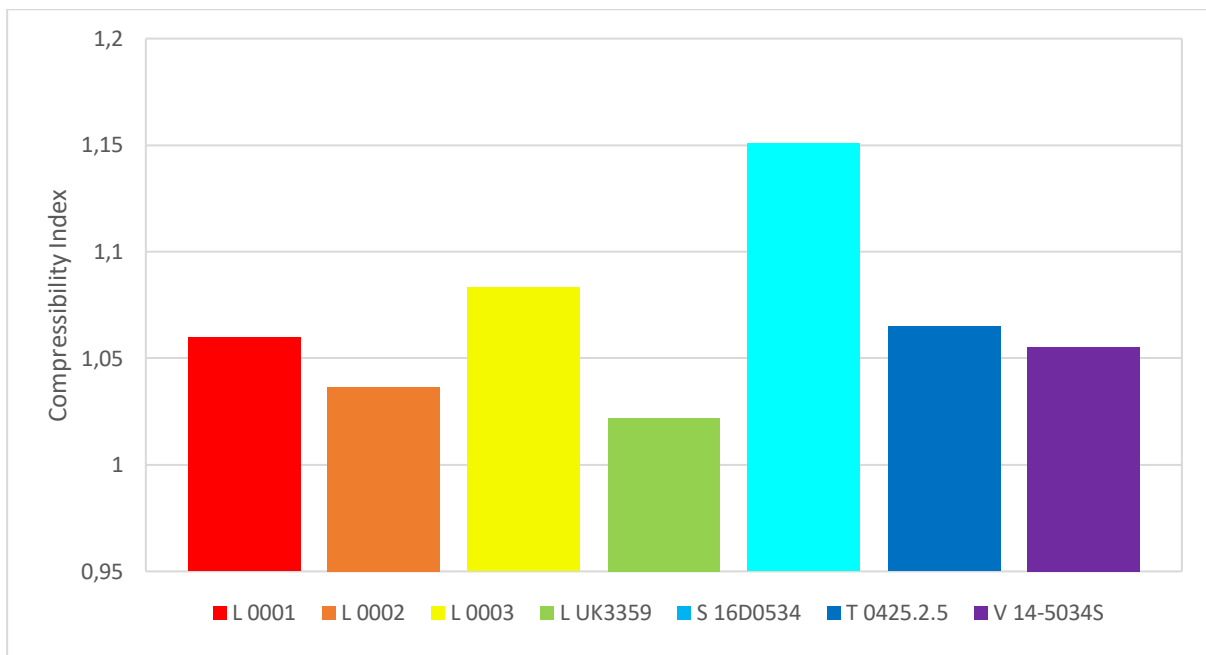


Figure 3.64: Compressibility index bar chart relative to all the AlSi10Mg powders.

In general, cohesive powders contain a high amount of entrained air, which require the vented piston to travel a long distance before the imposed compressive stress can be withstand by the sample. On the opposite, non-cohesive powders are already packed efficiently and the piston needs to travel just a short distance to make the stress be supported by the powder itself, in fact their amount of entrained air is low. This phenomenon usually leads to a situation where the density variation, that can be evaluated through the compressibility index, is far greater for cohesive powders, because entrained air, which is contained in a greater content, is freed during the compression process and escapes through the piston.

As a consequence of the above explained phenomenon, all the analysed powder, besides S 16D0534, have been considered as non-cohesive, due to their density variation being small (always below 10%). Although it must be considered that S 16D0534's satellites break apart during the process, as previously explained. The increase in the compressibility index is then caused by the more efficient rearranging of the smaller particles that used to be satellites, that

leads to a more close-packed structure, able to release more entrained air. For this reason, also that powder has not being considered cohesive.

The interpretation of the data available from that test supports the conclusion made during the analysis of both the aeration test and the permeability test.

3.6.5. Shear Cell Results

The compressibility test results are shown in Table 3.18 and Fig. 3.65, graph in which the shear stress is evaluated as the normal applied stress increases:

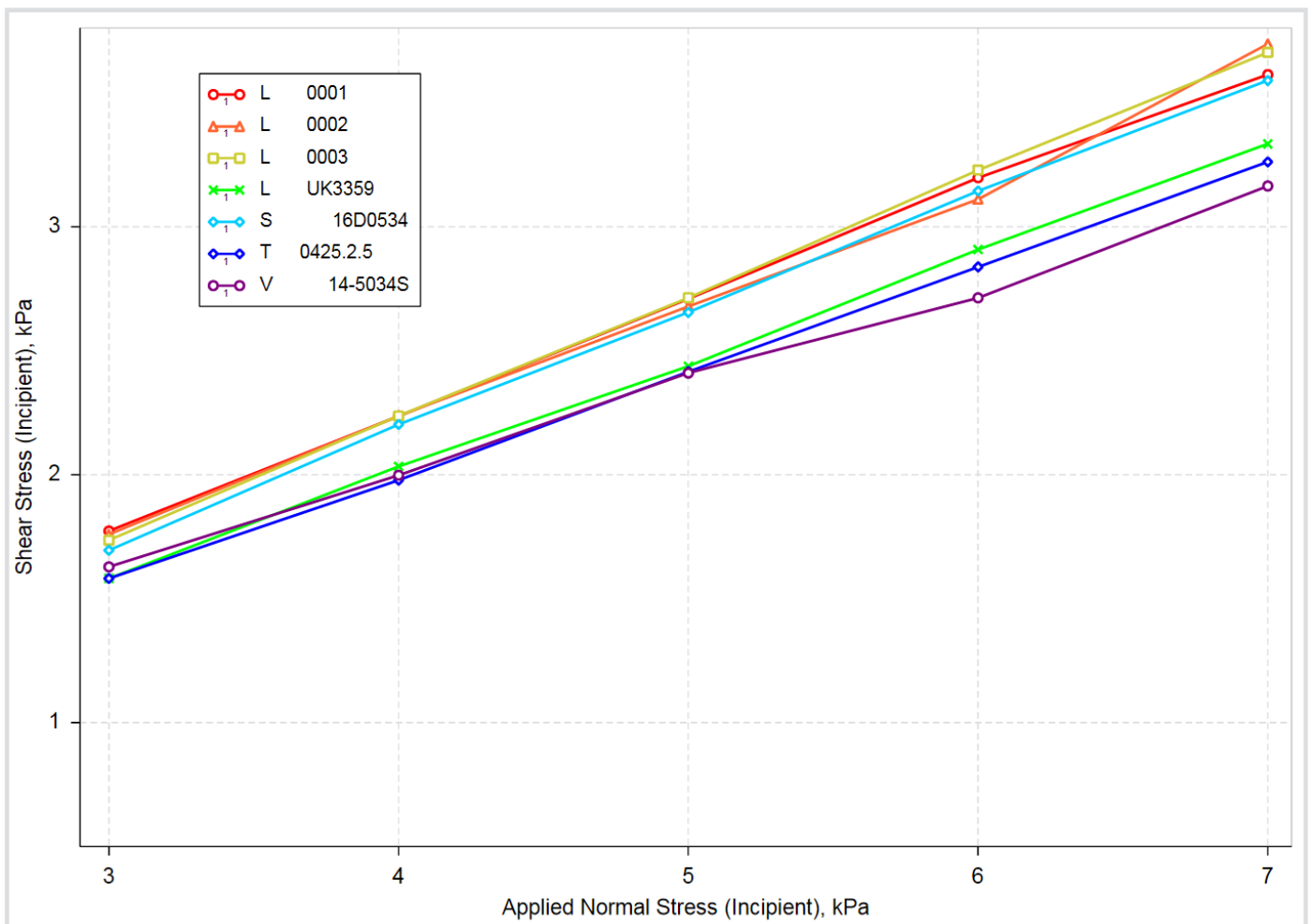


Figure 3.65: Shear cell results.

Table 3.18: Shear cell results.

Powder	Cohesion (kPa)	σ_c (kPa)	σ_1 (kPa)	σ_2 (kPa)	ff_c	Rel(p)	AIF (°)
L 0001	0.385	1.21	12.9	4.78	10.7	6.76	24.9
L 0002	0.288	0.918	12.9	4.72	14.1	8.93	25.8
L 0003	0.260	0.837	12.8	4.63	15.3	9.77	26.2
L UK3359	0.270	0.826	12.3	4.92	14.9	8.97	23.6
S 16D0534	0.292	0.923	13.0	4.85	14.1	8.85	25.3
T 0425.2.5	0.304	0.918	12.4	5.03	13.5	7.98	22.9
V 14-5034S	0.487	1.41	12.5	5.30	8.89	5.13	20.8

In the previous table, there are a lot of parameters that must be explained. To help the process, they are graphically represented in Fig. 3.66, where L UK3359 has been used as an example.

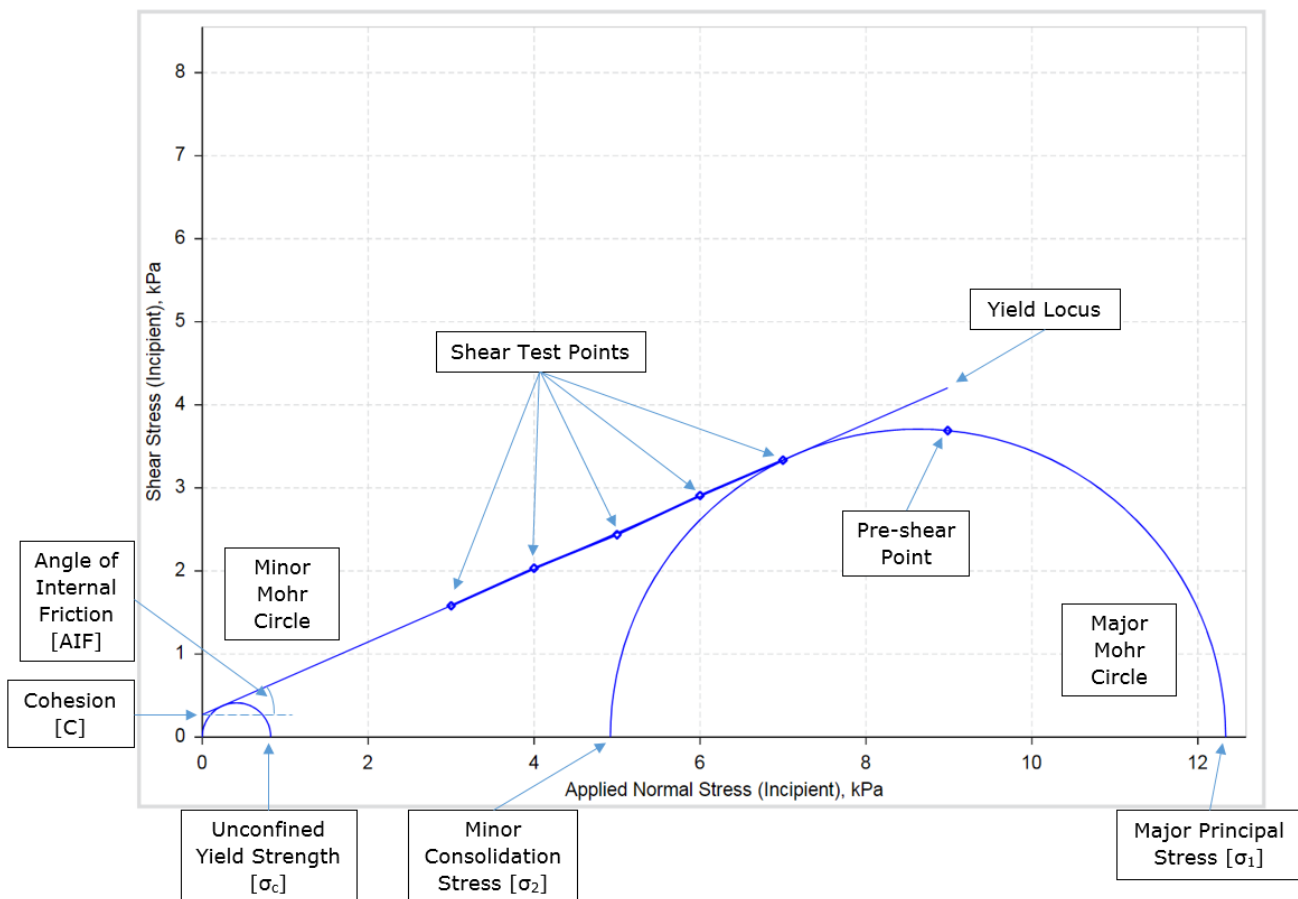


Figure 3.66: Test parameters graphical representation, the powder shown is L UK3359 (Courtesy of Freeman Technology). [46]

During the test, a normal stress is applied on the powder bed, then, whilst it keeps being applied, the shear cell head rotates to induce a shear stress. The powder initially resists that

movement, until it is overcome and the bed shears. The couple of normal stress and shear stress values (σ_i, τ_i) that results on the powder bed failure is defined as Yield Point. Of course, a different value of applied normal stress corresponds to a different shear stress for the Yield point. The Yield Locus is obtained by plotting on the graph all the five yield points obtained during the test.

Once the Yield Locus is obtained, it can be used to further analyse test data by applying the Mohr stress circles. First of all, a best fit line is applied to the Yield points obtained, so that the yield locus can be drawn. Then the smallest circle is obtained by drawing a semi-circle that passes through the origin and is tangential to the yield locus. The larger circle is drawn as the semi-circle that passes through the pre-shear point and is tangential to the yield locus.

Once the Mohr circles have been drawn, the following parameters can be derived:

- Cohesion (C): the shear stress corresponding to normal stress = 0, it is the point where the yield locus intercepts the Y-axis.
- Major Principal Stress (σ_1): the greater of the two values at which the bigger Mohr Circle intercepts the X-axis.
- Minor Consolidation Stress (σ_2): the smaller of the two values at which the bigger Mohr Circle intercepts the X-axis.
- Unconfined Yield Strength (σ_c): the greater of the two values at which the smaller Mohr circle intercepts the x-axis.
- Angle of Internal Friction (AIF): the angle created by the Yield locus and the X-axis.

A useful index can be used to study the test data. It is called Flow Function (FF or ff_c) and is defined as:

$$ff_c = \frac{\sigma_1}{\sigma_c} \quad (3.8)$$

Where:

$\sigma_1 = \text{Major principal stress [kPa]}$

$\sigma_c = \text{Unconfined yield strength [kPa]}$

Generally, a more cohesive powder will show high cohesion values, hence high values of σ_c and consequently a low ff_c . If that index is high instead, it should indicate a good flowing behaviour when in an environment characterised by a stress range close to that used in the test. [44, 46]

The full results graph, comprehensive of the Mohr Circles and the Pre-Shear Points, is shown in Fig. 3.67:

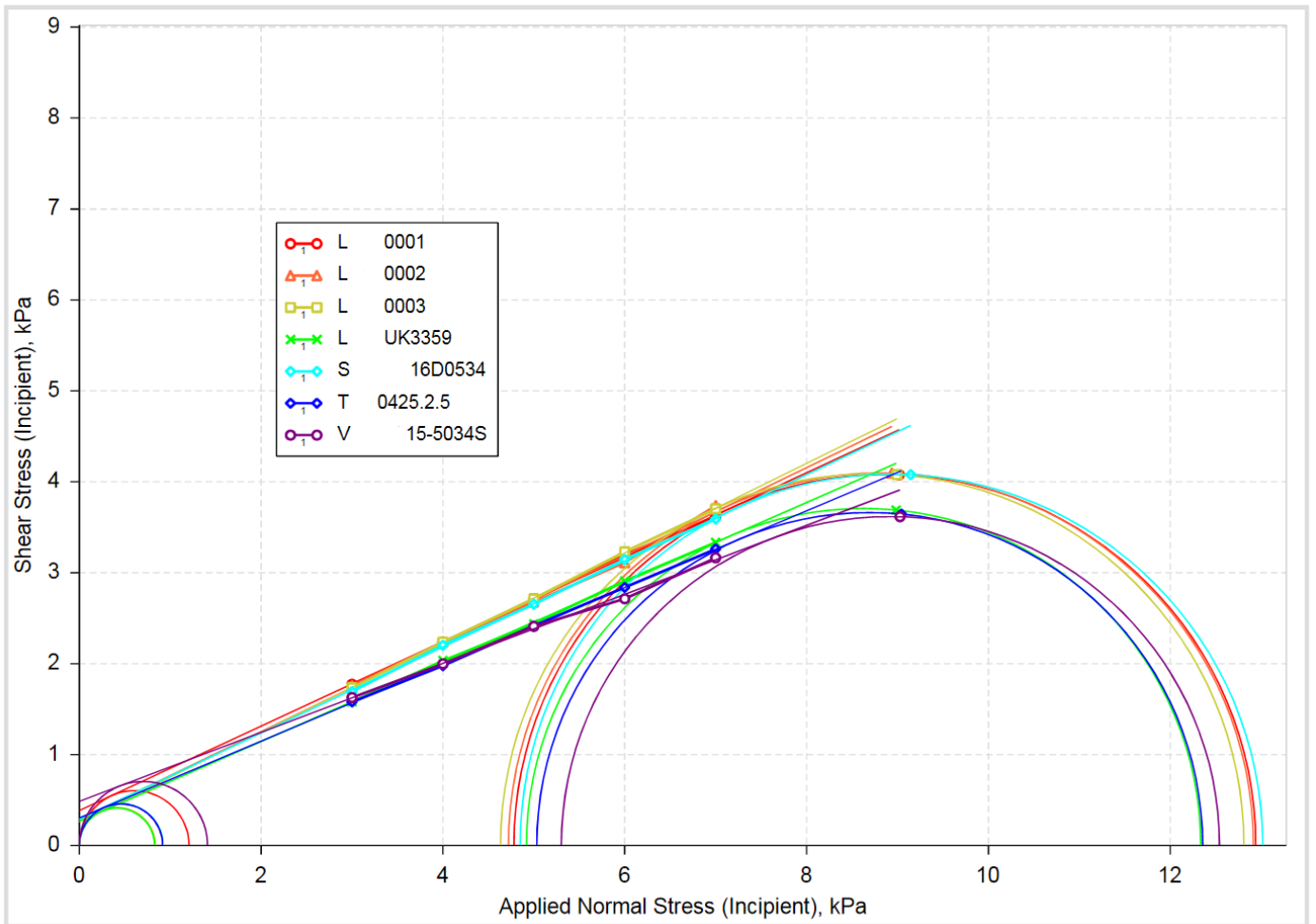


Figure 3.67: Shear cell full results graph.

As it can be already noticed from the previous graph, for this stress range, L 0001 and V 15-5034S proved to be more cohesive than most of all the other powders. The easy comparison can be made looking at the different σ_c values. This can be confirmed by the flowability analysis studied by Jenike [47] that revolves around the ff_c . According to that study, powder flowability can be determined in function of the flow function value as shown in Table 3.19:

Table 3.19: Correlation between ff_c and powder flowability (Courtesy of Freeman Technology). [46]

Type of flow	ff_c
Free-flowing	$10 < ff_c$
Easy-flowing	$4 < ff_c < 10$
Cohesive	$2 < ff_c < 4$
Very cohesive/Non-flowing	$ff_c < 2$

According to that, all the powder, except V 15-5034S, can be labelled as “free-flowing”, confirming what was stated before.

A graphical representation that makes it easier to visualize the concept is provided in Fig. 3.68:

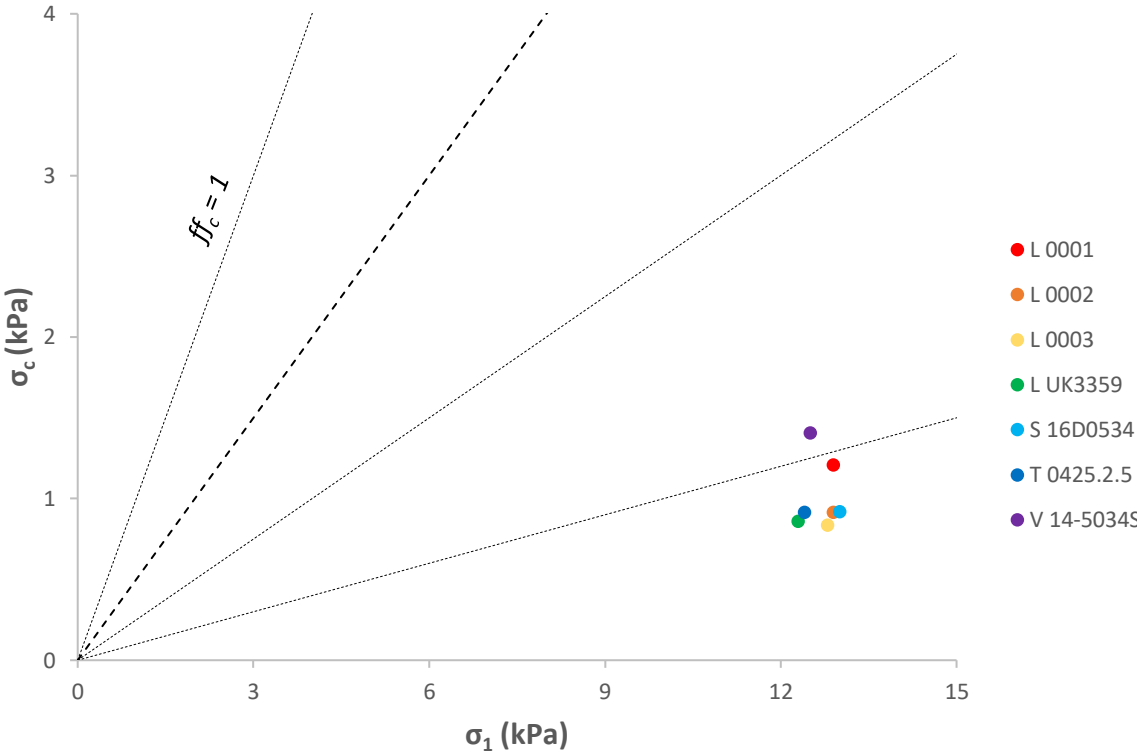


Figure 3.68: Application of the Jenike study.

ff_c can also be directly compared with the compressibility test results, as shown by Leturia et al. [48]. For doing that, test data must be referred to the same normal stress value. The applied normal stresses during the compressibility test were: 1, 2, 4, 6, 7, 10, 12, 15 kPa. While the only stress value used during the shear cell was 9 kPa. To make the comparison possible, it has been considered as the compressibility value for 9 kPa was the average value between the ones relative to 8 kPa and 10 kPa. The graphical representation of the results is shown in Fig. 3.69:

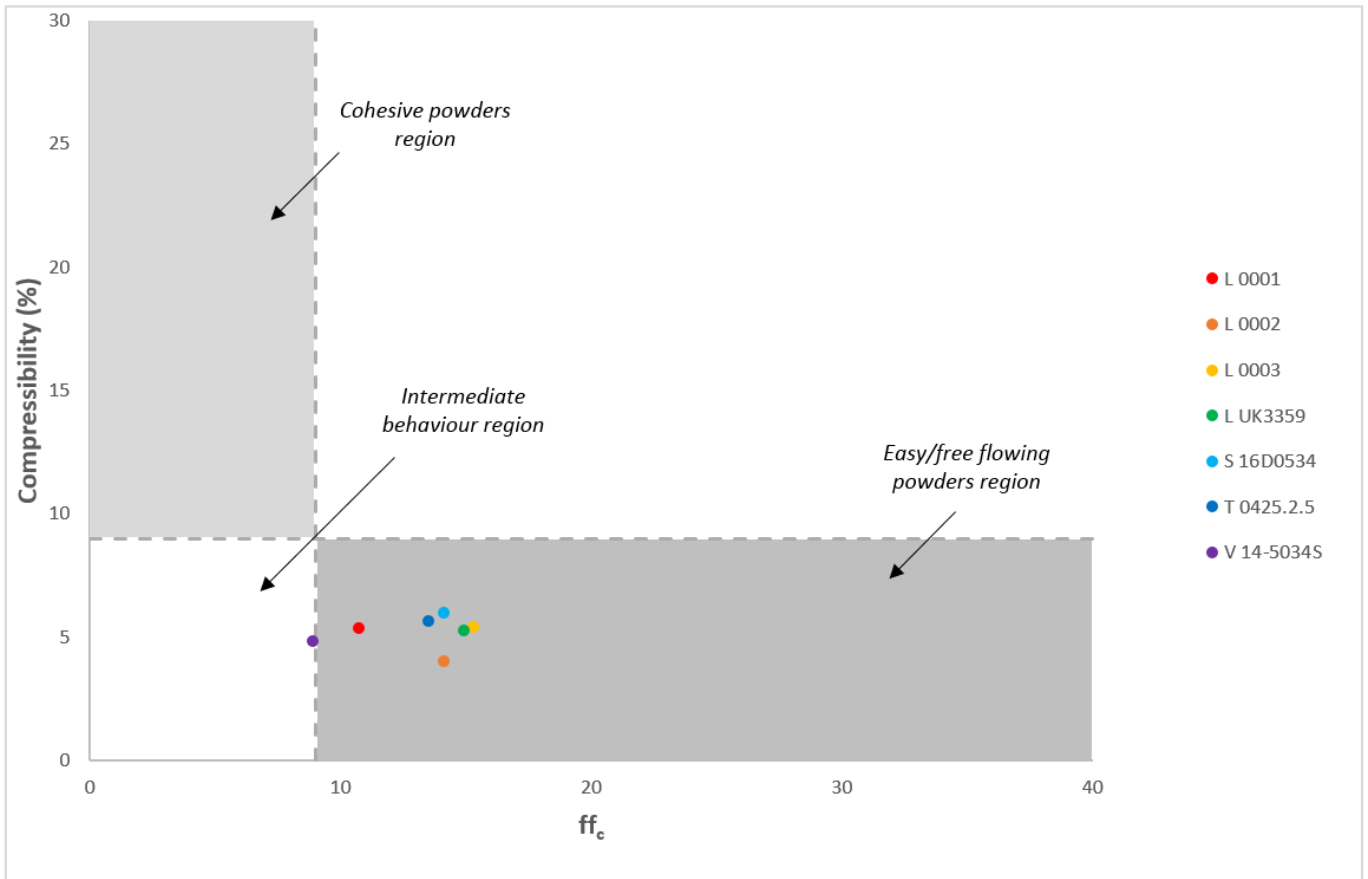


Figure 3.69: Shear cell and compressibility test results combined interpretation.

It is evident again the worse flowing behaviour of V 14-5034S, probably due to high cohesion (Fig. 3.67), maybe caused by the efficient powder packing due to the presence of very small particles, that were satellites at the beginning of the test.

But ff_c is not the only parameter that can be used to evaluate powder flowability, others have been developed. In this case $Rel(p)$ will be discussed [49]. The term “Rel” refers to relative flowability, “(p)” relates to Dr Ivan Peschl, the person who firstly suggested this parameter as an alternative to Jenike’s Flow Function (ff_c). It can be defined as:

$$Rel(p) = \frac{\sigma_1 - \sigma_2}{\sigma_c} \quad (3.9)$$

Where:

σ_1 = Major principal stress [kPa]

σ_2 = Minor consolidation stress [kPa]

σ_c = Unconfined yield strength [kPa]

Powder flowability can be classified using this parameter as explained in Table 3.20:

Table 3.20: Rel(p) and powder flowability correlation (Courtesy of Freeman Technology). [46]

Cohesion	Rel(p)
Bonding, solid	< 1
Plastic material	= 1
Extremey cohesive	1 – 2
Very cohesive	2 – 4
Cohesive	4 – 10
Slightly cohesive	10 – 15
Cohesionless	15 – 25

Compraing these table ranges with the test data (Table 3.18), all the analysed powders result being cohesive, which seems to contradict the ff_C results. Although it must be considered that this is a different type of analysis and in general the first one is preferred. In fact, the standardazide design protocol for mass flow hoppers (designed by Jenike) uses a plot of σ_1 and σ_C , obtained from several shear tests conducted ad different consolidating stresses.

It is although interesting to consider that even if all the powders fall in the 4 – 10 range, the general trend is the same shown during the ff_C analysis: most of the powders show similar values (8-9), suggesting similar characteristics, beside L 0001 which is slightly more cohesive (6.76) and most of all V 14-5034S (5.13), that is very close to the limit with the “very cohesive” range. Just a visual comparison between that and, for example, Fig. 3.68 show that there is coherency between Rel(p) and ff_C . In fact, even if these two parameters are obtained in different ways, their results show the same trend.

It must be also noted that V 14-5034S is the powder that shows the highest cohesion value (0.487 kPa). One possible cause may be again the satellite loss during the test, that leads to a packed, more cohesive sample, which results in a stronger energy/force required to make it flow.

The reason why L 0001 is more cohesive than the other powders is still unknown. It is not sure if the cause is due to the powder itself or the testing conditions. It is possible that a sample particularly rich of impurities was analysed, even if it seems quite unlikely, because L 0003, the powder with the highest impurities content, had the best test results. In fact, by analysing Rel(p) and ff_C , it appears as the least cohesive powder.

4. Results and Discussion for the A205 Powder

4.1. SEM/EDS

4.1.1. Shape and Morphology

V 15-6053S appears as a powder characterised by some oblong and irregular big particles. That can be noted in Fig. 4.1, where some of them have been highlighted.

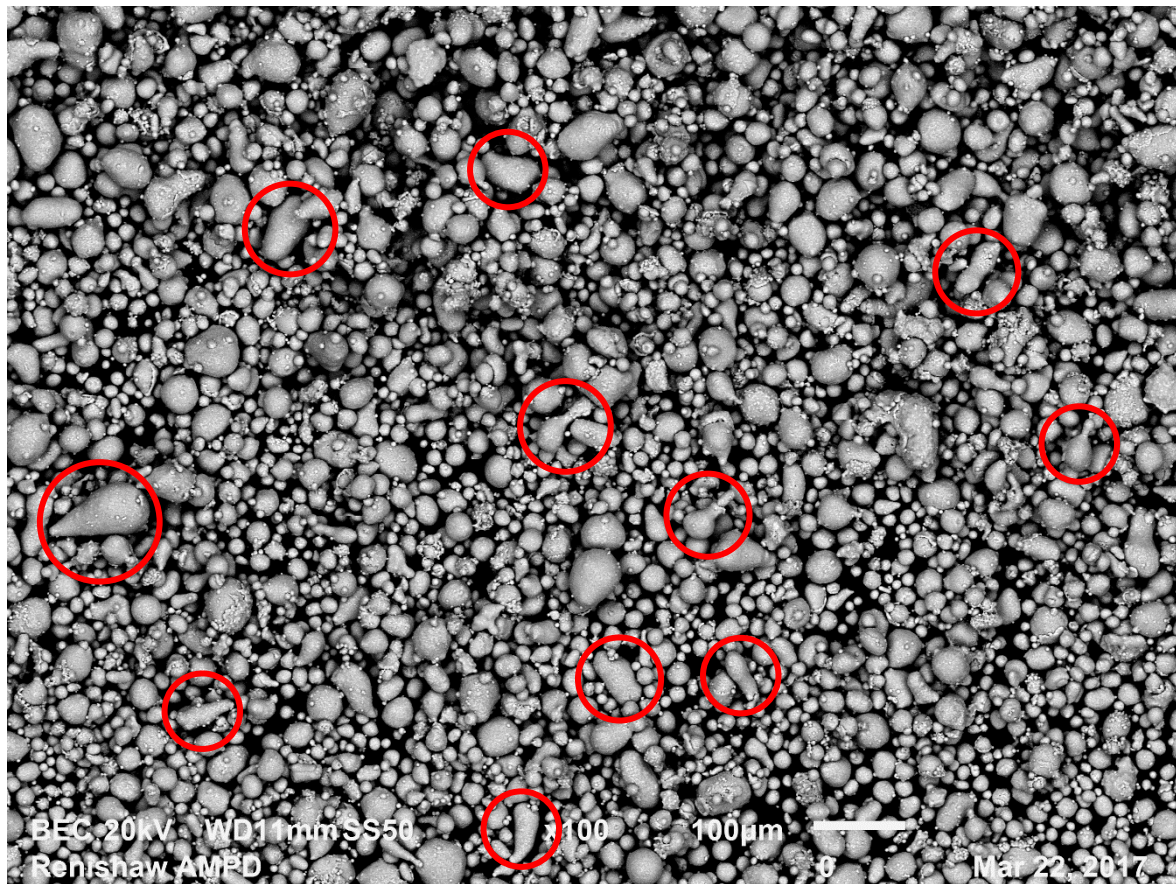


Figure 4.1: SEM image (backscattered electrons, 100x) of V 15-6053S.

By using a higher magnification and switching to secondary electrons (Fig. 4.2), it can be noticed the presence of satellites, even if they are not as common as they were in some of the powders analysed before. Some “splashes”, like the ones found in T 0425.2.5, can also be found.

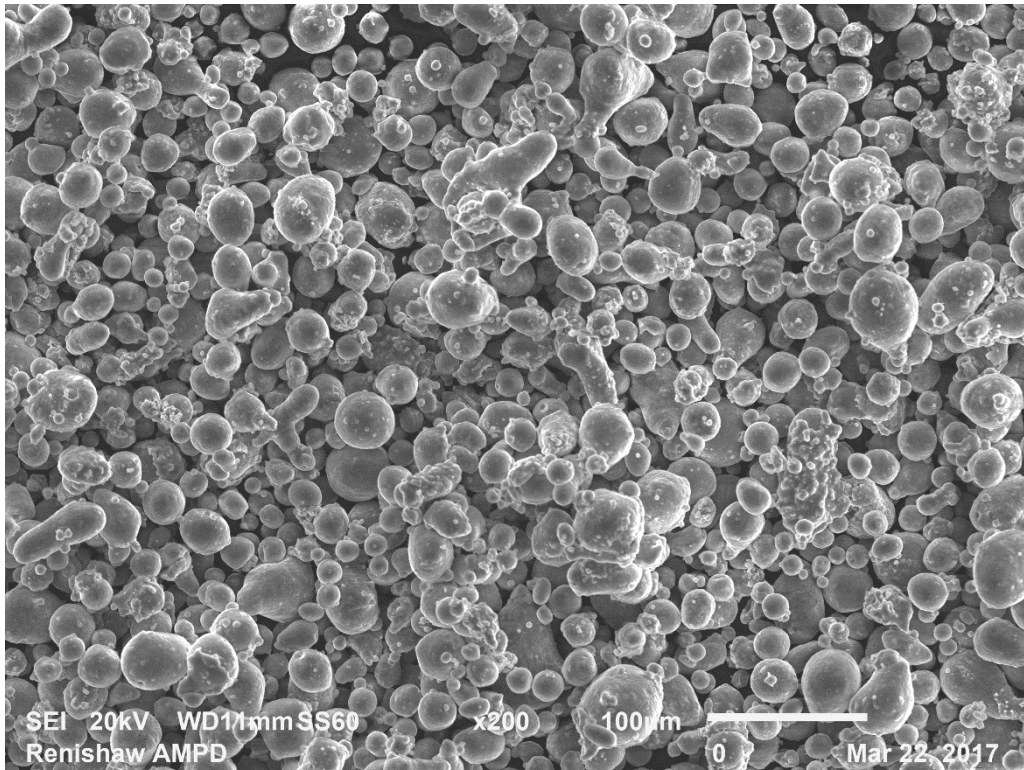


Figure 4.2: SEM image (secondary electrons, 200x) of V 15-6053S.

If an even higher magnification is used (Fig. 4.3), it is possible to visualize particle surfaces, that seems to be quite rough.

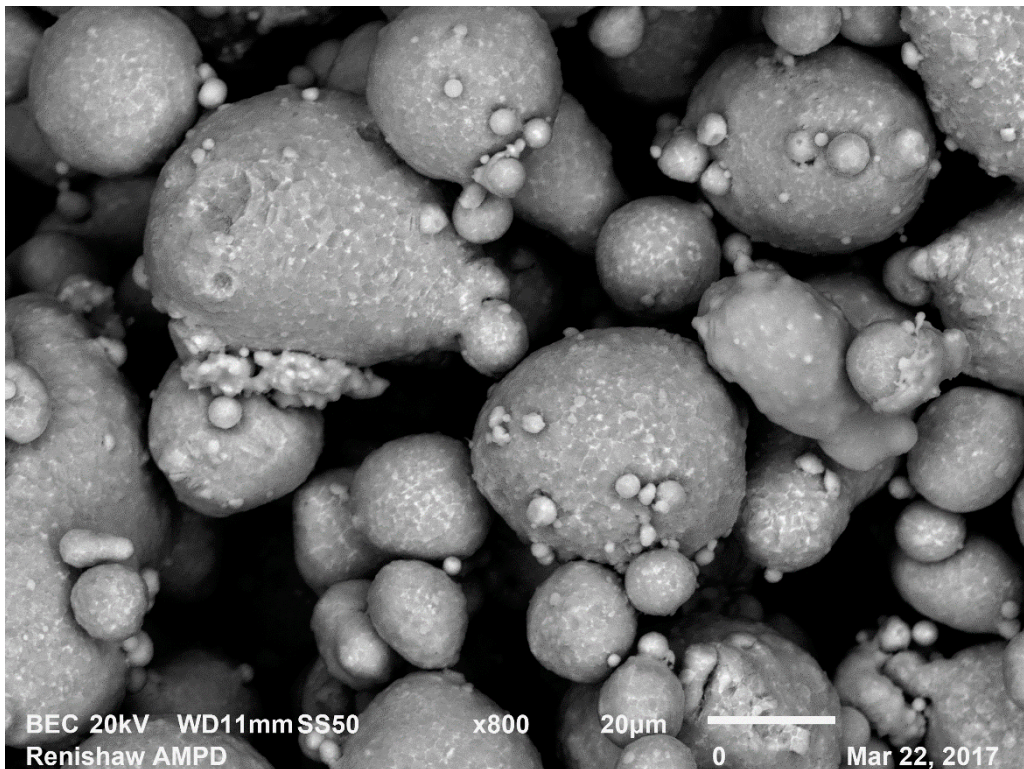


Figure 4.3: SEM image (backscattered electrons, 800x) of V 15-6053S.

To sum up, according to the preliminary imaging analysis that has been performed, any problem that may be related to this powder flowability can be linked to the following morphological causes:

- Presence of a lot of oblong, big, irregular particles.
- High splashes content.
- Rough surfaces.

4.1.2. Chemical Composition Analysis

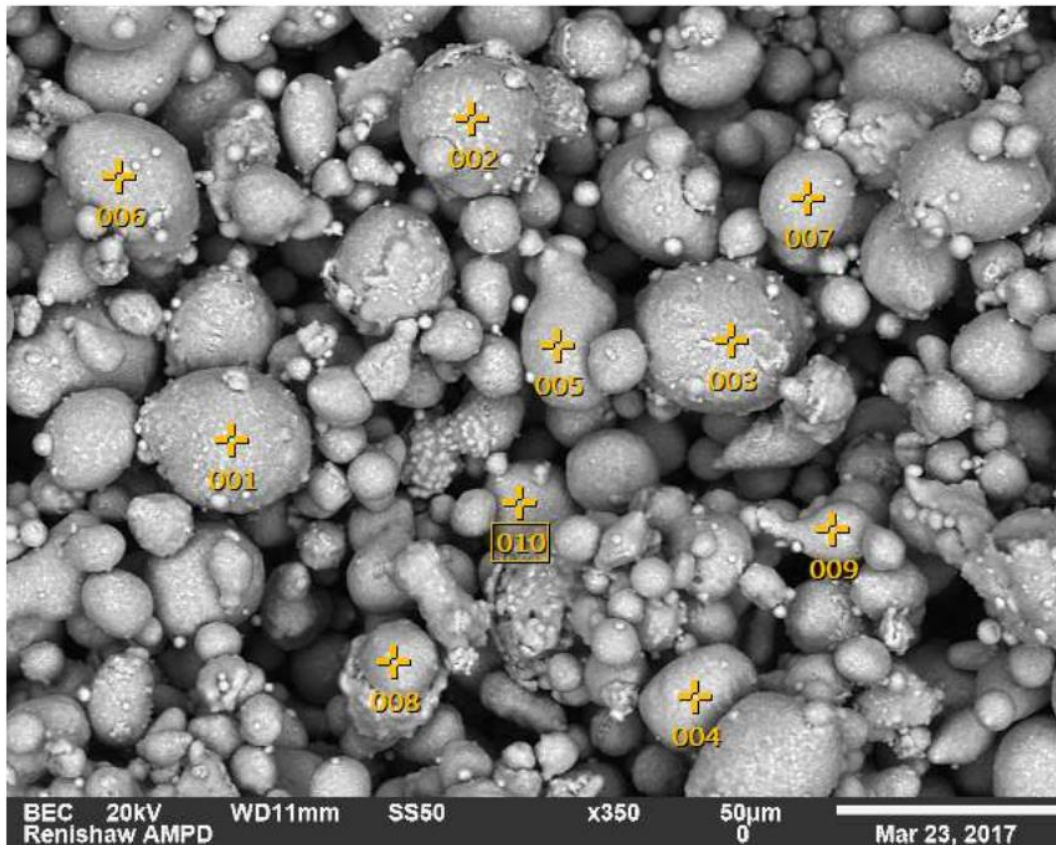


Figure 4.4: Spots selected for the EDS analysis (350x) of V 15-6053S.

The results of the EDS analysis are shown at both 350x (Fig. 4.4) and 500x magnification in Table 4.1. Although it must just be noted that, according to the certificate provided by the supplier, that powder contains approximately 1.6% of boron, that cannot be detected, being a light element, during the EDS analysis, hence it will not appear in the results.

Table 4.1: EDS analysis results.

Magnification	Al (%)	Al St Dev (%)	Ag (%)	Ag St Dev (%)	Mg (%)	Mg St Dev (%)	Ti (%)	Ti St Dev (%)	Cu (%)	Cu St Dev (%)
350x	90.41	0.57	1.28	0.25	0.24	0.03	2.21	0.11	5.86	0.96
500x	86.47	1.60	1.35	0.03	0.22	0.01	2.17	0.35	9.92	1.34

4.2. Density measurement

The analysed sample resulted in a density of 2.8816 g/cm³, with a standard deviation of 0.0017 g/cm³. As it can be seen in Fig. 4.5, both the temperature and density variation during the test were small, hence the result can be considered reliable.

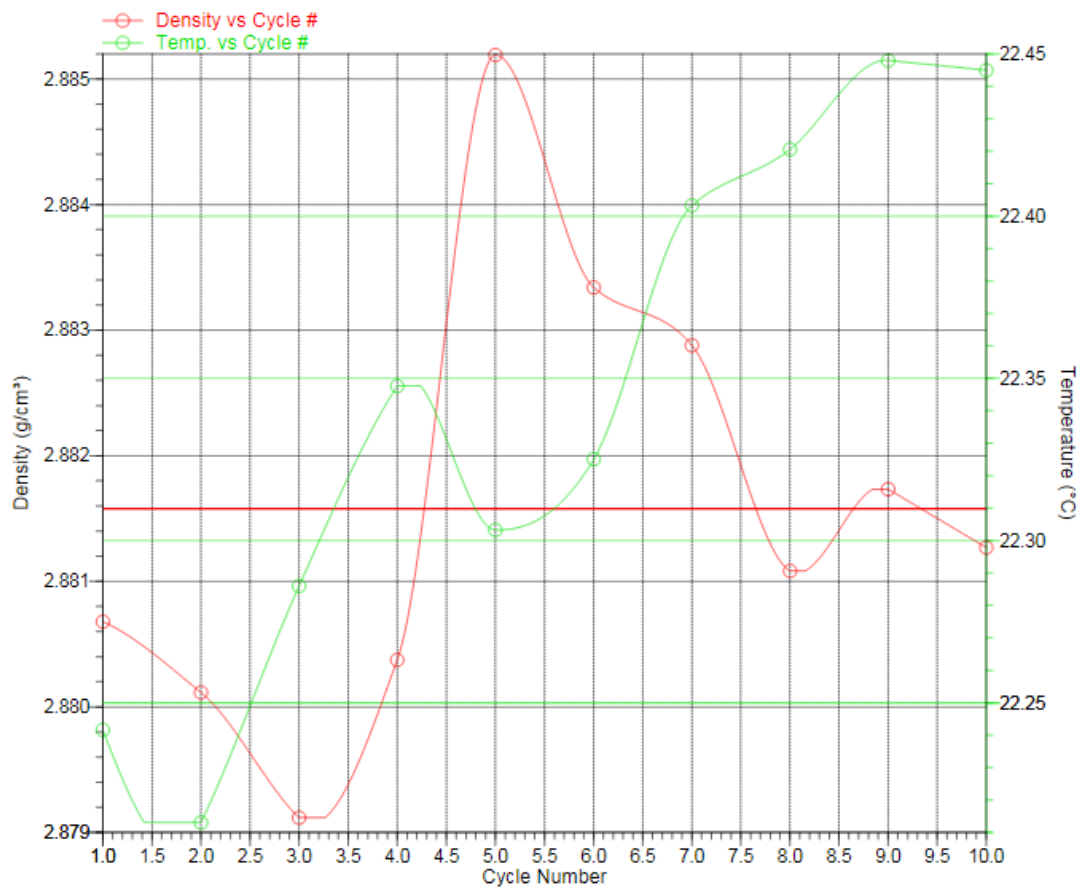


Figure 4.5: Temperature and density trend during the V 15-6053S test.

4.3. Particle Size Distribution

This test results are shown in Fig. 4.6 and Table 4.2.

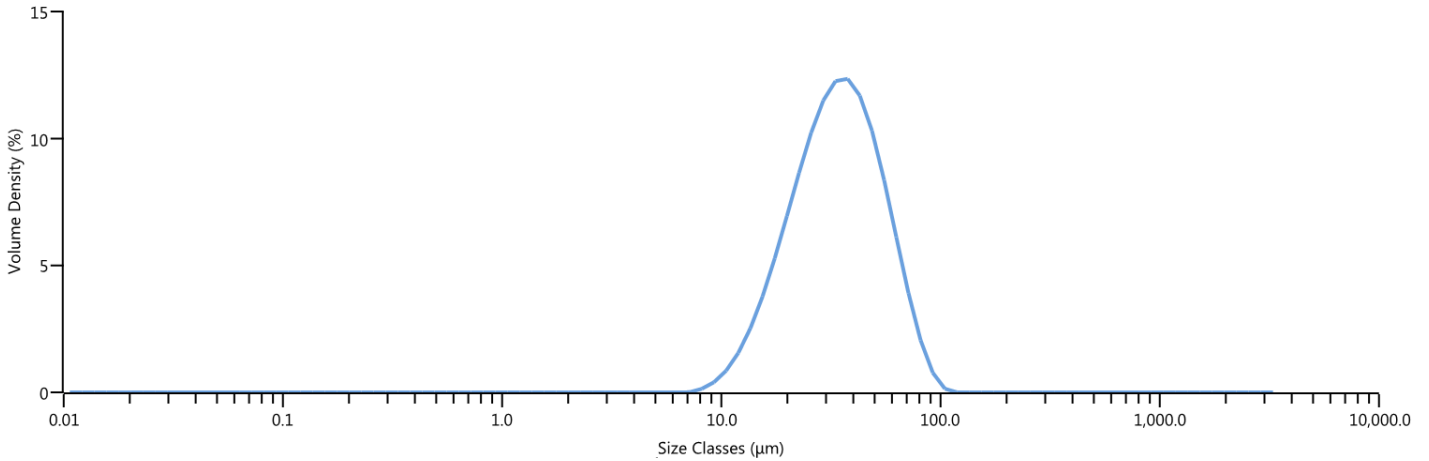


Figure 4.6: Particle size distribution graph of V 15-6053S.

Table 4.2: Particle size distribution analysis results for V 15-6053S.

Powder	D(10) (µm)	D(50) (µm)	D(90) (µm)
V 15-6053S	17.6	33.8	59.9

The curve appears symmetrical, suggesting from that point of view a good flowing behaviour. It must be although noticed that the D(50) value is quite low. Moreover D(10) is the lowest of all the powders analysed. This information suggests a more cohesive behaviour, in fact, being the particles on average smaller, their surface over volume ratio is higher, hence the cohesive forces are stronger. But it must be considered that this material has a higher density, hence the gravitational force is consequently stronger ($\propto m$). As a consequence of that, any consideration about the force equilibrium between cohesive and gravitational forces cannot be done by comparing A205 particles and AlSi10Mg particles, until further experiments are conducted, because of the different density values.

In Fig. 4.7 a visual comparison of SEM images at the same magnification between V 15-6053S (left) and L 0001 (right) makes it easier to visualize the big difference in particle size.

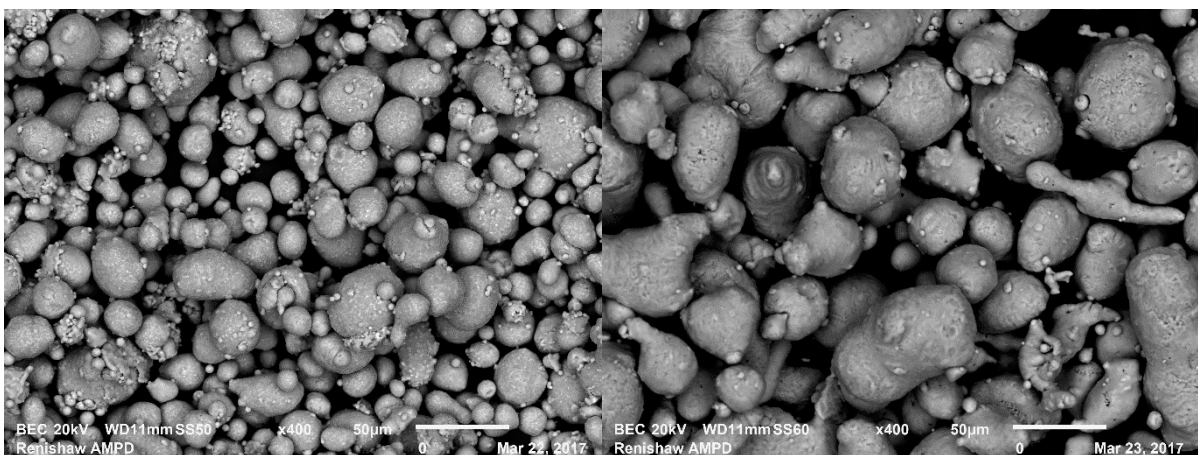


Figure 4.7: SEM images (backscattered electrons, 400x) of V 15-6053S (left) and L 0001 (right).

4.4. Powder Flow Test

The V 15-6053S powder was not able to flow through the Hall funnel nor the Carney funnel. That suggest a bad flowing behaviour, that makes it impossible for the powder to be processed.

4.5. Moisture Content

V 15-6053S moisture content was evaluated to be equal to 0.016%.

Exactly as it happened during the test for the other V powder, even in that case, after 2 hours in the oven, the sample showed a little amount of agglomeration on the surface, as shown in Fig. 4.8.



Figure 4.8: Agglomeration on V 15-6053S sample surface after the moisture content test.

Considering that and the powder flow test results, it is possible to state that the cohesive forces are strong enough to make the powder unable to flow properly and to cause agglomeration if heated. Of course, the latter phenomenon is not as relevant as it was for V 14-5034S, in fact just a small number of particles agglomerated (Fig. 4.9).



Figure 4.9: Agglomeration comparison between V 14-5034S (AlSi10Mg, left) and V 15-6053S (A205, right).

It must be considered again that a direct comparison between the two powders can also be indicative and it is not that accurate because these two samples are different materials, so they have different properties (e.g. density).

4.6. Powder Rheometer

4.6.1. Stability Test and Variable Flow Rate Test Results

The results of these tests are shown in Fig. 4.10 and Table 4.3.

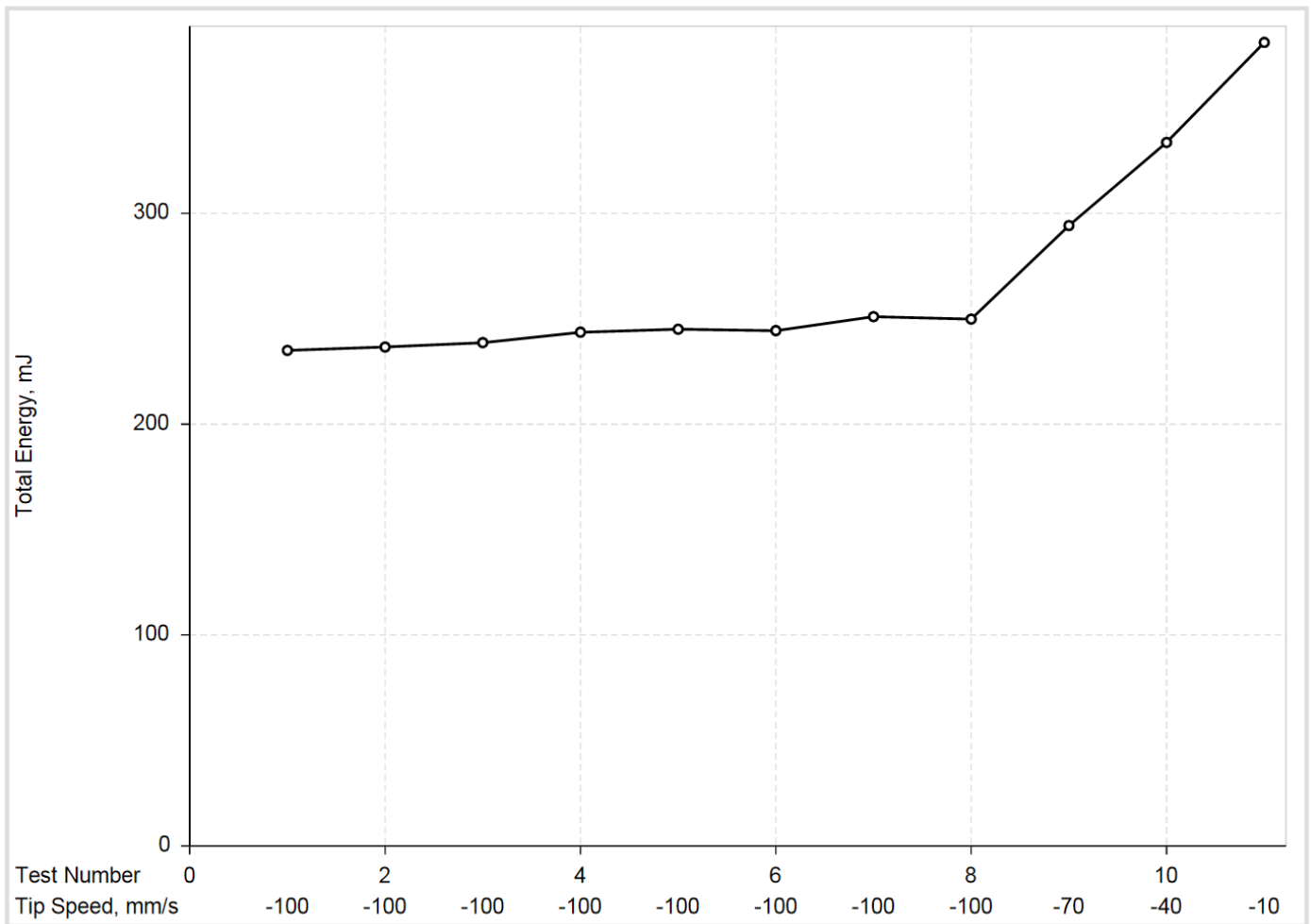


Figure 4.10: Stability test and variable flow rate test results for V 15-6053S.

Table 4.3: Stability and variable flow rate test results for V 15-6053S.

SI	BFE (mJ)	SE (mJ/g)	FRI	CBD (g/cm ³)
1.07	251	3.55	1.53	1.44

From a graphical point of view, that powder does not seem to be highly influenced by being conditioned, in fact its stability index is very close to 1. Its low BFE value makes it likely to be easily made flow by shearing stresses. The other indexes describe it as not very cohesive and characterised by an average flow sensitivity.

If compared with the AlSi10Mg powders, taking account of the fact that the comparison is not completely accurate due to the different compositions, this is the only powder that lies in the 1.5 – 3.0 range for FRI.

It must be stated that this powder’s CBD will not be compared with the AlSi10Mg samples. In fact, that value is influenced by the actual material density, which is completely different due to different chemical composition (see pycnometer results).

4.6.2. Aeration Test Results

The results of the aeration test are shown in Fig.4.11 and Table 4.4.

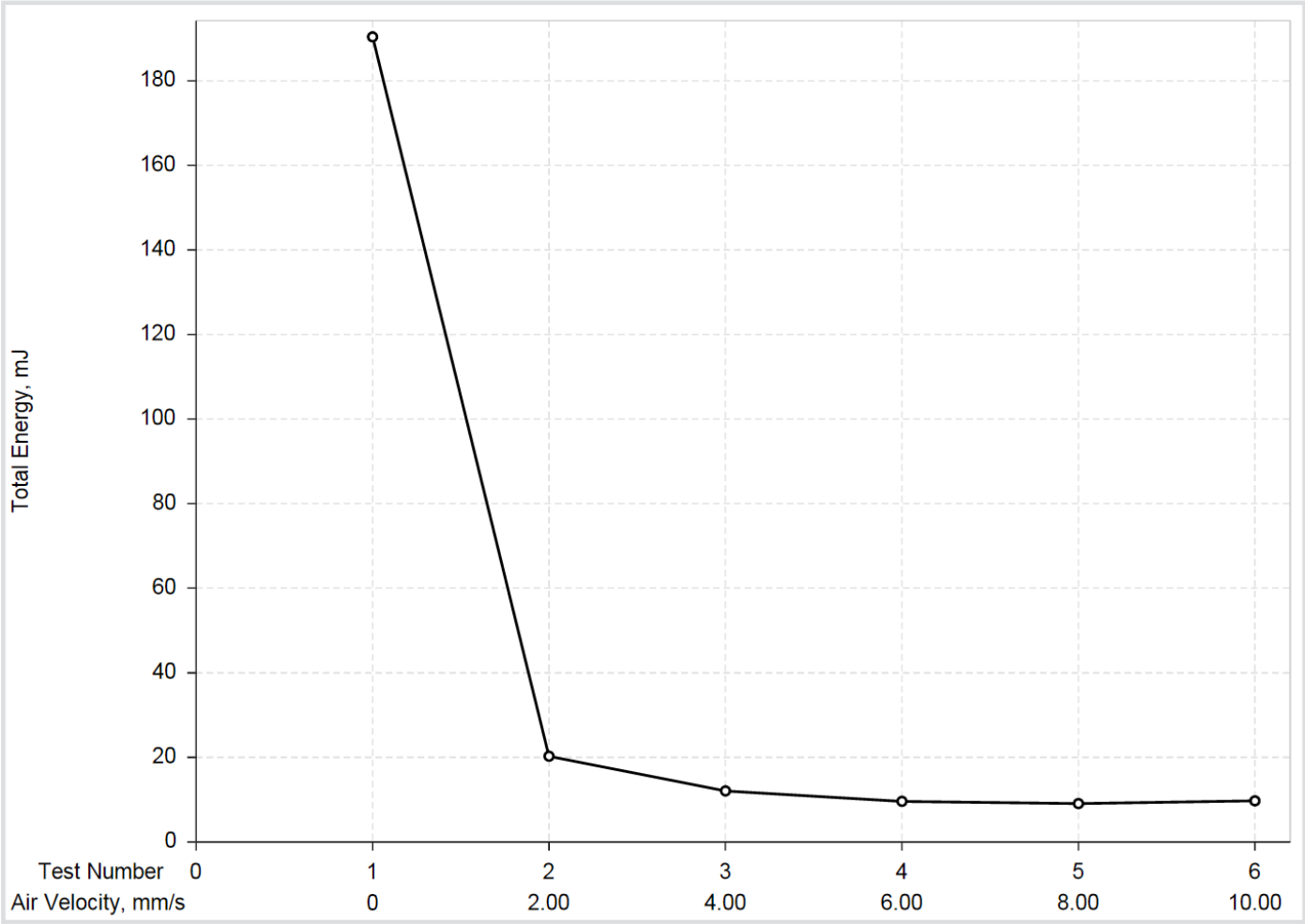


Figure 4.11: Aeration test results for V 15-6053S.

Table 4.4: Aeration test results for V 15-6053S.

AR_10	BFE (mJ)	AE_10 (mJ)
19.6	190	9.71

Considering that AE_10 is lower than 10 mJ, it means that the powder was fluidised during the test, so it can be considered reliable.

This powder minimum fluidisation velocity lies between 3 and 4 mm/s.

Its BFE is lower during that test, if compared with its value during the previous one. That suggests that the possibility to release entrained air during the conditioning cycle from both the top and the bottom of the vessel was more influencing than any electrostatic interaction that can happen between the powder itself and the metallic base.

Its AR_10 suggests an average sensitivity to aeration, hence cohesion. The limit to be defined as highly sensitive is 20, so V 15-6053S is close to that. Considering that a particle sensitivity to aeration is not that important for an additive manufacturing process, this test is more useful when used to compare different powder properties. V 15-6053S shows the lowest AR_10 value, when compared with the AlSi10Mg powders, suggesting that it is less sensitive to aeration. Although it must be considered again that a direct comparison is not that accurate, because in this test the gravitational force is very important and the different powder density plays an important role. Hence it is not possible to state if that difference is completely due to the density or if it is partially influence by some powder properties.

4.6.3. Permeability Test Results

The permeability test results are shown in Fig. 4.12 and Fig. 4.13.

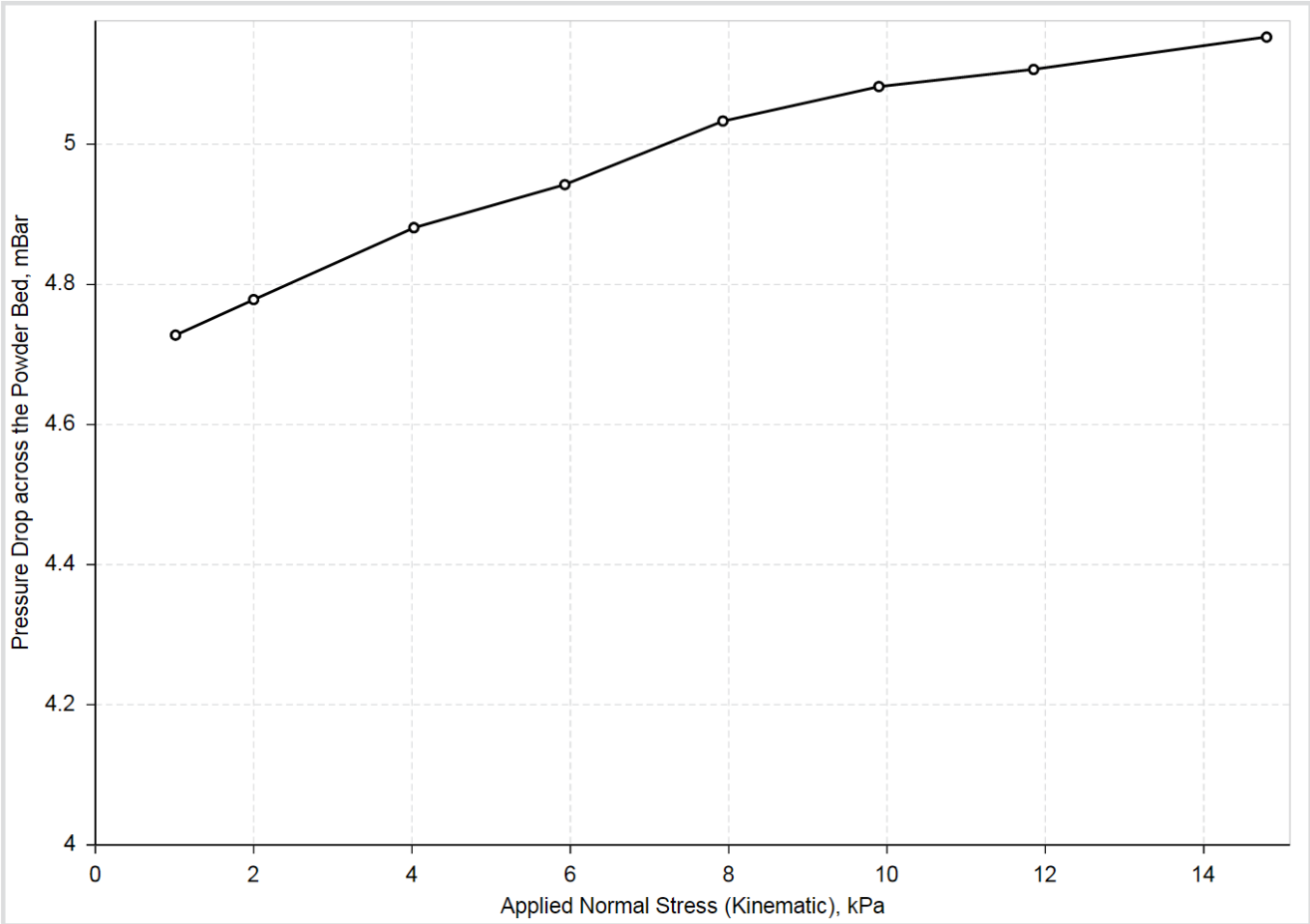


Figure 4.12: Permeability test result for V 15-6053S.

It is possible to noticed, from the previous graph, that V 15-6053S is characterised by a high pressure drop across the powder bed. That result is in line with the other powders data, considering that it did not flow through the Carney funnel.

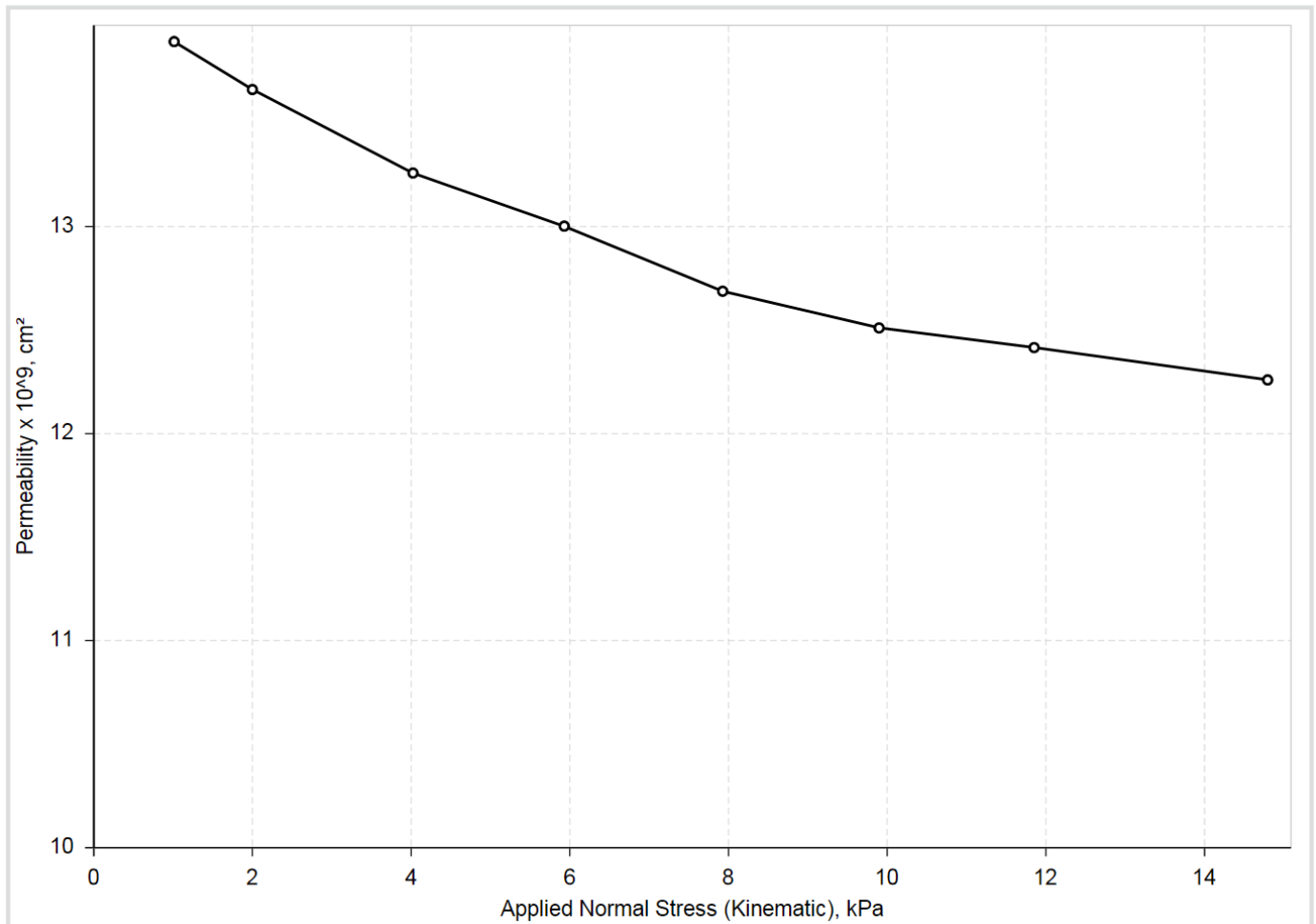


Figure 4.13: Permeability test results for V 15-6053S, where permeability is plotted instead of pressure drop.

By comparing the graph from Fig. 13 with the one relative to the AlSi10Mg powders (Fig. 3.53), it is possible to notice that the V 15-6053S line corresponds to low permeability values. It has been previously stated that there is a correspondence between these graphs and the flowing behaviour. It seems to work even in that case, because V 15-6053S would lie in the lowest part of the graph, in agreement with the result of its flowability test.

4.6.4. Compressibility Test Results

The compressibility test results are shown in Fig. 4.14.

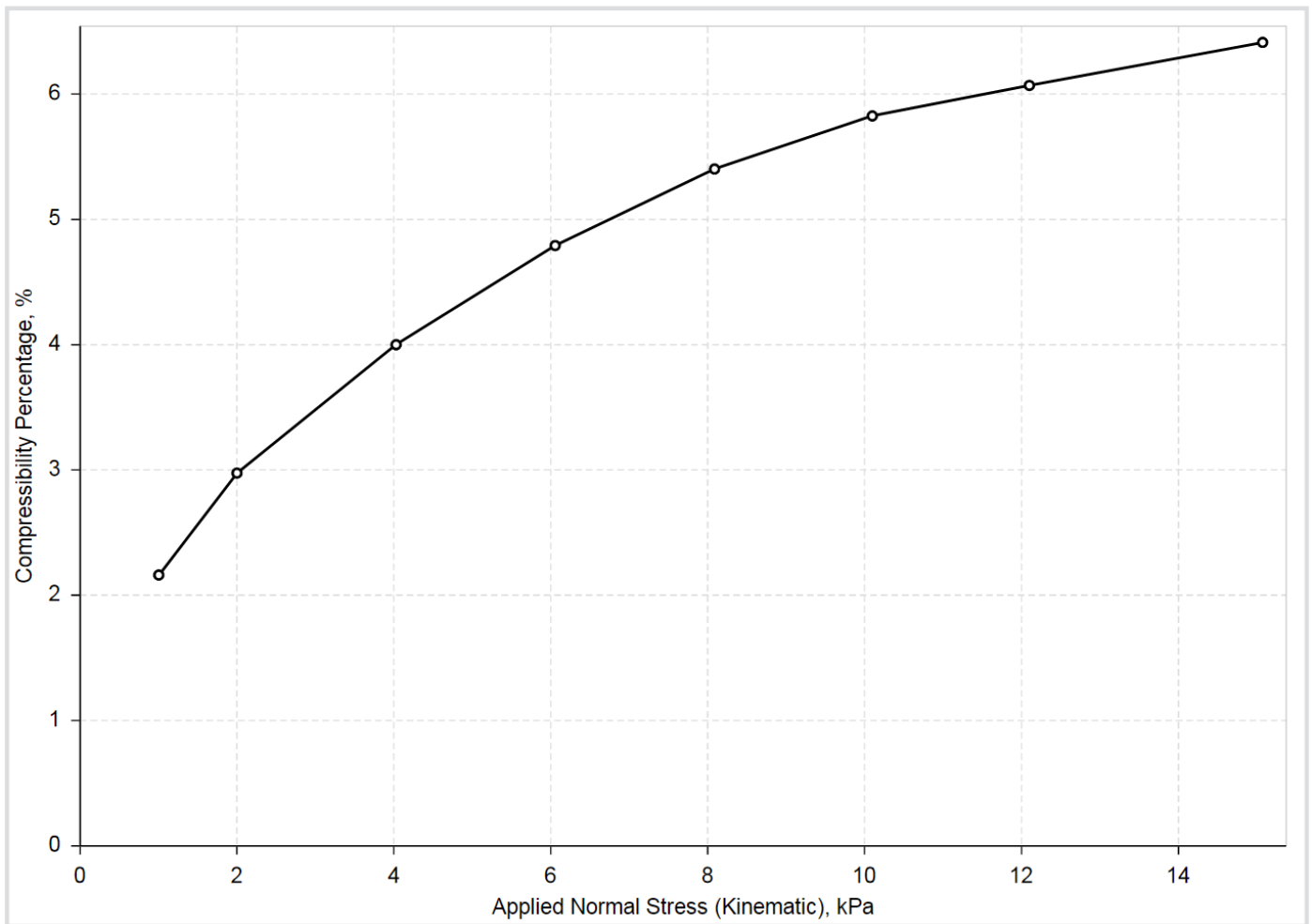


Figure 4.14: Compressibility test results for V 15-6053S.

For this powder, it was reached a 5.15% value of compressibility during the test at 15 kPa. If compared with previously analysed powder, that value is quite low, even if it was even lower for L 0002 (4.52%). Although It must be considered that comparing powders with different chemical compositions may lead to wrong interpretations, because there may be compressibility variations due to these powders having different elastic moduli.

4.6.5. Shear Cell Results

The shear cell results are shown in Fig. 4.15 and Table 4.5.

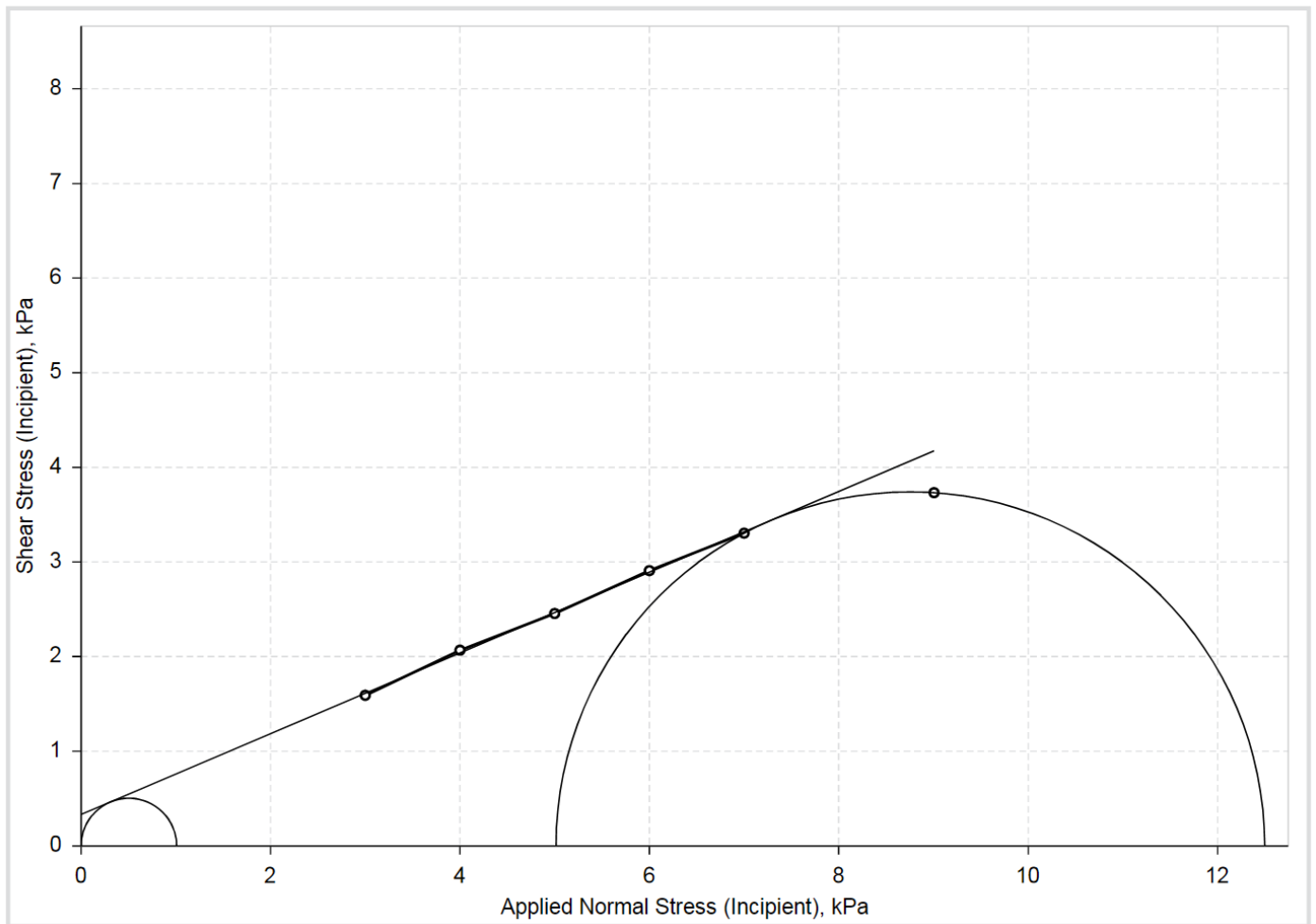


Figure 4.15: Shear cell results for V 15-6053S.

Table 4.5: Shear cell results for V 15-6053S.

Cohesion (kPa)	σ_c (kPa)	σ_1 (kPa)	σ_2 (kPa)	ff_c	Rel(p)	AIF (°)
0.333	1.01	12.5	5.01	12.4	7.42	23.1

According to the results interpretation provided in the previous chapter, this powder's ff_c value describes it as free-flowing, while the Rel(p) value defines it as a cohesive powder. There is again an apparent contradiction between these two values, as explained in the previous chapter. This test results are very similar to the other AlSi10Mg powders ones, not suggesting a lot of information. In fact, in the previous tests powders that had very different flowing behaviour resulted in having similar value as a result of this test.

5. Conclusions

One of the goals of this report was to establish some sort of relationship between the results of all the tests that have been conducted and flowing behaviour, with particular regard to the results of the flowability test.

It is important to understand the causes that prevented some powders to flow, so that they can be used in the future to predict the flowing behaviour of other samples.

V 14-5034S did not flow even through the Carney funnel, hence it does not meet the minimal requirements to be processed. Some test results that confirm its bad flowing behaviour consists in:

- High level of surface agglomeration during the moisture content evaluation. This suggests a very cohesive powder for which a short rest period and a thermal stimulus are enough to trigger agglomeration.
- If compared with all the other powders, it shows the highest conditioned bulk density. This is probably due to a very efficient packing state.
- Very high air velocity required to fluidise the powder, suggesting a compact bed with small and rare channels that let air flow through it
- Very high pressure drop across the powder bed during the permeability test, which means that it is offering great resistance to the air flowing. This leads to a very low permeability value, in agreement with the previous point.

The main possible causes that have been found to explain the previously named consequences are:

- High satellites content. This characteristic makes mechanical interlocking between particles likely and increase dramatically the number of contact points between particles, augmenting friction, hence making the powder itself mechanically more resistant and less prone to flow. This effect is so important that makes the otherwise good morphology (spherical particles, regularly shaped) negligible.
- Low particle size, in particular low D(50). Small particles are more sensitive to cohesive forces. Being this powder characterized by components so small, it is more prone to agglomerate, hence to show a bad flowing behaviour.
- Approximately more than 25% of its particles size is below 20 μm . This empirical limit defines when the cohesion forces are particularly critical. Having so many particles that small makes the powder's packing more efficient, leading to more difficulty in making it flow.

Regarding **L 0003**, it is difficult to understand the possible causes of its behaviour. During most of the test conducted, this powder's results were in line with all the other L samples. Although its flowing behaviour is worse, because it did not flow during the flowability test. The powder rheometer did not give any relevant data in that case. The only possible cause found consists in the very high impurities content of this powder. It contained several foreign particles with different chemical compositions, organic fibres both stretched and entangled. It has then been theorized that most of the tests performed are not able to fully discriminate chemically homogeneous powders and contaminated samples. In fact, all the possible interactions between powder, foreign particles and fibres are unknown, but they are likely to make the general

flowing behaviour worse due to phenomena like entanglement, electrostatic interactions, mechanical interlocking.

V 15-6053S is not AlSi10Mg , so comparisons are less accurate. Its bad flowing behaviour has been confirmed by:

- Surface agglomeration during the moisture content evaluation. Even if this phenomenon was not as relevant as in the V 14-5034S sample, it still suggests a cohesive enough powder to agglomerate.
- Low permeability (high pressure drop across the powder bed) detected during the permeability test. This suggests the powder resisting very well to air flowing, possibly due to the low presence of air channels.

The main possible causes that have been found to explain the previously named consequences are:

- Simultaneous presence of Irregular and oblong particles, splashes, satellites, rough and irregular surfaces. This irregularities content is not particularly high, but the compresence of them all makes the result critical.
- Low particle size, in particular low $D(50)$. Small particles are more sensitive to cohesive forces. Being this powder characterized by components so small, it is more prone to agglomerate, hence to show a bad flowing behaviour.

Another key point consists in using the test results to predict whether the powders with an uncertain behaviour, the ones that flowed through the Carney funnel, will be processable or not. To do so, it has been decided to evaluate the possible causes that would prevent these powders to flow and then discuss if these are consistent enough to compromise the flowing behaviour.

First of all, the powders that did not require a tap to flow during the flowability test will be analysed.

L 0001 should be compared to **L 0003**, because its bad flowing behaviour is due to foreign particle presence too. These two powders are very similar morphologically: by analysing their SEM images, they almost seem the same sample. They are in fact sold by the same supplier, hence it is likely that their producing methods are similar, providing analogous results. During imaging and the EDS analysis, impurities presence was far greater in the **L 0003** sample. Of course, this is not a reliable method to establish if a batch is more contaminated than another one. Although it seems likely to consider **L 0003** more contaminated, due to its worse results during the flowability test and the fact that the presence of impurities has been considered as the main cause of it. **L 0001** showed slightly higher $D(10)$, $D(50)$ and $D(90)$ values for its particle size distribution, suggesting particles a little bigger on average, hence cohesion less likely. Although this powder's Cohesion value obtained from the shear cell (0.385) is much greater than it is for **L 0003** (0.260), suggesting the opposite of what was previously stated. This last results is also confirmed by the fact that in all the tests, **L 0001**'s CBD is greater than it is for **L 0003**. This is probably due to the higher content of impurities preventing the latter to pack properly, leaving a lot of entrained air. This last phenomenon is probably why **L 0003** shows better properties during the powder rheometer tests: being shear stresses involved, a high amount of entrained air facilitates the blade/shear cell head movement, accommodating its motion. As a consequence of that, considering that during the additive manufacturing process shear stresses are more negligible, the cohesion results obtained during the shear cell are less

important. In conclusion, it has been decided that not enough information are available to determine whether this powder fill act properly during the manufacturing process or not, because its behaviour is deeply influenced by its impurities content, which cannot be directly evaluated by the tests conducted. Moreover, especially for contaminants, batch-to-batch variations can be very significant.

T 0425.2.5 is the other powder that was able to flow through the Carney funnel without the necessity of a tap. The possible causes that prevented it from flowing through the Hall funnel were:

- Frequent presence of splashes of particle's surface. This are likely to increase the chance of mechanical interlocking between particles, worsening the general powder flowing behaviour. This defect moreover increases surface roughness, which is another factor that worsens a powder's ability to flow.
- Highly asymmetrical particle size distribution curve, characterised by a high quantity of small particles (about 10% particles smaller than 20 μm). This leads to a better-packed structure, where smaller particles can fill the gap between the bigger ones, leading to a generally greater than average CBD value and a worse flowing behaviour.

This powder is also characterised by the lowest permeability value among all the samples analysed, excluding the ones that flowed through the Hall funnel. Moreover, its particle shape, besides the presence of splashes, is surprisingly regular. In particular, it is the powder with the more spherical particles, which is an important factor. In conclusion, considering that surface splashes are not as critical as a high content of satellites and that, even if the particle size distribution curve is asymmetrical, the volumetric quantity of powders smaller than 20 μm is just 10%, T 0425.2.5 is probably an acceptable powder, hence machinable. It must also be noticed that this powder showed an average flow of 11.3 s/50g, which is lower than the 12.5 s/50g showed by the L 0001 powder. This results suggest that, coherently with the previous analysis, T 0425.2.5 will show a better flowing behaviour.

S 16D0534 required a tap to flow through the Carney funnel during the powder flow test. Moreover, its average flow is 13.5 s/50g, which is greater than it is for the other two powders. This fact should be enough to prove that this is the worst of these three powders. If it has been suggested that L 0001 flowing behaviour will not be good enough to be processed, then the same should be stated for that powder too. Its bad flowing behaviour is mainly caused by the very high satellites content. This suggests a certain number of phenomena that make flowing complex and less efficient, such as mechanical interlocking, increasing number of contact points between particles, that leads to more relevant attrition phenomena. Moreover, these satellites have been proven to be highly unstable and likely to break. As a consequence of that, the conditioned powder becomes more packed, increasing the powder density and making agglomeration more likely to happen. This is more negligible in an environment where shear stress is prevalent (e.g. stability test), but in case of flow (e.g. process itself, powder flow test), where other forces are more relevant (e.g. gravity), it is critical. The results of the tests conducted using the powder rheometer, the SEM and the particle size distribution analyser then confirm what can be foreseen by the comparison of the average flow.

The other important goal of this project consisted in trying to determine the usefulness of the FT4 tests for aluminium powders used in additive manufacturing. In particular, the key point was to understand if these tests can provide any extra information that can be used to better discriminate the results of the powder flow test. As a result of the experiments conducted,

every single test proved to be somehow useful to confirm the information that was gathered previously. Although there have been two scenarios in which this is not true, where the powder rheometer proved to be very useful by giving important data, otherwise not obtainable:

- The results of all the tests that provided a Conditioned bulk density value, combined with the compressibility test, allowed to determine the satellite instability of the S 16D0534 powder. Moreover, it was possible to evaluate the precise stress value that caused particle breaking.

- The permeability test in general, proved to be a very useful tool to rank powders according to their flowing behaviour, in an apparently even more accurate way than the flowability test itself. By having a look at Fig. 5.1, it can be seen how the powders that showed a better flowing behaviour lies in the upper part of the graph (highest permeability values). The only exceptions to this trend are the L powders characterized by a high content of contaminants. Considering that, it has been concluded that this a very useful tool to rank powders, as long as they are compositionally homogeneous and not contaminated.

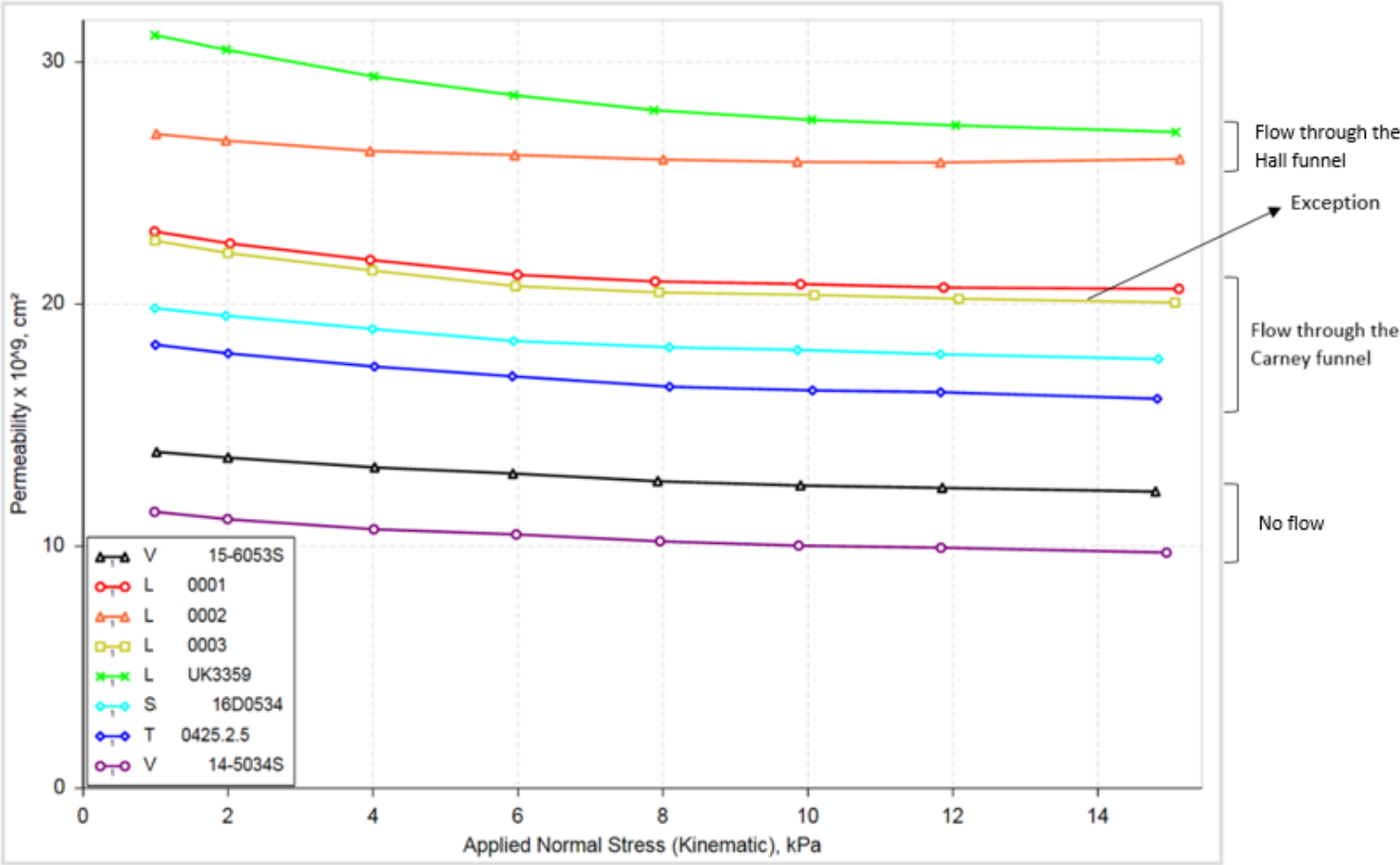


Figure 5.1: Permeability test results for all the analysed powders, where permeability is plotted instead of pressure drop.

6. List of Symbols

Symbol	Description	Unit
μ	Air viscosity	[Pa · s]
A	Area of the powder bed	[cm ²]
AR	Aeration ratio	[-]
BFE	Basic flowability energy	[mJ]
CBD	Conditioned bulk density	[g/cm ³]
CI	Compressibility index	[-]
$E_{(\text{air velocity} = n)}$	Flowing energy when the air velocity equals n mm/s	[mJ]
$E_{\text{Test } n}$	Flowing energy evaluated at the end of test number n	[mJ]
$E_{\text{up, Cycle } n}$	Flowing energy when the blade is moving upward during test number n	[mJ]
ff_c	Flow function	[-]
FRI	Flow rate index	[-]
$f_{y, \text{coh}}$	Vertical component of the cohesive force between two particles	[N]
g	Acceleration of gravity	[m/s ²]
k	Permeability	[cm ²]
L	Length of the powder bed	[cm]
m_i	Mass of particle i	[kg]
m_{split}	Sample mass once the vessel has been split	[g]
Q	Air volume per unit time	[cm ³ /s]
q	Air flow rate	[cm/s]
Rel(p)	Peschl relative flowability parameter	[-]
SE	Specific energy	[mJ/g]
SI	Stability index	[-]
V	Volume	[m ³]

ΔP	Pressure drop across powder bed	[Pa]
σ_1	Major principal stress	[kPa]
σ_2	Minor consolidation stress	[kPa]
σ_c	Unconfined yield strength	[kPa]

7. References

- [1] Mani M., Lane B., Donmez A., Feng S., Moylan S. and Fesperman R., 2015, Measurement Science Needs for Real-time Control of Additive Manufacturing Powder Bed Fusion Processes. NIST Interagency/Internal Report (NISTIR) – 8036, 1-7.
- [2] ASTM Standard 2792, 2012, Standard terminology for additive manufacturing technologies. *ASTM International*, West Conchocken, PA.
- [3] EPMA, Promoting Powder Metallurgy Technology, Additive Manufacturing Technology (Leaflet). Online version: www.epma.com/am
- [4] A. T. Sutton, C. S. Kriewall, M. C. Leu, J. W. Newkirk, 2016, Powders for Additive Manufacturing Processes: Characterization Techniques and Effects on Part Properties. *Solid Freeform Fabrication 2016 - Proceedings of the 26th Annual International*, 1004-1022.
- [5] C. Aumund-Kopp, A. Riou, 2015, Introduction to Additive Manufacturing Technology, A guide for Designers and Engineers. *Promoting Powder Metallurgy Technology*, 3-38.
- [6] J. A. Slotwinski, E. J. Garboczi, 2015, Metrology Needs for Metal Additive Manufacturing Powders. *Journal of Minerals, Metals & Materials Society*, Vol. 67, No. 3, 538-540.
- [7] M. Actis Grande, *Tecnologie di Formatura – Lecture Notes*. Polytechnic University of Turin, unpublished, academic year 2016/2017.
- [8] J. Gardan, 2016, Additive Manufacturing Technologies: State of the Art and Trends. *International Journal of Production Research*, 3118-3128.
- [9] G. N. Levy, R. Schindel, J. P. Kruth, 2003, Rapid Manufacturing and Rapid Tooling with Layer Manufacturing (LM) Technologies, State of the Art and Future Perspectives. *CIRP Annals*, Vol. 52, 1-10.
- [10] F. Calignano, D. Manfredi, E. P. Ambrosio, S. Biamino, M. Lombardi, E. Atzeni, A. Salmi, P. Minetola, L. Iuliano and P. Fino, 2017, Overview on Additive Manufacturing Technologies. *Proceedings of the IEEE*, Vol. 105, No. 4, 593-606.
- [11] W. Meiners, K. D. Wissenbach and A. D. Gasser, 1998, *Shaped Body Especially Prototype or Replacement Part Production*. U.S. Patent Appl. No. DE19649849C1.
- [12] Powder Metallurgy. *ALD Vacuum Technologies website*. Online version: <http://web.ald-vt.de/cms/vakuum-technologie/anlagen/powder-metallurgy/>
- [13] A. B. Spierings, M. Voegtlin, T. Bauer, K. Wegener, 2015, Powder Flowability Characterisation Methodology for Powder-Bedbased Metal Additive Manufacturing. *Progress in Additive Manufacturing*, Vol. 1, 9-12.
- [14] M. Krantz, H. Zhang, J. Zhu, 2009, Characterization of Powder Flow: Static and Dynamic Testing. *Powder Technology*, Vol. 194.

- [15] A. Simchi, 2004, The Role of Particle Size on the Laser Sintering of Iron Powder. *The Metallurgical and Materials Transactions B*, Vol. 35, 937-948.
- [16] E.O. Olakanmi, 2013, Selective Laser Sintering/Melting (SLS/SLM) of Pure Al, Al-Mg, and Al-Si Powders: Effect of Processing Conditions and Powder Properties. *Journal of Materials Processing Technology*, Vol. 213, 1387-1405.
- [17] E. J. R. Parteli, T. Poschel, 2016, Particle-Based Simulation of Powder Application in Additive Manufacturing. *Powder Technology*, Vol. 288, 96-102.
- [18] A. Castellanos, J. M. Valverde, M. A. S. Quintanilla, 2004, The Sevilla Powder Tester: a Tool for Characterizing the Physical Properties of Fine Cohesive Powders at Very Small Consolidations. *KONA Powder and Particle Journal*, Vol. 22, 66–81.
- [19] M. Leturia, M. Benali, S. Lagarde, I. Ronga, K. Saleh, 2014, Characterization of Flow Properties of Cohesive Powders: A Comparative Study of Traditional and New Testing Methods. *Powder Technology*, Vol. 253, 406-421
- [20] W. C. Yang, 2005, Fluidization of Fine Cohesive Powders and Nanoparticles - a Review. *Journal of the Chinese Institute of Chemical Engineers*, Vol. 36, 1-15.
- [21] J. Visser, 1989, Van der Waals and Other Cohesive Forces Affecting Powder Fluidization. *Powder Technology*, Vol. 50, 1-10.
- [22] J. P. K. Seville, C. D. Willett, P. C. Knight, 2000, Interparticle Forces in Fluidisation: a Review. *Powder Technology*, Vol. 113, 261-268.
- [23] J. Clayton, D. Millington-Smith and B. Armstrong, 2015, The Application of Powder Rheology in Additive Manufacturing. *Journal of Minerals, Metals & Materials Society*, Vol. 67, No. 3, 544-548.
- [24] J. M. Valverde, 2012, Fluidization of Fine Powders: Cohesive Versus Dynamical Aggregation. *Springer*.
- [25] R. Freeman, 2005, Powder Testing-Dealing with the Daily Challenges, Powder Handling and Processing, Vol. 17, 294-296.
- [26] M.K. Taylor, J. Ginsburg, A. Hickey, F. Gheyas, 2000, AAPS PharmSciTech. *Springer*.
- [27] G. B. M. Cervera and G. Lombera, 1999, Numerical Prediction of Temperature and Density Distributions in Selective Laser Sintering Processes. *Rapid Prototyping. Journal*, Vol. 5, 21-26.
- [28] A. V. Gusarov, T. Laoui, L. Froyen, V. Titov, 2003, Contact Thermal Conductivity of a Powder Bed in Selective Laser Sintering. *International Journal of Heat and Mass Transfer*, Vol. 46, 1103-1109.
- [29] B. Liu, R. Wildman, C. Tuck, I. Ashcroft, R. Hague, 2011, Investigation the Effect of Particle Size Distribution on Processing Parameters Optimisation in Selective Laser Melting Process. *Solid Freeform Fabrication Proceedings*, Austin, TX.
- [30] J. P. Kruth, G. Levy, F. Klocke, T. H. C. Childs, 2007, Consolidation Phenomena in Laser and Powder-Bed Based Layered Manufacturing. *CIRP Annuals - Manufacturing Technology*, Vol. 56, No. 2, 730-759.
- [31] Sample-electron interaction. *NanoScience Instruments*. Online version: <http://www.nanoscience.com/technology/sem-technology/sample-electron-interaction/>

- [32] Micromeritics, 2015, ACCUPYC II, gas displacement pycnometry system (Brochure).
Online version: <http://www.micromeritics.com/product-showcase/AccuPyc-II-1340.aspx>
- [33] Malvern, MASTERZISER 3000, smarter particle sizing (Brochure). Online version:
<https://www.malvern.com/en/products/product-range/mastersizer-range>
- [34] Copley Scientific, 2016, Quality Solutions for the Testing of Pharmaceuticals
(Brochure). Online version: <http://www.copleyscientific.com/home/pharmaceutical-testing/powder-testing/powder-flowability-testers/angle-of-repose>
- [35] Freeman Technology, 2006, The Conditioning Process, W7006.
- [36] Freeman Technology, 2013, Compressibility, W7008.
- [37] Freeman Technology, 2010, Stability Method, W7011.
- [38] Freeman Technology, 2007, Stability & Variable Rate Flow Method, W7013.
- [39] Freeman Technology, 2013, The Basic Flowability Energy, W7030.
- [40] Freeman Technology, 2008, Specific Energy, W7031.
- [41] Freeman Technology, 2007, Variable Flow Rate Method, W7012.
- [42] Freeman Technology, 2013, Aeration Method, W7015.
- [43] Freeman Technology, 2009, Permeability, W7017.
- [44] Freeman Technology, 2010, Shear Cell, W7018.
- [45] Malvern, 2015, Mastersizer 3000 User Manual. 146-148.
- [46] Freeman Technology, 2013, Additional Parameters Derived from Shear Cell Data,
W7108.
- [47] A. W. Jenike, 1964, Storage and Flow of Solids. *University of Utah, Bulletin*, Vol. 123.
- [48] M. Leturia, M. Benali, S. Lagarde, I. Ronga, K. Saleh, 2014, Characterization of Flow
Properties of Cohesive Powders: A Comparative Study of Traditional and New Testing
Methods. *Powder Technology*, Vol. 253, 406–423.
- [49] I. A. S. Z. Peschl and H. Colijn, 1977, New Rotational Shear Testing Technique.
Journal of Powder & Bulk Solids Technology, Vol. 1, 55-60.

Acknowledgements

I owe my deepest gratitude to all the Renishaw staff that worked with me in Stone. In particular, Laura, Ravi and Mark deserve a special thanks for sharing their knowledge with me and for all the excellent advices they gave me. Most of all, they should receive an award because they had a lot of patience with me.

Giunto al termine di questo percorso di studi, mi sembra doveroso ringraziare le persone che più mi sono state vicine e mi hanno aiutato a raggiungere questo traguardo che mi sono imposto cinque anni fa.

Un enorme grazie va ai miei genitori, che mi sono sempre stati vicini e mi hanno supportato, non solo economicamente, in questi lunghi anni. Siete sicuramente l'aiuto più grande che io abbia ricevuto e senza di voi sono sicuro che sarebbe stato tutto molto più difficile.

Un altro sentito ringraziamento va a tutti i miei amici, che mi sono rimasti a fianco nonostante riversassi su di loro i miei malumori e lo stress legato all'università (scusate ancora!). Grazie per non essere scappati via da me, come un minimo di saggezza avrebbe imposto. Grazie di avere poco buonsenso.

Un ringraziamento particolare va a Simone, Alessio, Patrizia e Monica per essersi dimostrati i meno sensati di tutti!